technische universität
dortmund

A Model-Building Approach to the Origin of Flavor

Dissertation
zur Erlangung des akademischen Grades

Dr. rer. nat.
im Fach Physik

Vorgelegt von
Erik Schumacher

Fakultät Physik
Technische Universität Dortmund

Dortmund, Oktober 2016

Gutachter dieser Arbeit:
Prof. Dr. Heinrich Päs und Prof. Dr. Gudrun Hiller
Vorsitzender des Promotionsausschusses:
Prof. Dr. Götz Uhrig

Datum der mündlichen Promotionsprüfung:
24. Januar 2017

This thesis contains the following work previously published by the author, ordered by appearance in the thesis:

- A. E. Cárcamo Hernández, I. de Medeiros Varzielas, and E. Schumacher. *Fermion and scalar phenomenology of a two-Higgs-doublet model with S_3.* Phys.Rev. D93 (2016) no.1, 016003. doi:10.1103/PhysRevD.93.016003 [2015]

- M. D. Campos, A. E. Cárcamo Hernández, S. Kovalenko, I. Schmidt, and E. Schumacher. *Fermion masses and mixings in an SU(5) grand unified model with an extra flavor symmetry.* Phys.Rev. D90 (2014) no.1, 016006. doi:10.1103/PhysRevD.90.016006 [2014]

- M. D. Campos, A. E. Cárcamo Hernández, H. Päs, and E. Schumacher. *Higgs $\to \mu\tau$ as an indication for S_4 flavor symmetry.* Phys.Rev. D91 (2015) no.11, 116011. doi:10.1103/PhysRevD.91.116011 [2014]

- H. Päs, E. Schumacher. *Common origin of R_K and neutrino masses.* Phys.Rev. D92 (2015) no.11, 114025. doi:10.1103/PhysRevD.92.114025 [2015]

- F. F. Deppisch, S. Kulkarni, H. Päs, and E. Schumacher. *Leptoquark patterns unifying neutrino masses, flavor anomalies, and the diphoton excess.* Phys.Rev. D94 (2016) no.12, 013003. doi:10.1103/PhysRevD.94.013003 [2016]

- A. E. Cárcamo Hernández, I. de Medeiros Varzielas, and E. Schumacher. *The 750 GeV diphoton resonance in the light of a 2HDM with S_3 flavor symmetry.* Unpublished manuscript. arXiv:1601.00661 [hep-ph] [2016]

ABSTRACT

In this thesis we link the recent anomalies reported in B meson and $h \to \mu\tau$ decays to the smallness of neutrino masses and aspects of the flavor puzzle, including the hierarchy of the Yukawa couplings and the disparate fermion mixings. By formulating various new models we attempt to shed light on the potential common origin of the distinct measurements in the flavor sector. To this end, discrete symmetries are utilized in this work as the governing principle behind all fermion interactions. The first two models based on the S_3 and the A_4 symmetry, respectively, aim to unify the diverse fermion masses and mixings. Special features separate the frameworks from the flavor models in the literature that often lack testable predictions. While the first model provides interesting flavor-violating signatures in top quark decays, the second one ties the flavor to the grand unification scale in a novel way. In the three following models we focus on the anomalies that hint at lepton flavor and universality violation. We propose that the large flavor violation observed in $h \to \mu\tau$ decays is dictated by the scalar mixing of an enlarged S_4-symmetric Higgs sector. By constructing two leptoquark models we show for the first time that leptoquark couplings shaped by a Froggatt-Nielsen mechanism can accommodate the B meson anomalies and simultaneously generate naturally-small neutrino masses. Emphasizing the importance of testability, we demonstrate how these models can be probed by future diphoton resonances, using the recent 750 GeV excess as an example scenario.

ZUSAMMENFASSUNG

In dieser Arbeit verknüpfen wir die jüngsten Anomalien in B Meson- und $h \to \mu\tau$-Zerfällen mit den verschwindend geringen Neutrinomassen und verschiedenen Aspekten des Flavorproblems wie den hierarchischen Yukawa-Kopplungen und den ungleichen Fermionmischungen. Indem wir diverse neue Modelle konstruieren, versuchen wir eine mögliche gemeinsame Ursache der verschiedenen Messungen im Flavorsektor zu finden. Dazu nutzen wir diskrete Symmetrien, um sämtliche Fermionwechselwirkungen in dieser Arbeit zu modellieren. Die ersten zwei Modelle, basierend auf der S_3- und der A_4-Symmetrie, zielen auf die Vereinheitlichung der Fermionmassen und -mischungen ab. Besondere Eigenschaften differenzieren diese von bisherigen Flavormodellen, die oft experimentell schwer zu unterscheiden sind. Während das eine Modell interessante flavorverletztende Top-Quarkzerfälle aufweist, schlägt das andere den Bogen zu großen vereinheitlichten Theorien. In drei weiteren Modellen betrachten wir die Anomalien, die auf eine Verletzung von Leptonflavor und -universalität hindeuten. Wir nehmen an, dass die Flavorverletzung in $h \to \mu\tau$-Zerfällen die Folge zusätzlicher Higgs Bosonen ist, deren Mischung durch eine S_4-Symmetrie beschrieben wird. Weiterhin zeigen wir erstmalig mithilfe eines Froggatt-Nielsen-Mechanismus, dass Leptoquarks nicht nur die anomalen Zerfälle der B Mesonen, sondern gleichzeitig auch die leichten Neutrinomassen erklären können. Um den Stellenwert von überprüfbaren Vorhersagen aufzuzeigen, analysieren wir am Beispiel des 750 GeV Signals, wie diese Modelle in Hinblick auf mögliche zukünftige Resonanzen im Diphotonkanal getestet werden können.

ACKNOWLEDGMENTS

Nach vier Jahren und geschätzten 1500 Tassen Kaffee geht für mich leider mit dem Schreiben dieser Dissertation ein besonderer Abschnitt zu Ende. Die Arbeit an den Lehrstühlen von T3 und T4 war spannend, abwechslungsreich, gesellig, fordernd und auch manchmal frustrierend, aber immer lustig und wird mir vor allem dank der vielen netten Leute lange in Erinnerung bleiben.

Zunächst einmal muss ich allen danken, die mich trotz der regelmäßigen Streiche so lange ausgehalten haben. Das betrifft wohl vor allem Maggi, Diganta, Wei-Chih, Dennis und Philipp – aber auch alle anderen, die länger mit mir zu tun hatten, dürfen sich angesprochen fühlen. Auch die Kaffeepausen, Group Meetings mit Bullshit Button, Movie Nights, und Aktionen wie den Office War oder die Wette mit Pokéballkuchen werde ich in Zukunft vermissen. Eine so tolle und rundum motivierende Arbeitsatmosphäre hat man wohl selten. Darum sei an dieser Stelle allen Mitgliedern von T3 und T4 der letzten vier Jahre für die schöne Zeit gedankt!

Aber in Wirklichkeit bestand das Doktorandenleben natürlich nicht nur aus Kaffee und Kuchen, sonst wäre ich mit dieser Arbeit wohl nicht fertig geworden. Da bedanke ich mich an erster Stelle bei meinem Doktorvater, Heinrich Päs, für die stets angenehme und unkomplizierte Zusammenarbeit, die Unterstützung meiner Forschung sowie die vielen Reisen, die er mir ermöglicht hat.

Dann wären da noch die übrigen Experten, die ich häufiger mal um Rat fragen durfte, weil es schneller ging als zu googlen, allen voran meine Lieblingsbürokollegen, Philipp und Mr. Chih. Auch die Flavor-Mitstreiter Dennis und Stefan konnte ich häufiger mal aushorchen, wenn es um Fragen zu B, K und D ging, sowie Peter bei mathematischen Diskussionen. Allen Genannten möchte ich außerdem für das Korrekturlesen diverser Kapitel meiner Arbeit und das kommende “Defense Training” danken.

Zu guter Letzt danke ich meinen Eltern, Ina und Fred, genauso wie meinen Freunden außerhalb der Physik für die moralische Unterstützung während dieser Zeit.

Finally, I would like to thank my English-speaking friends for the great opportunity to collaborate with them. I had the pleasure to work with Antonio and Ivo on many projects, who introduced me to the field of model building and answered all of my beginners' questions patiently. It was motivating to work on and learn from my first projects together with Miguel (Mígüelito), and I am grateful that he kept me alive during my stay in Chile. I also thank Frank Deppisch, Suchita Kulkarni, Sergey Kovalenko, and Ivan Schmidt for the fruitful discussions we had during our enjoyable collaborations.

CONTENTS

ACRONYMS

$0\nu\beta\beta$	Neutrinoless Double-Beta.
2HDM	Two-Higgs Doublet Model.
3HDM	Three-Higgs Doublet Model.
BSM	Beyond the Standard Model.
CKM	Cabibbo–Kobayashi–Maskawa.
CLFV	Charged Lepton Flavor Violation.
EW	Electroweak.
FCNC	Flavor-Changing Neutral Current.
FN	Froggatt-Nielsen.
GIM	Glashow-Iliopoulos-Maiani.
GUT	Grand Unified Theory.
IH	Inverted Hierarchy.
LFT	Lepton Flavor Triality.
LFV	Lepton Flavor Violation.
LHC	Large Hadron Collider.
NH	Normal Hierarchy.
NHDM	Multi-Higgs Model.
NP	New Physics.
PMNS	Pontecorvo–Maki–Nakagawa–Sakata.
SM	Standard Model.
TBM	Tribimaximal.
UV	Ultraviolet.
VEV	Vacuum Expectation Value.

1

INTRODUCTION

Two recent Nobel Prizes in physics attest the great progress of the field of particle physics and the success of the standard model (SM). After Peter Higgs and François Englert were recognized for their proposal of the Higgs boson on October 3, 2013, another Nobel Prize was awarded on October 6, 2015, to the particle physicists Takaaki Kajita and Arthur B. McDonald for their key contributions to the experiments that discovered neutrino oscillations. However, these outstanding achievements also exposed that the theory is incomplete since neutrino masses, implied by their oscillations, do not exist in the SM.

The current lack of evidence of new physics (NP) that could solve the remaining problems questions some well-established theories and the naturalness of the SM itself. As a result, an excess in the diphoton channel announced on December 14, 2015, motivated hundreds of physicists to come up with an explanation for what soon after turned out to be just a statistical fluctuation. However, other searches have revealed deviations from the SM in rare meson and Higgs boson decays that are yet to be verified and concern the origin of flavor.

This thesis addresses some of the issues directly related to the Nobel Prizes in physics of 2013 and 2015. The flavor problem referring to the peculiar patterns of fermion masses and mixings is arguably one of the most striking puzzles of the SM. It is plausible to assume that the distinct behavior of quarks and leptons, the smallness of neutrino masses, and the recent flavor anomalies all have a common origin. To this end we propose unified models, dealing with several of these problems at the same time.

The large leptonic mixing angles could be the first indication of the presence of a discrete flavor symmetry. Such theories are intertwined with an extended particle content that mediates flavor violation at detectable rates. This offers great model-building opportunities both to explain the deviations in the flavor observables and to provide testable predictions. The latter are crucial to distinguish between the many possible extensions of the SM. We show that the experimental anomalies can be connected with the diverse fermion mixings and the small neutrino masses by virtue of flavor symmetries. We utilize the scalar sector to extract characteristic model features.

In this chapter we recapitulate the current status of the SM and outline its shortcomings related to the flavor problem. Chapter 2 deals with the model-building tools at our disposal, which include additional symmetries and enlarged Higgs sectors. In Chapter 3 we present models to unify the fermion masses and mixings, whereas the models discussed in Chapter 4 attempt to combine the anomalies and the flavor problem. We explore how the inclusion of resonances like the recent excess in the diphoton channel can improve the testability of models in Chapter 5. The conclusions are presented in Chapter 6.

1.1 THE STANDARD MODEL OF PARTICLE PHYSICS

The SM of particle physics is a widely accepted theory describing the elementary particles and their interactions. It combines the electromagnetic, the weak, and the strong force acting between particles by imposing local gauge invariance under the symmetries $SU(3) \otimes SU(2) \otimes U(1)$ on the fundamental matter interactions.
Historically, the first steps towards the SM were taken when the electromagnetic and the weak force were combined to the electroweak (EW) force described by the $SU(2)_L \otimes U(1)_Y$ gauge symmetry in 1961 [1]. The Higgs mechanism explaining the generation of masses was introduced in 1967 [2]. Since then the SM has been extremely successful in predicting the missing pieces of the puzzle that complete the theory, including the top quark [3] and the Higgs boson, discovered only recently in 2012 [4, 5].
The fermion content of the SM consists of six quarks, classified as up-type (u, c, t; $Q = {}^{2}/_{3}$) and down-type (d, s, b; $Q = {}^{-1}/_{3}$), and leptons, divided into charged leptons (e, μ, τ; $Q = -1$) and neutrinos (ν_e, ν_μ, ν_τ; $Q = 0$) according to their electric charge Q. Furthermore, a number of gauge bosons arise from gauge invariance under $SU(3)_C \otimes SU(2)_L \otimes U(1)_Y$, where C, L, and Y stand for color, left, and hypercharge, respectively. The strong force is characterized by the $SU(3)_C$ symmetry affecting all particles that carry color charge, i.e., the quarks. Its mediators are the eight gluons. The EW force is jointly described by the $SU(2)_L \otimes U(1)_Y$ symmetries. Together they have four generators, which only after breaking down to $U(1)_{\mathrm{EM}}$ become the massive gauge bosons $W^{\pm}, Z$ and the massless photon γ.
The breaking of $SU(2)_L \otimes U(1)_Y \to U(1)_{\mathrm{EM}}$ is an integral part of the SM that is achieved by introducing the Higgs boson, which is the remaining piece to complete the self-consistent theory. The Higgs boson not only explains the masses of the $W^{\pm}$ and Z bosons, it also generates the masses of all the SM fermions. Besides the discovery of the Higgs boson, many predictions of the SM have been tested and confirmed at the Large Hadron Collider (LHC) with excellent precision. In the following subsections, two vital aspects of the SM are reviewed in detail, the Glashow-Salam-Weinberg theory (Sec. 1.1.1) and the Higgs-mechanism (Sec. 1.1.2). In its current state the SM is extremely robust, yet some challenges remain that are discussed in Sec. 1.2 and are addressed in the final chapters of this thesis.

1.1.1 *Glashow-Salam-Weinberg-Theory*

Although the electromagnetic and the weak force appear very different at low energies, it was found that at a scale of around 100 GeV they unify to a single force, known as the EW force. The corresponding energy where this takes place is referred to as the EW scale. Besides embedding these forces above and below the EW scale, an appropriate theory should account for why they diverge at low energies. This can be achieved by the spontaneous $SU(2)_L \otimes U(1)_Y \to U(1)_{\mathrm{EM}}$ gauge symmetry breaking.
The $SU(2)_L$ symmetry plays a special role in the Glashow-Salam-Weinberg model, as it distinguishes between fields with different chiralities. Left-handed fields are assigned to $SU(2)$ doublets, while their right-handed counterparts transform trivially under the symmetry. The charged leptons and neutrinos are accommodated in three copies of $SU(2)$ doublets, classifying the SM fermions in terms of three families or generations.

Similarly, each down-type quark is paired with one up-type quark, forming three generations of $SU(2)$ doublets. The explicit assignments of the SM fermions under $SU(3)_C \otimes SU(2)_L \otimes U(1)_Y$ are summarized in Tab. 1.1. These quantum numbers successfully accommodate the measured electric charges of the fields given by the equality $Q = T_3 + Y/2$.

Field	$SU(3)_C$	$SU(2)_L$	Y	T_3	Q
$\begin{pmatrix}\nu_e\\ e\end{pmatrix}_L, \begin{pmatrix}\nu_\mu\\ \mu\end{pmatrix}_L, \begin{pmatrix}\nu_\tau\\ \tau\end{pmatrix}_L$	**1**	**2**	-1	$1/2$ $-1/2$	0 -1
$\begin{pmatrix}u\\ d\end{pmatrix}_L, \begin{pmatrix}c\\ s\end{pmatrix}_L, \begin{pmatrix}t\\ b\end{pmatrix}_L$	**3**	**2**	$1/3$	$1/2$ $-1/2$	$2/3$ $-1/3$
$e_R,\, \mu_R,\, \tau_R$	**1**	**1**	-2	0	-1
$u_R,\, c_R,\, t_R$	**3**	**1**	$4/3$	0	$2/3$
$d_R,\, s_R,\, b_R$	**3**	**1**	$-2/3$	0	$-1/3$

Table 1.1: SM fermions with their quantum numbers or assignments under the SM symmetries, where Y denotes the weak hypercharge, T_3 is the weak isospin, and Q is the electric charge. L and R denote the left-handed and right-handed chirality of the fields, respectively.

In order to describe the EW force realistically, the gauge symmetry has to be broken spontaneously by a scalar field ϕ in a nontrivial representation of $SU(2)$. Once this scalar field acquires a vacuum expectation value (VEV), it will trigger the desired breaking of $SU(2)_L \otimes U(1)_Y \to U(1)_{\mathrm{EM}}$. The physical properties of the EW theory are a consequence of the local gauge transformation of ϕ and its interactions with the generators. Imposing $SU(2)_L \otimes U(1)_Y$-invariance implies that ϕ transforms as

$$\phi \to \exp\left(i \sum_{a=1}^{3} \alpha^a(x) t^a\right) \exp\left(i \frac{\beta(x)}{2}\right) \phi(x)\,, \tag{1.1}$$

where $t^a = \sigma^a/2$ are the $SU(2)$ generators. Therefore, the $\alpha^a(x)$ denote the local parameters of the $SU(2)$ transformation, while $\beta(x)$ corresponds to the $U(1)$ symmetry. Gauge invariance further requires introducing the covariant derivative

$$D_\mu = \partial_\mu - ig \sum_{a=1}^{3} A_\mu^a t^a - \frac{i}{2} g' B_\mu\,, \tag{1.2}$$

where A_μ^a and B_μ are the $SU(2)_L$ and the $U(1)_Y$ gauge bosons with their respective couplings g and g'. The $SU(2)$ structure is successfully broken once the field ϕ acquires a nonvanishing VEV in one component of the doublet

$$\langle \phi \rangle = \frac{1}{\sqrt{2}} \begin{pmatrix} 0 \\ v \end{pmatrix}\,, \tag{1.3}$$

which should happen at the EW scale and is known as the Higgs-mechanism. This VEV $v = 246$ GeV [6] eventually gives masses to the gauge bosons $W^{\pm}, Z$, and all the SM fermions. Explicitly, we obtain the gauge boson masses from the kinetic term of the Lagrangian

$$\mathcal{L} \supset \frac{1}{2}(D_\mu \phi)^2 = \frac{1}{2}\frac{v^2}{4}\left[g^2(A_\mu^1)^2 + g^2(A_\mu^2)^2 + (-gA_\mu^3 + g'B_\mu)^2\right] \tag{1.4}$$

yielding

$$\begin{aligned} W_\mu^{\pm} &= \frac{1}{\sqrt{2}}(A_\mu^1 \mp iA_\mu^2)\,, \\ Z_\mu^0 &= \frac{1}{\sqrt{g^2+g'^2}}(gA_\mu^3 - g'B_\mu)\,, \\ A_\mu &= \frac{1}{\sqrt{g^2+g'^2}}(g'A_\mu^3 - gB_\mu)\,, \end{aligned} \tag{1.5}$$

with the masses

$$m_W = g\frac{v}{2}\,, \qquad m_Z = \sqrt{g^2+g'^2}\frac{v}{2}\,, \qquad m_A = 0\,. \tag{1.6}$$

The SM gauge bosons are actually a mixture of the $SU(2)_L \otimes U(1)_Y$ generators, which explains why the Z boson, unlike the $W^{\pm}$, to some part also couples to right-handed particles. The mixing angle of the A_μ^3 and the B_μ generators in the neutral sector is defined by the Weinberg angle θ_{W}, i.e.,

$$\cos\theta_{\mathrm{W}} = \frac{g}{\sqrt{g^2+g'^2}}\,, \qquad \sin\theta_{\mathrm{W}} = \frac{g'}{\sqrt{g^2+g'^2}}\,. \tag{1.7}$$

Using this definition, the parameter budget defining EW interactions can be reduced to the three basic parameters e, θ_{W}, and m_W since

$$g = \frac{e}{\sin\theta_{\mathrm{W}}}\,, \qquad m_W = m_Z\cos\theta_{\mathrm{W}}\,. \tag{1.8}$$

These parameters have been measured with excellent precision, turning the Glashow-Salam-Weinberg framework into a cornerstone of the SM. The latter equality is typically defined as the ρ parameter

$$\rho \equiv \frac{m_W}{m_Z\cos\theta_{\mathrm{W}}}, \tag{1.9}$$

which has been measured experimentally to be very close to 1, thereby tightly constraining all NP models that modify charged or neutral currents at the EW scale. At tree level, ρ can also be expressed in terms of the weak isospin T_i and the hypercharge Y_i [7]

$$\rho = \frac{\sum_{i=1}^n \left[T_i(T_i+1) - \frac{Y_i^2}{4}\right] v_i}{\frac{1}{2}\sum_{i=1}^n Y_i^2 v_i}\,. \tag{1.10}$$

It is easy to verify that $SU(2)$ singlets ($T_i = 0, Y_i = 0$) and doublets ($T_i = 1/2, Y_i = 1$) preserve $\rho = 1$, while higher representations are subject to constraints from EW precision measurements.

1.1.2 *The Higgs-Mechanism and Flavor Mixing*

In the most general case, the complex scalar doublet ϕ can be parametrized in terms of real scalar fields with different CP properties

$$\phi = \frac{1}{\sqrt{2}} \begin{pmatrix} \eta^+ + i\sigma^+ \\ v + h + iA \end{pmatrix}, \tag{1.11}$$

where h and A are the CP-even and CP-odd neutral scalars, respectively, and η^+ and σ^+ are the corresponding charged components. Consequently, the scalar doublet has in total four degrees of freedom, out of which only one remains after EW symmetry breaking, the Higgs boson h. What happens to the other three fields?
The scalar field ϕ acquires its VEV due to its specifically shaped scalar potential

$$V(\phi) = -\mu^2(\phi^\dagger\phi) + \lambda(\phi^\dagger\phi)^2 \tag{1.12}$$

that has a continuum of nonvanishing absolute minima at $v^2 = -\mu^2/\lambda$. Choosing a specific configuration in this potential breaks the initial symmetry.
By acquiring a VEV ϕ in turn gives masses to the EW gauge bosons. Being massive, the gauge bosons each have one additional degree of freedom compared to massless vector particles, corresponding to their longitudinal polarization. These extra degrees of freedom are absorbed from the components of ϕ, leaving it with only the Higgs boson h. Hence, the Goldstone bosons η^+, σ^+ and A manifest themselves as the longitudinal polarizations of the EW force carriers $W^\pm$ and Z, respectively. The situation is different in theories with several Higgs doublets, where more scalar fields are present than can be "eaten" by the EW gauge bosons. Such models are discussed in Sec. 2.2.
Once ϕ acquires a VEV, it also gives masses to the fermions. These masses stem from the Yukawa sector of the SM Lagrangian, which in first-generation notation reads

$$-\mathcal{L}_{\text{Yuk}} = Y_u \overline{Q}_L \tilde{\phi} u_R + Y_d \overline{Q}_L \phi d_R + Y_l \overline{L}_L \phi e_R + \text{h.c.}\,, \tag{1.13}$$

where Q_L denotes the left-handed $SU(2)$ quark doublets, u_R and d_R are the right-handed up-type and down-type quark singlets, respectively, and L_L and e_R are the equivalent fields from the lepton sector. The constant Yukawa couplings are defined by Y_u, Y_d, and Y_l, while $\tilde{\phi} \equiv i\sigma_2\phi^*$. In three generations the Yukawa couplings become 3×3 matrices in flavor space that are connected to the fermion masses by

$$M_{u,d,l} = \frac{1}{\sqrt{2}} v Y_{u,d,l}\,. \tag{1.14}$$

Note that these 3×3 matrices are in general not diagonal; in fact M_u and M_d cannot be diagonalized at the same time. The mismatch between the up-type and down-type quark sector is accounted for by the Cabibbo–Kobayashi–Maskawa (CKM) matrix.[1]
The CKM matrix enters charged current interactions mediated by the W^+ boson

$$\overline{u}_L \gamma^\mu W^+_\mu d_L = \overline{u}'_L V_u \gamma^\mu W^+_\mu V_d^\dagger d'_L = \overline{u}'_L \gamma^\mu W^+_\mu V_{\text{CKM}} d'_L\,, \tag{1.15}$$

[1] The corresponding matrix of the lepton sector is the Pontecorvo–Maki–Nakagawa–Sakata (PMNS) matrix, which is discussed in Sec. 1.2.1.

where $V_{u,d}$ are the unitary matrices transforming the fields u_L and d_L from the flavor into the mass basis u'_L and d'_L, and

$$V_{\text{CKM}} \equiv V_u V_d^\dagger = \begin{pmatrix} V_{ud} & V_{us} & V_{ub} \\ V_{cd} & V_{cs} & V_{cb} \\ V_{td} & V_{ts} & V_{tb} \end{pmatrix} . \tag{1.16}$$

Much like the ρ parameter, the elements of the CKM matrix have been determined experimentally with percent-level precision or better, constraining all beyond the SM (BSM) scenarios that modify quark flavor transitions. The uncertainty of the theory lies in the origin of these elements and their peculiar hierarchy, which is discussed in Sec. 1.2.1.
Note that the mixing does not appear in neutral currents involving the Z boson. Flavor-changing neutral currents (FCNCs) are absent in the SM at tree level by virtue of the Glashow-Iliopoulos-Maiani (GIM) mechanism and occur only at second order in the weak interaction [8].

1.2 SHORTCOMINGS AND MOTIVATION FOR NEW PHYSICS

The fact that the SM describes only 5% of the matter content of the Universe implies that there must be something else in the vast "desert" spanned by the 17 orders of magnitude between the EW and the Planck scale, where the effects of gravity become relevant. While pressing matters such as dark matter and gravity are prominent subjects in the literature, this work is largely motivated by the flavor problem, which is introduced below. Lepton flavor violation and universality are being tested at low-energy experiments as well as the LHC and show interesting discrepancies between the measurements and the SM expectations. Besides these deviations, we are puzzled by the Yukawa couplings, the fermion mixings, and the source of neutrino masses as these are not predicted by the SM.
This section deals with selected shortcomings of the SM in more detail and highlights some promising channels to probe flavor models. We start by introducing the flavor problem in Sec. 1.2.1. Different types of neutrino mass mechanisms are outlined in Sec. 1.2.2, while Sec. 1.2.3 deals with rare fermion decays, which are crucial for NP searches. Finally, Sec. 1.2.4 reviews the diphoton anomaly that received a lot of attention from the community in 2016.

1.2.1 *The Origin of Flavor, Masses, and Mixings*

The so-called flavor problem refers to many unanswered questions at the same time: the puzzling pattern of Yukawa couplings defining the fermion masses and mixings is well measured but not predicted by the SM; it does not explain where these parameters come from, nor why the top quark is so much heavier than all the other fermions. The seemingly random pattern of fermion masses is illustrated schematically in Fig. 1.1 and the explicit experimental values are summarized in the Tabs. A.1, A.2, and A.3 of App. A.1.
Aside from the large hierarchy between the top quark and the up quark mass, a special feature of the quark sector is the hierarchical structure of the CKM matrix, reflected by

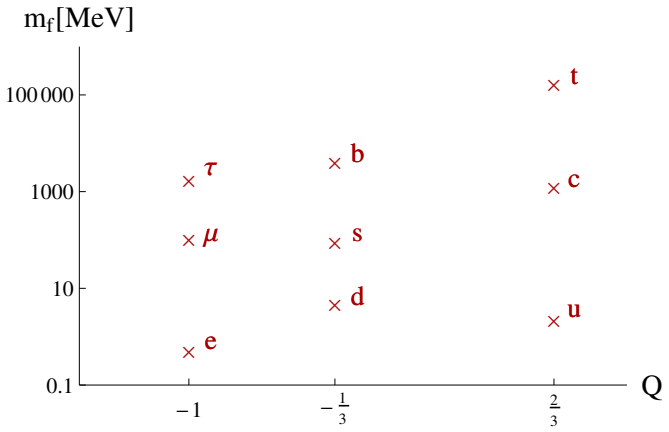

Figure 1.1: Pattern of the SM fermion masses, depicted in a logarithmic plot to accommodate the large hierarchies among them.

the values listed in Tab. A.4. This is in stark contrast with the large mixing present in the PMNS matrix that appears almost anarchic. The fundamental difference of the mixing matrices suggests a different origin of lepton and quark flavor. Until 2013, when $\theta_{13} \simeq 9°$ was measured by the reactor experiments Reno, Daya Bay, and Double Chooz [9–11], the lepton mixing data was in excellent agreement with tribimaximal (TBM) mixing,

$$U_{\text{TBM}} = \begin{pmatrix} \frac{2}{\sqrt{6}} & \frac{1}{\sqrt{3}} & 0 \\ -\frac{1}{\sqrt{6}} & \frac{1}{\sqrt{3}} & -\frac{1}{\sqrt{2}} \\ -\frac{1}{\sqrt{6}} & \frac{1}{\sqrt{3}} & \frac{1}{\sqrt{2}} \end{pmatrix} , \tag{1.17}$$

corresponding to $\theta_{12} = 33°$, $\theta_{23} = 45°$, and $\theta_{23} = 0°$. This structure, first proposed in Ref. [12], could very well be explained by a discrete symmetry acting on the lepton families as discussed further in Sec. 2.1.4. As of today, the neutrino mixing angles have been measured with great precision, resulting in increasingly contrived models that attempt to resolve the parameter puzzle. New data on θ_{23} is expected to clarify whether $\mu - \tau$ mixing truly is maximal, which in turn will rule out a number of these models. One could assume that nature chose all of these parameters randomly, but such an anthropic solution is unsatisfying and defies naturalness: An origin by chance is highly improbable due to the large hierarchies among the parameters. An overview of the physical observables in the neutrino sector and the respective experiments that currently measure them is given in Tabs. A.5 and A.6. For a detailed review see, e.g., Ref. [13]. A question closely related to the flavor puzzle concerns the origin of the neutrino masses. Absent from weak interactions, right-handed neutrinos were originally excluded from the SM. However, since the discovery of neutrino oscillations, they are known to be massive, which begs the question of how their masses are actually generated. If neutrinos receive their masses from the Higgs boson, their Yukawa couplings will be tiny, increasing the large hierarchy of the parameters even further, e.g.,

$$\frac{Y_\nu}{Y_e} \sim \mathcal{O}\left(10^{-7}\right) , \qquad \frac{Y_\nu}{Y_t} \sim \mathcal{O}\left(10^{-13}\right) . \tag{1.18}$$

Many alternatives have been considered that rely on the unique Majorana nature of the neutrino, some of which are highlighted in Sec. 1.2.2.
In the case that neutrinos are indeed Majorana particles, the PMNS matrix contains two more unknown parameters, referred to as Majorana phases,

$$U_{\text{PMNS}} = U_l^\dagger U_\nu P\,, \quad \text{with} \quad P = \text{diag}(1, e^{i\alpha}, e^{i\beta})\,. \tag{1.19}$$

Since neutrino oscillations are insensitive to these phases, they are very hard to track experimentally. A notable observable that depends on the Majorana phases, is the effective Majorana mass decisive for neutrinoless double-beta decay ($0\nu\beta\beta$), outlined in Sec. 1.2.2.[2]

1.2.2 *Neutrino Masses*

First predicted in 1957 by Pontecorvo [15], it took until 2001 to prove that neutrinos indeed oscillate, when the Sudbury Neutrino Observatory confirmed the deficit of solar neutrinos due to neutrino oscillations [16]. Meanwhile, also Super-Kamiokande observed a deficit in the atmospheric neutrino flux [17]. Only recently, both experiments were recognized for their efforts with the Nobel Prize for Physics in 2015.
This groundbreaking result not only states the obvious that neutrinos can change their flavor, it also implies that neutrinos must have masses, which are not yet embedded in the SM. The probability for a neutrino with the flavor α to oscillate into the flavor β can be expressed in terms of the neutrino mass squared differences $\Delta m^2_\nu \equiv m^2_2 - m^2_1$. For clarity, the transition probability can be written in the two-neutrino case as

$$P(\nu_\alpha \to \nu_\beta) = \sin^2(2\theta)\sin^2\left(\frac{\Delta m^2_\nu L}{4E}\right) \qquad (\alpha \neq \beta)\,, \tag{1.20}$$

where θ denotes the mixing angle between the neutrino flavors, L is the oscillation length, and E defines the energy. To observe oscillations at all, Δm^2_ν must not vanish. The actual observed mass squared differences are denoted as Δm^2_{sol} and Δm^2_{atm} (cf. Tab. A.2), implying the existence of at least three neutrinos.[3]
As of today, the observation of neutrino oscillations is still the only indication of neutrino masses. Direct detection experiments such as KATRIN aim to determine the absolute mass explicitly, but so far are only able to place upper limits [19]. Such bounds on the sum of the neutrino masses can also be inferred from observations of the cosmic microwave background. Latest results from the PLANCK satellite predict that [18, 20]

$$\sum_i m^\nu_i \lesssim 0.183 \text{ eV}\,. \tag{1.21}$$

Aside from the absolute mass scale, also the mass ordering is unknown. The two possible orderings that are determined by the sign of Δm^2_{atm} are referred to in the literature as normal hierarchy (NH) and inverted hierarchy (IH):

$$\text{NH:} \quad m_1 < m_2 \ll m_3\,, \qquad \text{IH:} \quad m_3 \ll m_1 < m_2\,, \tag{1.22}$$

which are illustrated schematically in Fig. 1.2.

[2] It is also possible to probe the Majorana phases at colliders in charged lepton flavor-violating processes. See, e.g., Ref. [14] for an analysis in the context of the seesaw mechanism type II.
[3] The composition of elements in our early universe and today indicates that the number of light neutrinos is likely three, to not interfere with big bang nucleosynthesis [18].

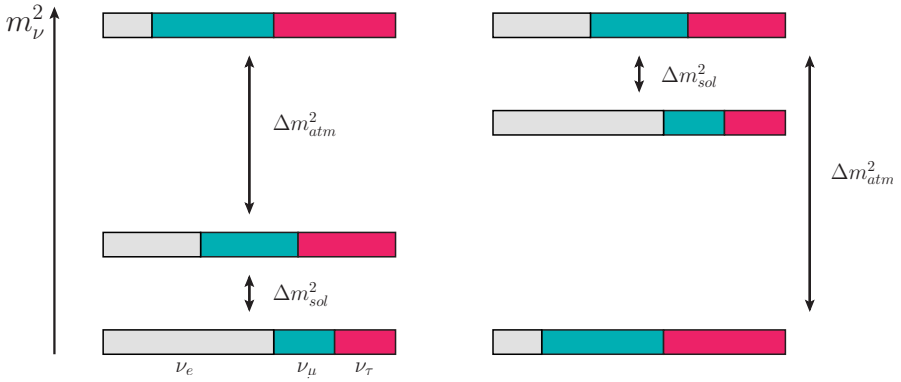

Figure 1.2: Schematic depiction of the normal (left) and the inverted neutrino mass hierarchy (right). The colors denote the flavor compositions of each mass eigenstate, while the height of the bars determines their masses relative to the other states.

Note that the lower limits on the sum of the neutrino masses for NH and IH are very close to the upper limits determined by PLANCK [cf. Eq. (1.21)]

$$\sum_i m_i^\nu \gtrsim 0.06 \text{ eV} \quad (\text{NH})\,, \qquad \sum_i m_i^\nu \gtrsim 0.10 \text{ eV} \quad (\text{IH})\,, \tag{1.23}$$

implying that experiments should slowly close in on the neutrino masses in the near future. For certain is that the neutrino mass is tiny compared to the other SM fermions, yet its origin remains unclear. The most common neutrino mass mechanisms are summarized in the following paragraphs.

Figure 1.3: Mass generation for the Dirac neutrino (left) and the Majorana neutrino (right).

DIRAC MASSES: A straightforward possibility to generate neutrino masses is to introduce right-handed neutrinos as singlets under the SM symmetries. The neutrino masses are then generated the same way as all the other fermion masses in the SM: via a coupling to the Higgs boson as depicted in Fig. 1.3. The respective Dirac mass term for the neutrino reads

$$\mathcal{L}_D = -\frac{1}{2} y_D \overline{L}\,\tilde{\phi}\,\nu_R + \text{h.c.}\,, \tag{1.24}$$

where y_D denotes the Yukawa coupling, with D standing for Dirac. While technically correct, this method cannot explain the smallness of the neutrino

mass compared to the other SM fermions, which is why many theorists resort to mechanisms relying on the unique Majorana property of the neutrino.

SEESAW MECHANISM (I – III): The fact that neutrinos are electrically neutral allows them to be their own antiparticles, which defines their Majorana nature. The right-handed neutrinos required for the mass term can hence be replaced by the complex conjugate left-handed counterparts, resulting in the nonrenormalizable interaction known as the Weinberg operator [21]

$$\mathcal{L}_\nu = -\frac{y}{\Lambda}(\overline{L^c}\tilde{\phi})(\tilde{\phi}^\dagger L) + \text{h.c.}\,, \tag{1.25}$$

with a model-dependent constant y. Because of its higher mass dimension, the operator is suppressed by the energy scale Λ, where the new particles come into play to generate the neutrino masses. The three minimal ultraviolet (UV) completions are denoted as the seesaw mechanisms I – III, emphasizing how the light neutrinos are lifted by the weight of the heavy messenger particles [22]. The respective diagrams are shown in Fig. 1.4, and the details about the messengers are summarized in Tab. 1.2.

Seesaw	Mediator	$SU(2)_L$	D
I	ν_R	**1**	3/2
II	Δ	**3**	1
III	Σ	**3**	3/2

Table 1.2: Overview of the seesaw mechanisms I – III. D denotes the mass dimension of the mediator, where 3/2 corresponds to a fermion, and 1 is a scalar field.

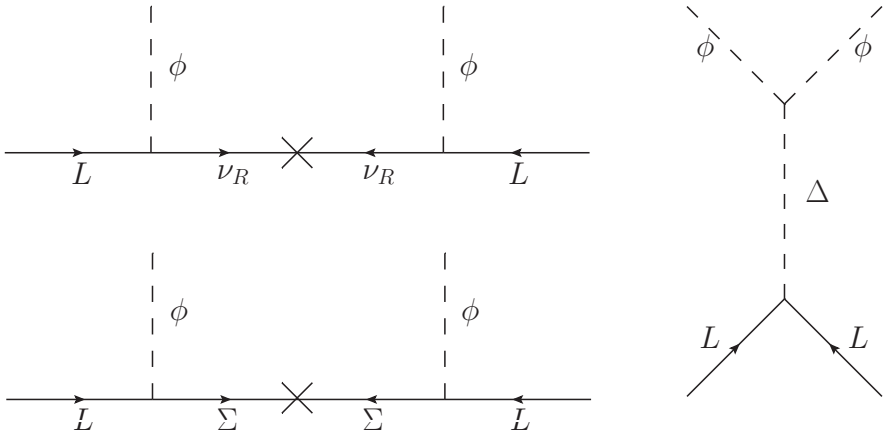

Figure 1.4: UV completions of the dimension five Weinberg operator, known as the seesaw mechanism I (top left), II (right), and III (bottom left).

By far the most common solution to the neutrino mass problem is to introduce heavy right-handed neutrinos ν_R to the SM field content, corresponding to the seesaw mechanism type I. In a simplified notation with one active and one right-handed neutrino, the UV complete form of the Weinberg operator reads

$$\mathcal{L}_\nu^{\text{UV}} = -\frac{1}{2}\overline{\nu^c}_L\, m_D\, \nu_R^c - \frac{1}{2}\overline{\nu}_R\, m_D\, \nu_L - \frac{1}{2}\overline{\nu}_R\, M_R\, \nu_R^c + \text{h.c.}\,, \tag{1.26}$$

where $m_D \equiv y_D v$ is the Dirac neutrino mass, and M_R is the mass of the heavy right-handed neutrino. For convenience this expression can also be written in matrix form

$$\mathcal{L}_\nu^{\text{UV}} = -\frac{1}{2}\begin{pmatrix} \overline{\nu^c}_L & \overline{\nu}_R \end{pmatrix}\begin{pmatrix} 0 & m_D \\ m_D & M_R \end{pmatrix}\begin{pmatrix} \nu_L \\ \nu_R^c \end{pmatrix} + \text{h.c.} \tag{1.27}$$

A back-of-the-envelope calculation of the neutrino masses then yields a light mass eigenstate m_1 suppressed by the heavy state M_R

$$m_1 \approx \frac{m_D^2}{M_R}\,, \qquad m_2 \approx M_R\,. \tag{1.28}$$

By assuming that the right-handed neutrinos are extraordinarily heavy, one can explain why the SM neutrinos are so much lighter than the other fermions. Indeed, the neutrino mass comes out naturally in the sub-eV range for $M_R \sim \mathcal{O}(10^{15}\text{ GeV})$ and $y_D \sim \mathcal{O}(1)$. Extending this framework to three active neutrinos is straightforward using three right-handed neutrinos to fit Δm^2_{sol} and Δm^2_{atm}.

RADIATIVE SEESAW MECHANISM: Other realizations of the Weinberg operator are plausible that go beyond the minimal seesaw mechanism. The fact that the heavy messengers in the seesaw I – III are way beyond the reach of current or next generation experiments, motivates ideas that invoke NP at a testable energy scale, preferably even at the LHC. One such idea is to generate the neutrino mass *radiatively* by producing it at loop level with messenger particles at the TeV scale [23], as shown in Fig. 1.5. The smallness of the neutrino mass is then primarily explained by the loop suppression.

The loop level neutrino mass is typically generated with scalar particles, but also vector solutions are possible if the renormalization of the loop is taken care of. Three types of mediators are presented in this thesis that generate neutrino masses radiatively: Higgs-like scalar fields (Sec. 3.2), scalar leptoquarks (Sec. 4.3.1), and vector leptoquarks (Sec. 4.3.2).

Note that the Weinberg operator violates lepton number by $\Delta L = 2$ units, which is an accidentally preserved but not a true symmetry of the SM. Lepton number violation is a distinct feature of many theoretical NP models and is actively searched for by various experiments. The most prominent among them are the $0\nu\beta\beta$ experiments. According to the black-box theorem, if $0\nu\beta\beta$ decay is found, at least one neutrino has to be a Majorana particle [24]. The rare process can occur if a neutrino is emitted and simultaneously absorbed in the beta decays of two nuclei, as depicted in Fig. 1.6. The $0\nu\beta\beta$ decay rate is approximately given by

$$\Gamma_{0\nu\beta\beta} = G|M|^2|m_{\beta\beta}|^2\,, \tag{1.29}$$

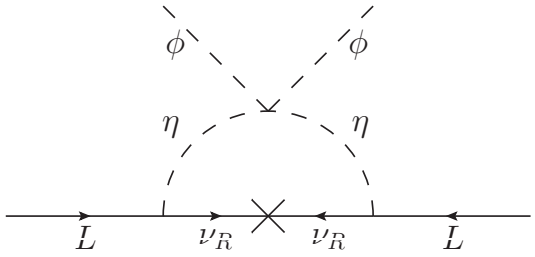

Figure 1.5: Example of a Majorana neutrino mass generated radiatively by a scalar field η coupling to the SM Higgs ϕ.

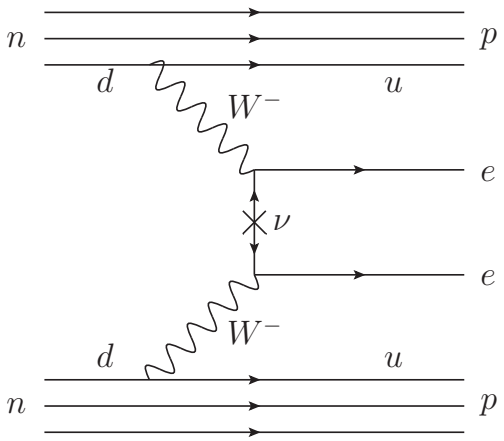

Figure 1.6: $0\nu\beta\beta$ decay enabled by a Majorana neutrino mass insertion.

where G is the two-body phase space factor, M is the nuclear matrix element, and $m_{\beta\beta}$ denotes the effective Majorana mass

$$m_{\beta\beta} = \sum_{i=1}^{3} m_i U_{ei}^2 \,. \tag{1.30}$$

As seen from Eq. (1.29), the $0\nu\beta\beta$ decay is strongly suppressed by the small neutrino masses entering $m_{\beta\beta}$. Consequently, detecting this decay is in practice possible only in elements that are stable against single-beta decay. This is the case for isotopes with even-numbered protons and neutrons, which have increased stability due to the spin coupling [25]. Observing the $0\nu\beta\beta$ decay is the key to understanding most of the remaining neutrino properties because of its sensitivity to the absolute mass scale, the Majorana phases and possibly also the mass ordering. Unfortunately, the reverse is not true: nonobservation of $0\nu\beta\beta$ does not exclude Majorana neutrinos. As shown in Fig. 1.7, $m_{\beta\beta}$ can vanish in the NH case for a specific set of neutrino masses and Majorana phases, although the neutrino itself could in fact be a Majorana particle.

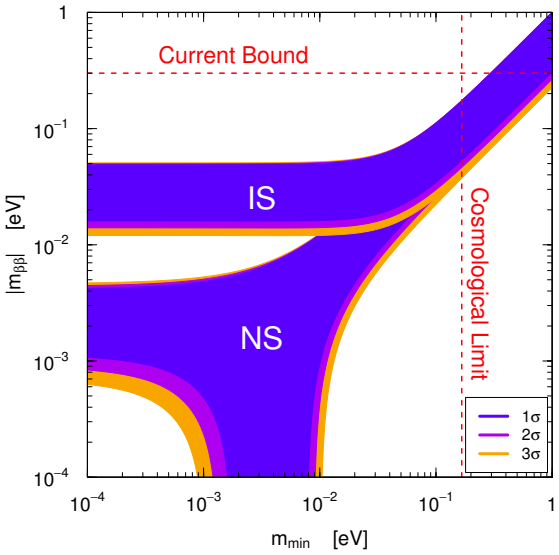

Figure 1.7: The effective Majorana mass $m_{\beta\beta}$ as a function of the lightest neutrino mass depicted for NH and IH. Figure taken from Ref. [26].

Aside from $m_{\beta\beta}$, also the nuclear matrix element $|M|$ is a decisive factor for the $0\nu\beta\beta$ decay rate, depending strongly on the considered nucleus. Typical materials used in $0\nu\beta\beta$ experiments include ^{136}Xe (EXO, KamLAND-Zen) and ^{76}Ge (GERDA, MAJORANA). Currently, the best limit for the half-life of ^{76}Ge is provided by GERDA [27] with

$$T_{1/2}^{0\nu\beta\beta}(^{76}\mathrm{Ge}) > 2.1 \times 10^{25}\ \mathrm{yr}\,, \tag{1.31}$$

while KamLAND-Zen predicts for ^{136}Xe [28]

$$T_{1/2}^{0\nu\beta\beta}(^{136}\mathrm{Xe}) > 1.07 \times 10^{26}\ \mathrm{yr} \tag{1.32}$$

at 90% C.L. Proposed experiments such as SuperNEMO and NEXT intend to push the limit on the $0\nu\beta\beta$ half-life further to close in on the inverse neutrino mass hierarchy in the near future [29, 30].

1.2.3 *Flavor Violation as a Probe of New Physics*

With *direct* detection being limited to TeV scale energy ranges, decays of light fermions are excellent tools to probe NP *indirectly*. Operating at low energies, indirect detection experiments are complementary to direct collider searches. Heavy new particles are produced only virtually and observed through their effect on well-known processes that are suppressed or even forbidden in the SM. If NP indeed affects the flavor sector, it is sure to manifest in rare meson decays or any lepton flavor-violating transitions.
Flavor experiments such as Belle and BaBar push the limits on new interactions involving quarks and charged leptons. A number of deviations from the SM have been observed in these experiments, which are discussed in the following subsections together with the most interesting decay channels for NP searches.

Rare B decays

Some meson decays are termed rare because of their strong suppression in the SM, which allows to test energy scales even beyond the reach of the LHC, limited only by precision and statistics. This suppression is due to large numbers of EW vertices or loops that are required to mediate the rare process in the SM. New particles and interactions can simplify the topology of the diagram and thereby result in an observable effect.
Searches for rare meson decays are historically motivated by the kaon channel $K_L^0 \to \mu\mu$ that lead to the discovery of the charm quark and thereby established the GIM mechanism. At the time, the decay was known to be induced by a box diagram involving the up-quark (Fig. 1.8). However, only the contribution from the new charm quark could explain the discrepancy between the theory prediction and the experimental observations.

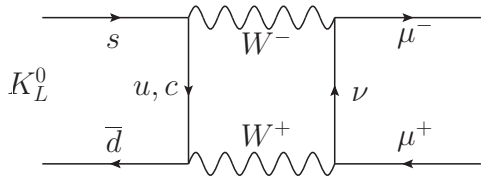

Figure 1.8: SM decay of $K_L^0 \to \mu\mu$.

While kaons were studied extensively in the past, the focus of today's experiments are B meson decays. The most notable experiments currently searching for rare B decays are the hadron collider experiment LHCb, and the B-Factories BaBar and Belle. The follow-up experiment Belle II located in Japan is expected to take new data in late fall 2018 [31]. The B-factories are experiments based at e^+e^- colliders that are specifically designed to produce 10.6 GeV $\Upsilon(4S)$ resonances decaying into pairs of B mesons. As such, the B mesons are easily identifiable, which is a powerful advantage in the search for rare decays.
Some of the key channels are outlined in the following paragraphs with respect to their current status and future prospects. A summary can be found in Tab. A.7. Similar bounds can be obtained from kaon and lepton decays, which are summarized in Tabs. A.8 and A.9. Measurements of D meson decays can constrain $c \to u$ flavor transitions, but the respective bounds are relatively weak, restricting the NP models in this thesis barely beyond the limits from the down-type quark sector.

$b \to s\gamma$: The $b \to s\gamma$ decay is dominated in the SM by a loop diagram with a W^- and a top or charm quark, respectively, as shown in Fig. 1.9. The current experimental data is in very good agreement with the SM prediction [6, 32]

$$\begin{aligned} \mathcal{B}_{\text{SM}}(b \to s\gamma) &= (3.36 \pm 0.23) \times 10^{-4}\,, \\ \mathcal{B}_{\text{exp}}(b \to s\gamma) &= (3.49 \pm 0.19) \times 10^{-4}\,, \end{aligned} \tag{1.33}$$

imposing stringent bounds on NP models with couplings to down-type quarks. Potential candidates are two-Higgs-doublet models (2HDMs), in which the W boson line is replaced by a charged Higgs H^+. The newest measurements indicate that the charged Higgs mass in the 2HDM type II should be heavier than 500 GeV to comply with the constraint from $b \to s\gamma$ [32].

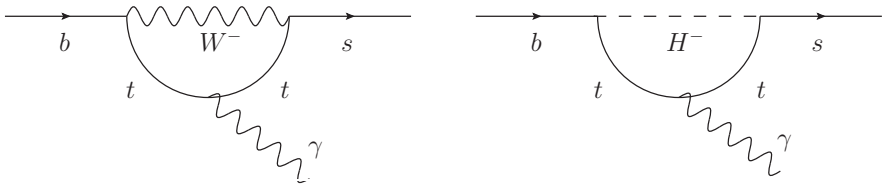

Figure 1.9: $b \to s\gamma$ in the SM (left) and with a charged Higgs boson (right).

$b \to sll$: This lepton universal decay occurs at one-loop level with an equally dominant box diagram depicted in Fig. 1.10. The observed branching ratios for $l = e, \mu$ and the corresponding SM expectation are [33, 34]

$$\begin{aligned} \mathcal{B}_{\text{exp}}(b \to see) &= (4.7 \pm 1.3) \times 10^{-6}\,, \\ \mathcal{B}_{\text{exp}}(b \to s\mu\mu) &= (4.3 \pm 1.3) \times 10^{-6}\,, \\ \mathcal{B}_{\text{SM}}(b \to sll) &= (4.15 \pm 0.70) \times 10^{-6}\,. \end{aligned} \tag{1.34}$$

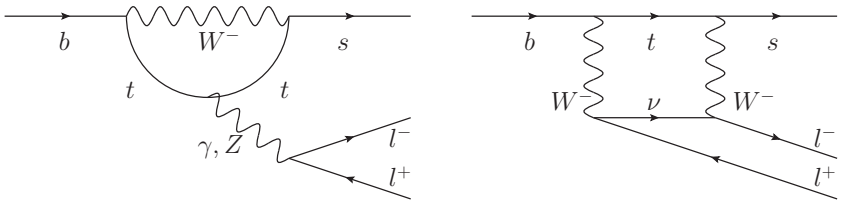

Figure 1.10: SM contributions to $b \to sll$.

$B^0_{(s)} \to \mu\mu$: In the SM this decay is induced by a box diagram, as shown in Fig. 1.11. Again, a potential NP candidate is a charged Higgs that replaces the W line in the diagram, coupling more strongly to heavier quarks. Once more, the measurements are consistent with the SM, leaving a little more room for BSM contributions than $b \to s\gamma$ [35, 36]

$$\begin{aligned} \mathcal{B}_{\text{SM}}(B^0 \to \mu\mu) &= (1.06 \pm 0.09) \times 10^{-10}\,, \\ \mathcal{B}_{\text{exp}}(B^0 \to \mu\mu) &= (3.9^{+1.6}_{-1.4}) \times 10^{-10}\,, \\ \mathcal{B}_{\text{SM}}(B^0_s \to \mu\mu) &= (3.66 \pm 0.23) \times 10^{-9}\,, \\ \mathcal{B}_{\text{exp}}(B^0_s \to \mu\mu) &= (2.8^{+0.7}_{-0.6}) \times 10^{-9}\,. \end{aligned} \tag{1.35}$$

$B \to l\nu$: Decays with ν final states are typically clean but experimentally challenging as neutrinos appear only as missing energy. The decay $B^+ \to l^+\nu$ is helicity suppressed by the small lepton masses. Therefore, the only decay measured so far is the channel involving the τ lepton [6, 37]

$$\begin{aligned} \mathcal{B}_{\text{SM}}(B^+ \to \tau^+\nu) &= (0.76^{+0.08}_{-0.06}) \times 10^{-4}\,, \\ \mathcal{B}_{\text{exp}}(B^+ \to \tau^+\nu) &= (1.14 \pm 0.27) \times 10^{-4}\,. \end{aligned} \tag{1.36}$$

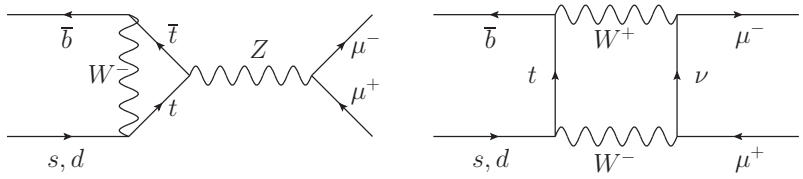

Figure 1.11: Dominant SM contributions to $B^0_{(s)} \to \mu\mu$.

The Belle II experiment intends to close the gap left for NP models in this channel.

$B \to K^{(*)}ll$: The exclusive decay $B \to K^*ll$ related to $b \to sll$ has a q^2 dependence with a longstanding anomaly in the angular observable P_5' [38], corresponding to a deviation of $3.7\,\sigma$ in the bins 4 GeV $< q^2 <$ 8 GeV.

The hadronic uncertainties of this channel cancel in the theoretically clean observable

$$R_K = \frac{\mathcal{B}(B \to K\mu\mu)}{\mathcal{B}(B \to Kee)}\,, \tag{1.37}$$

which is very close to unity in the SM [39]

$$R_K^{\mathrm{SM}} = 1.0003 \pm 0.0001\,. \tag{1.38}$$

Interestingly, the LHCb Collaboration has reported a $2.6\,\sigma$ deviation from the SM in R_K that hints at a violation of lepton universality, which has yet to be confirmed by other experiments. The reported result amounts to [40]

$$R_K^{\mathrm{LHCb}} = 0.745^{+0.090}_{-0.074} \pm 0.036\,. \tag{1.39}$$

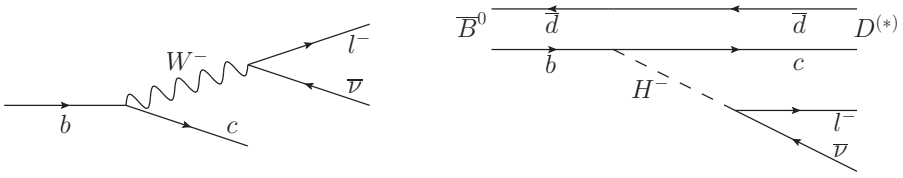

Figure 1.12: Tree-level decay of $b \to cl\nu$ in the SM (left). Tree-level decay of $\bar{B}^0 \to D^{(*)}l\nu$ induced by a charged Higgs boson in a multi-Higgs model (right).

$B \to D^{(*)}l\nu$: A number of experiments have observed deviations [41–43] in the ratios

$$R_D = \frac{\mathcal{B}(B \to D\tau\nu)}{\mathcal{B}(B \to Dl\nu)}\,, \qquad R_{D^*} = \frac{\mathcal{B}(B \to D^*\tau\nu)}{\mathcal{B}(B \to D^*l\nu)}\,. \tag{1.40}$$

Indicating lepton nonuniversality, the measurement has caused a lot of activity in the field because of its high statistical significance. Currently the experimental global average amounts to

$$R_D^{\mathrm{exp}} = 0.388 \pm 0.047\,, \qquad R_{D^*}^{\mathrm{exp}} = 0.321 \pm 0.021\,, \tag{1.41}$$

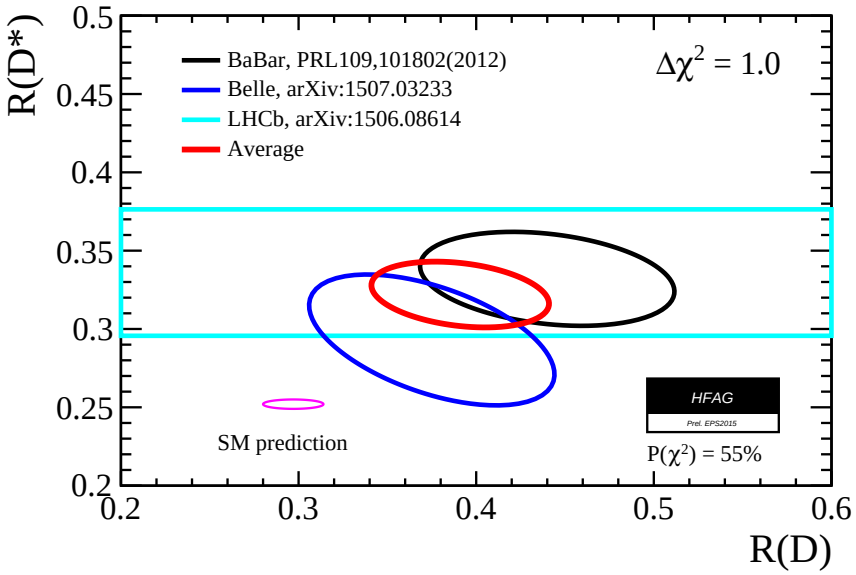

Figure 1.13: Global average of R_D and R_{D^*} based on data from BaBar, Belle, and LHCb. Plot taken from Ref. [45].

which results in a $3.9\,\sigma$ deviation from the theory prediction [44]

$$R_D^{\mathrm{SM}} = 0.300 \pm 0.010\,, \qquad R_{D^*}^{\mathrm{SM}} = 0.252 \pm 0.005\,, \tag{1.42}$$

assuming a correlation of the ratios. See also Fig. 1.13 for an illustration of the data in the R_D - R_{D^*} plane. Since the decay is mediated at tree level in the SM, the NP effects must be sizable to explain the data, which can cause tension with other B decay channels.

Combining the $b \to s$ channels in global fits shows that the current measurements prefer NP in the coefficient C_9, excluding the SM by at least $3\,\sigma$ (Fig. 1.14). The deviations in $b \to sll$ and $B \to Kll$ point towards NP in muons, while R_K alone could also be explained with NP in electrons [46].
Closely related to the rare decays are neutral meson oscillations. These are historically relevant since CP violation was first observed in $K^0 - \overline{K}^0$ oscillations back in 1964 [47]. New particles can modify the meson mixing measured in $K^0 - \overline{K}^0$, $B^0_{(s)} - \overline{B}^0_{(s)}$, and $D - \overline{D}$. The oscillations are sensitive to the mean mass of the eigenstates, their lifetimes and the CP mixing phase. Consequently, new particles can increase the decay rate and thereby shorten the lifetime of the mesons, letting them decay too fast before they can oscillate. The lowest order SM contribution to $K^0 - \overline{K}^0$ mixing is depicted in Fig. 1.15.

Charged Lepton Flavor Violation

While rare decays of K and B mesons led the way for NP searches in the hadronic sector, limits are pushed in the lepton sector by searches for charged lepton flavor violation (CLFV). Since CLFV is forbidden in the SM, these processes are even more suppressed than rare meson decays despite the flavor transitions due to neutrino oscillations. An

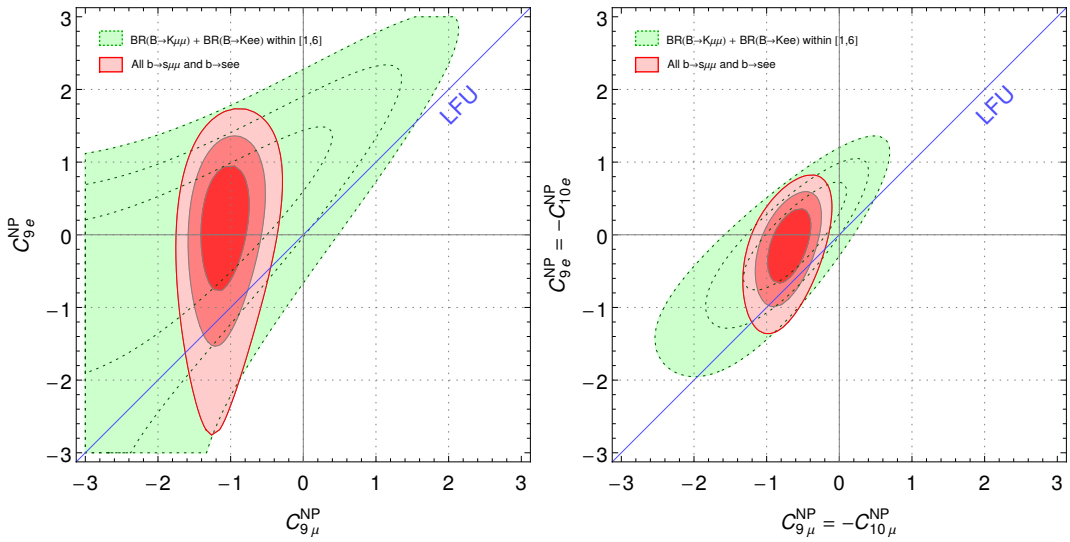

(a) (b)

Figure 1.14: Global fit of C_9^{NP} taking into account $b \to sll$ and $B \to Kll$ (a), and assuming $C_9^{\text{NP}} = -C_{10}^{\text{NP}}$ (b). The blue line denotes lepton flavor universality. Taking into account data from $b \to sll$ and $B \to Kll$ points to NP in muons. Figures taken from Ref. [46]

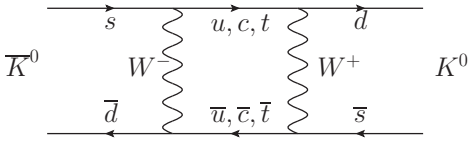

Figure 1.15: Lowest order contribution in the SM to $K^0 - \overline{K}^0$ oscillations.

estimate of $\mathcal{B}(\mu \to e\gamma)$ shows that the effect of massive neutrinos on the forbidden processes is tiny. Its branching ratio with neutrino oscillations is given by [48]

$$\mathcal{B}_{\nu\text{SM}}(\mu \to e\gamma) = \frac{3\alpha}{32\pi} \left| \sum_l U_{\mu l}^* U_{el} \frac{m_\nu^2}{m_W^2} \right|^2 \sim \mathcal{O}(10^{-54}) \,, \tag{1.43}$$

where U_{ij} denote the PMNS matrix elements and m_ν and m_W are the masses of the neutrino and the W boson, respectively. Being proportional to $(m_\nu/m_W)^4$, the decay rate is negligible as a consequence of the tiny neutrino mass. On the other hand, a lepton flavor-violating Higgs coupling $y_{e\mu}$ arising in multi-Higgs models affects the branching ratio significantly (cf. Fig. 1.17) [49]

$$\mathcal{B}_{he\mu}(\mu \to e\gamma) \approx 10^{-12} \left(\frac{500 \text{ TeV}}{\Lambda} \right)^4 (|y_{e\mu}|^2 + |y_{\mu e}|^2) \,, \tag{1.44}$$

which means that any observation of CLFV would be a smoking gun of NP.
Besides $\mu \to e\gamma$, notable limits on CLFV are provided by $\mu \to 3e$, $\mu \to e$ conversion in nuclei, and the various τ decay modes. Some of the most prominent channels are

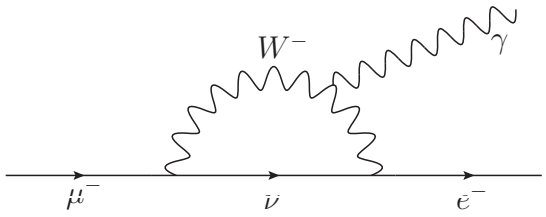

Figure 1.16: Dominating SM contribution to $\mu \to e\gamma$ with massive neutrinos.

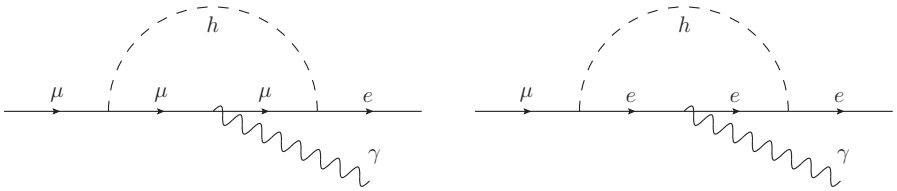

Figure 1.17: Leading order diagrams for $\mu \to e\gamma$ with flavor-violating Higgs boson couplings.

outlined as follows. A summary of the bounds on lepton decays with CLFV is given in Tab. A.9.

$l \to l'\gamma$: The radiative decays $l \to l'\gamma$, including $\mu \to e\gamma$, $\tau \to \mu\gamma$, and $\tau \to e\gamma$, currently provide the strongest constraints on NP with charged leptons. The B factories also produce a lot of tauons allowing for measurements of many flavor-violating τ decay modes. The upper bounds reported by BaBar are

$$\begin{aligned} \mathcal{B}_{\text{exp}}(\tau \to e\gamma) &\lesssim 3.3 \times 10^{-8}\,, \\ \mathcal{B}_{\text{exp}}(\tau \to \mu\gamma) &\lesssim 4.4 \times 10^{-8}\,. \end{aligned} \tag{1.45}$$

A much stronger limit on μ decays is provided by the MEG experiment [50]

$$\mathcal{B}_{\text{exp}}(\mu \to e\gamma) \lesssim 5.7 \times 10^{-13}\,. \tag{1.46}$$

Special attention has to be paid to higher order corrections, particularly in the case of $\mu \to e\gamma$, where the one-loop and two-loop corrections can be of the same order of magnitude in some BSM scenarios [51].

LHCb and the upcoming experiment Belle II expect to improve their limits on $\tau \to l\gamma$ to $\mathcal{O}(10^{-10} - 10^{-9})$ [52]. Also MEG plans to increase their sensitivity to $\mu \to e\gamma$ by another order of magnitude with their next upgrade [53].

$l \to 3l'$: In analogy to $l \to l'\gamma$, the SM contribution to the decay $l \to 3l'$ is suppressed by the tiny neutrino mass and is hence negligible (cf. Fig. 1.18). Alternatively this decay could be mediated at tree level by a flavor-violating Higgs coupling of a multi-Higgs model, as shown in the right diagram of Fig. 1.18 [51].

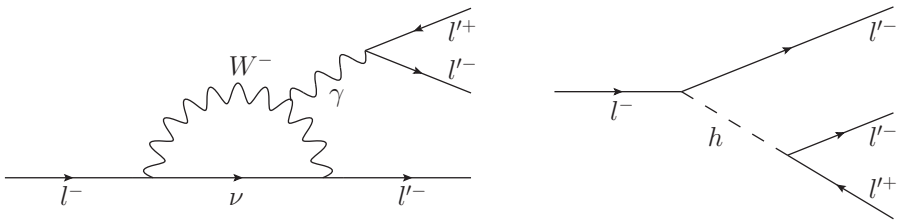

Figure 1.18: $l \to 3l'$ in the SM with neutrino masses (left) and with flavor-violating Higgs couplings (right).

In the tauon sector, the best limits on $\tau \to 3\mu$, and $\tau \to 3e$ are given by Belle [54]

$$\begin{aligned} \mathcal{B}_{\text{exp}}(\tau \to 3e) &\lesssim 2.7 \times 10^{-8}\,, \\ \mathcal{B}_{\text{exp}}(\tau \to 3\mu) &\lesssim 2.1 \times 10^{-8}\,. \end{aligned} \tag{1.47}$$

Once again, the bounds on μ are stronger [55]

$$\mathcal{B}_{\text{exp}}(\mu \to 3e) \lesssim 1 \times 10^{-12}\,. \tag{1.48}$$

According to their proposal, the Mu3e experiment intends to push the limit on $\mu \to 3e$ further to 10^{-16} [56].

$\mu N \to eN$: Searches for $\mu \to e$ conversion in nuclei are a promising alternative to the $\mu \to e\gamma$ channel with excellent future prospects. The current limit from SINDRUM II [57]

$$\mathcal{B}_{\text{Au}}(\mu N \to eN) \lesssim 7 \times 10^{-13}\,, \tag{1.49}$$

is expected to improve significantly in the near future with the upcoming experiments Mu2e at Fermilab [58], and COMET at J-PARC [59]. At the moment, both $\mu \to e\gamma$ and $\mu N \to eN$ already probe scales up to $10^3 - 10^4$ TeV.

$g_\mu - 2$: In the SM, the gyromagnetic ratio of the muon g_μ is predicted by the Dirac equation to be exactly 2. The deviation from this number is called the anomalous magnetic moment and is caused by EW and hadronic loop-level effects [60]

$$a_\mu^{\text{SM}} = \frac{g_\mu - 2}{2} = 0.00116591814(51)\,. \tag{1.50}$$

Even though the observed value [61]

$$a_\mu^{\text{exp}} = 0.00116592091(54)(33) \tag{1.51}$$

differs from the prediction only by $\mathcal{O}(10^{-9})$, the result corresponds to a $3.4\,\sigma$ deviation because of the excellent precision of both the theory prediction and the measurement.

Loop corrections with new particles coupling to muons could compensate for this discrepancy. However, fairly large effects are necessary that can cause tension with other observables, including $\tau \to \mu\gamma$ and $\mu \to e\gamma$ [62]. Possible diagrams generated by a scalar leptoquark coupling muons to top quarks are depicted in Fig. 1.19.

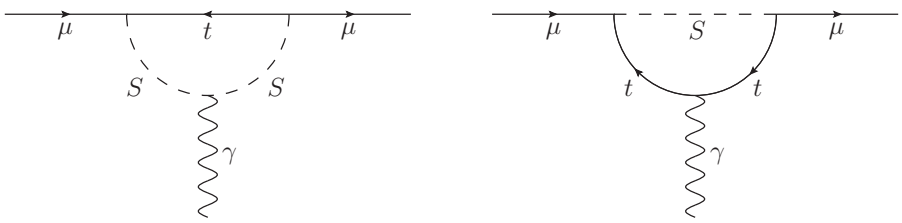

Figure 1.19: Possible loop corrections to the anomalous magnetic moment of the muon from a scalar leptoquark S.

Flavor-Violating Higgs Boson Decays

Since diagonalizing the fermion mass matrices is equivalent to diagonalizing the fermion Yukawa couplings, Higgs boson decays always preserve flavor in the SM. The Yukawa couplings that define the Higgs decay rates in the SM are known very precisely

$$y_{ij} = \sqrt{2}\frac{m_i}{v}\delta_{ij}\,, \tag{1.52}$$

where the diagonal couplings y_{ii} are proportional to the fermion mass m_i. In general BSM theories the Higgs decay rate into two arbitrary fermions is given by

$$\Gamma(h \to \psi_i \overline{\psi}_j) = N_c \frac{m_h}{8\pi}\left(|y_{ij}|^2 + |y_{ji}|^2\right)\,, \tag{1.53}$$

where N_c is the color factor ($N_c = 3$ for quarks, $N_c = 1$ for leptons). Higgs decay searches, therefore, directly constrain the absolute value of the Yukawa couplings, but in many cases indirect searches of rare or flavor-violating decays can provide better limits. As shown, e.g., in Fig. 1.17, typical channels to pin down the Higgs couplings are the radiative decays $l \to l'\gamma$, which are easier accessible because the light fermions can be produced in large numbers at low energies.
Since the discovery of the Higgs boson the LHC placed first limits on some Higgs decay channels with fermionic final states to confirm the SM hypothesis, Eq. (1.52). ATLAS and CMS reported the following best-fit values for the Yukawa couplings normalized to the SM expectation [63–66]

$$\begin{aligned} \mu_{h\tau\tau}^{\text{ATLAS}} &= 1.43^{+0.43}_{-0.37} \quad (4.5\,\sigma)\,, & \mu_{h\tau\tau}^{\text{CMS}} &= 0.78 \pm 0.27 \quad (3.7\,\sigma)\,, \\ \mu_{hb\bar{b}}^{\text{ATLAS}} &= 0.52 \pm 0.56 \quad (1.4\,\sigma)\,, & \mu_{hb\bar{b}}^{\text{CMS}} &= 1.0 \pm 0.5 \quad (2.1\,\sigma)\,. \end{aligned} \tag{1.54}$$

Because of the limited LHC sensitivity to small Yukawa couplings, only an upper bound could be placed on $h \to \mu\mu$ decays [67]

$$\mathcal{B}_{\text{ATLAS}}(h \to \mu\mu) < 1.5 \times 10^{-3}\,, \quad \text{or} \quad \frac{\mathcal{B}_{\text{exp}}(h \to \mu\mu)}{\mathcal{B}_{\text{SM}}(h \to \mu\mu)} < 7.0\,. \tag{1.55}$$

All the other fermion channels are far out of reach, being either polluted by QCD background or just too rare to be observed at the LHC. An overview of the couplings measured so far, based on the combined ATLAS and CMS data of Run 1 is shown in Fig. 1.20.

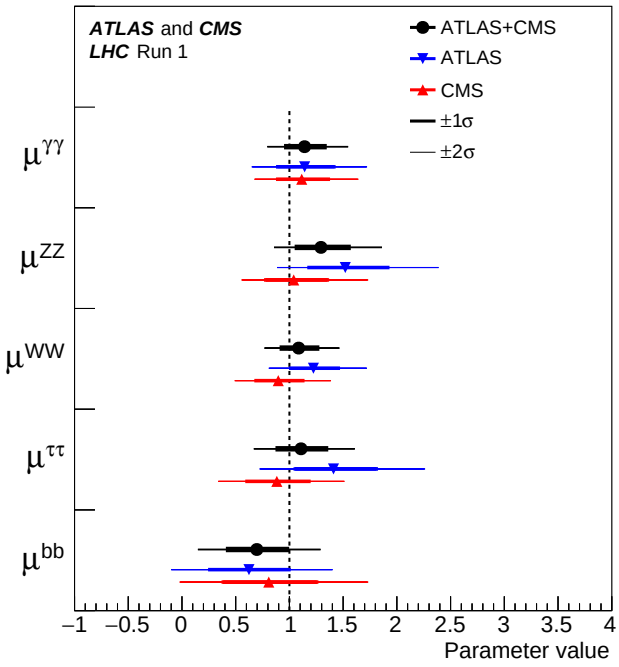

Figure 1.20: Measured Higgs decay rates normalized to the respective SM predictions from a combined analysis of ATLAS and CMS data. All listed decay channels are consistent with the SM expectation, the constraints on $h \to b\bar{b}$ and $h \to \tau\tau$ being the weakest. Figure taken from Ref. [68].

Like in the case of the rare B and charged lepton decays, any signal in a Higgs decay channel with a flavor-violating final state is a clear sign of BSM physics. The off-diagonal Higgs couplings are only weakly constrained by experimental searches, allowing for branching ratios of up to 10% with great model building opportunities in the lepton sector [51]. The limits on quark couplings are generally stronger thanks to the extensive searches for K and B meson decays. The y_{bs} coupling has the weakest bounds, allowing for [69]

$$\mathcal{B}(h \to bs) \lesssim 2 \times 10^{-3}\,, \tag{1.56}$$

which is still far too small to ever be observed at the LHC because of the large QCD background.
In 2014, the CMS Collaboration presented preliminary results from a $h \to \mu\tau$ search indicating CLFV in Higgs decays with a $2.4\,\sigma$ statistical significance [70]. The anomaly caused a lot of excitement in the field as it requires the SM to be changed fundamentally in order to accommodate the data. If confirmed, the best-fit branching ratio

$$\mathcal{B}_{\text{CMS}}(h \to \mu\tau) = (0.84^{+0.39}_{-0.37})\%\,, \tag{1.57}$$

would likely be caused by NP at the EW scale to have such a large effect. Potential new particles would either be well hidden, or should be found very soon in the LHC data.
In 2015, also ATLAS published their result [71]

$$\mathcal{B}_{\text{ATLAS}}(h \to \mu\tau) = (0.77 \pm 0.62)\%\,, \tag{1.58}$$

neither confirming, nor disproving the CMS signal. With first data from LHC Run 2, these branching ratios were updated in May 2016 [72]

$$\mathcal{B}_{\text{CMS}}(h \to \mu\tau) = (-0.76^{+0.81}_{-0.84})\%\,, \qquad \mathcal{B}_{\text{ATLAS}}(h \to \mu\tau) = (0.53 \pm 0.51)\%\,, \quad (1.59)$$

suggesting that the excess might just be a statistical fluctuation. However, since the updated limits are still consistent with the original claim, the situation remains unclear. If not $h \to \mu\tau$, then $h \to e\tau$ might still exhibit large flavor violation. The preliminary results [72, 73]

$$\mathcal{B}_{\text{ATLAS}}(h \to e\tau) < 1.04\%\,, \qquad \mathcal{B}_{\text{CMS}}(h \to e\tau) < 0.69\% \quad (1.60)$$

at 95% C.L. do not exclude large flavor violation in $e\tau$ final states yet.

1.2.4 *The 750 GeV Diphoton Excess*

On December 15, 2015, the CMS and ATLAS collaborations presented new data regarding a potential excess in $pp \to \gamma\gamma$ at the invariant mass of around 750 GeV with $3.4\,\sigma$ and $3.9\,\sigma$ local significance, respectively [74, 75]. The deviation reduced to $1.6\,\sigma$ and $2.3\,\sigma$ taking into account the look-elsewhere effect.
Although the significance was rather low, the signal received a lot of attention for the fact that it appeared in both experiments in the same invariant mass region. Updated results with slightly improved statistics were presented during Moriond 2016, further encouraging research on the resonance. The huge activity in the field amounted to 545 and counting publications to date that attempt to explain the data provided by CMS and ATLAS. On August 5, 2016, new LHC Run 2 results were presented at ICHEP, Chicago, finally clarifying the picture [76, 77]. Even though the excess turned out to be merely a statistical fluctuation, the potential signal led to a plethora of interesting models that allow for extensive studies of future diphoton resonances. Given that also the Higgs boson was first observed in $h \to \gamma\gamma$, the diphoton final state is still a very promising channel to discover NP.
The most common explanation was given by the so-called "everybody's model" [78], which is the simplest interpretation of the resonance as a scalar singlet field F coupling to exotic color particles that decay into gg and $\gamma\gamma$. The production and decay of the resonance in the everybody's model is shown schematically in Fig. 1.21.

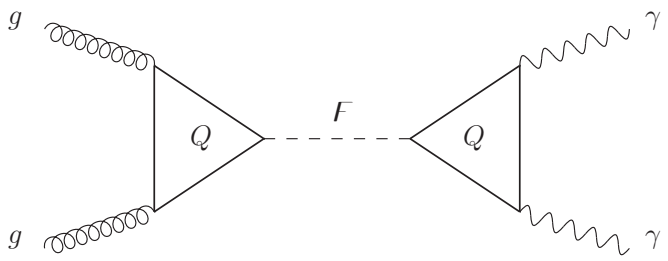

Figure 1.21: Production and decay of a singlet scalar resonance F coupling to color charged particles Q.

A number of properties of F could be deduced from the first measurements presented by CMS and ATLAS, which are summarized below based on the review [78]. Since it was observed in the $\gamma\gamma$ final state, the resonance had to be either a spin-0 or a spin-2 state. The latter was disfavored for predicting a similar signal in leptons, i.e., $\sigma(pp \to F \to e^+e^- + \mu^+\mu^-) = \sigma(pp \to F \to \gamma\gamma)$.
Explicitly, the total diphoton cross section of a boson with spin J, Mass M and width Γ_{tot} can be written in the narrow-width approximation in terms of its production and decay rate [78]

$$\sigma(pp \to F \to \gamma\gamma) = \frac{2J+1}{M \cdot \Gamma_{\text{tot}} \cdot s} \sum_q C_{qq} \Gamma(F \to qq) \Gamma(F \to \gamma\gamma)\,, \tag{1.61}$$

where s is the center-of-mass energy and $q = \{u, d, s, c, b, g\}$.
In order to achieve a large F production rate, the field had to couple to colored particles enabling the production at the LHC through gluon fusion. The high luminosity of gluons compared to quarks increases the total diphoton cross section significantly, which allows for a relatively small $\Gamma(F \to \gamma\gamma)$ (cf. Tab. 1.3).

$\sqrt{s}$ [TeV]	$C_{b\bar{b}}$	$C_{c\bar{c}}$	$C_{s\bar{s}}$	$C_{d\bar{d}}$	$C_{u\bar{u}}$	C_{gg}
8	1.07	2.7	7.2	89	158	174
13	15.3	36	83	627	1054	2137

Table 1.3: Quark and gluon luminosity factors at the LHC [78].

The charged particles mediating the decays into gg and $\gamma\gamma$ are typically heavy exotic quarks or (color) charged scalars which enhance the diphoton cross section through large hypercharges or Yukawa couplings. They could not be SM particles, which would couple to the resonance at tree level and, therefore, lead to observable signals in other decay channels dominating the F width. Particles in larger $SU(2)$ representations couple to the EW gauge bosons and are further constrained by nonobservation of $F \to WW, ZZ, Z\gamma$.
Furthermore, as a neutral scalar, F can also mix with the SM Higgs boson. However, the corresponding mixing angle should be tiny since $\Gamma(F \to ZZ) \lesssim \Gamma(F \to \gamma\gamma)$.
While CMS favored a narrow decay width, the width predicted by ATLAS was large with a best fit of about 45 GeV, or equivalently $\Gamma/M_F \approx 0.06$. From the theory point of view, the narrow width is strongly favored as models predicting a wide width come with a number of problems: The broad width entails a large diphoton decay rate of the order $\Gamma_{\gamma\gamma}/M_F \sim 10^{-4} - 10^{-3}$, which requires either a large Yukawa coupling, a high electric charge, or a large number of fields running in the loop. Sizable couplings can become nonperturbative and hit a Landau pole at high energies, whereas the multi-fields solution is disfavored for modifying the running of the gauge couplings sharply. Therefore, most theoretical models consider only the narrow width predicted by CMS.
In this thesis, two variations of the everybody's model are explored that provide a joint explanation of the 750 GeV diphoton excess and other anomalies of the SM: a flavor symmetry-based model (Sec. 5.1) and a vector leptoquark solution (Sec. 5.2).

2

MODEL BUILDING

New symmetries and fields can alter well-known SM observables and thereby explain the unanswered questions and anomalies outlined in the previous chapter. The process of working out theoretical models that determine and predict the behavior of the (B)SM particles is referred to as model building.

The following subsections focus on some of the most frequently used model-building tools: discrete and continuous symmetries (Sec. 2.1), extended Higgs sectors (Sec. 2.2) and unification (Sec. 2.3).

2.1 DISCRETE AND CONTINUOUS SYMMETRIES

Symmetry groups are essential tools in particle physics to explain the fundamental properties of the SM. Continuous gauge symmetries have been proven to describe the SM fermions and their interactions with percent-level precision and better. On the other hand, many of the fundamental symmetries such as charge conjugation C, parity P, and time reversal T are discrete. Therefore, discrete and continuous symmetries are both motivated by the SM but in practice employed for different purposes.

While gauge symmetries describe the fundamental SM interactions, they do not explain the origin of the Yukawa couplings. Instead, so-called "flavor symmetries" can make sense of the SM flavor puzzle by reducing the number of free parameters of the theory. Suitable flavor symmetries are typically discrete subgroups of $SU(3)$ with triplet representations to unify the three families of the SM, including but not limited to A_4, S_4, and $\Delta(27)$.

An exception is the symmetric group S_3, which is a popular choice in model building for being the simplest nonabelian flavor symmetry [79]. Two fermion families can be accommodated in the doublet representation, which is useful, e.g., to describe an approximate $\mu - \tau$ symmetry. This doublet representation also complements two-Higgs-doublet models well, which are discussed in Sec. 2.2.

Since no Goldstone or gauge bosons appear in the breaking of discrete symmetries, they are less constrained by experimental data, but at the same time difficult to rule out for their lack of distinguishable features. Therefore, their fundamental properties have been studied extensively for unique model predictions, see, e.g., Refs. [80–82].

The most prominent symmetries in (flavor) model building are outlined in the subsections 2.1.2 to 2.1.4. First, the necessary vocabulary for the use of groups in particle physics is introduced in Sec. 2.1.1.

2.1.1 *A Short Group Theory Primer*

The following introduction is based on Ref. [83] focusing on the group properties relevant for the application in particle theory. For a comprehensive review, see also Ref. [84].

A group G is defined by a set of elements and the operation $\bullet$ satisfying the following fundamental axioms:

CLOSURE: If $a, b \in G$ then $ab \in G$.

ASSOCIATIVITY: For all $a, b, c \in G$, $(ab)c = a(bc)$.

IDENTITY: There exists an identity element $e \in G$ such that $ea = a$, $\forall a \in G$.

INVERSE: For every $a \in G$ there exists an inverse element $a^{-1} \in G$ with $a^{-1}a = e$.

The *order* of a group is defined by its number of elements and can be *finite* or *infinite*. If these elements commute, the group is called *abelian*, otherwise *nonabelian*. A simple example of a nonabelian group is the $SO(3)$ describing rotations in three dimensional space.
Noncontinuous changes in a system are described by *discrete* symmetries. While a circle possesses a continuous rotation symmetry, a square keeps its original shape only if rotated by multiples of 90 degrees.
A subset H of G is a *subgroup* of G if H is also a group. A *representation* maps the elements $g \in G$ onto matrices $D(g)$ acting on the *representation space*. Its dimension n corresponds to the *dimension* of the representation space. Representations can be *reducible* or *irreducible* depending on whether they have an *invariant subspace*, i.e., H is an invariant subspace of G if $v \in H, g \in G$, then $D(g)v \in H$. The number of irreducible representations is equal to the number of *conjugacy classes*, which comprise the sets of elements $g^{-1}ag$, $a, g \in G$ that are *conjugate* to a. A special property of irreducible representations is that they are indecomposable. Particle multiplets can be decomposed into a direct sum of irreducible representations, which define their properties on a fundamental level.

2.1.2 $U(1)$ *and the Froggatt-Nielsen Mechanism*

The Froggatt-Nielsen (FN) mechanism was first proposed in Ref. [85] to explain the large fermion mass ratios and the hierarchical mixing of the CKM matrix. Since then it has become a popular model building tool to shape the mass and mixing matrices of the quark sector.
To suppress the Yukawa couplings of the light fermions, the mechanism employs an additional $U(1)$ flavor symmetry with nontrivial fermion field charges. The Yukawa Lagrangian is not invariant under this symmetry, unless a new scalar field η is taken into account that cancels the sum of the fermion field charges. This scalar field typically carries a $U(1)$ charge (-1) so that invariant mass terms are obtained with several insertions of η, depending on the sum of the fermion charges. Consequently, the now

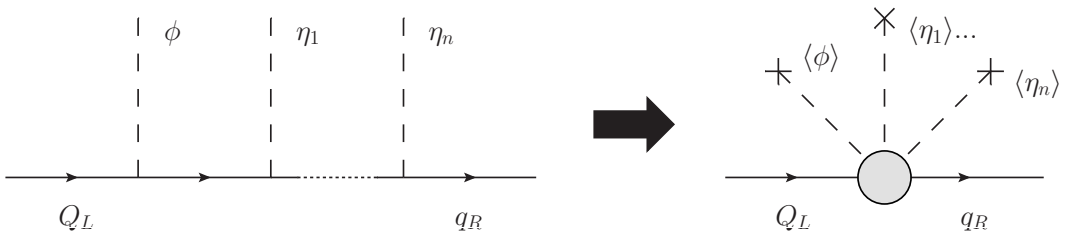

Figure 2.1: Schematic diagram of a quark mass term in the FN mechanism with n flavon insertions above (left) and below the energy scale Λ (right).

nonrenormalizable Yukawa interactions are suppressed by the energy scale Λ, where the flavon field η receives its mass. The resulting (lepton) Yukawa terms take the form

$$y_{ij}\overline{L}_i H e_j \left(\frac{\langle\eta\rangle}{\Lambda}\right)^{n_{ij}}, \tag{2.1}$$

with $n_{ij} = q_j - q_i$, where q_i denotes the FN charge q of the particle i.
Once the flavon acquires a VEV, it will break the $U(1)$ symmetry and suppress the fermion interactions by powers of $\left(\frac{\langle\eta\rangle}{\Lambda}\right)^{n_{ij}}$. Traditionally, this energy scale Λ is chosen such that it is out of reach of current experiments to avoid implications of a new massive gauge boson that accompanies the broken gauge symmetry.
Since only the ratio $\langle\eta\rangle/\Lambda$ is phenomenologically sensitive, there is some freedom in the choice of $\langle\eta\rangle$. The ratio

$$\frac{\langle\eta\rangle}{\Lambda} = \lambda\,, \quad \text{with} \quad \lambda \approx 0.22\,, \tag{2.2}$$

is motivated by the Wolfenstein parametrization of the CKM matrix [86]

$$V_{\text{CKM}} = \begin{pmatrix} 1-\frac{\lambda^2}{2} & \lambda & A\lambda^3(\rho - i\eta) \\ -\lambda & 1-\frac{\lambda^2}{2} & A\lambda^2 \\ A\lambda^3(1-\rho-i\eta) & -A\lambda^2 & 1 \end{pmatrix} + \mathcal{O}(\lambda^4) \tag{2.3}$$

and reproduces the Cabibbo mixing angle $\theta_{\text{C}} \approx 0.22$.
Note that the FN mechanism determines couplings only up to $\mathcal{O}(1)$ coefficients, accounting merely for hierarchies among them. Additional tools are necessary to predict specific relations between observables that are of the same order of magnitude, e.g., $m_b/m_\tau \approx 2.5$. Neglecting the $\mathcal{O}(1)$ coefficients, the fermion masses and mixing matrices are determined only by their fermion $U(1)$ charges, i.e.,

$$\frac{m_i}{m_j} \sim \lambda^{|q_i^R - q_i^L| - |q_j^R - q_j^L|}\,, \quad \text{and} \quad V_{ij}^{L(R)} \sim \lambda^{|q_i^{L(R)} - q_j^{L(R)}|}\,, \tag{2.4}$$

where $q_i^{L(R)}$ denotes the $U(1)$ charge q of the left-handed (right-handed) fermion i, and $V_{ij}^{L(R)}$ defines the matrix element mixing the left-handed (right-handed) fermions i and

j. Since the left-handed quarks are combined into an $SU(2)$ doublet, they share the same $U(1)$ FN charge, which implies

$$V_{ij}^{u,L} \sim V_{ij}^{d,L} \sim V_{ij}^{\text{CKM}} \sim \lambda^{|q_{Q_i} - q_{Q_j}|}\,, \tag{2.5}$$

where V^u and V^d denote the rotation matrices for the up- and down-type quarks, respectively.
The FN charges of the fermions then have to reproduce the experimentally observed fermion mass hierarchies (normalized to m_t)

$$\begin{array}{ccccccccccc} m_u & : & m_c & : & m_t & \approx & \lambda^8 & : & \lambda^4 & : & 1\,, \\ m_d & : & m_s & : & m_b & \approx & \lambda^7 & : & \lambda^5 & : & \lambda^3\,, \\ m_e & : & m_\mu & : & m_\tau & \approx & \lambda^9 & : & \lambda^5 & : & \lambda^3\,. \end{array} \tag{2.6}$$

On the other hand, they should accommodate the observed CKM mixing, placing additional constraints on the choice of quark charges

$$V_{us} \approx \lambda\,, \quad V_{ub} \approx \lambda^3\,, \quad V_{cb} \approx \lambda^2\,. \tag{2.7}$$

No such constraint applies to the PMNS matrix since the origin of neutrino masses and mixings is unknown in the SM. The freedom in the choice of the $U(1)$ lepton charges opens up model building opportunities, for instance, in leptoquark UV completions, which are discussed in Sec. 4.3.
The FN mechanism comes with a number of caveats that are summarized in the following:

1. If the $U(1)$ FN symmetry is treated as a gauge symmetry, it can give rise to chiral anomalies, i.e., divergent triangular loop diagrams. A specific choice of fermion charges can ensure cancellation of these diagrams, which in the case of a $U(1)$ gauge symmetry is given by [87]

   $$\sum_i q_i^3 = 0\,, \tag{2.8}$$

   where q_i denotes the $U(1)$ charge q of the fermion i. Anomaly cancellation is often ignored in FN models, given that the issue can be evaded, either by promoting the $U(1)$ to a global symmetry, or by imposing a discrete symmetry instead.

2. A broken gauge symmetry leads to massive gauge bosons, which are subject to constraints from ongoing collider searches as well as low-energy flavor experiments since additional gauge bosons can mediate new flavor transitions.

3. If the symmetry is not gauged, its breaking entails a massless Goldstone boson unobserved in experiments.

These caveats can be evaded by using a discrete Z_N symmetry in place of the $U(1)$, which for large enough N behaves almost like a continuous symmetry without its typical drawbacks. Instead, the breaking of a discrete symmetry leads to domain walls, which can influence early structure formation and the cosmic microwave background. However, these effects are negligible if the symmetry is broken after the cosmological inflation is complete [88].
The FN mechanism is utilized in all models of this thesis, realized in most cases by a discrete Z_N symmetry. We do not consider anomaly cancellation in the $U(1)$-based models knowing that the issue can be avoided by using a cyclic symmetry instead.

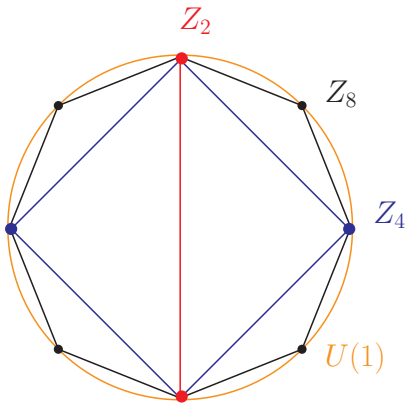

Figure 2.2: Cyclic graphs of Z_N symmetries compared to continuous $U(1)$ symmetry. The graphs become approximately circular for large N.

2.1.3 *Cyclic Groups Z_N*

Cyclic groups are abelian groups, where each group element can be generated by powers of a single element g

$$\langle g \rangle = \left\{ g^0, g^1, \ldots, g^{N-1} \right\} , \tag{2.9}$$

and $g^N = g^0$ for a group of order N. All subgroups of cyclic groups themselves are cyclic.
The Z_N symmetry can be visualized as an n-sided polygon, where each vertex denotes one of the N complex roots of unity that comprise the elements of the Z_N group. Therefore, with increasing number of N, the cyclic groups become approximately continuous (cf. Fig. 2.2), which makes them a convenient model building tool to replace a $U(1)$ FN symmetry.
Cyclic symmetries find use in many fields of BSM physics, e.g., Z_2 symmetries are commonly used to stabilize dark matter particles, and R-parity, preventing rapid proton decay in supersymmetric models, is also essentially a Z_2 symmetry.

2.1.4 *Symmetric and Alternating Groups S_N and A_N*

Nonabelian family symmetries had their breakthrough with the experimental discovery of neutrino oscillations [16, 17] and the measurements of the large parameters in the PMNS matrix. Until 2013, when the remaining mixing angle θ_{13} was measured [9–11], θ_{12} and θ_{23} were in excellent agreement with TBM mixing, corresponding to $\theta_{12} = 33°$, $\theta_{23} = 45°$, and $\theta_{13} = 0$, cf. Eq. (1.17). First proposed in Ref. [12], this structure could be explained exceptionally well using the discrete family symmetries A_4 and S_4. Pioneering works like Refs. [89, 90] led the way for model building with discrete symmetries. Even though the TBM mixing pattern has been ruled out by $\theta_{13} \neq 0$, the

groups A_4 and S_4 are still popular choices today, not only to explain the large PMNS mixing angles, but also to shed light on SM anomalies such as $h \to \mu\tau$ or R_D [91,92]. With respect to neutrino masses and mixings, a typical ansatz is to start from symmetries that predict TBM, "golden ratio" [93] or "bimaximal" [94] mixing, and to explain the data by the subsequent breaking of the symmetries. The small corrections of the mixing angles are hence linked to the symmetry breaking parameters, forming stronger ties between group theory and phenomenology. In all cases, making sense of the flavor puzzle usually requires intricate models with complex breaking patterns that may seem arbitrary and unappealing. The fact that the origin of the masses and mixings cannot be explained in a simple way has caused authors to consider also anarchic neutrino mixing and anthropic solutions, see, e.g., Refs. [95,96].
In this thesis, the symmetric and alternating groups S_N and A_N are prime tools to address some of the reported SM anomalies. Therefore, their basic properties and differences are outlined in the following subsections.

Symmetric Group S_3

The symmetric group S_3 consists of all possible permutations of three objects and is represented geometrically by an equilateral triangle, as shown in Fig. 2.3. The order of S_N groups is $N!$, i.e., six in the case of S_3. Since the smallest symmetric group S_1, with only one element, is trivial, and the group S_2 is equivalent to the cyclic group Z_2, S_3 is among the most studied groups in the literature as the smallest nonabelian symmetric group. See, e.g., Refs. [97–105] for fermion mixing models in the context of S_3 since the measurement of θ_{13}. The elements of S_3 can be denoted as

$$(x_i, x_j, x_k)\,, \tag{2.10}$$

which is short for the permutation

$$(x_1, x_2, x_3) \to (x_i, x_j, x_k)\,, \tag{2.11}$$

with $i, j, k \in [1, 2, 3]$ and $i \neq j \neq k$. Explicitly, the six elements of S_3 are

$$\begin{aligned} e:&\quad (x_1, x_2, x_3)\,, & a_3:&\quad (x_1, x_3, x_2)\,,\\ a_1:&\quad (x_2, x_1, x_3)\,, & a_4:&\quad (x_3, x_1, x_2)\,,\\ a_2:&\quad (x_3, x_2, x_1)\,, & a_5:&\quad (x_2, x_3, x_1)\,, \end{aligned} \tag{2.12}$$

which can be expressed entirely in terms of $a_1 = a$ and $a_2 = b$

$$\{e, a, b, ab, ba, bab\} \tag{2.13}$$

since $a_1 a_2 = a_5$, $a_2 a_1 = a_4$, and $a_3 = a_2 a_1 a_2$. They form the three conjugacy classes

$$C_1 : \{e\}\,, \qquad C_2 : \{ab, ba\}\,, \qquad C_3 : \{a, b, bab\}\,. \tag{2.14}$$

Consequently, the group consists of the three irreducible representations $\mathbf{1}$, $\mathbf{1'}$, and $\mathbf{2}$. A proof can be found in the literature [83].
In models with discrete symmetries, the particle content is assigned to the fundamental representations of the group. In order to construct a Lagrangian invariant under this symmetry, the representations are contracted with tensor products. Denoting the basis

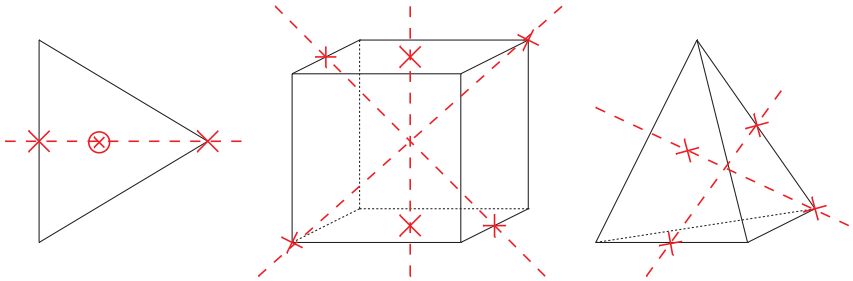

Figure 2.3: Geometrical representations of the nonabelian symmetries S_3, S_4, and A_4, respectively. The red lines denote rotation axes of the symmetry transformations.

vectors for two S_3 doublets as $(x_1, x_2)^T$ and $(y_1, y_2)^T$ and y' a nontrivial S_3 singlet, the S_3 multiplication rules are [83]:

$$\begin{aligned} \begin{pmatrix} x_1 \\ x_2 \end{pmatrix}_{\mathbf{2}} \otimes \begin{pmatrix} y_1 \\ y_2 \end{pmatrix}_{\mathbf{2}} &= \begin{pmatrix} x_2 y_2 - x_1 y_1 \\ x_1 y_2 + x_2 y_1 \end{pmatrix}_{\mathbf{2}} \oplus (x_1 y_1 + x_2 y_2)_{\mathbf{1}} \oplus (x_1 y_2 - x_2 y_1)_{\mathbf{1}'} \,, \\ \begin{pmatrix} x_1 \\ x_2 \end{pmatrix}_{\mathbf{2}} \otimes (y')_{\mathbf{1}'} &= \begin{pmatrix} -x_2 y' \\ x_1 y' \end{pmatrix}_{\mathbf{2}} \,, \qquad (x')_{\mathbf{1}'} \otimes (y')_{\mathbf{1}'} = (x'y')_{\mathbf{1}} \,, \end{aligned} \tag{2.15}$$

or in short

$$\mathbf{2} \otimes \mathbf{2} = \mathbf{1} \oplus \mathbf{1}' \oplus \mathbf{2} \,, \qquad \mathbf{2} \otimes \mathbf{1}' = \mathbf{2} \,, \qquad \mathbf{1}' \otimes \mathbf{1}' = \mathbf{1} \,. \tag{2.16}$$

The multiplication rules [Eq. (2.16)] are basis independent, i.e., the physics do not change under unitary transformations of the form $U^\dagger D(g) U$, where g is any element of the group. However, the components of the representations in Eq. (2.15) may be written in a different way depending on the choice of basis.

Symmetric Group S_4

The S_4 group is appealing for being the smallest symmetric group with a fundamental triplet representation. The S_4 symmetry and the TBM mixing scheme are strongly intertwined, which has been shown with purely group theoretical arguments [106–108] as well as in explicit flavor models [109–111]. This makes the S_4 group a popular tool in model building with leptons.

Geometrically, the S_4 symmetry is represented by a cube as depicted in Fig. 2.3. The 24 group elements form five conjugacy classes, resulting in the five irreducible representations $\mathbf{1}$, $\mathbf{1}'$, $\mathbf{2}$, $\mathbf{3}$, and $\mathbf{3}'$. The S_4 multiplication rules can be found in App. B.1.

Alternating Group A_4

The alternating groups A_N are obtained by taking only the even permutations of the symmetric groups S_N. Alternating groups, therefore, consist of $N!/2$ elements. As an example, the group A_3 is composed of the three even permutations of S_3

$$e : (x_1, x_2, x_3)\,, \quad a_4 : (x_3, x_1, x_2)\,, \quad a_5 : (x_2, x_3, x_1)\,. \tag{2.17}$$

Since $(a_{4,5})^2 = a_{5,4}$ and $(a_{4,5})^3 = e$, the group is isomorphic to the cyclic group Z_3. Consequently, the smallest alternating group considered in the literature is A_4 with $4!/2 = 12$ elements, corresponding to the symmetry of a tetrahedron shown in Fig. 2.3. The 12 elements are classified in four conjugacy classes, resulting in the four irreducible representations $\mathbf{1}$, $\mathbf{1'}$, $\mathbf{1''}$, and $\mathbf{3}$. The fact that the A_4 group has one triplet and three distinct singlet representations makes it particularly attractive for model-building purposes, since those representations accommodate the three SM fermion families nicely. See Refs. [112–115] for a selection of A_4 models since the measurement of θ_{13}.
The product rules for the A_4 group used in the construction of the models in this thesis are given in App. B.2.

2.2 EXTENDED HIGGS SECTORS

The family symmetries describing the fermion masses and mixings eventually have to be broken by higher dimensional scalar representations. These comprise distinct fields for each vector component in the symmetry space, implying that the scalar sector has to be extended with respect to the SM. The scalars breaking the symmetry are typically called "flavons". As such, they can be trivial or nontrivial $SU(2)_L$ multiplets.
The VEVs of $SU(2)_L$ singlet scalars preserve the SM symmetry, i.e., the flavor symmetry is completely separated from the EW scale and can be broken at a much higher energy. The exotic fields attributed to this symmetry breaking then acquire unobservably large masses beyond the reach of current experimental searches.
Alternatively, $SU(2)_L$ doublet flavons simultaneously break the flavor and the EW symmetry resulting in at least one or more Higgs copies at the EW scale. Such models are usually referred to as multi-Higgs models (NHDMs), where N denotes the number of scalar $SU(2)_L$ doublets in the theory. The additional light messengers entailed by the low breaking scale induce dangerous FCNCs that are a typical feature of NHDMs. Therefore, by relating the flavor symmetry to the EW scale, these models are subject to tight constraints but in turn become more predictive. This is helpful to distinguish and consequently rule out the plethora of models on the market through experimental searches.
Extending the SM field content with just one extra Higgs doublet is appealing not just for its simplicity; among the many motivations to study 2HDMs, the most compelling one is supersymmetry, which makes the 2HDM one of the most studied extensions of the SM. A second Higgs doublet must be present in all supersymmetric theories to cancel the gauge anomalies induced by its fermionic superpartner.
On the other hand, 3HDMs often appear in combination with discrete symmetries that accommodate the three fermion families in triplet representations. Symmetries such as A_4 and S_4 have been particularly successful in describing the lepton phenomenology, thereby motivating multiple Higgs doublets from a bottom-up perspective.

For these reasons, NHDMs are utilized in this thesis towards their potential to explain some of the recent SM anomalies, e.g., the 2.4σ excess in $h \to \mu\tau$ decays observed by CMS [70].
The general properties of NHDMs, of which most are easiest described in terms of 2HDMs, are discussed in Sec. 2.2.1. The overview concludes with 3HDM-specific details in Sec. 2.2.2. A comprehensive review on 2HDMs can also be found in Ref. [116].

2.2.1 *2HDMs*

In the presence of two scalar fields, the fermion mass matrices generally receive contributions from two Higgs bosons, which cannot be simultaneously diagonalized. As a consequence, NHDMs typically have tree-level FCNCs unless prevented by an additional mechanism. One possibility is to couple each fermion to only one of the Higgs bosons, which can for instance be achieved by applying a discrete symmetry. Such frameworks are referred to as Yukawa alignment models or models with natural flavor conservation and belong to the class of flavor-conserving NHDMs [117, 118].
2HDMs in particular are usually classified according to their fermion-Higgs couplings into types I – III, where I and II conserve and III violates flavor. In type I, the fermions acquire their masses from only one of the scalars, while in type II, one scalar is responsible for up-type and the other for down-type quark masses. As it is closely related to the minimal supersymmetric SM, type II is the most studied type of 2HDM. For the sake of brevity, the flavor-conserving variations called "flipped" and "lepton-specific" [116] are omitted in this review.
From a model building perspective, type I and type II are implemented easily by imposing a discrete Z_2 symmetry: To obtain a type I model, one of the scalars has to be odd under a Z_2 transformation, preventing interactions of the scalar with all other SM particles; Type II on the other hand is implemented by charging one scalar and the down-type quarks under this symmetry. An overview of the three standard types of 2HDMs is shown in Tab. 2.1, where the fermion-Higgs couplings can be inferred from the Z_2 charge assignments.

2HDM	ϕ_1	ϕ_2	u_R	d_R	e_R
I	$-$	$+$	$+$	$+$	$+$
II	$-$	$+$	$+$	$-$	$-$
III	$+$	$+$	$+$	$+$	$+$

Table 2.1: Overview of the 2HDMs and the corresponding Z_2 parities of the fields in the first-generation notation. Conventionally, ϕ_2 is chosen to couple to up-type quarks.

The models discussed in this thesis do not correspond to any of the classic types of 2HDMs as the couplings are dictated by intricate symmetries and hence do not follow the simplified classifications. Since the models generally allow for FCNCs, they resemble to some extent the type III 2HDM with modified fermion and gauge boson couplings.
Flavor-violating models face stringent constraints from meson oscillations as well as rare meson decays. The best-measured channels typically involve kaon decays, which

are induced by $d \to s$ quark transitions. In the lepton sector the strongest limits come from searches of $\mu \to e\gamma$. For more details see Sec. 1.2.3.
In this thesis we do not concern ourselves with the effects of additional sources of CP violation. Therefore, only CP-conserving models are considered to simplify the large parameter space of extended Higgs sectors. The scalar potential of a CP-conserving 2HDM is given by [116]

$$\begin{aligned} V(\phi_1,\phi_2) = {} & \mu_1^2\phi_1^\dagger\phi_1 + \mu_2^2\phi_2^\dagger\phi_2 - \mu_{12}^2(\phi_1^\dagger\phi_2 + \phi_2^\dagger\phi_1) + \frac{\lambda_1}{2}(\phi_1^\dagger\phi_1)^2 + \frac{\lambda_2}{2}(\phi_2^\dagger\phi_2)^2 \\ & + \lambda_3\phi_1^\dagger\phi_1\phi_2^\dagger\phi_2 + \lambda_4\phi_1^\dagger\phi_2\phi_2^\dagger\phi_1 + \frac{\lambda_5}{2}\left[(\phi_1^\dagger\phi_2)^2 + (\phi_2^\dagger\phi_1)^2\right], \end{aligned} \tag{2.18}$$

where the couplings μ_i and λ_i are real parameters.
The two complex scalar doublets have eight degrees of freedom, which can be decomposed as

$$\phi_l = \begin{pmatrix} \varphi_l^+ \\ \frac{1}{\sqrt{2}}(v_l + \rho_l + i\eta_l) \end{pmatrix}, \qquad l = 1, 2\,, \tag{2.19}$$

where φ_l^+ denotes the complex charged scalar, and ρ and η are the CP-even and CP-odd neutral scalars, respectively. The Higgs doublets acquire VEVs v_l that define the mixing angle β of the charged and CP-odd neutral scalars

$$\tan\beta = \frac{v_2}{v_1} \qquad \text{with} \quad v_{\text{SM}} = \sqrt{v_1^2 + v_2^2}\,. \tag{2.20}$$

Three of the eight degrees of freedom are absorbed by the masses of the SM gauge bosons $W^\pm$ and Z after the EW symmetry breaking. The remaining massive states form two CP-even neutral scalars h and H, one CP-odd neutral scalar A, and a complex charged scalar $H^\pm$. Assuming that CP is conserved, the CP-even and CP-odd scalars do not mix, resulting in 2×2 dimensional mixing matrices with

$$\begin{pmatrix} h \\ H \end{pmatrix} = \begin{pmatrix} \sin\alpha & -\cos\alpha \\ -\cos\alpha & -\sin\alpha \end{pmatrix} \begin{pmatrix} \rho_1 \\ \rho_2 \end{pmatrix}, \tag{2.21}$$

$$\begin{pmatrix} G_0 \\ A \end{pmatrix} = \begin{pmatrix} \cos\beta & \sin\beta \\ \sin\beta & -\cos\beta \end{pmatrix} \begin{pmatrix} \eta_1 \\ \eta_2 \end{pmatrix}, \tag{2.22}$$

$$\begin{pmatrix} G^\pm \\ H^\pm \end{pmatrix} = \begin{pmatrix} \cos\beta & \sin\beta \\ \sin\beta & -\cos\beta \end{pmatrix} \begin{pmatrix} \varphi_1^\pm \\ \varphi_2^\pm \end{pmatrix}, \tag{2.23}$$

where the linear combinations G_0 and $G^\pm$ correspond to the massless Goldstone bosons. The angle α is defined by the mixing of the CP-even neutral scalar fields and can be expressed as a function of their masses

$$\tan 2\alpha = \frac{2m_{12}^2}{m_{\rho_1}^2 - m_{\rho_2}^2}\,, \tag{2.24}$$

where m_{12} denotes the off-diagonal element of the CP-even neutral scalar mass matrix. Because of the few free parameters in the scalar potential, the charged and pseudoscalar mass eigenstates are related to each other and are given by

$$\begin{aligned} m_A^2 &= \frac{v^2}{v_1 v_2}\left[\mu_{12}^2 - 2\lambda_5 v_1 v_2\right], \\ m_{H^+}^2 &= m_A^2 + (\lambda_5 - \lambda_4)v^2\,. \end{aligned} \tag{2.25}$$

The CP-even scalar sector is slightly more complicated and, being model-dependent, omitted for the sake of brevity.

For $\mu_{12} = \lambda_5 = 0$ the pseudoscalar A becomes massless, leading to a model with too many Goldstone bosons. This is the case if the scalar potential preserves an additional global $U(1)$ due to the discrete symmetry [116]. A soft breaking of this symmetry in the scalar sector is required to obtain a viable model. An example is discussed in Chapter 3.1.

Using the angles α and β to parametrize the fermion-Higgs interactions, the 2HDM Yukawa couplings can be neatly expressed in terms of only two parameters in the flavor-conserving cases. For the 2HDMs type I and II the couplings are summarized in Tab. 2.2. In the literature, limits are typically presented as a function of $\tan\beta$. However, as indicated by Tab. 2.2, these bounds depend crucially on the fermion couplings with widely differing results for each 2HDM.

2HDM	y_u^h	y_d^h	y_l^h	y_u^H	y_d^H	y_l^H	y_u^A	y_d^A	y_l^A
I	c_α/s_β	c_α/s_β	c_α/s_β	s_α/s_β	s_α/s_β	s_α/s_β	$1/t_\beta$	$-1/t_\beta$	$-1/t_\beta$
II	c_α/s_β	$-s_\alpha/c_\beta$	$-s_\alpha/c_\beta$	s_α/s_β	c_α/c_β	c_α/c_β	$1/t_\beta$	t_β	t_β

Table 2.2: Diagonal Yukawa couplings in the 2HDMs type I and II normalized to the corresponding SM couplings with $\sin \equiv s$, $\cos \equiv c$, and $\tan \equiv t$. The light and heavy CP-even neutral scalars are denoted by h and H, respectively, and A is the CP-odd neutral scalar.

The Higgs-gauge boson interactions confine the Higgs parameter space the most since they are well measured as opposed to the Yukawa couplings (compare Fig. 1.20). As seen from

$$\mathcal{L}_{\text{kin}} = |D_\mu \phi_1|^2 + |D_\mu \phi_2|^2 \supset \frac{1}{2} g^2 W_\mu W^\mu (v_1 \rho_1^0 + v_2 \rho_2^0)\,, \tag{2.26}$$

the scalar-gauge boson couplings relative to the SM Higgs depend only on the mass basis transformation of the scalars. These transformations are independent of the fermion sector, i.e., they are the same for all types of 2HDMs. For convenience, the couplings can again be expressed in terms of the mixing angles α and β. Normalized to the corresponding SM coupling, they read

$$\begin{aligned} g_{hWW} &= \sin(\beta-\alpha)\,, & g_{hZZ} &= \sin(\beta-\alpha)\,, \\ g_{HWW} &= \cos(\beta-\alpha)\,, & g_{HZZ} &= \cos(\beta-\alpha)\,, \\ g_{AWW} &= 0\,, & g_{AZZ} &= 0\,. \end{aligned} \tag{2.27}$$

Note that the pseudoscalars do not couple to SM gauge boson pairs, and hence are not constrained by searches in these channels. Possible decay channels to look for pseudoscalars include, e.g., $H \to ZA$, and $A \to Zh$, depending on the mass m_A compared to the other states.

It is convenient to rotate into a basis in which one scalar doublet behaves exactly like the SM doublet ϕ, while the other accounts for all the BSM effects due to the extended scalar sector. This is the so-called Higgs basis

$$\begin{pmatrix} H_1 \\ H_2 \end{pmatrix} = \frac{1}{v_{\rm SM}} \begin{pmatrix} v_1 & v_2 \\ -v_2 & v_1 \end{pmatrix} \begin{pmatrix} \phi_1 \\ \phi_2 \end{pmatrix}, \tag{2.28}$$

with

$$H_1 = \begin{pmatrix} G^+ \\ \frac{1}{\sqrt{2}}\left(v_{\rm SM} + h_{\rm SM} + G_0\right) \end{pmatrix}, \qquad H_2 = \begin{pmatrix} H_2^+ \\ \frac{1}{\sqrt{2}}\left(H_2^0 + A_2\right) \end{pmatrix}. \tag{2.29}$$

A distinct feature of the Higgs basis is that only one of the doublets acquires a VEV, which, consequently, is the only one giving masses to the fermions. Therefore, the H_1 Yukawa couplings can be exactly diagonalized, leaving all potential FCNCs in the model to H_2. By denoting the SM Yukawa couplings $Y_{ij}^{u,d}$ and the new BSM couplings $\eta_{ij}^{u,d}$ the Yukawa Lagrangian can be written as

$$\begin{aligned} -\mathcal{L}_{\rm yuk} &\supset \overline{Q}_{iL} y^u_{ij} \tilde{H}_1 u_{jR} + \overline{Q}_{iL} y^d_{ij} H_1 d_{jR} + \overline{Q}_{iL} \eta^u_{ij} \tilde{H}_2 u_{jR} + \overline{Q}_{iL} \eta^d_{ij} H_2 d_{jR} \\ &= m^u \overline{u}'_{iL} u'_{jR} + m^d \overline{d}'_{iL} d'_{jR} + \overline{u}'_{iL} \tilde{\eta}^u_{ij} H_2^{0*} u'_{jR} + \overline{d}'_{iL} \tilde{\eta}^d_{ij} H_2^0 d'_{jR}\,, \end{aligned} \tag{2.30}$$

with

$$V_L^{u,d\dagger} y^{u,d} V_R^{u,d} = \frac{1}{v} m^{u,d}, \quad \text{and} \quad V_L^{u,d\dagger} \eta^{u,d} V_R^{u,d} = \tilde{\eta}^{u,d}. \tag{2.31}$$

Using this basis, it is easy to verify that the off-diagonal Yukawa couplings can always be rotated away if only one Higgs field is associated with one type of fermion.

2.2.2 *3HDMs*

The properties of 3HDMs are very similar to 2HDMs. However, because of the large parameter space, the mass eigenstates and the mixing angles are difficult to determine analytically without a mechanism to simplify the scalar potential. The models in this thesis employ discrete nonabelian symmetries that allow for compact analytical expressions to describe the scalar sector of the 3HDM. For example, the symmetries A_4, S_4, and $\Delta(27)$[1] have a common set of terms, here denoted by V_0

$$V_0 = \sum_{i=1}^{3} \left[-\mu_i^2 \phi_i^\dagger \phi_i + \alpha (\phi_i^\dagger \phi_i)^2\right] + \sum_{i,j=1}^{3} \left[\beta (\phi_i^\dagger \phi_i)(\phi_j^\dagger \phi_j) + \gamma (\phi_i^\dagger \phi_j)(\phi_j^\dagger \phi_i)\right], \tag{2.32}$$

while the additionally allowed terms that distinguish the potentials are

$$V_{A_4} = \delta \sum_{i,j=1}^{3} (\phi_i^\dagger \phi_j)^2 \quad (i \neq j), \tag{2.33}$$

$$V_{\Delta(27)} = \delta \sum_{i \neq j \neq k}^{3} (\phi_i^\dagger \phi_j)(\phi_i^\dagger \phi_k) \quad (i \neq j \neq k). \tag{2.34}$$

[1] Note that the $\Delta(27)$-symmetric 3HDM potential also extends to $\Delta(54)$ [119].

The S_4 potential can be obtained from V_{A_4} by assuming δ to be real. Consequently, the 3HDM potential can have even fewer parameters than the general 2HDM one [Eq. (2.18)] by virtue of the flavor symmetries.

The additional Higgs doublet adds four degrees of freedom to the scalar sector compared to the 2HDM, implying that after EW symmetry breaking a total of nine states become massive. However, discrete symmetries with certain vacuum alignments can further reduce the huge parameter space of 3HDMs by predicting specific relations between the masses of the scalars. These alignments ensure that the chosen VEVs correspond to an actual global minimum of the 3HDM potential, which have been determined by means of geometric minimization for A_4, S_4, and $\Delta(27)$ [120] and are

$$v(0,0,1)\,, \quad v(1,1,1)\,, \quad v(e^{i\pi/3}, e^{-i\pi/3}, \pm 1)\,, \quad v(1,i,0)\,, \tag{2.35}$$

and permutations thereof.

Once the scalar fields acquire VEVs in one of these alignments, they will either preserve a remnant (or residual) subgroup of the flavor symmetry, or break it entirely. In the case of A_4, S_4, and $\Delta(27)$, the CP conserving alignments $v(0,0,1)$ and $v(1,1,1)$ break the symmetry down to a residual Z_2 and Z_3 subgroup, respectively [119]. These leftover symmetries can be utilized to predict fermion masses and mixings or to suppress unwanted FCNCs. For example, the Majorana neutrino mass matrix respects the Klein symmetry $Z_2 \times Z_2$ [121], suggesting that the flavor symmetry should be broken in the neutrino sector by the VEV alignment $v(0,0,1)$. On the other hand, a remnant Z_3 symmetry in the charged lepton sector can preserve flavor on a renormalizable level, known as lepton flavor triality (LFT) [122]. This triality is exploited to explain the $h \to \mu\tau$ anomaly in an S_4 symmetric 3HDM discussed in Sec. 4.1.

Reproducing the large PMNS mixing angles requires a mismatch between the symmetries of the charged leptons and the neutrinos, implying that these leptons are associated with distinctly aligned flavons. Consequently, any symmetry solution to the flavor problem demands a multitude of new particles and cannot be simple. Extending the framework possibly even to quarks with a reasonable amount of additional field content becomes a highly involved endeavor to balance elegance and predictivity.

It is again useful to change into the Higgs basis, where only one of the doublets acquires a VEV. Explicitly, the Higgs basis doublets take the form

$$H_1 = \begin{pmatrix} G^+ \\ \frac{1}{\sqrt{2}}(v_{\rm SM} + h_{\rm SM} + G_0) \end{pmatrix}, \quad H_{2,3} = \begin{pmatrix} H^+_{2,3} \\ \frac{1}{\sqrt{2}}\left(H^0_{2,3} + iA_{2,3}\right) \end{pmatrix}. \tag{2.36}$$

In this basis only H_1 generates fermion masses $\propto y^{u,d}_{ij} v$ which can be diagonalized to yield the SM fermion masses. The H_2 and H_3 couplings $\eta^{u,d}_{ij}$ and $\xi^{u,d}_{ij}$, respectively, are then in general nondiagonal matrices inducing FCNCs. Interestingly, the Goldstone bosons G^+ and G_0 are already gathered in the doublet H_1, hence only one more 2D rotation is required to obtain the charged scalar and pseudoscalar mass eigenstates from $H^+_{2,3}$ and $A_{2,3}$.

Let $u = (v_1, v_2, v_3)^T$ and $w = (v, 0, 0)^T$, then the Higgs basis transformation rotating u into w corresponds to a 2D rotation around the normal $u \times w$. This orthogonal matrix ($v_{23}^2 \equiv v_2^2 + v_3^2$)

$$R_{v_1 v_2 v_3} = \frac{1}{v_{23}^2 v} \begin{pmatrix} v_1 v_{23}^2 & v_2 v_{23}^2 & v_3 v_{23}^2 \\ -v_2 v_{23}^2 & v_1 v_2^2 + v_3^2 v & v_2 v_3 (v - v_1) \\ -v_3 v_{23}^2 & v_2 v_3 (v - v_1) & v_1 v_3^2 + v_2^2 v \end{pmatrix} \tag{2.37}$$

depends only on the VEVs $v_{1,2,3}$ and is therefore valid in any 3HDM without specifying the potential. The typical VEV alignments favored by flavor symmetries $v(0, 0, 1)$ and $v(1, 1, 1)$ result in the rotation matrices $R_{v00} = I$ and

$$R_{vvv} = \frac{1}{\sqrt{3}} \begin{pmatrix} 1 & 1 & 1 \\ -1 & \frac{1}{2}(1 + \sqrt{3}) & \frac{1}{2}(1 - \sqrt{3}) \\ -1 & \frac{1}{2}(1 - \sqrt{3}) & \frac{1}{2}(1 + \sqrt{3}) \end{pmatrix}. \tag{2.38}$$

The Higgs basis notation is particularly useful for charged scalar interactions, which are completely determined by the matrices η and ξ. This feature is exploited in Sec. 4.2 to study the $R_{D^{(*)}}$ anomaly in the 3HDM.

2.3 UNIFICATION

Besides aesthetic reasons, the main purpose of unification is to find a single framework describing the SM gauge groups and the fermion interactions. So-called grand unified theories (GUTs) proclaim the SM symmetries as remnants of one larger gauge group and thereby motivate their common origin. This section deals with advances in GUTs, outlining some viable candidates and their shortcomings in Sec. 2.3.1.
The unification of quark and lepton interactions in particular is phenomenologically interesting. Leptoquarks can mediate B- and L-violating processes that are relevant also at low energies and, if found, could shed light on some of the unresolved SM anomalies. Sec. 2.3.2 focuses on the implications of leptoquarks and how they can emerge from GUTs.

2.3.1 *Grand Unified Theories*

The idea of GUTs is to unify the three distinct gauge interactions of the SM into a single force arising from one larger gauge group. The three, seemingly uncorrelated couplings of the SM hence emerge in the breaking of this larger gauge symmetry from one unified coupling constant. Ideally, the SM couplings converge in a single point thereby defining this unification scale. The running depends not only on the considered gauge group, but also on the additional particles affecting the evolution of the gauge couplings. While specific statements are strongly model-dependent, the running of the SM gauge couplings generally suggests that the scale of unification lies shortly below the Planck scale around $M_{\text{GUT}} \gtrsim 10^{15}\,\text{GeV}$ [123], implying that the expected NP is way beyond the reach of current or next-generation experiments. Implications of GUTs are therefore testable mostly indirectly, e.g., through their predictions for the half-life of the proton.

By uniting the SM fields in common multiplets GUTs also unify matter interactions and explain the peculiar assignments of fermions to the representations of the SM symmetries. Finally, they shed light on the quantized nature of the electric charge, and why the charges of the electron and the proton cancel each other to a high precision. Embedding the SM symmetries into a larger, unified framework fixes the arbitrary choice of the $U(1)_Y$ hypercharge to allow only for discrete electric charges that are exact multiples of $1/3$. Indeed, explaining the electric charge quantization was one of the main motivations to construct the $SU(5)$ GUT [124].
Common issues of GUTs lie in their specific predictions for gauge and Yukawa unification. The unification of quark and lepton interactions allows for B and L violating mediators that can shorten the lifetime of the proton, which is measured by experiments to be longer than the age of our current universe. Furthermore, the most appealing candidates such as the $SU(5)$ fall short of unifying the gauge couplings in their most minimal, nonsupersymmetric versions, as will be explained below.
As it stands, unified theories fail to simplify the rather intricate SM, which is why there is no generally accepted GUT model. In the following the most popular GUT groups, the $SU(5)$ and the $SO(10)$, are reviewed with respect to their features and shortcomings.

$SU(5)$

The $SU(5)$ GUT was first proposed by Georgi and Glashow in 1974 with the intent to unify the SM gauge groups and their associated gauge couplings [124]. The $SU(5)$ symmetry is a very appealing candidate since it is the simplest group to include the SM symmetries as a maximal subgroup. All known SM particles fit nicely into three copies of the smallest fundamental representations of $SU(5)$ with the correct observed electric charges

$$\overline{\mathbf{5}}_F = \begin{pmatrix} d_1^c \\ d_2^c \\ d_3^c \\ e^- \\ -\nu \end{pmatrix}, \qquad \mathbf{10}_F = \begin{pmatrix} 0 & u_3^c & -u_2^c & u_1 & d_1 \\ -u_3^c & 0 & u_1^c & u_2 & d_2 \\ u_2^c & -u_1^c & 0 & u_3 & d_3 \\ -u_1 & -u_2 & -u_3 & 0 & e^+ \\ -d_1 & -d_2 & -d_3 & -e^+ & 0 \end{pmatrix}. \tag{2.39}$$

The condition of gauge coupling unification [125]

$$\alpha_{\mathrm{GUT}} = \frac{5}{3}\alpha_Y = \alpha_{\mathrm{W}} = \alpha_{\mathrm{S}} \tag{2.40}$$

leads to the model-independent prediction for the Weinberg mixing angle at the unification scale

$$\sin^2\theta_{\mathrm{W}}(\Lambda_{\mathrm{GUT}}) = \frac{3}{8}. \tag{2.41}$$

Taking into account the renormalization group running between the EW and the GUT scale, this value can be compared with the very precise measurement at the M_Z scale [6]

$$\sin^2\theta_{\mathrm{W}}(M_Z) = 0.23126(5) \tag{2.42}$$

as opposed to $\sin^2\theta_{\rm W}(M_Z)\sim 0.20$ expected by the minimal $SU(5)$ GUT framework [125]. The deviation suggests that, if $SU(5)$ is indeed realized in nature, additional particle content is needed to modify the running of the couplings. Also supersymmetric extensions are known to solve the problem [126].
The minimal Higgs sector of an $SU(5)$ GUT includes a $\mathbf{5}_H$ containing the SM Higgs doublet and the adjoint $\mathbf{24}_H$ inducing the $SU(5)$ breaking

$$\begin{aligned} &SU(5)\xrightarrow{\langle\mathbf{24}_H\rangle} SU(3)_C\otimes SU(2)_L\otimes U(1)_Y \\ &\text{with}\quad \langle\mathbf{24}_H\rangle=\frac{v}{\sqrt{15}}\text{diag}\,(2,2,2,-3,-3)\,. \end{aligned} \tag{2.43}$$

The Yukawa Lagrangian then comprises only two fundamental interactions

$$-\mathcal{L}_Y=\overline{\mathbf{5}}_F Y_5\mathbf{10}_F\mathbf{5}_H^*+\frac{1}{8}\epsilon_5\mathbf{10}_F Y_{10}\mathbf{10}_F\mathbf{5}_H\,, \tag{2.44}$$

reducing the number of Yukawa matrices from three to two compared to the SM. This results in simple relations between the Yukawa interactions, referred to as the Georgi-Jarlskog mass relations [127]

$$m_b\sim m_\tau\,,\quad 3m_s\sim m_\mu\,,\quad m_d\sim 3m_e\,, \tag{2.45}$$

which have to be fulfilled at the GUT scale. The Yukawa couplings are subject to renormalization group running and therefore have to be evolved down to the EW scale to be compared with experimental data. As it turns out, the above relations are far from satisfied [123], e.g.,

$$\left(\frac{m_b}{m_\tau}\right)_{SU(5)}\sim 0.8\,,\qquad \left(\frac{m_b}{m_\tau}\right)_{\rm exp}\sim 2.5\,. \tag{2.46}$$

This simple prediction excludes the minimal $SU(5)$ as a valid candidate to unify the gauge interactions.
One either has to resort to nonrenormalizable operators or to an extended Higgs sector in order to relax the constraints from Yukawa unification. A common solution is to complement the $\mathbf{5}_H$ representation with an additional $\mathbf{45}_H$ multiplet that allows to tune the predicted fermion mass relations. To make a relevant contribution to the fermion mass matrices, some of the states in the $\mathbf{5}_H$ and $\mathbf{45}_H$ multiplet must be relatively light, while others are required to be heavy to avoid rapid proton decay. The implied fine-tuning is an issue of most GUTs. Once the $SU(5)$ is broken, the $\mathbf{5}_H$ Higgs representation is decomposed into an $SU(3)_C$ triplet T and the SM Higgs $SU(2)$ doublet H. The masses of T and H should naturally be of the same order of magnitude since they are part of the same multiplet. The T scalar, however, leads to proton decay due to dimension six diquark operators of the form

$$\mathcal{L}^T_{d=6}=-\frac{1}{2m_T^2}(qY_{10}q)(lY_5q)-\frac{1}{m_T^2}(d^cY_5u^c)(e^cY_{10}u^c)+\text{h.c.} \tag{2.47}$$

A typical $SU(5)$ proton decay mode is $p\to e^+\pi^0$, which due to dimension six operators has the expected partial half-life [128]

$$\tau_p\sim\frac{M_X^4}{\alpha_{\rm GUT}^2 m_p^2}=10^{29}\text{ yr}\,, \tag{2.48}$$

with $M_X \sim 10^{14}$ GeV, where M_X is the mass of the decay-inducing particle, and m_p is the proton mass. For comparison, Super-Kamiokande sets the lower bound $\tau_p > 1.67 \times 10^{34}$ yr on the partial half-life of the proton in this channel [129], which entails even larger values of M_X. The fine-tuning required to explain the large mass difference of T and H is referred to as the doublet-triplet splitting problem.
In conclusion, fixing the fermion mass ratios requires a plethora of new scalar fields with a specific mass hierarchy that makes an $SU(5)$ GUT less appealing. An upside of the extended scalar sector is, however, that the many additional states can contribute favorably to the running of the gauge couplings and thereby solve also the gauge unification problem.
Alternatively, the issues of matter unification can be addressed with nonrenormalizable operators, first proposed in [130]. The existence of higher-dimensional operators implies that the theory is not complete and another breaking takes place somewhere between Λ_{GUT} and $\Lambda_{\text{Planck}} \sim 10^{19}$ GeV. The additional terms in the Yukawa Lagrangian modify the predictions for the fermion mass ratios but do not affect the running of the parameters. Realistic GUT models typically employ a combination of nonrenormalizable operators and an extended particle content to address all the problems of the minimal $SU(5)$ GUT. An example is presented in Sec. 3.2. See also Refs. [131–135] for a selection of GUT flavor models.
Finally, the $SU(5)$ framework does not naturally provide right-handed neutrinos, hence neutrino masses and mixings cannot originate from an $SU(5)$ breaking. Another scale beyond the GUT scale is needed to realize the Weinberg operator for neutrinos with a seesaw mechanism.[2]

$SO(10)$

The $SO(10)$ as a GUT was found independently by Fritzsch, Minkowski [138], and Georgi [139]. An enticing feature of $SO(10)$ is that all fermionic matter of the SM is contained in the fundamental representation **16**, reducing the number of Yukawa matrices from three to a single matrix that describes all interactions. An $SO(10)$ GUT can be broken in various ways, yielding many possibilities to accommodate the SM particles, including [140]

$$\begin{aligned}
&SO(10) \xrightarrow{\langle \mathbf{45}\rangle,\langle \mathbf{16}\rangle} && SU(5) && \text{(standard } SU(5)\text{)} \\
&SO(10) \xrightarrow{\langle \mathbf{45}\rangle,\langle \mathbf{16}\rangle} && SU(5)\otimes U(1)_X && \text{(flipped } SU(5)\text{)} \\
&SO(10) \xrightarrow{\langle \mathbf{54}\rangle,\langle \mathbf{16}\rangle} && SU(4)\otimes SU(2)_L \otimes SU(2)_R && \text{(Pati-Salam)} \\
&SO(10) \xrightarrow{\langle \mathbf{54}\rangle,\langle \mathbf{45}\rangle,\langle \mathbf{16}\rangle} && SU(3)_C \otimes SU(2)_L \otimes U(1)_Y && \text{(SM)}
\end{aligned} \tag{2.49}$$

Aside from $SU(5)$, an important subgroup of $SO(10)$ is the $SU(4)_C \otimes SU(2)_L \otimes SU(2)_R$ Pati-Salam group, where leptons and quarks are accommodated in the same multiplets. The Pati-Salam framework has been studied extensively because of its potentially low breaking scale, making it a viable candidate for leptoquark UV completions, see, e.g., Refs. [141–144].

[2] A viable alternative is the "flipped" $SU(5)$ [136], where ν^c and e^c as well as u^c and d^c switch places in the $\overline{\mathbf{5}}$- and **10**-plets. See, e.g., Ref. [137] for a realization of neutrino masses in the flipped $SU(5)$ framework.

However, the appeal of the $SO(10)$ GUT to provide only one Yukawa interaction $\sim \mathbf{16}_F\mathbf{16}_F\mathbf{10}_H$ is also its drawback: the SM fermion mass relations cannot be accommodated at all without introducing a scalar $\mathbf{126}_H$ multiplet to modify them [145]. Consequently the $SO(10)$ Higgs sector is even bigger than the $SU(5)$ one. On the positive side, the **126** generates naturally-small Majorana mass terms for the neutrinos included in the **16**-plet by virtue of a seesaw mechanism [146].

2.3.2 *Leptoquarks*

The so-called leptoquarks are typical byproducts of theories with unified Yukawa interactions mediating transitions between quarks and leptons. They can appear as spin-0 or spin-1 messengers, referred to as scalar or vector type, respectively. Scalar leptoquarks arise as a consequence of an extended Higgs sector, while vector leptoquarks correspond to the vector bosons of a broken gauge theory. In both cases, leptoquark interactions can affect a variety of low energy and high energy processes, giving rise to tightly constrained rare decays (cf. Sec. 1.2.3). If the leptoquark interactions are also L- and B-violating, they can even induce rapid proton and $0\nu\beta\beta$ decays, both so far unobserved.
Despite the constraints, leptoquarks could be the missing puzzle piece to resolve the many anomalies in the flavor sector. To this end, two GUT frameworks are outlined in this section which contain leptoquarks that can modify the anomalous flavor observables. It is plausible that these leptoquarks are also responsible for neutrino masses. Two specific model realizations exploring this idea are presented in Chapter 4.3.
A complete list of scalar and vector leptoquarks that can interact with the SM fermions is given in Tab. 2.3. The corresponding interactions are [147]

$$\begin{aligned}
-\mathcal{L}_{\text{SQL}} = \;& \lambda^R_{S_0}\overline{u^c}P_R e S_0^\dagger + \lambda^R_{\tilde{S}_0}\overline{d^c}P_R e \tilde{S}_0^\dagger + \lambda^R_{S_{1/2}}\overline{u}P_L l S_{1/2}^\dagger + \lambda^R_{\tilde{S}_{1/2}}\overline{d}P_L l \tilde{S}_{1/2}^\dagger \\
+ \;& \lambda^L_{S_0}\overline{q^c}P_L i\sigma_2 l S_0^\dagger + \lambda^L_{S_{1/2}}\overline{q}P_R i\sigma_2 e S_{1/2}^\dagger + \lambda^L_{S_1}\overline{q^c}P_L i\sigma_2 \hat{S}_1^\dagger l + \text{h.c.}\,, \\
-\mathcal{L}_{\text{VQL}} = \;& \lambda^R_{V_0}\overline{d}\gamma^\mu P_R e V_{0\mu}^\dagger + \lambda^R_{\tilde{V}_0}\overline{u}\gamma^\mu P_R e \tilde{V}_{0\mu}^\dagger + \lambda^R_{V_{1/2}}\overline{d^c}\gamma^\mu P_L l V_{1/2\mu}^\dagger \\
+ \;& \lambda^R_{\tilde{V}_{1/2}}\overline{u^c}\gamma^\mu P_L l \tilde{V}_{1/2\mu}^\dagger + \lambda^L_{V_0}\overline{q}\gamma^\mu P_L l V_{0\mu}^\dagger \\
+ \;& \lambda^L_{V_{1/2}}\overline{q^c}\gamma^\mu P_R e V_{1/2\mu}^\dagger + \lambda^L_{V_1}\overline{q}\gamma^\mu P_L \hat{V}_{1\mu}^\dagger l + \text{h.c.}\,,
\end{aligned} \tag{2.50}$$

where P_L and P_R denote the projection operators and σ_2 is the Pauli matrix. The leptoquark couplings $\lambda^{L,R}_{LQ}$ are understood as 3×3 matrices in the quark-lepton space. The leptoquarks are typically assumed to couple exclusively to left-handed or right-handed quarks as they otherwise affect the well-measured ratio $\mathcal{B}(\pi\to e\nu)/\mathcal{B}(\pi\to\mu\nu)$ [148]. Such leptoquarks are referred to as chiral.
Furthermore, leptoquarks are also often assumed to couple to only one generation of fermions to avoid rare decays like $K_L\to\mu e$. Leptoquarks with generation-diagonal couplings are appropriately labeled first, second, and third generation leptoquarks. We will specifically allow cross-generation interactions in this thesis to explain the recently reported flavor anomalies. Adopting this assumption imposes stringent constraints on our model parameters, which are discussed in detail in Sec. 4.3.2.
Direct collider searches usually consider only leptoquarks with generation-diagonal couplings. The latest results exclude first generation leptoquark masses below 1 TeV at 95% C.L. [149], which is often adopted as a conservative lower limit in model building

with leptoquarks. A comprehensive collection of leptoquark interactions with their respective bounds is given in Ref. [150].

Leptoquark	$(SU(3)_C, SU(2)_L)_{U(1)_Y}$	Q_{EM}	B	L
S_0	$(\mathbf{3},\mathbf{1})_{-1/3}$	$-1/3$	$1/3$	1
$\tilde{S}_0$	$(\mathbf{3},\mathbf{1})_{-4/3}$	$-4/3$	$1/3$	1
$S_{1/2}$	$(\overline{\mathbf{3}},\mathbf{2})_{-7/6}$	$(-2/3,-5/3)$	$-1/3$	1
$\tilde{S}_{1/2}$	$(\overline{\mathbf{3}},\mathbf{2})_{-1/6}$	$(1/3,-2/3)$	$-1/3$	1
S_1	$(\mathbf{3},\mathbf{3})_{-1/3}$	$(2/3,-1/3,-4/3)$	$1/3$	1
V_0	$(\overline{\mathbf{3}},\mathbf{1})_{-2/3}$	$-2/3$	$-1/3$	1
$\tilde{V}_0$	$(\overline{\mathbf{3}},\mathbf{1})_{-5/3}$	$-5/3$	$-1/3$	1
$V_{1/2}$	$(\mathbf{3},\mathbf{2})_{-5/6}$	$(-1/3,-4/3)$	$1/3$	1
$\tilde{V}_{1/2}$	$(\mathbf{3},\mathbf{2})_{1/6}$	$(2/3,-1/3)$	$1/3$	1
V_1	$(\overline{\mathbf{3}},\mathbf{3})_{-2/3}$	$(1/3,-2/3,-5/3)$	$-1/3$	1

Table 2.3: Possible scalar and vector leptoquarks and their SM quantum numbers.

Leptoquarks in Pati-Salam Models

The simplest framework to unify quarks and leptons is provided by the $SU(4)_C$ Pati-Salam gauge theory [151], in which the SM fermions of each generation are accommodated in the same multiplets with leptons as the "fourth color".[3] The gauge group of Pati-Salam models is extended and broken in two steps [152]

$$\begin{array}{c} SU(4)_C \otimes SU(2)_L \otimes SU(2)_R \\ \downarrow \\ SU(3)_C \otimes SU(2)_L \otimes U(1)_Y \\ \downarrow \\ SU(3)_C \otimes U(1)_{\mathrm{EM}}\,, \end{array} \tag{2.51}$$

while the SM fields are usually accommodated in the following representations under $(SU(4)_C, SU(2)_L, SU(2)_R)$:

$$\begin{aligned} f_L &= (\mathbf{4},\mathbf{2},\mathbf{1})_L = \begin{pmatrix} u_r & u_g & u_b & \nu \\ d_r & d_g & d_b & e \end{pmatrix}_L , \\ f_R &= (\mathbf{4},\mathbf{1},\mathbf{2})_R = \begin{pmatrix} u_r^c & u_g^c & u_b^c & \nu^c \\ d_r^c & d_g^c & d_b^c & e^c \end{pmatrix}_R . \end{aligned} \tag{2.52}$$

However, variations of these assignments are possible, which require different scalar representations to generate the fermion masses and initiate the breaking. For the

[3] The fourth color is often called lilac to resemble the "l" of leptons.

purpose of this thesis we discuss only the general aspects of Pati-Salam models with respect to leptoquark interactions.

A few comments are in order to clarify the breaking chain in Eq. (2.51):

1. Pati-Salam models achieve only partial unification as they do not attempt to unify the gauge couplings, which usually pushes the breaking scale to around $M_{\text{GUT}} \sim 10^{15}\,\text{GeV}$ or higher. Without this constraint, the breaking scale can be as low as a few TeV allowing Pati-Salam models to be tested at current or next-generation experiments. The scale is then constrained only by low-energy experiments and Yukawa unification. The latter predicts $y_\tau \sim y_b$ at the unification scale, which is consistent with the measured values at the M_Z scale thanks to renormalization group running if the gauge group is broken at a few TeV [142].

2. The $SU(4)_C$ alone breaks into $SU(3)_C \otimes U(1)_{B-L}$. The SM $U(1)_Y$ is hence a combination of the $U(1)_{B-L}$ and the broken $SU(2)_R$ [152]. A direct consequence of the unbroken $U(1)_{B-L}$ subgroup is that the $SU(4)_C$ leptoquarks do not violate $B-L$, i.e., they do not induce proton decay. This statement, however, does not hold for scalar leptoquarks, which emerge from the scalar representations and are unconstrained by the $B-L$ symmetry.

The Pati-Salam framework is a possible UV completion of leptoquark models, providing low-scale vector leptoquarks corresponding to the $SU(4)_C$ gauge bosons, see Refs. [141–144] for a selection of models. The fifteen generators λ_a ($a = 1 \dots 15$) of $SU(4)_C$ split into eight generators of $SU(3)_C$, one messenger corresponding to $U(1)_{B-L}$, and six new states mediating quark and lepton transitions that preserve $SU(3)_C \otimes U(1)_{B-L}$

$$A_\mu = \sum_{a=1}^{15} A_\mu^a \frac{\lambda^a}{2} \sim \left(\begin{array}{c|c} SU(3)_C & \begin{array}{c} SU(3)_C \\ \otimes \\ U(1)_{B-L} \end{array} \\ \hline SU(3)_C \otimes U(1)_{B-L} & U(1)_{B-L} \end{array}\right). \tag{2.53}$$

Since the $SU(4)_C$ symmetry is broken separately from $SU(2)_L$, the exotic gauge bosons appear as $(\mathbf{3},\mathbf{1})_{2/3}$ under the SM symmetries $SU(3)_C \otimes SU(2)_L \otimes U(1)_Y$, corresponding to the vector leptoquark V_0. A flavor model based on this leptoquark is presented in Sec. 4.3.2.

The scalar leptoquarks reside in the multiplets that form invariants with the matter representations. These can be derived from the products $(\overline{\mathbf{4}},\mathbf{2},\mathbf{1})_L \otimes (\mathbf{4},\mathbf{1},\mathbf{2})_R$, $(\overline{\mathbf{4}},\mathbf{2},\mathbf{1})_L \otimes (\mathbf{4},\mathbf{2},\mathbf{1})_L$ and $(\overline{\mathbf{4}},\mathbf{1},\mathbf{2})_R \otimes (\mathbf{4},\mathbf{1},\mathbf{2})_R$. In Young-tableau notation the $SU(4)_C$ product yields

$$\overline{\mathbf{4}} \otimes \mathbf{4} = \begin{array}{|c|}\hline \\ \hline \\ \hline \end{array} \otimes \begin{array}{|c|}\hline \\ \hline \end{array} = \mathbf{1} \oplus \mathbf{15}\,. \tag{2.54}$$

The **15**-plet can contain leptoquarks and decomposes under $SU(3)_C$ as

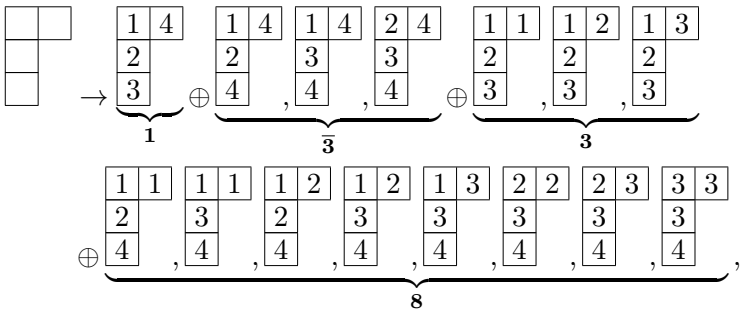

(2.55)

i.e.,

$$\mathbf{15} \to \mathbf{1} \oplus \overline{\mathbf{3}} \oplus \mathbf{3} \oplus \mathbf{8}\,. \tag{2.56}$$

Since the $SU(4)_C$ symmetry is first broken down to $SU(3)_C \otimes U(1)_{B-L}$, the resulting hypercharge Y is given by a linear combination of the $U(1)_{B-L}$ and $SU(2)_R$ charges [152]

$$Y = \frac{1}{2}(B-L) + I_{3R}\,. \tag{2.57}$$

$SU(2)_R$ singlets have $I_{3R} = 0$, while doublets decompose into the states $\frac{1}{2} \oplus -\frac{1}{2}$. Putting all the pieces together, the $(SU(4)_C, SU(2)_L, SU(2)_R)$ representations $(\mathbf{15}, \mathbf{2}, \mathbf{2})$, $(\mathbf{15}, \mathbf{1}, \mathbf{1})$, and $(\mathbf{15}, \mathbf{3}, \mathbf{1})$ split into the following $(SU(3)_C, SU(2)_L)_{U(1)_Y}$ fields:

$$\begin{aligned}
(\mathbf{15},\mathbf{2},\mathbf{2}) \to\ & (\mathbf{1},\mathbf{2})_{\pm 1/2} \oplus \underbrace{(\mathbf{3},\mathbf{2})_{1/6}}_{\tilde{S}^\dagger_{1/2}} \oplus \underbrace{(\mathbf{3},\mathbf{2})_{7/6}}_{S^\dagger_{1/2}} \\
& \oplus (\mathbf{8},\mathbf{2})_{\pm 1/2} \oplus \underbrace{(\overline{\mathbf{3}},\mathbf{2})_{-1/6}}_{\tilde{S}_{1/2}} \oplus \underbrace{(\overline{\mathbf{3}},\mathbf{2})_{-7/6}}_{S_{1/2}}\,, \\
(\mathbf{15},\mathbf{1},\mathbf{1}) \to\ & (\mathbf{1},\mathbf{1})_0 \oplus \underbrace{(\overline{\mathbf{3}},\mathbf{1})_{1/3}}_{S^\dagger_0} \oplus \underbrace{(\mathbf{3},\mathbf{1})_{-1/3}}_{S_0} \oplus (\mathbf{8},\mathbf{1})_0\,, \\
(\mathbf{15},\mathbf{3},\mathbf{1}) \to\ & (\mathbf{1},\mathbf{3})_0 \oplus \underbrace{(\overline{\mathbf{3}},\mathbf{3})_{1/3}}_{S^\dagger_1} \oplus \underbrace{(\mathbf{3},\mathbf{3})_{-1/3}}_{S_1} \oplus (\mathbf{8},\mathbf{3})_0\,.
\end{aligned} \tag{2.58}$$

The $(\mathbf{15}, \mathbf{2}, \mathbf{2})$ representation not only provides the leptoquarks $S_{1/2}$ and $\tilde{S}_{1/2}$ but also gives masses to the SM fermions through the Higgs residing in its $(\mathbf{1}, \mathbf{2})_{1/2}$ component. It is therefore a common ingredient of Pati-Salam models. All remaining scalar leptoquarks except $\tilde{S}_0$ can be obtained from the $SU(2)_L$ singlet and triplet versions of the **15**-plet.

Leptoquarks in $SU(5)$ Grand Unified Theories

The requirements of gauge unification and proton stability typically entail a very high breaking scale that would render all messenger particles unobservable. However, if this condition is dropped, the $SU(5)$ symmetry can be broken at a lower scale with a mechanism that prevents rapid proton decay. The question of gauge unification is then postponed until $SU(5)$ emerges from another symmetry, e.g., in the breaking of $SO(10)$.

When $SU(5)$ is broken to its maximal subgroup $SU(3)_C \otimes SU(2)_L \otimes U(1)_Y$, the twenty-four generators are divided into eight generators corresponding to the gluons of $SU(3)_C$, the four EW $SU(2)_L \otimes U(1)_Y$ gauge bosons, and twelve additional mediators with mixed $SU(3)_C \otimes SU(2)_L$ quantum numbers [124]

$$A_\mu = \sum_{a=1}^{24} A_\mu^a \frac{\lambda^a}{2} \sim \left(\begin{array}{c|c} SU(3)_C & \begin{array}{c} SU(3)_C \\ \otimes \\ SU(2)_L \end{array} \\ \hline SU(3)_C \otimes SU(2)_L & SU(2)_L \end{array} \right) . \tag{2.59}$$

Specifically, the adjoint representation splits up into

$$\mathbf{24} \to (\mathbf{8},\mathbf{1})_0 + (\mathbf{1},\mathbf{3})_0 + (\mathbf{1},\mathbf{1})_0 + (\mathbf{3},\mathbf{2})_{-5/6} + (\overline{\mathbf{3}},\mathbf{2})_{5/6}\,, \tag{2.60}$$

where the exotic gauge bosons $(\mathbf{3},\mathbf{2})_{-5/6}$ can be identified as the vector leptoquarks $V_{1/2}$. On the other hand, the flipped $SU(5)$ is paired with an additional $U(1)_X$, which modifies the hypercharge of the exotic $SU(5)$ gauge bosons. In this case the adjoint representation **24** decomposes into [136]

$$\mathbf{24} \to (\mathbf{8},\mathbf{1})_0 + (\mathbf{1},\mathbf{3})_0 + (\mathbf{1},\mathbf{1})_0 + (\mathbf{3},\mathbf{2})_{1/6} + (\overline{\mathbf{3}},\mathbf{2})_{-1/6} \tag{2.61}$$

yielding the $(\mathbf{3},\mathbf{2})_{1/6}$ vector leptoquarks $\tilde{V}_{1/2}$.
To avoid rapid proton decay, leptoquark and diquark operators induced by the $(\mathbf{3},\mathbf{2})_{-5/6}$ and $(\mathbf{3},\mathbf{2})_{1/6}$ states must not be present at the same time, requiring an underlying quantum number similar to R-parity to forbid one or the other interaction.
Scalar leptoquarks emerge in $SU(5)$ models that rely on extended Higgs sectors to address problems such as Yukawa unification and the proton decay. Since the quarks and charged leptons are accommodated in the fundamental representations **10** and $\overline{\mathbf{5}}$ of $SU(5)$, the leptoquark states should be found in the tensor products [153]

$$\begin{aligned} \mathbf{10} \otimes \mathbf{10} &= \overline{\mathbf{5}} \oplus \overline{\mathbf{45}} \oplus \overline{\mathbf{50}}\,, \\ \mathbf{10} \otimes \overline{\mathbf{5}} &= \mathbf{5} \oplus \mathbf{45}\,, \\ \overline{\mathbf{5}} \otimes \overline{\mathbf{5}} &= \overline{\mathbf{10}} \oplus \overline{\mathbf{15}}\,. \end{aligned} \tag{2.62}$$

The resulting multiplets decompose under $(SU(3)_C, SU(2)_L)_{U(1)_Y}$ into [153]

$$\begin{aligned} \mathbf{5} &= (\mathbf{1},\mathbf{2})_{1/2} \oplus \underbrace{(\mathbf{3},\mathbf{1})_{-1/3}}_{S_0}\,, \\ \mathbf{10} &= (\mathbf{1},\mathbf{1})_1 \oplus \underbrace{(\mathbf{3},\mathbf{1})_{-2/3}}_{\hat{S}_0} \oplus \underbrace{(\mathbf{3},2)_{1/6}}_{\tilde{S}^\dagger_{1/2}}\,, \\ \mathbf{15} &= (\mathbf{1},\mathbf{3})_1 \oplus \underbrace{(\mathbf{3},\mathbf{2})_{1/6}}_{\tilde{S}^\dagger_{1/2}} \oplus (\mathbf{6},1)_{-2/3}\,, \\ \mathbf{45} &\supset \underbrace{(\mathbf{3},\mathbf{3})_{-1/3}}_{S_1} \oplus \underbrace{(\overline{\mathbf{3}},\mathbf{2})_{-7/6}}_{S_{1/2}} \oplus \underbrace{(\mathbf{3},\mathbf{1})_{-1/3}}_{S_0} \oplus \underbrace{(\overline{\mathbf{3}},\mathbf{1})_{4/3}}_{\tilde{S}^\dagger_0}\,, \\ \mathbf{50} &\supset \underbrace{(\mathbf{3},\mathbf{1})_{-1/3}}_{S_0} \oplus \underbrace{(\overline{\mathbf{3}},\mathbf{2})_{-7/6}}_{S_{1/2}}\,, \end{aligned} \tag{2.63}$$

while the components of $\overline{\mathbf{5}}, \overline{\mathbf{10}}, \overline{\mathbf{15}}, \overline{\mathbf{45}}$, and $\overline{\mathbf{50}}$ follow from complex conjugation of Eq. (2.63). Consequently, most scalar leptoquarks are found in the **45** representation, which is an integral part of nonminimal $SU(5)$ models to fix the fermion mass ratios and proton decay predictions. Another representation in addition to **45** is necessary in order to incorporate the $\tilde{S}_{1/2}$ leptoquark, which, as will be shown in Sec. 4.3.1, is relevant for generating one-loop level Majorana neutrino masses. However, the fact that $\tilde{S}_{1/2}$ resides in a different multiplet can be viewed as an advantage of $SU(5)$ as it explains a possible leptoquark mass splitting. This mass difference can prove useful to suppress the leptoquark mixing in models where the smallness of the neutrino masses is explained with leptoquark interactions, cf. Sec. 4.3.

3

MODELS ADDRESSING THE FLAVOR PROBLEM

Various SM extensions with flavor symmetries have been proposed in the literature to solve some of the most pressing issues of the SM: the smallness of neutrino masses, the puzzling pattern of fermion masses and mixings, and the existence of the three families of quarks and leptons. Since the mixing patterns of leptons and quarks are significantly different, it is challenging to implement a unique symmetry, able to describe the small quark mixing angles and the large leptonic ones at the same time. Indeed, flavor models in the literature often lack distinguishing properties and predictions.

In this chapter we construct two new models that are aimed at combining the quark and lepton masses and mixings in one unified framework: a 2HDM with the S_3 flavor symmetry (Sec. 3.1), and a grand unified model based on the $SU(5)$ group (Sec. 3.2). The S_3 model can be tested with searches for top quark decays, and the $SU(5)$ flavor model links the gauge unification scale to the origin of the Yukawa couplings and fermion mixings by virtue of an FN mechanism. The conclusions are presented in Sec. 3.3.

3.1 AN S_3-SYMMETRIC FLAVOR MODEL

With neutrino experiments increasingly constraining the mixing angles in the leptonic sector, many models focus on explaining the near TBM structure of the PMNS matrix through a nonabelian symmetry. Discrete flavor symmetries have shown a lot of promise and S_3 in particular, as the smallest nonabelian group, has been studied considerably in the literature since [79], with interesting results for quarks, leptons or both, and remains a popular group [97–105].

In this section we make use of the S_3 group to provide an elegant description of the SM fermion masses and mixings in a 2HDM. By assigning the SM fermions under this symmetry and using scalars transforming under the different irreducible representations of S_3, an existence proof of models is provided leading to the viable mixing-inspired quark textures presented in Ref. [154].

The framework is extended to the lepton sector by modifying the down-type quark texture for the charged leptons. Viable lepton masses and mixings are obtained with the neutrino sector being completed with a type I seesaw mechanism.

The model itself can be tested through its specific predictions in the scalar sector. To this end, the scalar potential is discussed in some detail with respect to processes that constrain the parameters of the model such as $t \to ch$ and $h \to \gamma\gamma$. Moreover, it is shown that the VEVs required to explain the fermion masses indeed correspond to a natural minimum of the potential.

In Sec. 3.1.1 the field and symmetry content of the model is described, followed by a brief revision of the quark masses and mixing angles presented in Ref. [154] and the equivalent analysis for the lepton sector in Sec. 3.1.2. Sec. 3.1.3 deals with the implications of the extended scalar sector, presenting the Yukawa couplings, an analysis of rare top decays, then considering the $h \to \gamma\gamma$ rate and the T and S parameters. We relegate some technical discussions that are relevant for the model to App. C.1.

3.1.1 *The Model*

We consider an extension of the SM with additional scalar fields and discrete symmetries, which reproduces the predictive mixing inspired textures proposed in Ref. [154]

$$M_U = \frac{v}{\sqrt{2}} \begin{pmatrix} c_1\lambda^8 & 0 & a_1\lambda^3 \\ 0 & b_1\lambda^4 & a_2\lambda^2 \\ 0 & 0 & a_3 \end{pmatrix}, \qquad M_D = \frac{v}{\sqrt{2}} \begin{pmatrix} e_1\lambda^7 & f_1\lambda^6 & 0 \\ 0 & f_2\lambda^5 & 0 \\ 0 & 0 & g_1\lambda^3 \end{pmatrix}, \tag{3.1}$$

where a_k ($k = 1, 2, 3$), b_1, c_1, g_1, f_1, f_2, and e_1 are $\mathcal{O}(1)$ parameters. We assume that all of them are real except a_1. The matrices in Eq. (3.1) provide an elegant understanding of all SM fermion masses and mixing angles through their scaling by powers of the Wolfenstein parameter $\lambda = 0.225$ with $\mathcal{O}(1)$ coefficients.
The Cabibbo mixing arises from the down-type quark sector, whereas the up-type quark sector contributes to the remaining mixing angles. The distinct textures required by the observed mismatch of the down-type and up-type quark mixings are obtained using two Higgs doublets distinguished by a symmetry (in this model, a Z_3).
Besides the Z_3 symmetry, other discrete symmetries help to shape the patterns in Eq. (3.1). The purpose of each is summarized in Tab. 3.1 and explained in the following.

Symmetry	Function
S_3	Connects Yukawa couplings and reduces parameters
Z_3	Separates down-type from up-type quark mixing
Z_3'	Suppresses up quark and electron mass
Z_{14}	Implements FN mechanism

Table 3.1: Summary of symmetries and their function in the model.

The 2HDM is embedded in an S_3 flavor symmetry, which is particularly suitable for our purposes as it is the smallest nonabelian group with a doublet representation. By combining fields in this multiplet, we utilize the S_3 symmetry to reduce the number of free model parameters, unifying the corresponding couplings.
Additionally, a $Z_3' \otimes Z_{14}$ symmetry dictates the hierarchical structure of the fermion masses and mixing matrices. Specifically, the Z_{14} functions as an FN symmetry, being the smallest cyclic symmetry that can induce 11-dimensional operators. These nonrenormalizable operators are crucial to explain the hierarchical fermion masses with natural $\mathcal{O}(1)$ Yukawa couplings. To account even for the tiny up quark and electron

masses, the Z_3' then further suppresses the respective mass terms through additional scalar insertions.
The full symmetry $\mathcal{G}$ experiences a two-step symmetry breaking:

$$\begin{gathered}\mathcal{G} = SU(3)_C \otimes SU(2)_L \otimes U(1)_Y \otimes S_3 \otimes Z_3 \otimes Z_3' \otimes Z_{14} \\ \Downarrow \langle\chi\rangle, \langle\zeta\rangle, \langle\xi\rangle \sim \Lambda \\ SU(3)_C \otimes SU(2)_L \otimes U(1)_Y \otimes Z_3 \\ \Downarrow \langle\phi_2\rangle \sim \Lambda_{\mathrm{EW}} \\ SU(3)_C \otimes U(1)_{\mathrm{EM}}\,,\end{gathered} \tag{3.2}$$

where the different scales satisfy $\Lambda \gg \Lambda_{\mathrm{EW}}$ with $\Lambda_{\mathrm{EW}} = 246$ GeV.
The particle content and the assignments under the symmetry groups are shown in Tab. 3.2. In addition to the two Higgs doublets, four $SU(2)$ singlet scalars shape the fermion mass matrices, whose functions in the model are clarified as follows. Two scalars are unified into an S_3 doublet representation ξ. Its VEV breaks the S_3 symmetry and thereby generates a hierarchy between the first two rows of the down quark and charged lepton mass matrices. Charged as (-1) under Z_{14}, the scalar χ is responsible for the hierarchical flavor structure as the flavon in the FN mechanism. Finally, the field ζ breaks Z_3' and suppresses m_u and m_e once it develops its VEV.
Explicitly, the VEVs of these scalars are denoted by

$$\langle\xi\rangle = v_\xi\,(1,0)\,, \qquad \langle\chi\rangle = v_\chi, \qquad \langle\zeta\rangle = v_\zeta\,, \tag{3.3}$$

i.e., the VEV of ξ is aligned as $(1,0)$ in the S_3 direction. See App. C.1.4 for a discussion of the minima in the scalar potential. To simplify the analysis we assume that these VEVs have a common origin, manifesting at a the same scale Λ

$$v_\xi \sim v_\zeta \sim v_\chi = \lambda\Lambda\,. \tag{3.4}$$

The two Higgs doublets are defined according to the typical conventions

$$\phi_l = \begin{pmatrix} \varphi_l^+ \\ \frac{1}{\sqrt{2}}\left(v_l + \rho_l + i\eta_l\right) \end{pmatrix}, \tag{3.5}$$

with

$$\langle\phi_l\rangle = \begin{pmatrix} 0 \\ \frac{v_l}{\sqrt{2}} \end{pmatrix}, \qquad l = 1,2\,. \tag{3.6}$$

Their VEVs should be in the same order of magnitude to obtain realistic fermion masses and mixings, which is demonstrated in Sec. 3.1.2.
The assignments and symmetries shown in Tab. 3.2 lead to the following quark Yukawa Lagrangians:

$$\begin{aligned}-\mathcal{L}_Y^U = {}& \varepsilon_{33}^{(u)}\overline{q}_{3L}\widetilde{\phi}_1 u_{3R} + \varepsilon_{23}^{(u)}\overline{q}_{2L}\widetilde{\phi}_2 u_{3R}\frac{\chi^2}{\Lambda^2} + \varepsilon_{13}^{(u)}\overline{q}_{1L}\widetilde{\phi}_2 u_{3R}\frac{\chi^3}{\Lambda^3} \\ & + \varepsilon_{22}^{(u)}\overline{q}_{2L}\widetilde{\phi}_1 U_R\frac{\xi\chi^3}{\Lambda^4} + \varepsilon_{11}^{(u)}\overline{q}_{1L}\widetilde{\phi}_1 U_R\frac{\xi\chi^4\zeta^3}{\Lambda^8} + \mathrm{h.c.}\,,\end{aligned} \tag{3.7}$$

Field	$SU(2)_L$	S_3	Z_3	Z_3'	Z_{14}
q_{1L}	$\mathbf{2}$	$\mathbf{1}$	0	0	-3
q_{2L}	$\mathbf{2}$	$\mathbf{1}$	0	0	-2
q_{3L}	$\mathbf{2}$	$\mathbf{1}$	1	0	0
U_R	$\mathbf{1}$	$\mathbf{2}$	0	0	1
u_{3R}	$\mathbf{1}$	$\mathbf{1}$	1	0	0
d_{1R}	$\mathbf{1}$	$\mathbf{1}$	2	0	4
d_{2R}	$\mathbf{1}$	$\mathbf{1}$	2	0	3
d_{3R}	$\mathbf{1}$	$\mathbf{1}$	1	0	3
l_{1L}	$\mathbf{2}$	$\mathbf{1}$	2	0	-3
l_{2L}	$\mathbf{2}$	$\mathbf{1}$	0	0	0
l_{3L}	$\mathbf{2}$	$\mathbf{1}$	0	0	0
l_{1R}	$\mathbf{1}$	$\mathbf{1}'$	1	2	4
l_{2R}	$\mathbf{1}$	$\mathbf{1}$	0	0	5
l_{3R}	$\mathbf{1}$	$\mathbf{1}$	0	0	3
ν_{1R}	$\mathbf{1}$	$\mathbf{1}$	0	0	0
ν_{2R}	$\mathbf{1}$	$\mathbf{1}$	0	0	0
ϕ_1	$\mathbf{2}$	$\mathbf{1}$	0	0	0
ϕ_2	$\mathbf{2}$	$\mathbf{1}$	1	0	0
ξ	$\mathbf{1}$	$\mathbf{2}$	0	0	0
χ	$\mathbf{1}$	$\mathbf{1}$	0	0	-1
ζ	$\mathbf{1}$	$\mathbf{1}'$	0	1	0

Table 3.2: Full particle content and assignments under the flavor symmetries.

$$
\begin{aligned}
-\mathcal{L}_Y^D = {} & \varepsilon_{33}^{(d)} \overline{q}_{3L} \phi_1 d_{3R} \frac{\chi^3}{\Lambda^3} + \varepsilon_{22}^{(d)} \overline{q}_{2L} \phi_2 d_{2R} \frac{\chi^5}{\Lambda^5} + \varepsilon_{12}^{(d)} \overline{q}_{1L} \phi_2 d_{2R} \frac{\chi^6}{\Lambda^6} \\
& + \varepsilon_{21}^{(d)} \overline{q}_{2L} \phi_2 d_{1R} \frac{\chi^6}{\Lambda^6} + \varepsilon_{11}^{(d)} \overline{q}_{1L} \phi_2 d_{1R} \frac{\chi^7}{\Lambda^7} + \text{h.c.}\,,
\end{aligned}
\tag{3.8}
$$

where $\mathcal{L}_Y^U$ and $\mathcal{L}_Y^D$ refer to the up-type and down-type quark Yukawa interactions, respectively. The invariant Yukawa terms $\mathcal{L}_Y^l$ and $\mathcal{L}_Y^\nu$ for the charged leptons and neutrinos, respectively, are

$$
\begin{aligned}
-\mathcal{L}_Y^l = {} & \varepsilon_{33}^{(l)} \overline{l}_{3L} \phi_1 l_{3R} \frac{\chi^3}{\Lambda^3} + \varepsilon_{23}^{(l)} \overline{l}_{2L} \phi_1 l_{3R} \frac{\chi^3}{\Lambda^3} + \varepsilon_{22}^{(l)} \overline{l}_{2L} \phi_1 l_{2R} \frac{\chi^5}{\Lambda^5} \\
& + \varepsilon_{32}^{(l)} \overline{l}_{3L} \phi_1 l_{2R} \frac{\chi^5}{\Lambda^5} + \varepsilon_{11}^{(l)} \overline{l}_{1L} \phi_2 l_{1R} \frac{\chi^7 \zeta}{\Lambda^8} + \text{h.c.}\,,
\end{aligned}
\tag{3.9}
$$

$$
\begin{aligned}
-\mathcal{L}_Y^\nu = {} & \varepsilon_{11}^{(\nu)} \overline{l}_{1L} \widetilde{\phi}_2 \nu_{1R} \frac{\chi^3}{\Lambda^3} + \varepsilon_{12}^{(\nu)} \overline{l}_{1L} \widetilde{\phi}_2 \nu_{2R} \frac{\chi^3}{\Lambda^3} + \varepsilon_{21}^{(\nu)} \overline{l}_{2L} \widetilde{\phi}_1 \nu_{1R} \\
& + \varepsilon_{22}^{(\nu)} \overline{l}_{2L} \widetilde{\phi}_1 \nu_{2R} + \varepsilon_{31}^{(\nu)} \overline{l}_{3L} \widetilde{\phi}_1 \nu_{1R} + \varepsilon_{32}^{(\nu)} \overline{l}_{3L} \widetilde{\phi}_1 \nu_{2R} \\
& + M_1 \overline{\nu}_{1R} \nu_{1R}^c + M_2 \overline{\nu}_{2R} \nu_{2R}^c + M_{12} \overline{\nu}_{1R} \nu_{2R}^c + \text{h.c.}
\end{aligned}
\tag{3.10}
$$

These interactions are the source of the fermion masses and mixings, which are discussed in the following subsections.

3.1.2 *Fermion Masses and Mixings*

Quarks

Using Eqs. (3.7) and (3.8) we find the mass matrices for the up- and down-type quarks in the form:

$$
M_U = \frac{v}{\sqrt{2}} \begin{pmatrix} c_1 \lambda^8 & 0 & a_1 \lambda^3 \\ 0 & b_1 \lambda^4 & a_2 \lambda^2 \\ 0 & 0 & a_3 \end{pmatrix}, \qquad M_D = \frac{v}{\sqrt{2}} \begin{pmatrix} e_1 \lambda^7 & f_1 \lambda^6 & 0 \\ e_2 \lambda^6 & f_2 \lambda^5 & 0 \\ 0 & 0 & g_1 \lambda^3 \end{pmatrix}, \tag{3.11}
$$

where the combinations of order one coefficients $\epsilon_{ij}^{(u,d)}$ were redefined to resemble the textures in Eq. (3.1). The down-type quark matrix deviates only in $(M_D)_{21}$, which is a negligible perturbation of the original pattern.
The hermitian combinations $M_U M_U^\dagger$ and $M_D M_D^T$

$$
M_U M_U^\dagger = \frac{v^2}{2} \begin{pmatrix} |a_1|^2 \lambda^6 + c_1^2 \lambda^{16} & a_1 a_2 \lambda^5 & a_1 a_3 \lambda^3 \\ a_1^* a_2 \lambda^5 & a_2^2 \lambda^4 + b_1^2 \lambda^8 & a_2 a_3 \lambda^2 \\ a_1^* a_3 \lambda^3 & a_2 a_3 \lambda^2 & a_3^2 \end{pmatrix}, \tag{3.12}
$$

$$
M_D M_D^T = \frac{v^2}{2} \begin{pmatrix} \lambda^{14} e_1^2 + \lambda^{12} f_1^2 & e_1 e_2 \lambda^{13} + f_1 f_2 \lambda^{11} & 0 \\ e_1 e_2 \lambda^{13} + f_1 f_2 \lambda^{11} & \lambda^{12} e_2^2 + \lambda^{10} f_2^2 & 0 \\ 0 & 0 & \lambda^6 g_1^2 \end{pmatrix}, \tag{3.13}
$$

are approximately diagonalized by the unitary rotation matrices V_U and V_D

$$
\begin{aligned}
& V_U^\dagger M_U M_U^\dagger V_U = \text{diag}(m_u^2, m_c^2, m_t^2)\,, \qquad V_D^T M_D M_D^T V_D = \text{diag}(m_d^2, m_s^2, m_b^2)\,, \\
& V_U \simeq \begin{pmatrix} c_{13} & s_{13} s_{23} e^{i\delta} & -c_{23} s_{13} e^{i\delta} \\ 0 & c_{23} & s_{23} \\ s_{13} e^{-i\delta} & -c_{13} s_{23} & c_{13} c_{23} \end{pmatrix}, \qquad V_D = \begin{pmatrix} c_{12} & s_{12} & 0 \\ -s_{12} & c_{12} & 0 \\ 0 & 0 & 1 \end{pmatrix},
\end{aligned}
\tag{3.14}
$$

where $c_{ij} \equiv \cos\theta_{ij}$, $s_{ij} \equiv \sin\theta_{ij}$ (with $i \neq j$ and $i,j = 1,2,3$), while θ_{ij} and δ are the quark mixing angles and the CP violating phase, respectively. They are given by

$$\begin{aligned} \tan\theta_{12} &\simeq \tfrac{f_1}{f_2}\lambda\,, & \tan\theta_{23} &\simeq \tfrac{a_2}{a_3}\lambda^2\,, \\ \tan\theta_{13} &\simeq \tfrac{|a_1|}{a_3}\lambda^3\,, & \delta &= -\arg(a_1)\,. \end{aligned} \tag{3.15}$$

And consequently, the up- and down-type quark masses are approximately

$$\begin{aligned} m_u &\simeq c_1\lambda^8\tfrac{v}{\sqrt{2}}\,, & m_d &\simeq |e_1 f_2 - e_2 f_1|\,\tfrac{\lambda^7}{\sqrt{2}}v\,, \\ m_c &\simeq b_1\lambda^4\tfrac{v}{\sqrt{2}}\,, & m_s &\simeq f_2\lambda^5\tfrac{v}{\sqrt{2}}\,, \\ m_t &\simeq a_3\tfrac{v}{\sqrt{2}}\,, & m_b &\simeq g_1\lambda^3\tfrac{v}{\sqrt{2}}\,. \end{aligned} \tag{3.16}$$

From a comparison with the Wolfenstein parametrization of the CKM matrix [cf. Eq. (2.3)], we infer

$$\begin{aligned} a_1 &\simeq -A\sqrt{\rho^2+\eta^2}e^{i\delta} \simeq -0.3e^{i\delta}\,, & b_1 &\simeq \tfrac{m_c}{\lambda^4 m_t} \simeq 1.43\,, \\ a_2 &\simeq A \simeq 0.81\,, & c_1 &\simeq \tfrac{m_u}{\lambda^8 m_t} \simeq 1.27\,, \\ a_3 &\simeq 1\,, & \delta &= 67^\circ\,. \end{aligned} \tag{3.17}$$

To reproduce the Cabibbo mixing angle, the constants e_2 and f_2 in Eq. (3.1) should be approximately equal. The remaining parameters e_1, f_1, f_2, and g_1 are fitted to the down-type quark masses and mixing parameters. Note that the model has in total ten free parameters to fit the ten observables of the quark sector, i.e., the six quark masses, the three mixing angles, and the CP-violating phase δ. However, the large parameter budget not only reproduces these observables, but also accounts for the hierarchies among them without the need of fine-tuning. The values of the quark sector observables shown in Tab. 3.3 correspond to the best fit

$$e_1 \simeq 0.84\,, \quad f_1 \simeq 0.4\,, \quad f_2 \simeq 0.57\,, \quad g_1 \simeq 1.42\,. \tag{3.18}$$

The results are consistent with the measurements, which were taken from Refs. [6, 155] at the M_Z scale.

Leptons

We have demonstrated that the S_3 flavor model successfully produces the quark textures proposed in Ref. [154]. The analysis is now extended to the lepton sector for a unified description of quarks and leptons in one framework. The charged lepton mass matrix follows from Eq. (3.9) and takes the form

$$M_l = \frac{v}{\sqrt{2}}\begin{pmatrix} x_1\lambda^8 & 0 & 0 \\ 0 & y_1\lambda^5 & z_1\lambda^3 \\ 0 & y_2\lambda^5 & z_2\lambda^3 \end{pmatrix}, \tag{3.19}$$

where x_1, y_1, y_2, z_1, z_2, are $\mathcal{O}(1)$ parameters, for simplicity assumed to be real. Like the quark matrices, the symmetric product $M_l M_l^T$ can be diagonalized with a unitary rotation matrix V_l according to

$$V_l^T M_l M_l^T V_l = \mathrm{diag}(m_e^2, m_\mu^2, m_\tau^2)\,, \qquad V_l = \begin{pmatrix} 1 & 0 & 0 \\ 0 & \cos\theta_l & -\sin\theta_l \\ 0 & \sin\theta_l & \cos\theta_l \end{pmatrix}, \tag{3.20}$$

Observable	Model	Measurement ($\pm 1\,\sigma$)
m_u [MeV]	1.47	$1.45^{+0.56}_{-0.45}$
m_c [MeV]	641	635 ± 86
m_t [GeV]	172.2	$172.1 \pm 0.6 \pm 0.9$
m_d [MeV]	3.00	$2.9^{+0.5}_{-0.4}$
m_s [MeV]	59.2	$57.7^{+16.8}_{-15.7}$
m_b [GeV]	2.82	$2.82^{+0.09}_{-0.04}$
$\sin\theta_{12}$	0.2257	0.2254
$\sin\theta_{23}$	0.0412	0.0413
$\sin\theta_{13}$	0.00352	0.00350
δ	68°	68°

Table 3.3: Model and experimental values of the quark sector observables at the M_Z scale. The measurements were taken from Refs. [6, 155].

with $\tan\theta_l \simeq -\frac{z_1}{z_2}$. Consequently, the charged lepton masses are approximately given by

$$m_e = x_1 \lambda^8 \frac{v}{\sqrt{2}}\,, \quad m_\mu \simeq \frac{|y_1 z_2 - y_2 z_1|}{\sqrt{z_1^2 + z_2^2}} \lambda^5 \frac{v}{\sqrt{2}}\,, \quad m_\tau \simeq \sqrt{z_1^2 + z_2^2}\,\lambda^3 \frac{v}{\sqrt{2}}\,. \tag{3.21}$$

On the other hand, the neutrino masses are explained in this framework through a seesaw mechanism type I with two heavy right-handed neutrinos. The complete 5×5 neutrino mass matrix is

$$M_\nu = \begin{pmatrix} 0_{3\times 3} & M_\nu^D \\ \left(M_\nu^D\right)^T & M_R \end{pmatrix}, \tag{3.22}$$

with

$$M_\nu^D = \begin{pmatrix} \lambda^3 \varepsilon_{11}^{(\nu)} \frac{v_2}{\sqrt{2}} & \lambda^3 \varepsilon_{12}^{(\nu)} \frac{v_2}{\sqrt{2}} \\ \varepsilon_{21}^{(\nu)} \frac{v_1}{\sqrt{2}} & \varepsilon_{22}^{(\nu)} \frac{v_3}{\sqrt{2}} \\ \varepsilon_{31}^{(\nu)} \frac{v_1}{\sqrt{2}} & \varepsilon_{33}^{(\nu)} \frac{v_3}{\sqrt{2}} \end{pmatrix}, \qquad M_R = \begin{pmatrix} M_1 & \frac{1}{2} M_{12} \\ \frac{1}{2} M_{12} & M_2 \end{pmatrix}. \tag{3.23}$$

Since $(M_R)_{ii} \gg v$, the light neutrino masses are approximately given by

$$M_{\nu_L} = M_\nu^D M_R^{-1} \left(M_\nu^D\right)^T. \tag{3.24}$$

The resulting real symmetric matrix can be diagonalized separately for the normal and inverted neutrino mass hierarchy, predicting one mass eigenstate to be zero. The remaining nonvanishing mass eigenstates in these cases are

$$m_{\nu_\mp} = \frac{1}{2}\left(W^2 + X^2 + Y^2 \mp \sqrt{\left(W^2 - X^2 + Y^2\right)^2 - 4\kappa^2 X^2 \left(W^2 + Y^2\right)}\right). \tag{3.25}$$

The definition of the parameters W, X, Y, and κ, as well as the details of the computation can be found in App. C.1.1. The leptonic mixing angles for NH and IH can also be expressed as functions of these parameters and thus adjusted to the experimental data

$$\begin{aligned} \text{NH:} \qquad \sin^2\theta_{12} &= \frac{W^2\sin^2\theta_\nu}{Y^2+(1-\cos^2\theta_\nu)\,W^2}\,, \qquad \sin^2\theta_{13} = \frac{W^2\cos^2\theta_\nu}{W^2+Y^2}\,, \\ \sin^2\theta_{23} &= \frac{\left(\sqrt{W^2+Y^2}\sin\theta_\nu\cos\theta_l - Y\cos\theta_\nu\sin\theta_l\right)^2}{(1-\cos^2\theta_\nu)\,W^2+Y^2}\,, \end{aligned} \tag{3.26}$$

$$\begin{aligned} \text{IH:} \qquad \sin^2\theta_{12} &= \frac{Y^2\sin^2\theta_\nu}{W^2+(1-\cos^2\theta_\nu)\,Y^2}\,, \qquad \sin^2\theta_{13} = \frac{Y^2\cos^2\theta_\nu}{W^2+Y^2}\,, \\ \sin^2\theta_{23} &= \frac{\left(\sqrt{W^2+Y^2}\sin\theta_\nu\cos\theta_l - W\cos\theta_\nu\sin\theta_l\right)^2}{(1-\cos^2\theta_\nu)\,Y^2+W^2}\,. \end{aligned} \tag{3.27}$$

The analysis is further simplified by setting

$$x_1 = y_2 = z_1\,, \tag{3.28}$$

so that eventually the charged lepton masses are determined by the three dimensionless effective parameters x_1, y_1, and z_2, whereas the neutrino mass squared splittings and mixing angles are controlled by the four parameters κ, W, X, and Y. Therefore, the lepton sector has in total seven effective parameters to describe eight physical observables, i.e., the three charged lepton masses, the two neutrino mass squared splittings and the three leptonic mixing angles. The results shown in Tab. 3.5 correspond to the best-fit values listed in Tab. 3.4

Hierarchy	κ	W [eV$^{1/2}$]	X [eV$^{1/2}$]	Y [eV$^{1/2}$]	x_1	y_1	z_2
NH	0.444	0.12	0.11	0.18	0.43	1.57	0.58
IH	0.008	0.20	0.22	0.08	0.43	1.40	0.78

Table 3.4: Best-fit values that reproduce the observables in the lepton sector.

Given that the lightest neutrino is massless in this framework, the overall neutrino mass scale is beyond the current experimental reach, including also the cosmological bound $\sum_{k=1}^{3} m_{\nu_k} < 0.18$ eV on the sum of the neutrino masses [18, 20] and $0\nu\beta\beta$ decay.
The obtained masses and mixing angles are in excellent agreement with the experimental data, bearing some fine-tuning of the parameter κ in the IH case. The IH parameter set can fit m_τ better, implying a slight preference for IH in this framework. Note that for the sake of simplicity all leptonic parameters were assumed to be real. However, by allowing one or several parameters in the neutrino mass matrix to be complex, a nonvanishing CP-violating phase indicated by recent observations [13] can easily be incorporated.

Hierarchy	Observable	Model value	Measurement ($\pm 1\,\sigma$)
	m_e [MeV]	0.491	0.487
	m_μ [MeV]	102.8	102.8 ± 0.0003
NH	m_τ [GeV]	1.45	1.75 ± 0.0003
IH		1.77	
	Δm^2_{21} [eV^2]	7.49×10^{-5}	$7.49^{+0.19}_{-0.17} \times 10^{-5}$
	Δm^2_{31} [eV^2]	2.53×10^{-3}	$2.526^{+0.039}_{-0.037} \times 10^{-3}$
NH	$\sin^2\theta_{12}$	0.308	$0.308^{+0.013}_{-0.012}$
	$\sin^2\theta_{23}$	0.440	$0.440^{+0.023}_{-0.019}$
	$\sin^2\theta_{13}$	0.0216	0.02163 ± 0.00074
	Δm^2_{21} [eV^2]	7.49×10^{-5}	$7.49^{+0.19}_{-0.17} \times 10^{-5}$
	Δm^2_{13} [eV^2]	2.51×10^{-3}	$2.518^{+0.038}_{-0.037} \times 10^{-3}$
IH	$\sin^2\theta_{12}$	0.308	$0.308^{+0.013}_{-0.012}$
	$\sin^2\theta_{23}$	0.584	$0.584^{+0.018}_{-0.022}$
	$\sin^2\theta_{13}$	0.0217	0.02175 ± 0.00075

Table 3.5: Model and experimental values of the lepton sector observables, for the normal (NH) and inverted (IH) hierarchy using the best-fit values shown in Tab. 3.4. The experimental values were taken from NuFit 2.2 (2016) [13].

3.1.3 *Scalar Phenomenology*

With the plethora of flavor models on the market, an analysis of the scalar sector, including the mass hierarchies and decay channels, can be the most crucial tool to distinguish between the viable frameworks.

In this section the scalar potential is analyzed with respect to the physical states and their fermion couplings. To this end, the scalar sector is reduced to the low-energy field content, which has the biggest impact on testable FCNCs. As shown in the following, the model can be probed by searches for rare top decays, which have potentially large branching ratios in the model and are weakly constrained by current experimental data.

Since $v_\chi \sim v_\xi \sim v_\zeta \gg v_{\rm SM}$, the low-energy scalar sector consists only of the two Higgs doublets, implying that the scalar degrees of freedom are the same as in any 2HDM. Consequently, we expect two massive charged Higgses ($H^\pm$), one CP-odd Higgs (A^0) and two neutral CP-even Higgs (h, H^0) bosons. The scalar h is identified as the SM-like 126 GeV Higgs boson found at the LHC, while the neutral π^0 and charged $\pi^\pm$ Goldstone bosons are associated with the longitudinal components of the Z and $W^\pm$ gauge bosons, respectively.

The renormalizable scalar potential involving only the $SU(2)$ doublets $\phi_i (i = 1, 2)$ reads

$$\begin{aligned} V(\phi_i) &= -\sum_{i=1}^{2} \mu_i^2 (\phi_i^\dagger \phi_i) + \sum_{i=1}^{2} \kappa_i (\phi_i^\dagger \phi_i)^2 \,, \\ V(\phi_1, \phi_2) &= \gamma_{12} (\phi_1^\dagger \phi_1)(\phi_2^\dagger \phi_2) + \kappa_{12} (\phi_1^\dagger \phi_2)(\phi_2^\dagger \phi_1) \,, \\ V(\xi, \chi, \zeta, \phi_i) &= \left[\lambda_\xi (\xi\xi)_1 + \lambda_\chi (\chi^\dagger \chi) + \lambda_\zeta (\zeta^\dagger \zeta) \right] \sum_{i=1}^{2} \lambda_{1i} (\phi_i^\dagger \phi_i) \,, \end{aligned} \tag{3.29}$$

whereas the remaining terms are

$$\begin{aligned} V(\xi) &= -\mu_\xi^2 (\xi\xi)_1 + \gamma_{\xi,3} (\xi\xi)_2 \xi + \kappa_{\xi,1} (\xi\xi)_1 (\xi\xi)_1 + \kappa_{\xi,2} (\xi\xi)_2 (\xi\xi)_2 \,, \\ V(\chi) &= -\mu_\chi^2 (\chi^\dagger \chi) + \kappa_\chi (\chi^\dagger \chi)^2 \,, \\ V(\zeta) &= -\mu_\zeta^2 (\zeta^\dagger \zeta) + \kappa_\zeta (\zeta^\dagger \zeta)^2 \,, \\ V(\xi, \chi, \zeta) &= \lambda_2 (\xi\xi)_1 (\chi^\dagger \chi) + \lambda_3 (\xi\xi)_1 (\zeta^\dagger \zeta) + \lambda_4 (\zeta^\dagger \zeta)(\chi^\dagger \chi) \,. \end{aligned} \tag{3.30}$$

The high symmetry of the potential leaves an accidental ungauged $U(1)$ intact that results in an additional Goldstone boson, unobserved by experiments. Therefore, to obtain a viable low-energy model with only three massless Goldstone bosons, the following soft-breaking terms are considered

$$\begin{aligned} V_{\text{soft}}(\zeta, \chi) &= -\mu_{\chi\zeta}^2 (\zeta\chi + \zeta^\dagger \chi^\dagger) \,, \\ V_{\text{soft}}(\phi_i, \phi_j) &= -\mu_{12}^2 \left[\left(\phi_1^\dagger \phi_2 \right) + \left(\phi_2^\dagger \phi_1 \right) \right] . \end{aligned} \tag{3.31}$$

The mass matrices of the low-energy CP-even neutral scalars $\rho_{1,2}$, the CP-odd neutral scalars $\eta_{1,2}$, and the charged scalars $\varphi_{1,2}^\pm$ can be written as

$$M_1^\rho = \frac{1}{2} \begin{pmatrix} 2\kappa_1 v_1^2 + \frac{v_2}{v_1} \mu_{12}^2 & \gamma v_1 v_2 - \mu_{12}^2 \\ \gamma v_1 v_2 - \mu_{12}^2 & 2\kappa_2 v_2^2 + \frac{v_1}{v_2} \mu_{12}^2 \end{pmatrix} , \tag{3.32}$$

$$M_2^\eta = \frac{\mu_{12}^2}{2} \begin{pmatrix} \frac{v_2}{v_1} & -1 \\ -1 & \frac{v_1}{v_2} \end{pmatrix} , \tag{3.33}$$

$$M_3^\varphi = \frac{\mu_{12}^2 + \kappa_{12} v_1 v_2}{2} \begin{pmatrix} \frac{v_2}{v_1} & -1 \\ -1 & \frac{v_1}{v_2} \end{pmatrix} . \tag{3.34}$$

According to the typical 2HDM conventions, the physical scalar mass eigenstates are connected with the weak scalar states by the following relations [116, 156]

$$\begin{pmatrix} h \\ H \end{pmatrix} = \begin{pmatrix} \sin\alpha & -\cos\alpha \\ -\cos\alpha & -\sin\alpha \end{pmatrix} \begin{pmatrix} \rho_1 \\ \rho_2 \end{pmatrix} , \tag{3.35}$$

$$\begin{pmatrix} \pi^0 \\ A^0 \end{pmatrix} = \begin{pmatrix} \cos\beta & \sin\beta \\ \sin\beta & -\cos\beta \end{pmatrix} \begin{pmatrix} \eta_1 \\ \eta_2 \end{pmatrix} , \tag{3.36}$$

$$\begin{pmatrix} \pi^\pm \\ H^\pm \end{pmatrix} = \begin{pmatrix} \cos\beta & \sin\beta \\ \sin\beta & -\cos\beta \end{pmatrix} \begin{pmatrix} \varphi_1^\pm \\ \varphi_2^\pm \end{pmatrix} , \tag{3.37}$$

with

$$\tan 2\alpha = \frac{2 \left(\gamma v_1 v_2 - \mu_{12}^2 \right)}{2 \left(\kappa_1 v_1^2 - \kappa_2 v_2^2 \right) + \mu_{12}^2 \left(\frac{v_2}{v_1} - \frac{v_1}{v_2} \right)} , \qquad \tan\beta = \frac{v_2}{v_1} . \tag{3.38}$$

The physical scalar masses are hence given by

$$\begin{aligned} m_h^2 &= \frac{1}{2v_1}\left(\kappa_1 v_1^3 + \kappa_2 v_1 v_2^2 + \mu_{12}^2 v_2\right) \\ &\quad -\frac{1}{2}\sqrt{\gamma^2 v_1^2 v_2^2 - 2\gamma\mu_{12}^2 v_1 v_2 + \kappa_1^2 v_1^4 - 2\kappa_1\kappa_2 v_1^2 v_2^2 + \kappa_2^2 v_2^4 + \mu_{12}^4}\,, \\ m_H^2 &= \frac{1}{2v_1}\left(\kappa_1 v_1^3 + \kappa_2 v_1 v_2^2 + \mu_{12}^2 v_2\right) \\ &\quad +\frac{1}{2}\sqrt{\gamma^2 v_1^2 v_2^2 - 2\gamma\mu_{12}^2 v_1 v_2 + \kappa_1^2 v_1^4 - 2\kappa_1\kappa_2 v_1^2 v_2^2 + \kappa_2^2 v_2^4 + \mu_{12}^4}\,, \\ m_{A^0}^2 &= \frac{\mu_{12}^2}{2}\left(\frac{v_2}{v_1}+\frac{v_1}{v_2}\right), \qquad m_{H^\pm}^2 = \frac{\mu_{12}^2 + \kappa_{12} v_1 v_2}{2}\left(\frac{v_2}{v_1}+\frac{v_1}{v_2}\right), \end{aligned} \tag{3.39}$$

where h corresponds to the SM-like Higgs boson observed at the LHC. In the following section we determine the Yukawa couplings associated with each physical scalar to identify the allowed ranges of α, β, and the scalar masses.

Yukawa couplings and FCNCs

Thanks to the specific shape of the Yukawa couplings dictated by the discrete symmetries, the present model is flavor-conserving in the down-type and charged lepton sectors, which is a special case of Yukawa alignment [117, 157, 158]. The scalar ϕ_2 generates the masses of the first two down-type quark generations, whereas ϕ_1 is responsible only for the bottom Yukawa; conversely, ϕ_2 is associated only with the electron Yukawa, while ϕ_1 generates the masses of the remaining charged leptons. The Yukawa couplings of both scalar doublets are therefore aligned in these sectors. Due to the lack of FCNCs in the down-type sector, the tightly constrained K and B meson oscillations are protected against neutral scalar contributions. Mixing occurs exclusively in the up-type sector, where both ϕ_1 and ϕ_2 couple to the third generation of up-type quarks. Consequently, top quark FCNCs arise that can probe NP since the associated processes are strongly suppressed in the SM. Explicitly, we obtain the following structures for the up- and down-type Yukawas in the scalar and fermion mass bases using the rotation matrices (3.14), (3.20), (2.21) and the corresponding transformations of the right-handed fields:

$$Y_d^h = \begin{pmatrix} y_{dd}^h & y_{ds}^h & y_{db}^h \\ y_{sd}^h & y_{ss}^h & y_{sb}^h \\ y_{bd}^h & y_{bs}^h & y_{bb}^h \end{pmatrix} = \sqrt{2}\begin{pmatrix} -\frac{c_\alpha m_d}{v s_\beta} & 0 & 0 \\ 0 & -\frac{c_\alpha m_s}{v s_\beta} & 0 \\ 0 & 0 & \frac{m_b s_\alpha}{v c_\beta} \end{pmatrix}, \tag{3.40}$$

$$Y_d^H = \begin{pmatrix} y_{dd}^H & y_{ds}^H & y_{db}^H \\ y_{sd}^H & y_{ss}^H & y_{sb}^H \\ y_{bd}^H & y_{bs}^H & y_{bb}^H \end{pmatrix} = \sqrt{2}\begin{pmatrix} -\frac{m_d s_\alpha}{v s_\beta} & 0 & 0 \\ 0 & -\frac{m_s s_\alpha}{v s_\beta} & 0 \\ 0 & 0 & -\frac{c_\alpha m_b}{v c_\beta} \end{pmatrix}, \tag{3.41}$$

$$Y_u^h = \begin{pmatrix} y_{uu}^h & y_{uc}^h & y_{ut}^h \\ y_{cu}^h & y_{cc}^h & y_{ct}^h \\ y_{tu}^h & y_{tc}^h & y_{tt}^h \end{pmatrix} \simeq \sqrt{2}\begin{pmatrix} \frac{m_u s_\alpha}{v c_\beta} & 0 & \frac{m_t}{v} V_{tb} V_{ub}\left(\frac{c_\alpha}{s_\beta}+\frac{s_\alpha}{c_\beta}\right) \\ 0 & \frac{m_c s_\alpha}{v c_\beta} & \frac{m_t}{v} V_{tb} V_{cb}\left(\frac{c_\alpha}{s_\beta}+\frac{s_\alpha}{c_\beta}\right) \\ 0 & 0 & \frac{m_t}{v}\left(V_{tb}^2 \frac{s_\alpha}{c_\beta} - \mathcal{O}(\lambda^4)\right) \end{pmatrix}, \tag{3.42}$$

$$Y_u^H = \begin{pmatrix} y_{uu}^H & y_{uc}^H & y_{ut}^H \\ y_{cu}^H & y_{cc}^H & y_{ct}^H \\ y_{tu}^H & y_{tc}^H & y_{tt}^H \end{pmatrix} \simeq -\sqrt{2}\begin{pmatrix} \frac{c_\alpha m_u}{v c_\beta} & 0 & -\frac{m_t}{v} V_{tb} V_{ub}\left(\frac{s_\alpha}{s_\beta}-\frac{c_\alpha}{c_\beta}\right) \\ 0 & \frac{c_\alpha m_c}{v c_\beta} & -\frac{m_t}{v} V_{tb} V_{cb}\left(\frac{s_\alpha}{s_\beta}-\frac{c_\alpha}{c_\beta}\right) \\ 0 & 0 & \frac{m_t}{v}\left(V_{tb}^2 \frac{c_\alpha}{c_\beta} + \mathcal{O}(\lambda^4)\right) \end{pmatrix}, \tag{3.43}$$

where the V_{ij} denote the CKM matrix elements. Furthermore, the mixing angles α and β are defined in Eq. (2.21). Like in other 2HDMs, the couplings depend crucially on the parameters α and β, but should comply with the current bounds if $\tan\beta$ is neither unnaturally large nor small, in which cases deviations from the bottom and top Yukawa couplings with respect to the SM become very large. This agrees with the previous statement that the fermion mass hierarchies and mixings are best explained by $\tan\beta$ values of $\mathcal{O}(1)$. As explained above, FCNCs are absent in the down-type quark sector since the matrices $Y_d^{h,H}$ do not have off-diagonal entries. The up-type Yukawa couplings $Y_{ut,ct}^{h,H}$, however, allow for the tree-level decays $t \to hq$ ($q = u, c$), whose branching ratios are currently limited by ATLAS to $\mathcal{B}(t \to hq) < 0.79\%$ @ 95% C.L. [159] and by CMS to $\mathcal{B}(t \to hq) < 0.56\%$ @ 95% C.L (observed limit) and $\mathcal{B}(t \to hq) < 0.65^{+0.29}_{-0.19}\%$ (expected limit) [160]. Since $y_{ut}^{h,H}$ is negligibly small compared to $y_{ct}^{h,H}$, we consider only the stronger CMS constraint that can be interpreted as an upper bound on the off-diagonal top Yukawas

$$\sqrt{|y_{ct}^h|^2 + |y_{ct}^h|^2} = \frac{\sqrt{2}m_t}{v}\sqrt{\left|V_{tb}V_{cb}\left(\frac{s_\alpha}{c_\beta} + \frac{c_\alpha}{s_\beta}\right)\right|^2} < 0.14\,, \tag{3.44}$$

which translates to

$$\left|\frac{c_{\alpha-\beta}}{c_\beta s_\beta}\right| \lesssim 3.40\,. \tag{3.45}$$

The $t \to ch$ channel is particularly interesting since its branching ratio $\mathcal{B}(t \to hc)_{\text{SM}} \simeq 10^{-15}$ is extremely suppressed in the SM [159]. As shown in Figs. 3.1 and 3.2, the model predicts branching ratios of $\mathcal{O}(0.01\%)$ in some regions of the α-β plane, which can be probed at future collider experiments searching for flavor-violating top decays.
Recently an analysis of up-type FCNCs in the 2HDM type III has been performed [161] parametrizing the flavor-violating y_{ct}^h coupling as $y_{ct}^h = \frac{1}{v}\lambda_{ct}\sqrt{2m_t m_c}$ according to the Cheng–Sher ansatz [162]. Focusing on the $cc \to tt$ as well as the $t \to cg$ channels, the authors find that λ_{ct} can still take values of up to $10 - 20$ depending on the neutral heavy Higgs mass. With $y_{ct}^h \propto \frac{1}{v}V_{cb}V_{tb}\sqrt{2}m_t$ our model corresponds to $\lambda_{ct} \approx \frac{1}{2}$ and is therefore well below the critical region. Indeed, following the analysis of [163], we find numerically that the loop induced decays $t \to cg$, $t \to c\gamma$ and $t \to cZ$ are several orders of magnitude below the current LHC sensitivity. The respective loop functions were taken from Ref. [163] and are compiled in App. C.1.2. Explicitly, varying the free model parameters α, β, and the scalar masses m_H, m_A and $m_{H^\pm}$, we expect the branching ratios to be approximately

$$\mathcal{B}(t \to cg) \sim \mathcal{O}(10^{-9})\,, \quad \mathcal{B}(t \to c\gamma) \sim \mathcal{O}(10^{-12})\,, \quad \mathcal{B}(t \to cZ) \sim \mathcal{O}(10^{-13})\,, \tag{3.46}$$

which are way below the current upper limits from ATLAS and CMS [164, 165]

$$\mathcal{B}(t \to cg) < 1.6 \times 10^{-4}\,, \qquad \mathcal{B}(t \to c\gamma, cZ) < 5 \times 10^{-4}. \tag{3.47}$$

The largest branching ratio of the three channels in our model, $\mathcal{B}(t \to cg)$, is shown in Fig. 3.3 as a function of α and β for fixed m_H and m_A, as well as for variable m_H and m_A with fixed α and β in Fig. 3.4. As it turns out, the charged Higgs contribution is tiny and does not affect the prediction for any values of $m_{H^\pm}$.

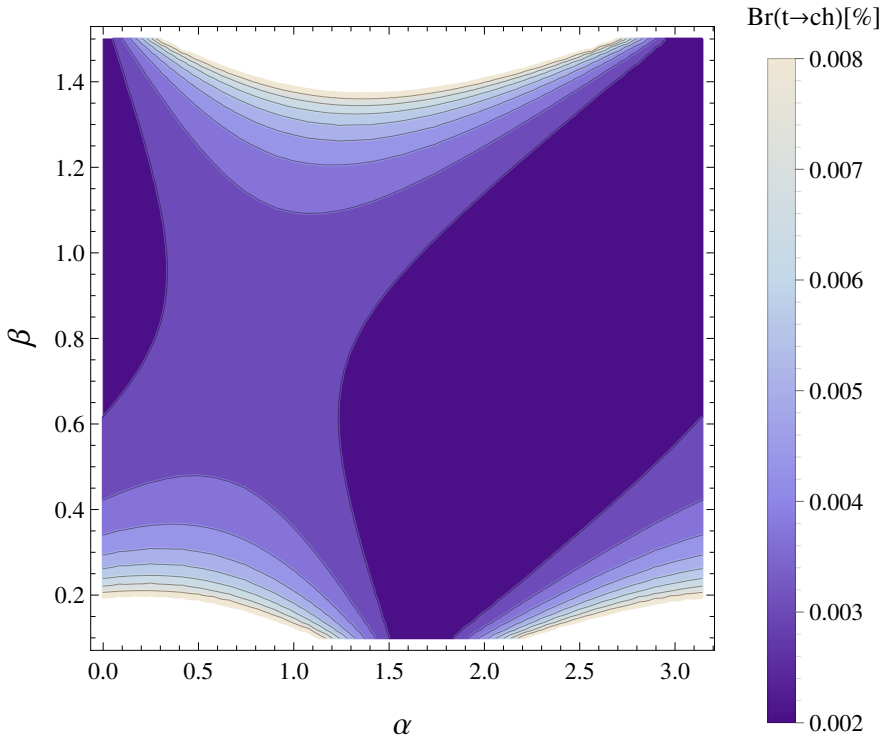

Figure 3.1: $\mathcal{B}(t \to hc)$ [%] shown in the α-β plane. The flavor-violating $y_{ct}^{h,H}$ couplings are enhanced for small β values leading to a potentially large $\mathcal{B}(t \to hc)$ observable at future experiments.

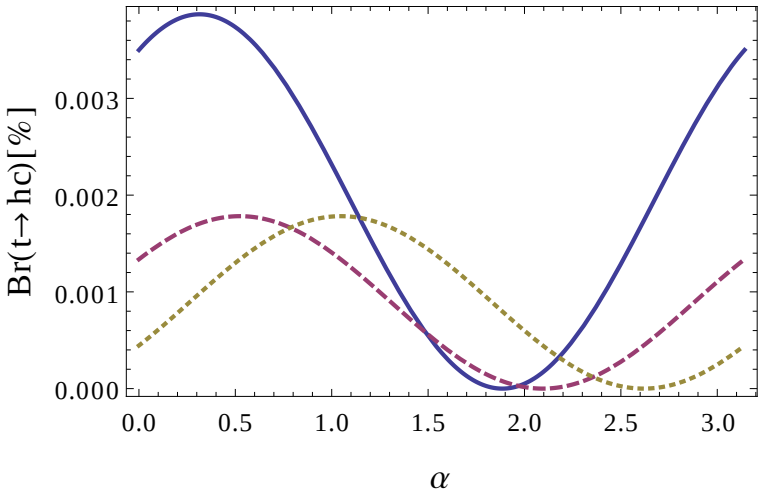

Figure 3.2: $\mathcal{B}(t \to hc)$ [%] shown as a function of α for $\beta = \pi/10$ (blue, solid), $\beta = \pi/6$ (red, dashed) and $\beta = \pi/3$ (yellow, dotted).

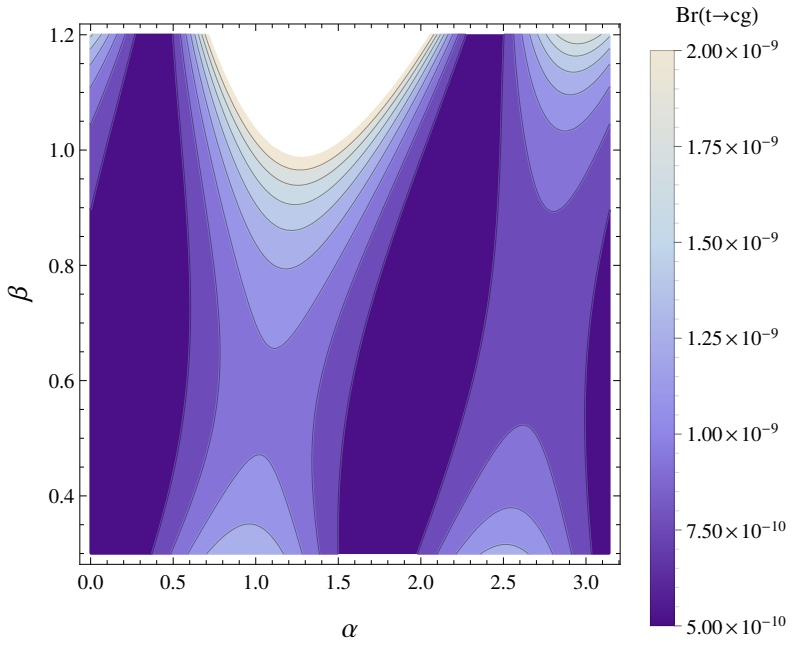

Figure 3.3: $\mathcal{B}(t \to hg)$ depicted in the α-β plane with $m_H = m_A = 500\,\text{GeV}$.

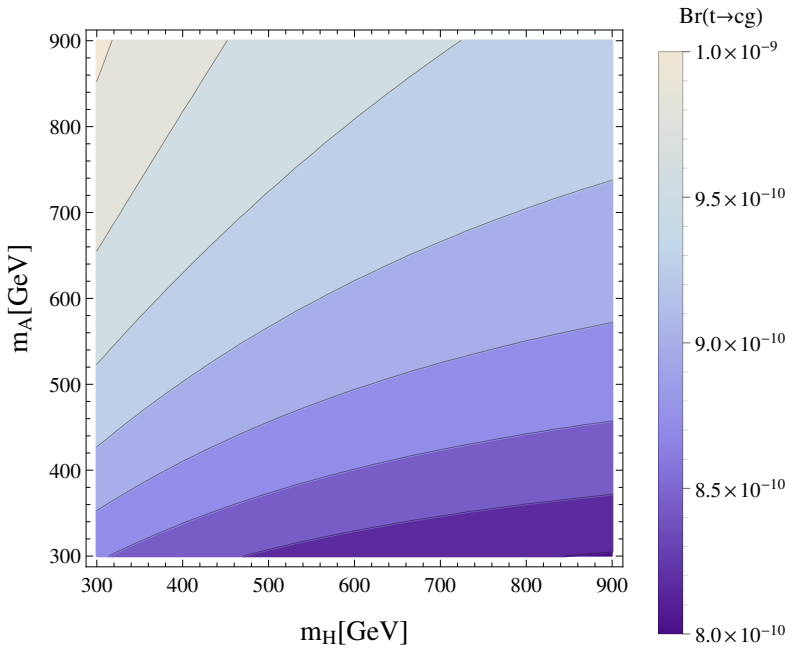

Figure 3.4: $\mathcal{B}(t \to hg)$ shown as a function of m_H and m_A for $\alpha = \pi/3$ and $\beta = \pi/4$. The decay rate is to a large extent independent of the charged Higgs mass $m_{H^\pm}$.

The charged lepton Yukawa matrices

$$Y_l^h = \sqrt{2}\begin{pmatrix} y_{ee}^h & y_{e\mu}^h & y_{e\tau}^h \\ y_{\mu e}^h & y_{\mu\mu}^h & y_{\mu\tau}^h \\ y_{\tau e}^h & y_{\tau\mu}^h & y_{\tau\tau}^h \end{pmatrix} = \sqrt{2}\begin{pmatrix} -\frac{c_\alpha m_e}{v s_\beta} & 0 & 0 \\ 0 & \frac{m_\mu s_\alpha}{v c_\beta} & 0 \\ 0 & 0 & \frac{m_\tau s_\alpha}{v c_\beta} \end{pmatrix}, \tag{3.48}$$

$$Y_l^H = \sqrt{2}\begin{pmatrix} y_{ee}^H & y_{e\mu}^H & y_{e\tau}^H \\ y_{\mu e}^H & y_{\mu\mu}^H & y_{\mu\tau}^H \\ y_{\tau e}^H & y_{\tau\mu}^H & y_{\tau\tau}^H \end{pmatrix} = \sqrt{2}\begin{pmatrix} -\frac{m_e s_\alpha}{v s_\beta} & 0 & 0 \\ 0 & -\frac{c_\alpha m_\mu}{v c_\beta} & 0 \\ 0 & 0 & -\frac{c_\alpha m_\tau}{v c_\beta} \end{pmatrix} \tag{3.49}$$

are also free of FCNCs due to the vanishing off-diagonal Yukawa couplings. Consequently, the $h \to \mu\tau$ channel is SM-like, which is not generally the case in multi-Higgs models with discrete symmetries. An example model with Higgs-mediated flavor violation explaining the $h \to \mu\tau$ anomaly is presented in Sec. 4.1.
Finally, the charged Higgs couplings that are relevant, e.g., for $B_{s,d}^0 - \overline{B}_{s,d}^0$ mixings and the radiative decays $b \to q\gamma$ $(q = s, d)$, are given by

$$Y_L^{H^\pm} = \sqrt{2}\begin{pmatrix} y_{du} & y_{dc} & y_{dt} \\ y_{su} & y_{sc} & y_{st} \\ y_{bu} & y_{bc} & y_{bt} \end{pmatrix} = \sqrt{2}\begin{pmatrix} \frac{V_{ud}}{V_{tb}^2+V_{cb}^2} t_\beta \frac{m_u}{v} & -\frac{V_{us}}{V_{tb}} t_\beta \frac{m_c}{v} & -V_{td}^* \frac{m_t}{v t_\beta} \\ \frac{V_{us}}{V_{tb}^2+V_{cb}^2} t_\beta \frac{m_u}{v} & \frac{V_{ud}}{V_{tb}} t_\beta \frac{m_c}{v} & -V_{ts}^* \frac{m_t}{v t_\beta} \\ 0 & 0 & V_{tb} t_\beta \frac{m_t}{v} \end{pmatrix}, \tag{3.50}$$

$$Y_R^{H^\pm} = \sqrt{2}\begin{pmatrix} y_{ud} & y_{us} & y_{ub} \\ y_{cd} & y_{cs} & y_{cb} \\ y_{td} & y_{ts} & y_{tb} \end{pmatrix} = \sqrt{2}\begin{pmatrix} V_{ud} \frac{m_d}{v t_\beta} & V_{us} \frac{m_s}{v t_\beta} & V_{ub} t_\beta \frac{m_b}{v} \\ V_{cd} \frac{m_d}{v t_\beta} & V_{cs} \frac{m_s}{v t_\beta} & V_{cb} t_\beta \frac{m_b}{v} \\ V_{td} \frac{m_d}{v t_\beta} & V_{ts} \frac{m_s}{v t_\beta} & V_{tb} t_\beta \frac{m_b}{v} \end{pmatrix}, \tag{3.51}$$

$$Y_{H^\pm}^{e\nu} = \frac{\sqrt{2} m_e}{v t_\beta}, \quad Y_{H^\pm}^{\mu\nu} = \frac{\sqrt{2} m_\mu}{v} t_\beta \left(c_{\theta_l} - s_{\theta_l}\right), \quad Y_{H^\pm}^{\tau\nu} = \frac{\sqrt{2} m_\tau}{v} t_\beta \left(c_{\theta_l} + s_{\theta_l}\right). \tag{3.52}$$

The last equation is understood as a sum over the neutrino mass eigenstates, as the neutrino flavor is typically inferred only from the signature of the corresponding charged lepton. The mixing angle θ_l was defined in Eq. (3.20).
The 2HDM type II is disfavored as an explanation of the anomaly observed in $B \to D^{(*)}\tau\nu$ decays [41]. However, flavor-violating 2HDMs provide two operators instead of one to fit the observable. This new operator is represented here by the $Y_L^{H^\pm}$ couplings, the relevant entry y_{bc} being zero. Hence, no deviation from 2HDMs of type II is expected in this channel.
Recently the lower bound $m_{H^\pm} > 480\,\text{GeV}$ at 95% C.L. was derived from $b \to s\gamma$ measurements for the 2HDM type II [32]. This constraint depends on higher-order QCD corrections, therefore, computing the limit in the present framework is beyond the scope of this analysis. Instead we adopt a conservative lower bound of $m_{H^\pm} > 500$ GeV in the following sections.

Constraints from $h \to \gamma\gamma$

In this model the $h \to \gamma\gamma$ decay receives additional contributions from loops with the charged scalars $H^\pm$, as shown in Fig. 3.5, and therefore constrains their masses as well as the mixing angles α and β.

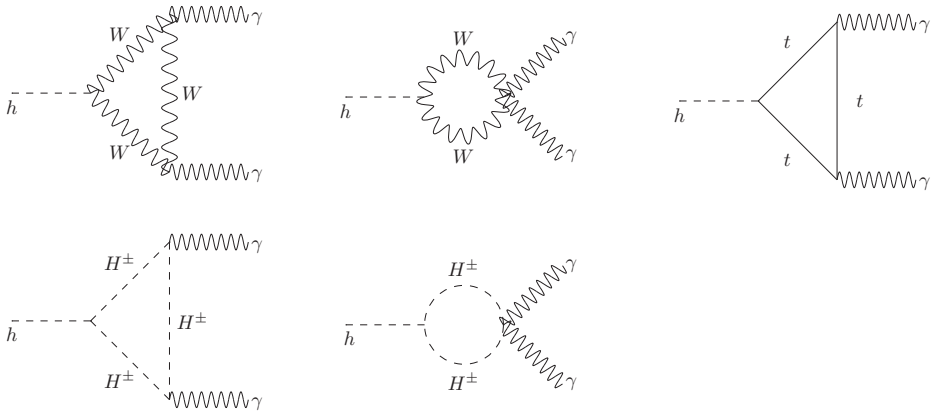

Figure 3.5: One-loop Feynman diagrams in the unitary Gauge contributing to the $h \to \gamma\gamma$ decay.

The explicit form of the $h \to \gamma\gamma$ decay rate is [166]

$$\begin{aligned}\Gamma\left(h \to \gamma\gamma\right) &= \frac{\alpha_{\rm EM}^2 m_h^3}{256\pi^3 v^2} \\ &\times \left| \sum_f a_{hff} N_c Q_f^2 F_{1/2}\left(\varrho_f\right) + a_{hWW} F_1\left(\varrho_W\right) + \frac{\lambda_{hH^\pm H^\mp} v}{2m_{H^\pm}^2} F_0\left(\varrho_{H^\pm}\right) \right|^2 .\end{aligned} \tag{3.53}$$

Here, ϱ_i are the mass ratios $\varrho_i = \frac{m_h^2}{4M_i^2}$, with $M_i = m_f, M_W$, and $m_{H^\pm}$, $\alpha_{\rm EM}$ is the fine structure constant, N_C is the color factor ($N_C = 1$ for leptons, $N_C = 3$ for quarks), and Q_f is the electric charge of the fermion in the loop, which is dominated by the top quark. Furthermore, $\lambda_{hH^\pm H^\mp}$ is the trilinear coupling between the SM-like Higgs and a pair of charged Higgses given by

$$\lambda_{hH^\pm H^\mp} = -\frac{\gamma_{12} + \kappa_{12}}{2} v \sin 2\beta \cos\left(\alpha + \beta\right). \tag{3.54}$$

The factors a_{htt} and a_{hWW} are defined as the $ht\bar{t}$ and the hW^+W^- coupling, respectively, normalized by their SM expressions to measure the deviation from the SM. In terms of α and β they read

$$a_{htt} \simeq \frac{\sin\alpha}{\cos\beta}, \qquad a_{hWW} = \sin\left(\alpha - \beta\right), \tag{3.55}$$

where in a_{htt} we neglected the contribution suppressed by small CKM entries.
The dimensionless loop factors $F_0\left(\varrho\right)$, $F_{1/2}\left(\varrho\right)$, and $F_1\left(\varrho\right)$ for spin-0, spin-1/2 and spin-1 particles in the loop, respectively, are [167, 168]

$$\begin{aligned} F_{1/2}\left(\varrho\right) &= 2\left[\varrho + \left(\varrho - 1\right) f\left(\varrho\right)\right] \varrho^{-2}, \\ F_1\left(\varrho\right) &= -\left[2\varrho^2 + 3\varrho + 3\left(2\varrho - 1\right) f\left(\varrho\right)\right] \varrho^{-2}, \\ F_0\left(\varrho\right) &= -\left[\varrho - f\left(\varrho\right)\right] \varrho^{-2}, \end{aligned} \tag{3.56}$$

with

$$f(\varrho) = \begin{cases} \arcsin^2 \sqrt{\varrho}\,, & \text{for } \varrho \leq 1 \\ -\frac{1}{4}\left[\ln\left(\frac{1+\sqrt{1-\varrho^{-1}}}{1-\sqrt{1-\varrho^{-1}}}\right) - i\pi\right]^2, & \text{for } \varrho > 1\,. \end{cases} \tag{3.57}$$

To determine the bounds imposed on the model by the Higgs diphoton channel, we introduce the ratio $R_{\gamma\gamma}$, which normalizes the $\gamma\gamma$ model prediction relative to the SM expectation

$$R_{\gamma\gamma} = \frac{\sigma(pp \to h)\,\Gamma(h \to \gamma\gamma)}{\sigma(pp \to h)_{\rm SM}\,\Gamma(h \to \gamma\gamma)_{\rm SM}} \simeq a_{htt}^2 \frac{\Gamma(h \to \gamma\gamma)}{\Gamma(h \to \gamma\gamma)_{\rm SM}}\,. \tag{3.58}$$

This ratio has been measured by CMS and ATLAS with the best-fit signals [169, 170]

$$R_{\gamma\gamma}^{\rm CMS} = 1.14^{+0.26}_{-0.23}\,, \qquad \text{and} \qquad R_{\gamma\gamma}^{\rm ATLAS} = 1.17 \pm 0.27\,. \tag{3.59}$$

Fig. 3.6 shows the sensitivity of $R_{\gamma\gamma}$ under variations of the mixing angle α for $m_{H^\pm} = 500$ GeV, $\gamma_{12} + \kappa_{12} = 1$ and different values of β. As the mixing angle β is increased, the range of α consistent with LHC observations of $h \to \gamma\gamma$ moves away from $\pi/2$. On the other hand, the decay rate is largely independent of the charged Higgs mass or the sum of the couplings $\gamma_{12} + \kappa_{12}$, which is consistent with the contribution mediated by charged scalars to the process being a small correction. In fact we checked numerically that it stays almost constant when $m_{H^\pm}$ is varied from 500 GeV to 1 TeV for fixed values of α, β, and the quartic couplings of the scalar potential. For the same values of the charged Higgs mass and quartic couplings, we show in Fig. 3.7 the Z-shaped allowed region in the α-β plane that is consistent with the $h \to \gamma\gamma$ decay rate at the LHC, and overlay it with the relatively weak bound (3.45) that arises from top quark FCNCs.

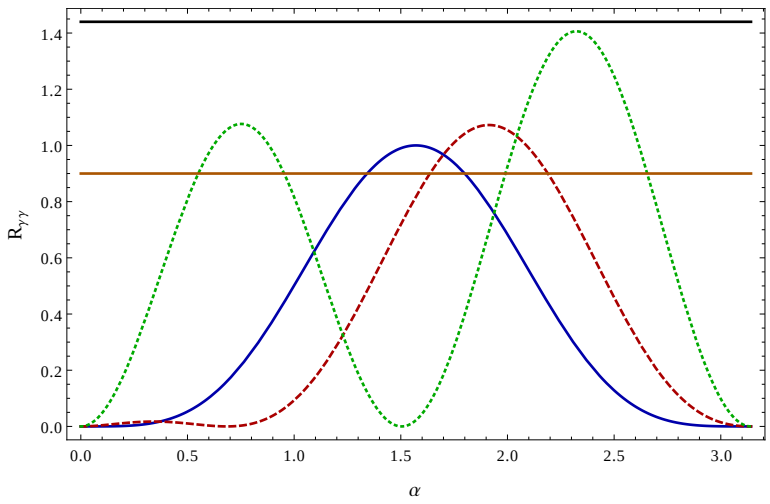

Figure 3.6: The ratio $R_{\gamma\gamma}$ shown as a function of the scalar mixing angle α for $m_{H^\pm} = 500$ GeV, $\gamma_{12} + \kappa_{12} = 1$ and different values of the mixing angle β; the blue, red and green curves correspond to β set to 0, $\frac{\pi}{6}$ and $\frac{\pi}{3}$, respectively, and the horizontal lines are the minimum and maximum values of $R_{\gamma\gamma}$ measured by ATLAS and CMS [169, 170].

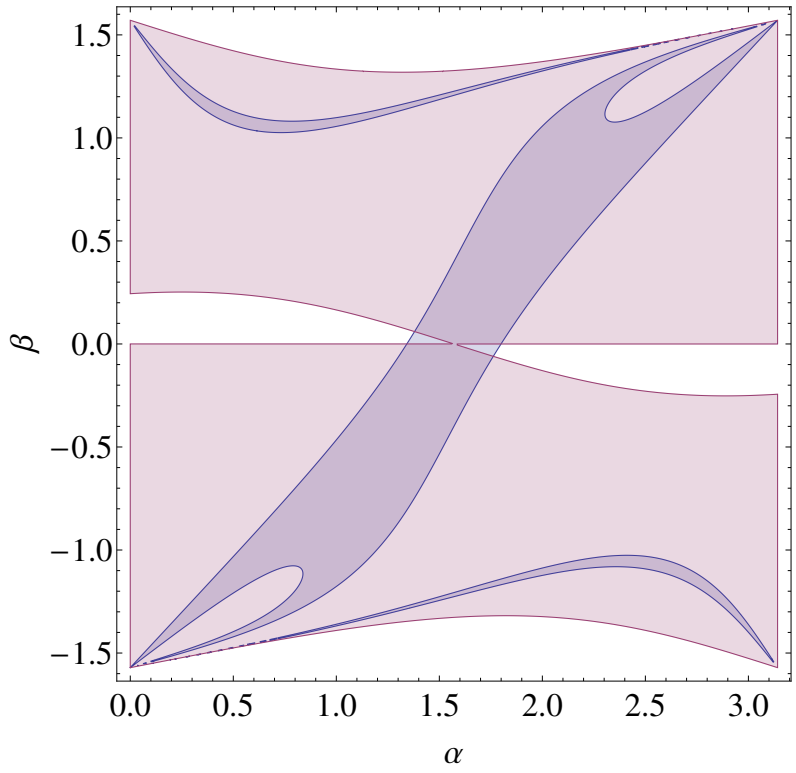

Figure 3.7: The allowed region in the α-β plane consistent with the Higgs diphoton decay rate at the LHC (purple), superimposed with the constraint (3.45) (red).

T and S Parameters

The additional scalars affect the oblique corrections of the SM parametrized in terms of the two well-known quantities T and S, which are measured in high-precision experiments. Consequently, they further confine the parameter space of the model. In this section we calculate one-loop contributions to the oblique parameters T and S defined as [171]

$$T = \left.\frac{\Pi_{33}\left(q^2\right) - \Pi_{11}\left(q^2\right)}{\alpha_{EM}(M_Z) M_W^2}\right|_{q^2=0}, \qquad S = \left.\frac{2\sin 2\theta_W}{\alpha_{EM}(M_Z)} \frac{d\Pi_{30}\left(q^2\right)}{dq^2}\right|_{q^2=0}. \tag{3.60}$$

$\Pi_{11}(0)$, $\Pi_{33}(0)$, and $\Pi_{30}\left(q^2\right)$ are the vacuum polarization amplitudes with the $\{W_\mu^1, W_\mu^1\}$, $\{W_\mu^3, W_\mu^3\}$ and $\{W_\mu^3, B_\mu\}$ external gauge bosons, respectively, where q is their momentum. Note that in the definitions of the T and S parameters, NP contributions are assumed to be heavy compared to M_W and M_Z.

To analyze the deviations from the SM, the T and S parameters are split into an SM and a BSM part $T \equiv T_{\rm SM} + \Delta T$ and $S \equiv S_{\rm SM} + \Delta S$. The reader is referred to App. C.1.3 for the Feynman diagrams contributing to the T and S parameters (Figs. C.1 and C.2) and the respective loop expressions.

The measurements of T and S confine the parameter space to an elliptic region in the ΔS-ΔT plane. These are the contours shown in Fig. 3.8 at 95% C.L., where the origin $\Delta S = \Delta T = 0$ is the SM value with $m_h = 125.5$ GeV and $m_t = 176$ GeV. We study the T and S parameter constraints by considering two benchmark scenarios, while setting $\alpha - \beta = \frac{\pi}{5}$. In the first case the CP-even and CP-odd neutral Higgs bosons are

assumed to have degenerate masses of 500 GeV. In this scenario, the T and S parameters constrain the charged Higgs masses to the range 550 GeV $\leq m_{H^\pm} \leq$ 580 GeV, which is consistent with the lower bound $m_{H^\pm} \gtrsim 500$ GeV obtained from $b \to s\gamma$ [32]. In the second scenario, the charged and CP-even neutral Higgses have degenerate masses of 500 GeV. In this case, the limits are fulfilled if the CP-odd neutral Higgs boson mass m_A^0 lies between 375 GeV and 495 GeV.

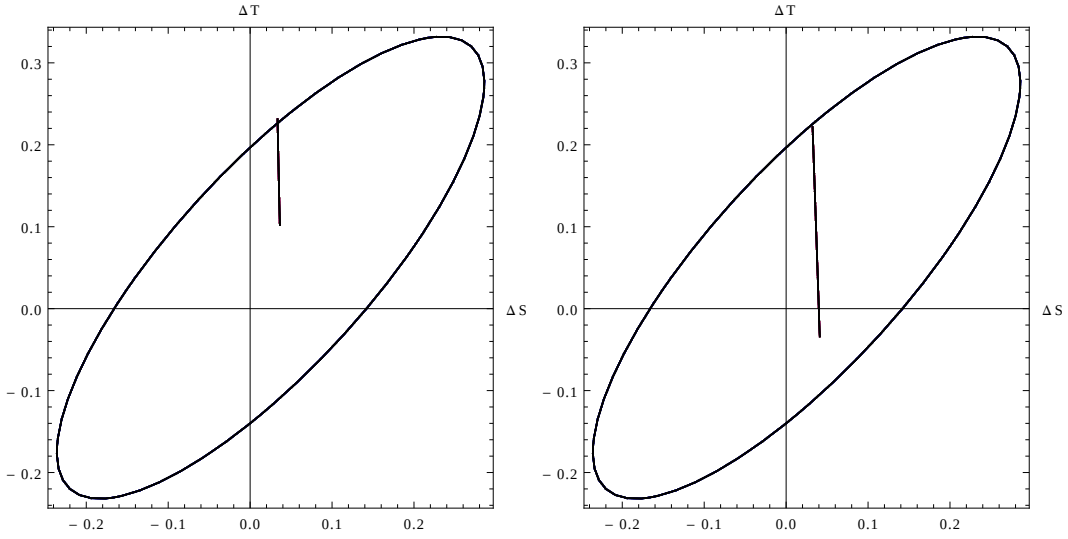

(a) (b)

Figure 3.8: The ΔS-ΔT plane, where the ellipses define the experimentally allowed region at 95% C.L. for $\alpha - \beta = \frac{\pi}{5}$. The figures (a) and (b) correspond to $m_{A^0} = m_{H^0} = 500$ GeV and $m_{H^0} = m_{H^\pm} = 500$ GeV, respectively. The charged Higgs and CP-odd neutral Higgs boson masses vary between 550 GeV $\leq m_{H^\pm} \leq$ 580 GeV (a), 375 GeV $\leq m_{A^0} \leq$ 495 GeV (b). The nearly vertical lines going up towards the ellipses define the values of ΔT and ΔS in our model as the masses are varied in the aforementioned ranges.

3.2 FERMION PHENOMENOLOGY IN AN $SU(5)$ GUT MODEL

GUTs supplemented with global flavor symmetries are a promising setup for a unified description of fermion interactions. This is motivated by the fact that leptons and quarks are part of the same multiplets of the GUT group, which connects their masses and mixings [172,173]. Various GUT models with flavor symmetries have been proposed in the literature to unify the fermion interactions [131–135]. For a general review see for example [121,174].

As pointed out in Sec. 2.3.1, the minimal $SU(5)$ GUT with fermions in the $\bar{\mathbf{5}} + \mathbf{10}$ and the scalars in the $\mathbf{5} + \mathbf{24}$ representations, predicts the wrong fermion mass relations, a short proton life-time, and the gauge unification is in tension with the values of α_S, $\sin\theta_W$, and α_{EM} at the M_Z scale.

Some of these problems can be solved by an extension of the model field content with a scalar $\mathbf{45}$ representation [7,127,130,175–177]. However, this extended $SU(5)$ GUT

fails to shed light on the Yukawa coupling hierarchies. This motivates implementing a generalized FN mechanism [178], where the fermion mass hierarchy is explained by special $U(1)_f$ charge assignments of the SM fermions.
Consequently, we propose an extended version of the $SU(5)$ GUT model with an additional global flavor symmetry $A_4 \times Z_2 \times Z_2' \times Z_2'' \times U(1)_f$. The discrete A_4 and the three different Z_2 symmetries shape the fermion mass and mixing matrices, while the $U(1)_f$ symmetry explains the hierarchies among them by virtue of a generalized FN mechanism [178].
Addressing the flavor problem with an $SU(5)$ GUT requires a significant extension of the scalar sector. The role of each scalar field and the corresponding assignments under the symmetry group of the model are explained in detail in Sec. 3.2.1.
On the other hand, the light neutrino masses are generated using only one right-handed neutrino with a radiative seesaw mechanism. The smallness of the neutrino masses is a consequence of the small one-loop contributions, implying that the TeV scale right-handed neutrino is in LHC reach. For a general discussion on the radiative seesaw in the context of flavor symmetries, the readers are referred to Ref. [179].
The model manages to describe the SM fermion masses and mixings with 14 free effective parameters that reproduce 18 observables, i.e., the nine charged fermion masses, two neutrino mass squared splittings, three lepton mixing angles, and the four CKM parameters. Sec. 3.2.2 contains a comprehensive study of the fermion masses and mixings in the model framework.

3.2.1 *The Model*

Besides the $U(1)_f$ FN symmetry, the model is supplemented with the tetrahedral symmetry A_4, which accommodates the three fermion families naturally in its triplet and three singlet representations. Furthermore, three distinct Z_2 symmetries are utilized to shape the Yukawa interactions and fermion mixing matrices. Their specific role will be clarified in the following paragraphs. The additional flavor symmetries and their function in the model are summarized in Tab. 3.6.

Symmetry	Function
$SU(5)$	Grand unification
A_4	Creates family structure and mixings
$U(1)_f$	Implements FN mechanism
Z_2	Forbids tree-level neutrino masses
Z_2'	Reduces model parameters in scalar potential
Z_2''	Separates down-type from up-type quarks for realistic CKM mixing

Table 3.6: Summary of symmetries and their function in the model.

The complete list of fields with their symmetry group assignments can be found in Tab. 3.7 and is explained as follows. All SM fermions are accommodated in three copies of

Field	$SU(5)$	A_4	Z_2	Z_2'	Z_2''	$U(1)_f$
$\psi = (\psi_1, \psi_2, \psi_3)$	$\overline{\mathbf{5}}$	$\mathbf{3}$	1	1	-1	Q^ψ
Ψ_1, Ψ_2, Ψ_3	$\mathbf{10}$	$\mathbf{1}, \mathbf{1}', \mathbf{1}''$	1	1	1	$Q_1^\Psi, Q_2^\Psi, Q_3^\Psi$
N_R	$\mathbf{1}$	$\mathbf{1}$	-1	1	-1	0
H_1	$\mathbf{5}$	$\mathbf{1}$	1	1	-1	Q_1^H
H_2, H_3, H_4	$\mathbf{5}$	$\mathbf{1}', \mathbf{1}'', \mathbf{1}$	1	1	1	Q_2^H, Q_3^H, Q_4^H
Φ	$\mathbf{45}$	$\mathbf{1}$	1	1	-1	Q^Φ
Σ	$\mathbf{24}$	$\mathbf{1}$	1	-1	1	$-1/2$
$\xi = (\xi_1, \xi_2, \xi_3)$	$\mathbf{1}$	$\mathbf{3}$	1	1	1	Q^ξ
$\chi = (\chi_1, \chi_2, \chi_3)$	$\mathbf{1}$	$\mathbf{3}$	1	-1	1	0
$S = (S_1, S_2, S_3)$	$\mathbf{5}$	$\mathbf{3}$	-1	1	1	Q^S

Table 3.7: Fields and their assignments under the additional symmetries.

the $SU(5)$ representations $\overline{\mathbf{5}}$ and $\mathbf{10}$, as shown in Eq. (2.39). The three quintuplets $\psi = (\psi_1, \psi_2, \psi_3)$ are combined in a triplet representation of A_4, while the three decuplets Ψ_1, Ψ_2, and Ψ_3 are assigned to the three distinct singlets $\mathbf{1}, \mathbf{1}'$, and $\mathbf{1}''$, respectively.

To build Yukawa interactions for the down-type quarks and charged leptons, the scalar sector contains a $\mathbf{5}$-plet H_1, and an A_4 triplet flavon ξ that contracts the A_4 triplet ψ. A total of three $\mathbf{5}$'s, $H_{2,3,4}$ in different A_4 singlets are responsible for the up-type quark masses. The Z_2'' symmetry is used to separate H_1 from $H_{2,3,4}$, which is necessary to generate the nontrivial CKM mixing as demonstrated in Sec. 3.2.2.

Finally, to generate neutrino masses radiatively, two more scalar A_4 triplets are introduced, $\chi = (\chi_1, \chi_2, \chi_3)$ and $S = (S_1, S_2, S_3)$. A Z_2 symmetry is exploited to forbid interactions between S and the SM fermions except the neutrinos. The same Z_2 also prevents S from acquiring a VEV by demanding the Z_2 to be preserved after EW symmetry breaking. As a consequence, the neutrinos do not obtain masses at tree level. The right-handed neutrino N_R is a singlet under A_4 as well as $SU(5)$, which is crucial to construct the necessary Majorana mass term.

Last but not least, the Σ field in the adjoint representation $\mathbf{24}$ simultaneously breaks the $SU(5)$ as well as the $U(1)_f$ symmetry, uniquely connecting the GUT scale with the origin of flavor. The full symmetry $\mathcal{G}$ is hence broken in two subsequent steps

$$\begin{aligned} \mathcal{G} = SU(5) \otimes A_4 \otimes Z_2 \otimes Z_2' \otimes Z_2'' \otimes U(1)_f & \\ \Downarrow \ \langle \Sigma \rangle, \langle \xi \rangle \sim \Lambda_{\text{GUT}} & \\ SU(3)_C \otimes SU(2)_L \otimes U(1)_Y \otimes Z_2 \otimes Z_2'' & \\ \Downarrow \ \langle H_i \rangle, \langle \Phi \rangle \sim \Lambda_{\text{EW}} & \\ SU(3)_C \otimes U(1)_{\text{EM}} \otimes Z_2 \,, & \end{aligned} \tag{3.61}$$

where the first set of symmetries is broken at the GUT scale $\Lambda_{\text{GUT}} \sim 10^{16}$ GeV. The second breaking is induced by the VEVs of H_i and Φ residing at the EW scale. Since it is not decisive for the breaking, the scalar χ may receive its VEV anywhere between these two scales. However, a value around the TeV scale can prove useful for explaining the small neutrino masses and TBM mixing, as will be clarified in Sec. 3.2.2.
The Z_2' symmetry, broken at the GUT scale, forbids terms with odd powers of χ. Besides reducing the number of parameters in the theory, the symmetry thereby selects a favored VEV alignment for χ in the A_4 space, cf. App. C.2.2.
With all these considerations, we find the Yukawa interactions given in App. C.2.1, which are the basis for the discussions of the lepton and quark masses and mixings in Sec. 3.2.2.
The lightest of the physical neutral scalars of $H_{1,2,3,4}$ and Φ should be interpreted as the SM-like 126 GeV Higgs observed at the LHC [5]. The SM Higgs receives its dominant contribution from the CP-even neutral scalar of H_3, which also dominates the top quark mass, as shown in Sec. 3.2.2.
However, considering the large number of scalar representations required to break down the intricate pattern of symmetries, the model is not predictive in the scalar sector. The low-energy effective theory corresponds to an 8HDM with three scalar singlets and one color octet, i.e., the model has a multitude of relatively light neutral scalars. For comparison, the LHC signatures of TeV octet scalars in an $SU(5)$ GUT model extended with the **45** representation are studied in Ref. [180]. Further details on the scalar potential and the VEV alignments are reserved for App. C.2.2.

3.2.2 *Fermion Phenomenology*

Leptons

The charged lepton mass matrix follows from Eq. (C.24) by using the A_4 product rules given in App. B.2,

$$M_l = V_{lL}^{\dagger} \text{diag}\left(m_e, m_\mu, m_\tau\right) , \tag{3.62}$$

with

$$\begin{aligned} m_e &= \frac{v_\xi}{\sqrt{2}\Lambda}(\alpha_1 \kappa^{a_1} v_H^{(1)} - 6\beta_1 \kappa^{b_1} v_\Phi) , \\ m_\mu &= \frac{v_\xi}{\sqrt{2}\Lambda}(\alpha_2 \kappa^{a_2} v_H^{(1)} - 6\beta_2 \kappa^{b_2} v_\Phi) , \\ m_\tau &= \frac{v_\xi}{\sqrt{2}\Lambda}(\alpha_3 \kappa^{a_3} v_H^{(1)} - 6\beta_3 \kappa^{b_3} v_\Phi) , \end{aligned} \tag{3.63}$$

and

$$V_{lL} = \frac{1}{\sqrt{3}} \begin{pmatrix} 1 & 1 & 1 \\ 1 & \omega & \omega^2 \\ 1 & \omega^2 & \omega \end{pmatrix} , \qquad \omega = e^{\frac{2\pi i}{3}} . \tag{3.64}$$

Since α_i and β_i $(i = 1, 2, 3)$ are roughly of the same order of magnitude, and the VEVs $v_H^{(1)}$ and v_Φ are of the order of the EW scale $v \simeq 246$ GeV, the hierarchy of the charged lepton masses is largely explained by their FN charges a_i and b_i (Eq. C.25).
As the scalar S does not acquire a VEV, the neutrino masses are generated only at one-loop level from radiative corrections by S interacting with the scalar χ, as depicted

in Fig. 3.9. These interactions are caused by the quartic terms in the scalar potential

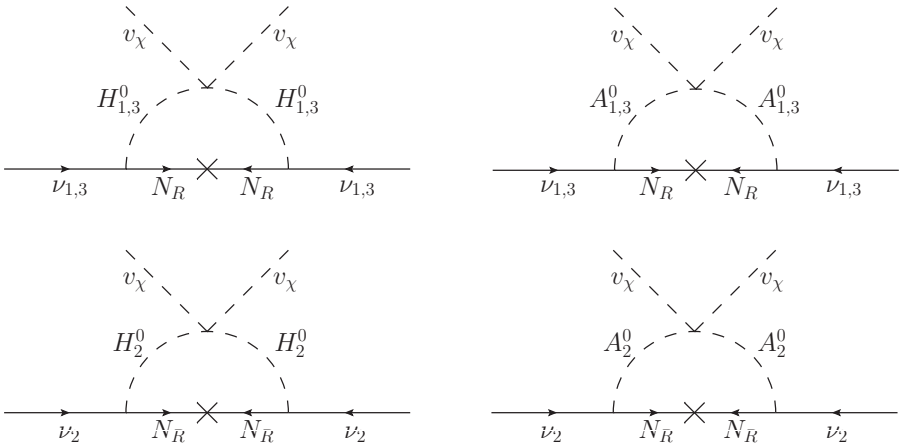

Figure 3.9: One-loop diagrams contributing to the neutrino mass matrix, where H^0_i and A^0_i denote the CP-even and CP-odd neutral components of the scalars S_i.

(assuming $v_\chi \gg v$)

$$\begin{aligned} V(S,\chi) = {} & \lambda_1^{(S\chi)} \left(S_l S^l\right)_{\mathbf{1}} (\chi\chi)_{\mathbf{1}} + \lambda_3^{(S\chi)} \left(S_l S^l\right)_{\mathbf{3s}} (\chi\chi)_{\mathbf{3s}} \\ & + \lambda_2^{(S\chi)} \left[\left(S_l S^l\right)_{\mathbf{1'}} (\chi\chi)_{\mathbf{1''}} + \left(S_l S^l\right)_{\mathbf{1''}} (\chi\chi)_{\mathbf{1'}}\right] \\ & + \lambda_4^{(S\chi)} \left[e^{i\frac{\pi}{2}} \left(S_l S^l\right)_{\mathbf{3a}} (\chi\chi)_{\mathbf{3s}} + \text{h.c.}\right], \end{aligned} \tag{3.65}$$

where the subscripts $\mathbf{1}, \mathbf{1'}, \mathbf{1''}, \mathbf{3a}$, and $\mathbf{3s}$ refer to the respective projection on the component of the products.
For simplicity, the quartic couplings are assumed to be nearly universal, i.e.,

$$\lambda = \lambda_2^{(S\chi)} = \lambda_3^{(S\chi)} = \lambda_1^{(S\chi)} - \varepsilon\,, \tag{3.66}$$

where the deviation from universality is measured by the parameter ϵ. A nonzero value of ϵ is necessary to generate the two mass squared differences, resulting in the neutrino mass matrix [112]

$$M_\nu \simeq \begin{pmatrix} Ae^{2i\psi} & 0 & A \\ 0 & B & 0 \\ A & 0 & Ae^{-2i\psi} \end{pmatrix}, \tag{3.67}$$

with

$$\begin{aligned} A \simeq {} & \frac{y_\nu^2}{16\pi^2 M_N} \left\{ \left(M^2_{A^0_1} - M^2_{A^0_2} + \frac{\varepsilon v_\chi^2}{2}\right) \left[D_0\left(\frac{M_{H^0_1}}{M_N}\right) - D_0\left(\frac{M_{A^0_1}}{M_N}\right)\right] \right. \\ & \left. + \left(M^2_{A^0_3} - M^2_{A^0_2} + \frac{\varepsilon v_\chi^2}{2}\right) \left[D_0\left(\frac{M_{A^0_3}}{M_N}\right) - D_0\left(\frac{M_{H^0_3}}{M_N}\right)\right] \right\}, \\ B \simeq {} & \frac{\varepsilon y_\nu^2 v_\chi^2}{16\pi^2 M_N} \left[D_0\left(\frac{M_{H^0_2}}{M_N}\right) - D_0\left(\frac{M_{A^0_2}}{M_N}\right)\right], \end{aligned} \tag{3.68}$$

and

$$\tan 2\psi \simeq \left[\frac{9}{4}\left(\frac{M_{A_3^0}^2 - M_{A_1^0}^2}{M_{A_3^0}^2 + M_{A_1^0}^2 - 2M_{A_2^0}^2}\right)^2 - 1\right]^{-1/2}, \tag{3.69}$$

where $M_{H_i^0}$ and $M_{A_i^0}$ $(i = 1, 2, 3)$ are the masses of the CP-even and CP-odd neutral components of the $SU(2)$ doublets S_i. The function $D_0(x)$ is defined as [181]

$$D_0(x) \equiv \frac{-1 + x^2 - \ln x^2}{(1 - x^2)^2}. \tag{3.70}$$

The neutrino mass matrix depends on the three effective parameters A, B and ψ, which are different combinations of the model parameters. To obtain two massive neutrinos, the parameters A and B must be nonzero, implying $\epsilon \neq 0$, and $m_{A_i} \neq m_{H_i}$. While the masses are determined solely by A and B, the PMNS matrix is fixed by the parameter ψ, as will be shown below.

The complex symmetric Majorana matrix M_ν is diagonalized by a unitary rotation of the form

$$\begin{aligned} V_\nu &= \begin{pmatrix} \cos\theta & 0 & \sin\theta e^{-i\phi} \\ 0 & 1 & 0 \\ -\sin\theta e^{i\phi} & 0 & \cos\theta \end{pmatrix} P_\nu, \quad \text{with} \\ P_\nu &= \operatorname{diag}\left(e^{i\alpha_1/2}, e^{i\alpha_2/2}, e^{i\alpha_3/2}\right), \quad \theta = \pm\frac{\pi}{4}, \quad \text{and} \quad \phi = -2\psi, \end{aligned} \tag{3.71}$$

where $\alpha_i (i = 1, 2, 3)$ are the Majorana phases. The system has two solutions $\theta = \pm\frac{\pi}{4}$, which are shown in Tab. 3.8, where the positive and negative solution correspond to NH and IH, respectively.

Hierarchy	θ	m_{ν_1}	m_{ν_2}	m_{ν_3}	α_1	α_2	α_3
NH	$\pi/4$	0	B	$2A$	0	0	ϕ
IH	$-\pi/4$	$2A$	B	0	$-\phi$	0	0

Table 3.8: Correlation between the model parameters and observables in the NH and IH case.

With V_{lL} [Eq. (3.64)] and V_ν [Eq. (3.71)], we can determine the PMNS matrix

$$U = V_{lL}^\dagger V_\nu \simeq \begin{pmatrix} \frac{\cos\theta}{\sqrt{3}} - \frac{e^{i\phi}\sin\theta}{\sqrt{3}} & \frac{1}{\sqrt{3}} & \frac{\cos\theta}{\sqrt{3}} + \frac{e^{-i\phi}\sin\theta}{\sqrt{3}} \\ \frac{\cos\theta}{\sqrt{3}} - \frac{e^{i\phi + \frac{2i\pi}{3}}\sin\theta}{\sqrt{3}} & \frac{e^{-\frac{2i\pi}{3}}}{\sqrt{3}} & \frac{e^{\frac{2i\pi}{3}}\cos\theta}{\sqrt{3}} + \frac{e^{-i\phi}\sin\theta}{\sqrt{3}} \\ \frac{\cos\theta}{\sqrt{3}} - \frac{e^{i\phi - \frac{2i\pi}{3}}\sin\theta}{\sqrt{3}} & \frac{e^{\frac{2i\pi}{3}}}{\sqrt{3}} & \frac{e^{-\frac{2i\pi}{3}}\cos\theta}{\sqrt{3}} + \frac{e^{-i\phi}\sin\theta}{\sqrt{3}} \end{pmatrix} P_\nu. \tag{3.72}$$

The mixing angles can be derived by comparing with the standard parametrization [6]

$$\begin{aligned}
\sin^2\theta_{12} &= \frac{|U_{e2}|^2}{1-|U_{e3}|^2} = \frac{1}{2\mp\cos\phi}\,,\\
\sin^2\theta_{13} &= |U_{e3}|^2 = \frac{1}{3}(1\pm\cos\phi)\,,\\
\sin^2\theta_{23} &= \frac{|U_{\mu 3}|^2}{1-|U_{e3}|^2} = \frac{2\mp(\cos\phi+\sqrt{3}\sin\phi)}{4\mp 2\cos\phi},
\end{aligned} \tag{3.73}$$

where the upper sign corresponds to NH ($\theta = +\pi/4$) and the lower one to IH ($\theta = -\pi/4$). Note that TBM mixing is best produced for $\phi = 0$ (IH) and $\phi = \pi$ (NH). Since $\theta = \pm\frac{\pi}{4}$, the Jarlskog invariant and the δ CP phase vanish in these limits

$$J = \mathrm{Im}\left(U_{e1}U_{\mu 2}U_{e2}^*U_{\mu 1}^*\right) \simeq -\frac{1}{6\sqrt{3}}\cos 2\theta = 0\,, \tag{3.74}$$

$$\sin\delta = \frac{8J}{\cos\theta_{13}\sin 2\theta_{12}\sin 2\theta_{23}\sin 2\theta_{13}} = 0\,. \tag{3.75}$$

The TBM ansatz is, however, only a first approximation to explain the actual data. Hence, in the following we adjust the free parameters of the model to reproduce the measurements given in Tabs. A.2, and A.5. It is noteworthy that, while A and B control the two mass splittings $\Delta m^2_{\mathrm{sol}}$ and $\Delta m^2_{\mathrm{atm}}$, only a single parameter ϕ determines all three neutrino mixing parameters $\sin^2\theta_{13}$, $\sin^2\theta_{12}$ and $\sin^2\theta_{23}$ as well as the Majorana phases α_i. Using the experimental values from Tabs. A.2, and A.5, we obtain the best-fit results shown in Tab. 3.9 for NH and IH. The mixing angles θ_{13} and θ_{23} are in good agreement with the data, while θ_{12} is within the $3\,\sigma$ range of its best-fit value. The deviation is reasonable given that no fine-tuned couplings or large dimensionful parameters were required to fit the observables.

Hierarchy	m_{ν_1}	m_{ν_2}	m_{ν_3}	$\sin^2\theta_{12}$	$\sin^2\theta_{23}$	$\sin^2\theta_{13}$	ϕ
NH	0 meV	9 meV	51 meV	0.341	0.396	0.0214	-0.115π
IH	49 meV	50 meV	0 meV	0.341	0.605	0.0216	0.115π

Table 3.9: Approximate best-fit values of the observables in the neutrino sector.

With the values derived from neutrino oscillations, we can also predict the amplitude for $0\nu\beta\beta$ decay, which is proportional to the effective Majorana neutrino mass $m_{\beta\beta}$ [Eq. (1.30)]

$$m_{\beta\beta} = \frac{1}{3}\left(B + 4A\cos^2\frac{\phi}{2}\right) = \begin{cases} 4\text{ meV} & \text{(NH)} \\ 50\text{ meV} & \text{(IH)} \end{cases}. \tag{3.76}$$

By comparing with the current limits on ^{76}Ge and ^{136}Xe, provided by GERDA and KamLAND-Zen, respectively [cf. Eqs. (1.31) and (1.32)], we conclude that this prediction is beyond the reach of the present and forthcoming $0\nu\beta\beta$ decay experiments. Considering the proposals for ton-scale next-to-next generation $0\nu\beta\beta$ experiments with ^{136}Xe [182] and ^{76}Ge [183,184] claiming sensitivities over $T^{0\nu\beta\beta}_{1/2} \sim 10^{27}$ yr, corresponding to $m_{\beta\beta} \sim 12 - 30$ meV, our estimate for $T^{0\nu\beta\beta}_{1/2}$ may be probed at next-to-next generation $0\nu\beta\beta$ experiments.

Quarks

The Yukawa Lagrangian in App. C.2.1 gives rise to the following quark mass matrices:

$$M_U = \begin{pmatrix} C & F & G \\ F & D & H \\ G & H & E \end{pmatrix}, \tag{3.77}$$

with

$$\begin{aligned} F &= 2\left(\gamma_{12}+\gamma_{21}\right)\kappa^{x_{12}} v_H^{(3)}, & D &= 4\gamma_{22}\kappa^{x_{22}} v_H^{(2)}, \\ G &= 2\left(\gamma_{13}+\gamma_{31}\right)\kappa^{x_{13}} v_H^{(2)}, & C &= 4\gamma_{11}\kappa^{x_{11}} v_H^{(4)}, \\ H &= 2\left(\gamma_{23}+\gamma_{32}\right)\kappa^{x_{23}} v_H^{(4)}, & E &= 4\gamma_{33}\kappa^{x_{33}} v_H^{(3)}, \end{aligned} \tag{3.78}$$

for the up-type quarks, and

$$M_D = \mathrm{diag}\left(m_d, m_s, m_b\right)\left(V_{lL}^{\dagger}\right)^T, \tag{3.79}$$

with

$$\begin{aligned} m_d &= \frac{v_\xi}{\sqrt{2}\Lambda}\left(\alpha_1\kappa^{a_1} v_H^{(1)} + 2\beta_1\kappa^{b_1} v_\Phi\right), \\ m_s &= \frac{v_\xi}{\sqrt{2}\Lambda}\left(\alpha_2\kappa^{a_2} v_H^{(1)} + 2\beta_2\kappa^{b_2} v_\Phi\right), \\ m_b &= \frac{v_\xi}{\sqrt{2}\Lambda}\left(\alpha_3\kappa^{a_3} v_H^{(1)} + 2\beta_3\kappa^{b_3} v_\Phi\right), \end{aligned} \tag{3.80}$$

for the down-type quarks.
In analogy to the lepton sector the dimensionless couplings $\alpha_i, \beta_i, \gamma_{ij} (i,j=1,2,3)$ are roughly of the same order of magnitude, with the VEVs $v_H^{(h)} (h=1,2,3,4)$ and v_Φ residing at the EW scale $v \simeq 246\,\mathrm{GeV}$. Then, the hierarchy among the quark masses can again be explained by the different combinations of $U(1)_f$ charges shown in Eq. (C.25). For the down-type quarks this hierarchy is approximately described by

$$m_d : m_s : m_b \approx \lambda^4 : \lambda^2 : 1\,, \qquad m_b \approx \lambda^3 m_t\,, \tag{3.81}$$

which can be reproduced using the values

$$a_1 = b_1 = 6\,, \quad a_2 = b_2 = 4\,, \quad a_3 = b_3 = 2\,, \quad v_H^{(1)} \sim v_\Phi \sim \frac{v}{\sqrt{2}}\,, \tag{3.82}$$

and $v_\xi = \lambda\Lambda$. Furthermore, setting

$$\beta_1 = \beta_3 = -\beta_2, \tag{3.83}$$

we assume that the Yukawa couplings are approximately equal to reduce the number of free parameters. The down-type quarks and charged lepton masses are then determined by the four dimensionless parameters α_1, α_2, α_3, β_1. We fit these parameters to reproduce the masses of the down-type quarks and charged leptons at the M_Z scale. For the best-fit values

$$\alpha_1 = 1.36\,, \quad \alpha_2 = 2.06\,, \quad \alpha_3 = 3.77\,, \quad \beta_1 = 0.18\,, \tag{3.84}$$

Observable	Model	Measurement ($\pm 1\,\sigma$)
m_d [MeV]	2.91	$2.9^{+0.5}_{-0.4}$
m_s [MeV]	57.1	$57.7^{+16.8}_{-15.7}$
m_b [GeV]	2.73	$2.82^{+0.09}_{-0.04}$
m_e [MeV]	0.487	0.487
m_μ [MeV]	102.8	102.8
m_τ [GeV]	1.75	1.75

Table 3.10: Best-fit values of the down-type quark and charged lepton masses compared with the measurements at the M_Z scale. The experimental values were taken from Ref. [155].

we obtain the results shown in Tab. 3.10, which are in good agreement with the measurements.
The rotation matrices V_U and V_D entering the CKM matrix $V_{\text{CKM}} = V_U^\dagger V_D$ can be derived from

$$V_U^\dagger M_U M_U^\dagger V_U = \text{diag}\left(m_u^2, m_c^2, m_t^2\right) , \quad V_D^\dagger M_D M_D^\dagger V_D = \text{diag}\left(m_d^2, m_s^2, m_b^2\right) . \tag{3.85}$$

We immediately conclude $V_D = 1_{3\times 3}$, since

$$M_D M_D^\dagger = \text{diag}\left(m_d^2, m_s^2, m_b^2\right) , \tag{3.86}$$

following from Eq. (3.79). Consequently, the CKM matrix is solely determined by the up-type quark sector.
Instead of computing V_U, which is analytically challenging, we exploit this special property of the model to relate $M_U M_U^\dagger$ directly to the CKM matrix. This can be accomplished by using

$$\begin{aligned} M_U M_U^\dagger &= V_{\text{CKM}}^\dagger \text{diag}\left(m_u^2, m_c^2, m_t^2\right) V_{\text{CKM}} \\ &\simeq m_t^2 \begin{pmatrix} |V_{td}|^2 & V_{td}^\dagger V_{ts} & V_{td}^\dagger V_{tb} \\ V_{ts}^\dagger V_{td} & |V_{ts}|^2 & V_{ts}^\dagger V_{tb} \\ V_{tb}^\dagger V_{td} & V_{tb}^\dagger V_{ts} & |V_{tb}|^2 \end{pmatrix} , \end{aligned} \tag{3.87}$$

and by comparing this result with $M_U M_U^\dagger$ expressed in terms of the model parameters. The details of this computation are shown in App. C.2.3. The results of the fit to the Wolfenstein parametrization of the CKM matrix (Eq. [C.38)] are listed in Tab. 3.11 and are compared with the experimental values taken from Refs. [6,155] at the M_Z scale. All observables are in excellent agreement with the measurements, except for m_u, and m_c, which reproduce the corresponding experimental values only with order-of-magnitude accuracy.

Observable	Model value	Experiment ($\pm 3\,\sigma$)
m_u [MeV]	5.4	$1.45^{+0.56}_{-0.45}$
m_c [MeV]	284	635 ± 86
m_t [GeV]	173.4	$172.1 \pm 0.6 \pm 0.9$
$\lvert V_{ud}\rvert$	0.974	$0.97425^{+0.00022}_{-0.00023}$
$\lvert V_{us}\rvert$	0.225	$0.22542^{+0.00101}_{-0.00097}$
$\lvert V_{ub}\rvert$	0.00348	$0.00371^{+0.00027}_{-0.00020}$
$\lvert V_{cd}\rvert$	0.225	$0.22529^{+0.00100}_{-0.00090}$
$\lvert V_{cs}\rvert$	0.973	$0.97339^{+0.00024}_{-0.00024}$
$\lvert V_{cb}\rvert$	0.0422	$0.04180^{+0.00097}_{-0.00164}$
$\lvert V_{td}\rvert$	0.00872	$0.00868^{+0.00027}_{-0.00058}$
$\lvert V_{ts}\rvert$	0.0415	$0.04107^{+0.00094}_{-0.00161}$
$\lvert V_{tb}\rvert$	0.999	$0.99912^{+0.00007}_{-0.00004}$
J	2.95×10^{-5}	$(2.96^{+0.20}_{-0.16}) \times 10^{-5}$
δ	66°	68°

Table 3.11: Model values and the corresponding measurements of the up-type quark masses and CKM parameters at the M_Z scale. Experimental values taken from Refs. [6, 185].

3.3 CONCLUSIONS

To shed light on the flavor puzzle, we have constructed two flavor models utilizing discrete family symmetries and extended scalar sectors: a two-Higgs doublet extension of the SM based on an S_3 flavor symmetry and an extended $SU(5)$ GUT model.
Overall, the models can fit the observed masses, CKM and PMNS mixing angles very well. The S_3 model has in total 17 effective free parameters, which are fitted to reproduce the 18 observables in the quark and lepton sectors. One neutrino is predicted to be massless in both NH and IH. Consequently, the effective Majorana neutrino mass, relevant for $0\nu\beta\beta$ decay, is beyond the reach of next generation $0\nu\beta\beta$ decay experiments. The additional scalars mediate FCNCs, but due to the specific shape of the Yukawa couplings dictated by the flavor symmetry these processes occur only in the up-type quark sector. Furthermore, the enlarged field content of the model is constrained by both rare top decays and the $h \to \gamma\gamma$ rate, which deviate from the SM prediction. Among the flavor-violating top decays, $t \to ch$ is a particularly promising channel for NP searches as its branching ratio can reach $\mathcal{O}(0.01\%)$ in our model. With respect to $h \to \gamma\gamma$, the dominant top quark and vector boson contributions allow for additional constraints on the mixing angles α and β that are much stronger than the limits from up-type quark FCNCs. In conclusion, the analysis of the scalar sector has revealed

distinct features of the model that can be probed at future collider experiments and set it apart from the various other flavor models.
To make the minimal $SU(5)$ framework phenomenologically viable, a multitude of scalar fields and additional symmetries were employed, which address also the issue of proton decay. A special feature of the model is that the same representation that breaks the $SU(5)$ symmetry is also responsible for the fermion mass hierarchies.
The model uses only 14 effective parameters to fit 18 observables from the distinct fermion sectors, and the solution is not fine-tuned. The lepton sector is particularly elegant since the PMNS matrix is reproduced by varying only one parameter.
However, considering that one of the main incentives to study GUTs is to simplify the SM gauge groups and fields, the model is highly intricate. Because of the large scalar sector, a thorough analysis of the scalar phenomenology is impossible due to the many free parameters in the potential.

4

MODELS EXPLAINING FLAVOR ANOMALIES

As pointed out in Sec. 1.2.3, any observation of CLFV is a smoking gun of NP that is generally realized by virtue of new particles and symmetries. It is therefore imperative not only to search for CLFV, but also to study models extensively for flavor-violating predictions. Indeed, many flavor models resort to extended scalar sectors combined with additional symmetries to explain the origin of flavor. It is reasonable to assume that the same NP is responsible for the flavor violation reported in multiple observables over the past years. The anomalies in $R_K, R_{D^{(*)}}$, and $h \to \mu\tau$ indicating either lepton nonuniversality, flavor violation, or both, have received a lot of attention in particular, see, e.g., Refs [92, 186–191].

In this chapter we build explicit models aimed at explaining the observed anomalies from a bottom-up approach and explore whether the measurements could have a common origin.

The large amount of flavor violation reported by CMS in $h \to \mu\tau$ calls for NP at the EW scale, which is most easily realized by a multi-Higgs model. Such frameworks face tight constraints from rare flavor decays that can be utilized to confine the Higgs parameter space. A possible solution based on an S_4-symmetric 3HDM is presented in Sec. 4.1.

The deviations in the B meson sector, R_K and $R_{D^{(*)}}$, can both be explained with NP at the TeV scale, suggesting that the anomalies have a common source. Viable candidates studied by many authors include leptoquark mediators. In this chapter we show that the same leptoquarks can also generate naturally-small neutrino masses through a $\Delta L = 2$ coupling to the SM Higgs boson. Before delving into leptoquark frameworks combining R_K, $R_{D^{(*)}}$ and neutrino masses in Sec. 4.3, we study in Sec. 4.2 if the ratio $R_{D^{(*)}}$ could also be accommodated by 3HDMs. We conclude the analyses in Sec. 4.4.

4.1 FLAVOR-VIOLATING HIGGS DECAYS IN S_4

LFV Higgs decays have been advocated as a harbinger of flavor symmetries explaining the large amount of lepton flavor mixing [192–195]. Indeed, substantial LFV Higgs couplings can arise naturally in such models as a consequence of the maximal atmospheric $\mu - \tau$ mixing in the PMNS matrix. To manifest itself in the physical mass basis, a misalignment of the Higgs doublets, typically utilized to yield a realistic symmetry breaking pattern, is necessary. While the scalar sector in Refs. [192–195] decomposes into an SM-like Higgs doublet and new exotic scalars experiencing LFV decays, in the following we present an S_4 flavor model where these states mix, resulting in sizable LFV decays of the SM-like Higgs boson. This is particularly interesting after the recent

report by the CMS Collaboration of a $2.4\,\sigma$ anomaly in the $h \to \mu\tau$ channel with a best fit of $\mathcal{B}(h \to \mu\tau) \approx 0.84\%$ [70].

The S_4 symmetry, chosen as the basis of this model, naturally reproduces the TBM mixing scheme [106–108]. This makes the group the ideal starting point for a realistic description of leptons in particular. To evade bounds from the tightly constrained radiative decays $l_\alpha \to l_\beta\gamma$, we consider the special case in which S_4 is broken down to a residual Z_3 subgroup. In the literature this case has also been referred to as LFT, e.g., in the context of the symmetry groups A_4, T_7, and $\Delta(27)$ [193]. The discrete Z_3 symmetry is obtained when scalar doublets in the irreducible triplet representation $\mathbf{3'}$ of S_4 are aligned as $(1,1,1)$ in the S_4 space [109]. To explain LFV Higgs decays by virtue of scalar mixing, we consider perturbations caused by other S_4 triplets that eventually break the Z_3 symmetry. These additional scalars arise if the framework is extended to quarks and neutrinos.

The large LFV Yukawa couplings required to explain $h \to \mu\tau$ are in tension with the limits from rare lepton decays such as $\tau \to \mu\gamma$, $\tau \to e\mu$, and also $\mu \to e\gamma$. To find a possible solution, we search the Higgs parameter space for a window where $|y_{\mu\tau}|^2 + |y_{\tau\mu}|^2$ is large enough to accommodate the $h \to \mu\tau$ CMS report and respects the radiative decay bounds at the same time.

The section is structured as follows. We introduce the concept of LFT in Sec. 4.1.1, which is followed by an explicit model with realistic fermion masses and mixings in Sec. 4.1.2. The breaking of LFT and its consequences for LFV Higgs decays with focus on $h \to \mu\tau$ are analyzed in Sec. 4.1.3.

Some technical details are relocated to the appendix, including the discussion of the quark sector (App. C.3.1), the consequences of the breaking on the lepton mixing (App. C.3.2), and the loop expressions to compute precision observables (App. C.3.4).

4.1.1 *Lepton Flavor Triality*

The notion of LFT was first introduced in Ref. [122], inspired by the success of flavor symmetries in reproducing the approximate TBM mixing in the lepton sector. Accommodating the data (before $\theta_{13} \neq 0$) was easiest accomplished by embedding the lepton fields in the A_4 tetrahedral symmetry such that A_4 is broken down to Z_3 in the charged lepton sector, and to Z_2 in the neutrino sector [89, 90]. The residual Z_3 symmetry can be used to test the A_4 flavor model through its specific predictions for charged lepton decays.

A typical feature of the TBM flavor models is the unique structure of the charged lepton mass matrix M_l, revealing that the mass eigenstates are also distinct Z_3 eigenstates[1]

$$M_l = v\frac{1}{\sqrt{3}}\begin{pmatrix} 1 & 1 & 1 \\ 1 & \omega^2 & \omega \\ 1 & \omega & \omega^2 \end{pmatrix} \mathrm{diag}(y_e, y_\mu, y_\tau) \tag{4.1}$$

[1] This was substantiated further in Ref. [193] using the symmetry groups T_7 and $\Delta(27)$.

with $\omega = e^{2i\pi/3} = -\frac{1}{2} + i\frac{\sqrt{3}}{2}$. Moreover, also the scalars that break A_4 and give masses to the fermions are pure Z_3 eigenstates, resulting in the Yukawa interactions

$$\begin{aligned} -\mathcal{L}_{\text{LFT}} = v^{-1} \Big\{ & \left(m_\tau \overline{L}_\tau \tau_R + m_\mu \overline{L}_\mu \mu_R + m_e \overline{L}_e e_R\right) \phi_0 \\ & \left(m_\tau \overline{L}_\mu \tau_R + m_\mu \overline{L}_e \mu_R + m_e \overline{L}_\tau e_R\right) \phi_1 \\ & \left(m_\tau \overline{L}_e \tau_R + m_\mu \overline{L}_\tau \mu_R + m_e \overline{L}_\mu e_R\right) \phi_2 \Big\} + \text{h.c.} \end{aligned} \tag{4.2}$$

The corresponding Z_3 properties of each field are summarized in Tab. 4.1. Only a few selected lepton decay channels are actually allowed by the remnant Z_3 symmetry

$$\tau^+ \to \mu^+ \mu^+ e^- \,, \qquad \tau^+ \to e^+ e^+ \mu^- \,, \tag{4.3}$$

excluding entirely the rare radiative decays $l \to l'\gamma$. In triality models the scalar sector, usually involving three Higgs doublets, separates into an SM-like Higgs boson h, and new exotic scalars $\psi_{1,2}$ with exciting flavor-violating signatures. These unique predictions can easily be tested, e.g., through the decay mode $h \to \psi_2^0 \overline{\psi}_2^0 \to (\tau^- e^+)(\tau^- \mu^+)$, provided that $2m_{\psi_2} < m_h$ [193].
Note that also permutations of the matrix (4.1) yield a triality model with interchanged Z_3 quantum numbers, which may result in different collider signatures. An example model is presented in the following section based on the S_4 flavor symmetry.

Field	e	μ	τ	u	c	t	d	s	b	ϕ_0	ϕ_1	ϕ_2
Z_3	1	ω^2	ω	1	ω^2	ω	1	ω^2	ω	1	ω	ω^2

Table 4.1: Example of Z_3 quantum numbers in triality models after the breaking of the global flavor symmetry.

Flavor triality can also extend to quarks in a scenario where both up- and down-type quarks are Z_3 invariant. In this case the CKM mixing is trivial, which is a good first order approximation of the small quark mixing angles. Quark flavor triality has interesting implications for rare meson decays, favoring the flavor-violating modes

$$\begin{aligned} B^0 &\to \tau^+ e^-,\ \mu^+ \tau^-,\ e^+ \mu^- \,, & D^0 &\to \tau^- e^+,\ e^- \mu^+ \,, \\ B_s^0 &\to \tau^+ \mu^-,\ \mu^+ e^-,\ e^+ \tau^- \,, & K^0 &\to \mu^+ e^- \,. \end{aligned} \tag{4.4}$$

Extensive searches for K and B meson decays tightly constrain triality models by placing lower bounds on the masses of the new mediators. The measurement of $K_L^0 \to \mu^\pm e^\mp$ in particular leads to [122]

$$\frac{m_{\psi_1} m_{\psi_2}}{\sqrt{m_{\psi_1}^2 + m_{\psi_2}^2}} > 510 \text{ GeV} \,. \tag{4.5}$$

Assuming LFT alone, the exotic scalars can be even lighter than the SM Higgs boson because the leptonic bounds are comparatively weak.

4.1.2 *The Model*

In the following the charged lepton sector is used as a starting point to introduce the relevant scalar content. Some of the additional scalars needed to accommodate quarks and neutrinos affect the lepton phenomenology, which we can exploit to explain the excess in $h \to \mu\tau$ reported by CMS, as will be discussed in Sec. 4.1.3.

Charged Leptons

The necessary ingredients to build a triality model in S_4 are three scalar $SU(2)$ doublets ϕ_i in the triplet representation $\mathbf{3'}$ of S_4. Together with the charged leptons, these scalars are the foundation of the model and jointly give masses to the fermions by acquiring VEVs at the EW scale. Furthermore, two EW scalar singlets, η_1 and η_2 are introduced to describe the charged lepton mass hierarchy through a Z_{12} FN symmetry. These fields acquire the VEVs $v_{\eta_{1,2}} = \lambda\Lambda$, where $\lambda \approx 0.22$ and $\Lambda \gg \Lambda_{\text{EW}}$ is a high scale defining the breakdown of the effective theory. The particle content and charge assignments of this minimal model are summarized in Tab. 4.2.

Field	$SU(2)_L$	S_4	Z_{12}
$L = (L_e, L_\mu, L_\tau)$	$\mathbf{2}$	$\mathbf{3'}$	0
τ_R	$\mathbf{1}$	$\mathbf{1}$	3
$l_R = (e_R, \mu_R)$	$\mathbf{1}$	$\mathbf{2}$	5
$\phi = (\phi_1, \phi_2, \phi_3)$	$\mathbf{2}$	$\mathbf{3'}$	0
η_1	$\mathbf{1}$	$\mathbf{1}$	-1
η_2	$\mathbf{1}$	$\mathbf{1'}$	-1

Table 4.2: Minimal field content for a realistic charged lepton model with lepton flavor triality in S_4.

The assignments lead to the following charged lepton Yukawa terms

$$\begin{aligned} -\mathcal{L}^l_{\text{yuk}} \supset\ & \frac{y_1}{\Lambda^3}\,[L\phi]_1\,\tau_R(\eta_1^3 + \varepsilon_0\eta_1\eta_2^2) \\ +\ & \frac{y_2}{\Lambda^5}\,[L\phi]_2\,l_R(\eta_1^5 + \varepsilon_1\eta_1^3\eta_2^2 + \varepsilon_2\eta_1\eta_2^4) \\ +\ & \frac{y_3}{\Lambda^5}\,[L\phi]_2\,l_R(\eta_2^5 + \varepsilon_3\eta_2^3\eta_1^2 + \varepsilon_4\eta_2\eta_1^4) + \text{h.c.} \end{aligned} \tag{4.6}$$

Like in the models presented in Chapter 3, the mass hierarchies are ensured by suitable Z_{12} charges for the charged leptons. In this case, the tau and muon masses arise from seven- and nine-dimensional Yukawa terms, respectively. The smallness of the electron mass on the other hand is explained by the destructive interference of two nine-dimensional operators.

Assuming that the $SU(2)$ singlets η_i are heavy, their mixing with the EW doublets ϕ_i is minimized. For simplicity the scalar potential can be reduced to its low-energy part

$$\begin{aligned} V(\phi) = &- \mu_1^2 \sum_{i=1}^{3} \phi_i^\dagger \phi_i + \alpha \left(\sum_{i=1}^{3} \phi_i^\dagger \phi_i \right)^2 \\ &+ \sum_{i,j=1, i\neq j}^{3} \left[\beta (\phi_i^\dagger \phi_i)(\phi_j^\dagger \phi_j) + \gamma |\phi_i^\dagger \phi_j|^2 + \delta (\phi_i^\dagger \phi_j)^2 \right] \end{aligned} \tag{4.7}$$

which coincides with the general CP-conserving S_4-invariant 3HDM potential. Expanding the fields as

$$\phi_j = \begin{pmatrix} \phi_j^+ \\ \frac{1}{\sqrt{2}} \left[\frac{v}{\sqrt{3}} + \phi_{jR}^0 + i \phi_{jI}^0 \right] \end{pmatrix}, \tag{4.8}$$

the scalar content includes three CP-even neutral scalars ϕ_{jR}^0 ($j = 1, 2, 3$), three CP-odd neutral scalars ϕ_{jI}^0, as well as three complex charged scalars (ϕ_j^+), of which three degrees of freedom are absorbed by the $W^\pm$ and Z gauge boson masses. The corresponding physical mass spectrum reads

$$\begin{array}{lllllllll} m^2_{\phi^0_{(a,b)R}} & = & -\frac{v^2}{3}\kappa\,, & m^2_{\phi^0_{cR}} & = & \frac{v^2}{3}(3\alpha + 2\kappa)\,, & m^2_{\phi^0_{cI}} & = & 0\,, \\ m^2_{\phi^0_{(a,b)I}} & = & -v^2\delta\,, & m^2_{\phi^\pm_{a,b}} & = & -v^2(\kappa - \beta)\,, & m^2_{\phi^\pm_{c}} & = & 0\,, \end{array} \tag{4.9}$$

with $\kappa \equiv \beta + \gamma + \delta$.

The mass eigenstates $\phi_{a,b,c}$ are given by the following linear combinations of the S_4 basis scalars $\phi_{1,2,3}$:

$$\begin{array}{lll} \phi_a & = & \frac{1}{\sqrt{2}}(\phi_3 - \phi_2)\,, \\ \phi_b & = & \frac{1}{\sqrt{6}}(2\phi_1 - \phi_2 - \phi_3)\,, \\ \phi_c & = & \frac{1}{\sqrt{3}}(\phi_1 + \phi_2 + \phi_3). \end{array} \tag{4.10}$$

These equations hold for the charged, CP-even and CP-odd components of ϕ implying that

$$\langle \phi_a \rangle = \langle \phi_b \rangle = 0 \quad \text{and} \quad \langle \phi_c \rangle = v. \tag{4.11}$$

The fact that ϕ_c is the only mass eigenstate of the S_4 triplet acquiring a VEV is essential for LFT. It suggests that ϕ_{cR}^0 can be identified as the SM Higgs particle found at the LHC with a mass of approximately 125 GeV.

Consequently, ϕ_c is also the only scalar giving masses to the SM gauge bosons, i.e., decaying via $\phi_{cR}^0 \to W^+W^-$ and $\phi_{cR}^0 \to ZZ$. This can be confirmed from the kinetic terms of the Lagrangian and the resulting three-point interactions. As a result, the masses of the exotic scalars (e.g., $\phi_{(a,b)R}^0$) are not constrained by the usual Higgs searches in the gauge boson channels performed in the LEP and LHC experiments [196, 197].

The charged lepton mass matrix follows from Eq. (4.7)

$$\begin{aligned} M_l &= \frac{1}{\sqrt{2}} \begin{pmatrix} v_1 (\widetilde{y}_2 - \widetilde{y}_3) \lambda^5 & v_1 (\widetilde{y}_2 + \widetilde{y}_3) \lambda^5 & v_1 \widetilde{y}_1 \lambda^3 \\ v_2 \omega^2 (\widetilde{y}_2 - \widetilde{y}_3) \lambda^5 & v_2 \omega (\widetilde{y}_2 + \widetilde{y}_3) \lambda^5 & v_2 \widetilde{y}_1 \lambda^3 \\ v_3 \omega (\widetilde{y}_2 - \widetilde{y}_3) \lambda^5 & v_3 \omega^2 (\widetilde{y}_2 + \widetilde{y}_3) \lambda^5 & v_3 \widetilde{y}_1 \lambda^3 \end{pmatrix} \\ &= v \frac{1}{\sqrt{6}} \begin{pmatrix} 1 & 1 & 1 \\ \omega^2 & \omega & 1 \\ \omega & \omega^2 & 1 \end{pmatrix} \mathrm{diag}((\widetilde{y}_2 - \widetilde{y}_3) \lambda^5, (\widetilde{y}_2 + \widetilde{y}_3) \lambda^5, \widetilde{y}_1 \lambda^3)\,, \end{aligned} \tag{4.12}$$

with $v_1 = v_2 = v_3 = \frac{v}{\sqrt{3}}$, $\omega = e^{2i\pi/3}$ and $\widetilde{y}_1$, $\widetilde{y}_2$, $\widetilde{y}_3$ given by

$$\widetilde{y}_1 = (1+\varepsilon_0)\, y_1\,, \qquad \widetilde{y}_2 = (1+\varepsilon_1+\varepsilon_2)\, y_2\,, \qquad \widetilde{y}_3 = (1+\varepsilon_3+\varepsilon_4)\, y_3\,, \tag{4.13}$$

where the dimensionless couplings y_1, y_2, y_3, ε_0, ε_1, ε_2, ε_3 and ε_4 are $\mathcal{O}(1)$ parameters. Consequently, the charged lepton masses are

$$m_e = (\widetilde{y}_2 - \widetilde{y}_3)\,\lambda^5 \frac{v}{\sqrt{2}}\,, \qquad m_\mu = (\widetilde{y}_2 + \widetilde{y}_3)\,\lambda^5 \frac{v}{\sqrt{2}}\,, \qquad m_\tau = \widetilde{y}_1 \lambda^3 \frac{v}{\sqrt{2}}\,, \tag{4.14}$$

which explain the observed mass hierarchy through their suppression by powers of λ. Eq.(4.12) shows a characteristic feature of LFT that the mass basis of the charged leptons coincides with the Z_3 basis; i.e., the charged lepton fields can be identified as the Z_3 eigenstates $e \sim 1, \mu \sim \omega^2, \tau \sim \omega$.
In the mass eigenstate basis the Yukawa matrices read

$$Y_a = \frac{i}{v\sqrt{2}} \begin{pmatrix} 0 & m_\mu \omega^2 & -m_\tau \omega \\ -m_e \omega & 0 & m_\tau \omega^2 \\ m_e \omega^2 & -m_\mu \omega & 0 \end{pmatrix}, \tag{4.15}$$

$$Y_b = \frac{1}{v\sqrt{2}} \begin{pmatrix} 0 & m_\mu \omega^2 & m_\tau \omega \\ m_e \omega & 0 & m_\tau \omega^2 \\ m_e \omega^2 & m_\mu \omega & 0 \end{pmatrix}, \tag{4.16}$$

$$Y_c = \frac{1}{v} \begin{pmatrix} m_e & 0 & 0 \\ 0 & m_\mu & 0 \\ 0 & 0 & m_\tau \end{pmatrix}. \tag{4.17}$$

Since ϕ_c couples only diagonally to the charged leptons it should be uncharged under Z_3, preserving the group after EW symmetry breaking. This can be understood by expressing the fields $\phi_{a,b,c}$ in terms of the Z_3 eigenstates $\phi_{x,y,z} \sim (1, \omega, \omega^2)$

$$\begin{pmatrix} \phi_x \\ \phi_y \\ \phi_z \end{pmatrix} = \frac{1}{\sqrt{3}} \begin{pmatrix} 1 & 1 & 1 \\ 1 & \omega^2 & \omega \\ 1 & \omega & \omega^2 \end{pmatrix} \begin{pmatrix} \phi_1 \\ \phi_2 \\ \phi_3 \end{pmatrix}, \tag{4.18}$$

and consequently realizing that

$$\phi_c = \phi_x, \qquad \phi_b = \frac{1}{\sqrt{2}}(\phi_y + \phi_z), \qquad \phi_a = \frac{1}{\sqrt{2}}(\phi_y - \phi_z). \tag{4.19}$$

In conclusion, Z_3 remains unbroken at this point since only ϕ_c, in the trivial Z_3 eigenstate, acquires a VEV. Note that the remnant Z_3 symmetry prevents mixing of ϕ_c with the other scalars. Therefore, as it stands, the model is robust against FCNC constraints but cannot account for the $h \to \mu\tau$ anomaly since the SM-like Higgs boson couples only diagonally to leptons. In the following we extend the framework to the other fermion sectors, eventually breaking LFT.

Neutrinos

To generate the neutrino masses via a type I seesaw mechanism, we add two heavy Majorana neutrinos N_{1R} and N_{2R} to the SM particle content as well as four S_4 triplets

scalar fields χ, ξ, σ and ζ, which are singlets under $SU(2)$. Because of the simplicity of the charged lepton sector, an intricate pattern of specifically aligned scalar fields is necessary to break the S_4 symmetry in the desired direction and at the same time obtain two massive neutrinos. Additionally, we employ two Z_2 symmetries to enforce a specific mass pattern and decouple the scalars from interactions with the other fermion sectors. The corresponding $S_4 \otimes Z_2 \otimes Z_2' \otimes Z_{12}$ assignments are shown in Tab. 4.3.

Field	$SU(2)_L$	S_4	Z_2	Z_2'	Z_{12}
N_{1R}	$\mathbf{1}$	$\mathbf{1}$	1	0	0
N_{2R}	$\mathbf{1}$	$\mathbf{1}$	1	1	0
χ	$\mathbf{1}$	$\mathbf{3'}$	1	0	0
ξ	$\mathbf{1}$	$\mathbf{3}$	1	0	0
σ	$\mathbf{1}$	$\mathbf{3'}$	1	1	0
ζ	$\mathbf{1}$	$\mathbf{3}$	1	1	0

Table 4.3: The additional field content and symmetries required to implement neutrinos.

Therefore the relevant $S_4 \otimes Z_2 \otimes Z_2' \otimes Z_{12}$ -invariant neutrino Yukawa terms read

$$\begin{aligned} -\mathcal{L}^{\nu}_{\text{yuk}} \supset\ & y_1^{(\nu)} \left[L\phi\right]_{3'} N_{1R}\, \frac{\chi}{\Lambda} + y_2^{(\nu)} \left[L\phi\right]_{3} N_{1R}\, \frac{\xi}{\Lambda} + y_3^{(\nu)} \left[L\phi\right]_{3'} N_{2R}\, \frac{\sigma}{\Lambda} \\ & + y_4^{(\nu)} \left[L\phi\right]_{3} N_{2R}\, \frac{\zeta}{\Lambda} + \frac{y_5^{(\nu)}}{\Lambda} L \left[\phi\chi\right]_{3'} N_{1R}\ + \frac{y_6^{(\nu)}}{\Lambda} L \left[\phi\xi\right]_{3'} N_{1R} \\ & + \frac{y_7^{(\nu)}}{\Lambda} L \left[\phi\sigma\right]_{3'} N_{2R} + \frac{y_8^{(\nu)}}{\Lambda} L \left[\phi\zeta\right]_{3'} N_{2R} + M_1 \overline{N}_{1R} N_{1R}^c + M_2 \overline{N}_{2R} N_{2R}^c \,. \end{aligned} \tag{4.20}$$

With the VEV patterns of the scalar fields χ, ξ, σ and ζ

$$\begin{aligned} \langle\chi\rangle &= v_\chi \left(1,0,0\right) , \qquad \langle\xi\rangle = v_\xi \left(1,0,0\right) , \\ \langle\sigma\rangle &= v_\sigma \left(0,i,0\right) , \qquad \langle\zeta\rangle = v_\zeta \left(0,1,0\right) , \end{aligned} \tag{4.21}$$

and assuming that

$$y_1^{(\nu)} = y_2^{(\nu)} = y_5^{(\nu)} = y_6^{(\nu)} = y^{(\nu)} \,, \tag{4.22}$$

the full 5×5 neutrino mass matrix is

$$M_L^{(\nu)} = \begin{pmatrix} 0_{3\times3} & M_\nu^D \\ \left(M_\nu^D\right)^T & M_R \end{pmatrix} , \tag{4.23}$$

where

$$M_\nu^D = \begin{pmatrix} 0 & a e^{i\tau} \\ b & 0 \\ 0 & a e^{-i\tau} \end{pmatrix} \frac{v}{\sqrt{3}} \,, \qquad M_R = \begin{pmatrix} M_1 & 0 \\ 0 & M_2 \end{pmatrix} , \tag{4.24}$$

with

$$\begin{aligned} a &= \lambda \sqrt{\left(y_4^{(\nu)} + y_6^{(\nu)}\right)^2 + \left(y_3^{(\nu)} + y_7^{(\nu)}\right)^2}\,, \\ b &= 4\lambda y^{(\nu)}\,, \\ \tau &= \arctan\left(-\frac{y_3^{(\nu)} + y_7^{(\nu)}}{y_4^{(\nu)} + y_6^{(\nu)}}\right)\,. \end{aligned} \tag{4.25}$$

Since $(M_R)_{ii} \gg v$, the light neutrino mass matrix arises from a type I seesaw mechanism and is given by

$$M_L^{(\nu)} = \begin{pmatrix} Ae^{2i\tau} & 0 & A \\ 0 & B & 0 \\ A & 0 & Ae^{-2i\tau} \end{pmatrix}\,, \tag{4.26}$$

with

$$A = a^2 \frac{v^2}{3M_2}\,, \qquad B = b^2 \frac{v^2}{3M_1}\,. \tag{4.27}$$

Hence, the neutrino mass matrix depends only on the three effective parameters A, B, and τ. The lepton phenomenology at this point coincides with the $SU(5)$ flavor model discussed in Sec. 3, the technical details of which can be found in Sec. 3.2.2. In conclusion, the model can accommodate the lepton observables well, predicting one massless neutrino as well as a small CP-violating phase δ_{CP}^L.

Quarks

To obtain realistic quark masses and mixings, the scalar sector has be extended even further. The new fields include two S_4 triplets, ρ, and φ, and three S_4 singlets Ω_1, Ω_2 and Ω_3 aligned as

$$\begin{aligned} \langle \rho \rangle = v_\rho\,(i,0,0)\,, \quad \langle \varphi \rangle = v_\varphi\,(1,0,0)\,, \\ \langle \Omega_1 \rangle = v_{\Omega_1}\,, \quad \langle \Omega_2 \rangle = v_{\Omega_2} e^{i\theta_\Omega}\,, \quad \langle \Omega_3 \rangle = v_{\Omega_3} \end{aligned} \tag{4.28}$$

in the S_4 space. Again we use a Z_2'' symmetry to decouple these scalars from the other fermion sectors, whereas a Z_6 symmetry accounts for the top and bottom mass hierarchy. The $S_4 \otimes Z_2'' \otimes Z_6 \otimes Z_{12}$ assignments are given in Tab. 4.4. Note that previously introduced symmetries are omitted here if they do not affect the quark sector. A complete list of the entire field content and all the flavor symmetries can be found in Tab. C.1 in App. C.3.

Applying the S_4 multiplication rules listed in App. B.1 to the Yukawa interactions (C.44) and (C.45), it follows that the quark mass matrices are given by

$$M_q = \begin{pmatrix} C_q e^{i\theta_{1q}} & 0 & 0 \\ D_q e^{-i\theta_{2q}} & E_q e^{-i\theta_{3q}} & F_q e^{-i\theta_{4q}} \\ D_q e^{i\theta_{2q}} & E_q e^{i\theta_{3q}} & F_q e^{i\theta_{4q}} \end{pmatrix}\,, \qquad q = U, D. \tag{4.29}$$

The matrix $J_q \equiv M_q M_q^\dagger$ can be rewritten as

$$J_q = \begin{pmatrix} X_q & Y_q & Y_q \\ Y_q & U_q & V_q \\ Y_q & V_q & U_q \end{pmatrix}\,, \tag{4.30}$$

Field	$SU(2)_L$	S_4	Z_2''	Z_6	Z_{12}
$Q = (Q_1, Q_2, Q_3)$	**2**	**3′**	1	0	0
u_R	**1**	**1**	0	0	6
c_R	**1**	**1**	0	0	0
t_R	**1**	**1**	0	0	0
d_R	**1**	**1**	0	3	6
s_R	**1**	**1**	0	3	0
b_R	**1**	**1**	0	3	0
ρ	**1**	**3′**	1	0	0
φ	**1**	**3**	1	0	0
Ω_1	**1**	**1**	0	0	3
Ω_2	**1**	**1**	1	0	2
Ω_3	**1**	**1**	0	1	0

Table 4.4: The quark fields and the scalars required to implement them.

which is a modification of the Fukuyama-Nishiura texture proposed in Ref. [154]. Since this pattern appeared previously in the S_3 flavor model in Chapter 3.1, the reader is referred to App. C.3.1 for a detailed discussion of the quark mixings and the Yukawa interactions.

4.1.3 Z_3 *Breaking*

Scalar Sector

The S_4 symmetry of the model is broken down to a residual Z_3 symmetry once the S_4 triplet ϕ acquires VEVs in the direction $v(1,1,1)$. However, perturbations can arise without a mechanism to protect the necessary VEV alignments; e.g., due to a scalar triplet χ acquiring a VEV in the $v_\chi(1,0,0)$ direction to generate neutrino masses and mixings [cf. Eq. (4.21)]. These perturbations are caused by quartic interactions of the form $(\phi^\dagger\phi)(\chi^\dagger\chi)$ that always appear in the scalar potential since the combinations $\phi^\dagger\phi$ and $\chi^\dagger\chi$ cannot be forbidden by a flavor symmetry.
Several scalars responsible for the mixings in the quark and neutrino sectors cause deviations from the $v(1,1,1)$ alignment through quartic interactions with ϕ. If we assume a VEV hierarchy among those scalars to simplify the discussion, i.e., $v_\rho, v_\varphi \gg v_\chi, v_\xi, v_\sigma, v_\zeta$, the perturbations coming from scalars involved in neutrino interactions can be neglected. The remaining fields

$$\begin{aligned} \rho &: (3', 1)\,, & \varphi &: (3, 1)\,, \\ \langle\rho\rangle &= v_\rho\,(i, 0, 0)\,, & \langle\varphi\rangle &= v_\varphi\,(1, 0, 0)\,, \end{aligned} \tag{4.31}$$

lead to the cross couplings in the scalar potential

$$V_{\text{int}} \supset \sum_{i=\mathbf{1},\mathbf{2},\mathbf{3},\mathbf{3'}} (\phi^\dagger\phi)_i \left[\lambda_{\rho_i}(\rho^\dagger\rho)_i + \lambda_{\varphi_i}(\varphi^\dagger\varphi)_i\right], \tag{4.32}$$

where $i = \mathbf{1}, \mathbf{2}, \mathbf{3}, \mathbf{3'}$ denotes the corresponding S_4 projection. Eventually only the $\mathbf{2}$-contractions, e.g.,

$$\sum_{j,k=1,j\neq k}^{3} 2|\phi_j|^2|\rho_j|^2 - |\phi_j|^2|\rho_k|^2,$$

result in perturbations of the VEV alignment $v(1,1,1)$. The other contractions are invariant under the Z_3-conserving generator after the scalars ρ and φ acquire their VEVs. Therefore, it suffices to consider only the following terms in the scalar potential to analyze the breaking of Z_3:

$$\begin{aligned} V_{\text{int}} &\supset (\phi^\dagger\phi)_{\mathbf{2}} \left[\lambda_\rho(\rho^\dagger\rho)_{\mathbf{2}} + \lambda_\varphi(\varphi^\dagger\varphi)_{\mathbf{2}}\right] \\ &= \sum_{j,k=1,j\neq k}^{3} |\phi_j|^2 \left[\lambda_\rho(2|\rho_j|^2 - |\rho_k|^2) + \lambda_\varphi(2|\varphi_j|^2 - |\varphi_k|^2)\right]. \end{aligned} \tag{4.33}$$

Assuming for simplicity that the coupling constants are the same order of magnitude, i.e., $\lambda_\rho \approx \lambda_\varphi \equiv \lambda_s/2$, the VEV alignment of the triplet ϕ is approximately shifted by a perturbation ϵ in the following way

$$\langle\phi\rangle = v(1+2\epsilon, 1-\epsilon, 1-\epsilon), \tag{4.34}$$

where the contributions from ρ and φ are summarized in the parameter ϵ. Doing so, we adopt a similar approach as the authors of Ref. [91], who recently analyzed a triality model based on an A_4 flavor symmetry.

As a consequence, one of the physical Higgs doublets which was inert before the breaking of Z_3, $\langle\phi_b\rangle = 0$, now acquires a small VEV depending on the size of the perturbation parameter ϵ

$$\begin{pmatrix} \langle\phi_a\rangle \\ \langle\phi_b\rangle \\ \langle\phi_c\rangle \end{pmatrix} = \begin{pmatrix} 0 & -\frac{1}{\sqrt{2}} & \frac{1}{\sqrt{2}} \\ \frac{\sqrt{2}}{\sqrt{3}} & -\frac{1}{\sqrt{6}} & -\frac{1}{\sqrt{6}} \\ \frac{1}{\sqrt{3}} & \frac{1}{\sqrt{3}} & \frac{1}{\sqrt{3}} \end{pmatrix} \begin{pmatrix} \frac{v}{\sqrt{3}}(1+2\epsilon) \\ \frac{v}{\sqrt{3}}(1-\epsilon) \\ \frac{v}{\sqrt{3}}(1-\epsilon) \end{pmatrix} = v \begin{pmatrix} 0 \\ \sqrt{2}\epsilon \\ 1 \end{pmatrix}. \tag{4.35}$$

Following Ref. [91] we use the parametrization

$$\langle(\phi_a, \phi_b, \phi_c)^T\rangle = v(0, \sin\theta, \cos\theta), \tag{4.36}$$

where θ is given by a combination of parameters from the scalar potential to account for the deviation from LFT.

The breaking of Z_3 induces new mixing of the doublets ϕ_b and ϕ_c, which were mass eigenstates prior to the breaking. The CP-odd neutral scalars $\phi^0_{(b,c),I}$ and the charged scalars $\phi^+_{b,c}$ mix via

$$\begin{aligned} \begin{pmatrix} H^\pm \\ \pi^\pm \end{pmatrix} &= \begin{pmatrix} c_\theta & s_\theta \\ -s_\theta & c_\theta \end{pmatrix} \begin{pmatrix} \phi_b^\pm \\ \phi_c^\pm \end{pmatrix}, \\ \begin{pmatrix} \eta_I^0 \\ \pi_I^0 \end{pmatrix} &= \begin{pmatrix} c_\theta & s_\theta \\ -s_\theta & c_\theta \end{pmatrix} \begin{pmatrix} \phi_{b,I}^0 \\ \phi_{c,I}^0 \end{pmatrix}, \end{aligned} \tag{4.37}$$

where $\pi^\pm$ and π_I^0 are the massless Goldstone bosons, $\sin\theta \equiv s_\theta$ and $\cos\theta \equiv c_\theta$. In the case of the CP-even neutral scalars the situation is more complicated and the mixing results in a mass splitting of the initially degenerate scalars. The complete mass spectrum reads

$$\begin{aligned} m^2_{\phi^0_{a,I}} &= m^2_{\eta^0_I} = -v^2\delta\,, & m^2_{\phi^0_{a,R}} &= \frac{1}{6}v^2(-2+2\sqrt{2}c_\theta s_\theta + s_\theta^2)\kappa\,, \\ m^2_{\phi^\pm_a} &= m^2_{H^\pm} = -v^2(\kappa-\beta)\,, & m^2_h &= \frac{1}{2}(v^2\alpha - m^2_{\phi^0_{a,R}}) - \Delta\,, \\ m^2_{\pi^\pm} &= m^2_{\pi^0_I} = 0\,, & m^2_H &= \frac{1}{2}(v^2\alpha - m^2_{\phi^0_{a,R}}) + \Delta\,, \end{aligned} \tag{4.38}$$

with

$$\Delta = \frac{1}{6}v^2\sqrt{9(\alpha+\kappa)^2 + 3\kappa s_\theta\left[2\sqrt{2}c_\theta(\alpha+\kappa) - 3s_\theta(5\alpha+3\kappa)\right] + \mathcal{O}(s_\theta^3)}\,. \tag{4.39}$$

Note that only the masses of the CP-even scalars depend on the perturbation parameter θ. Hence Z_3 breaking in this direction does not affect the phenomenology of the CP-odd and charged scalars in our triality model. In the triality limit $\theta \to 0$ the mixing vanishes and the original mass spectrum is recovered

$$m_h^2 \xrightarrow{\theta\to 0} m^2_{\phi^0_{c,R}}\,, \qquad m_H^2 \xrightarrow{\theta\to 0} m^2_{\phi^0_{b,R}} = m^2_{\phi^0_{a,R}}\,. \tag{4.40}$$

Therefore, the scalar h should play the role of the SM-like Higgs with $m_h \approx 125\,\text{GeV}$, whereas H will be a new heavy Higgs as in regular 2HDMs. The mixing angle ϑ between the CP-even neutral scalars is defined by

$$\begin{gathered} \begin{pmatrix} H \\ h \end{pmatrix} = \begin{pmatrix} c_\vartheta & s_\vartheta \\ -s_\vartheta & c_\vartheta \end{pmatrix} \begin{pmatrix} \phi^0_{b,R} \\ \phi^0_{c,R} \end{pmatrix} \qquad \text{and} \\ \tan 2\vartheta = -\frac{4s_\theta[\sqrt{2}\kappa s_\theta - 2c_\theta(3\alpha+\kappa)]}{6(-1+2s_\theta^2)\alpha + (-6-2\sqrt{2}c_\theta s_\theta + 11 s_\theta^2)\kappa} \end{gathered} \tag{4.41}$$

with $\vartheta \to 0$ for $\theta \to 0$ in the unbroken triality limit.
For the analysis the angle ϑ is more conveniently expressed in terms of the masses m_h and $m_{\phi^0_{a,R}} \equiv m_a$. The full expression can be found in Eq. (C.54) of App. C.3.2. Since m_h is fixed, the mixing angle ϑ depends only on the two parameters m_a and θ. Through the relation $m_a^2 = v^2\alpha - (m_h^2 + m_H^2)$ one can alternatively display the results in terms of m_H.
In the following we identify the new charged lepton mass eigenstates after Z_3 breaking to extract the relevant LFV Yukawa couplings for the $h \to \mu\tau$ analysis.

Consequences for Leptons

As a result of the perturbed alignment $v(0, s_\theta, c_\theta)$ the mass matrix of the charged leptons takes the form

$$\begin{gathered} M_l = \frac{v}{2}U_\omega \begin{pmatrix} \sqrt{2}c_\theta(\widetilde{y}_2 - \widetilde{y}_3)\lambda^5 & s_\theta(\widetilde{y}_2 + \widetilde{y}_3)\lambda^5 & s_\theta\widetilde{y}_1\lambda \\ s_\theta(\widetilde{y}_2 - \widetilde{y}_3)\lambda^5 & \sqrt{2}c_\theta(\widetilde{y}_2 + \widetilde{y}_3)\lambda^5 & s_\theta\widetilde{y}_1\lambda^3 \\ s_\theta(\widetilde{y}_2 - \widetilde{y}_3)\lambda^5 & s_\theta(\widetilde{y}_2 + \widetilde{y}_3)\lambda^5 & \sqrt{2}c_\theta\widetilde{y}_1\lambda^3 \end{pmatrix}, \\ \text{with} \qquad U_\omega = \frac{1}{\sqrt{3}}\begin{pmatrix} 1 & 1 & 1 \\ \omega^2 & \omega & 1 \\ \omega & \omega^2 & 1 \end{pmatrix}. \end{gathered} \tag{4.42}$$

Hence with off-diagonal elements that vanish in the limit $\theta \to 0$ it is no longer diagonal in the Z_3 basis of the charged leptons. The perturbed charged lepton mass matrix can be diagonalized to a good approximation by

$$V_L^\dagger M_l V_R = \mathrm{diag}(m_e, m_\mu, m_\tau) \tag{4.43}$$

with

$$\begin{aligned} V_R &\simeq \begin{pmatrix} 1 & -\frac{\sqrt{2}s_\theta(\widetilde{y}_2-\widetilde{y}_3)}{(\widetilde{y}_2+\widetilde{y}_3)} & -\frac{\sqrt{2}s_\theta(\widetilde{y}_2-\widetilde{y}_3)\lambda^2}{\widetilde{y}_1} \\ \frac{\sqrt{2}s_\theta(\widetilde{y}_2-\widetilde{y}_3)}{(\widetilde{y}_2+\widetilde{y}_3)} & 1 & -\frac{\sqrt{2}s_\theta(\widetilde{y}_2+\widetilde{y}_3)\lambda^2}{\widetilde{y}_1} \\ \frac{\sqrt{2}s_\theta(\widetilde{y}_2-\widetilde{y}_3)\lambda^2}{\widetilde{y}_1} & \frac{\sqrt{2}s_\theta(\widetilde{y}_2+\widetilde{y}_3)\lambda^2}{\widetilde{y}_1} & 1 \end{pmatrix}, \\ V_L &\simeq U_\omega R O_{23}(\theta) R^T O_{12}(\alpha_L), \qquad R = \begin{pmatrix} -\frac{1}{\sqrt{2}} & \frac{1}{\sqrt{2}} & 0 \\ \frac{1}{\sqrt{2}} & \frac{1}{\sqrt{2}} & 0 \\ 0 & 0 & 1 \end{pmatrix}, \end{aligned} \tag{4.44}$$

where O_{ij} are rotation matrices in the ij-plane and

$$\tan 2\alpha_L = \frac{s_\theta\left(4\sqrt{2}c_{3\theta} + 12\sqrt{2}c_\theta - 7s_{3\theta} - 3s_\theta\right)}{10c_{3\theta} + 6c_\theta + 8\sqrt{2}{s_\theta}^3}\,. \tag{4.45}$$

Using the rotation matrices V_L and V_R we find the charged lepton Yukawa couplings $y_{ll'}(l, l' = e, \mu, \tau)$ that eventually lead to flavor violation in the lepton sector. With

$$\begin{aligned} (\overline{L}_1, \overline{L}_2, \overline{L}_3) &= (\overline{L}_e, \overline{L}_\mu, \overline{L}_\tau) V_L^\dagger\,, \\ (e_1, e_2, e_3)^T &= V_R \cdot (e, \mu, \tau)^T\,, \\ (\phi_1, \phi_2, \phi_3)^T &= U_s \cdot (\phi_a, H, h)^T\,, \end{aligned} \tag{4.46}$$

where

$$U_s \equiv \begin{pmatrix} 0 & \sqrt{\frac{2}{3}} & \frac{1}{\sqrt{3}} \\ -\frac{1}{\sqrt{2}} & -\frac{1}{\sqrt{6}} & \frac{1}{\sqrt{3}} \\ \frac{1}{\sqrt{2}} & -\frac{1}{\sqrt{6}} & \frac{1}{\sqrt{3}} \end{pmatrix} \cdot \begin{pmatrix} 1 & 0 & 0 \\ 0 & c_\vartheta & -s_\vartheta \\ 0 & s_\vartheta & c_\vartheta \end{pmatrix}, \tag{4.47}$$

we can identify the coefficients of $h l_L l'_R$ as the Yukawa couplings $y_{ll'}$. In leading order, i.e., $m_e \ll m_\mu \ll m_\tau$, the dominant flavor-violating couplings are

$$\begin{aligned} y_{e\tau} &\simeq -\frac{m_\tau}{v}(c_{\alpha_L} - s_{\alpha_L}) s_{\vartheta+\theta}\,, \\ y_{\mu\tau} &\simeq -\frac{m_\tau}{v}(c_{\alpha_L} + s_{\alpha_L}) s_{\vartheta+\theta}\,, \\ y_{e\mu} &\simeq \frac{m_\mu}{4v}\Big\{2c_\vartheta\left[c_{\alpha_L}\left(c_\theta - 2{s_\theta}^2 - 1\right) - s_{\alpha_L}\left(c_\theta - 2{s_\theta}^2 + 1\right)\right] \\ &\quad - s_\vartheta\left(c_{\alpha_L}\left[c_\theta\left(4s_\theta + \sqrt{2}\right) - 2s_\theta + \sqrt{2}\right]\right. \\ &\quad + \left. s_{\alpha_L}\left[-c_\theta\left(4s_\theta + \sqrt{2}\right) + 2s_\theta + \sqrt{2}\right]\right)\Big\}\,. \end{aligned} \tag{4.48}$$

The remaining off-diagonal couplings are negligibly small and therefore irrelevant for the discussion since

$$y_{\tau e} \ll y_{e\tau}\,, \qquad y_{\mu e} \ll y_{e\mu}\,, \qquad y_{\tau\mu} \ll y_{\mu\tau}\,, \tag{4.49}$$

which means that $y_{\mu\tau}$ dominates the $h \to \mu\tau$ decay channel in our model.
The perturbation of the PMNS matrix due to the Z_3 breaking is negligible for sufficiently small values of θ. Explicitly, rotating by θ modifies the charged lepton contribution to the PMNS mixing matrix approximately as follows

$$V_L = U_\omega W_L \quad \text{with} \quad W_L \simeq \begin{pmatrix} 1 & \frac{\theta}{\sqrt{2}} - \frac{3\theta^2}{4} & \frac{\theta}{\sqrt{2}} \\ -\frac{\theta}{\sqrt{2}} + \frac{3\theta^2}{4} & 1 & \frac{\theta}{\sqrt{2}} \\ -\frac{\theta}{\sqrt{2}} & -\frac{\theta}{\sqrt{2}} & 1 \end{pmatrix} . \tag{4.50}$$

As will be pointed out in Sec. 4.1.3, the values required to explain the $h \to \mu\tau$ measurement are in the region $|\theta| \lesssim 0.10$ @ 95% C.L. The limiting factor is the mixing angle θ_{12}, which quickly exceeds the experimental $3\,\sigma$ bounds for positive values of the breaking parameter, resulting in $\theta \lesssim 0.02$. On the other hand, for negative θ values the fit to θ_{12} actually improves compared to the unbroken model. By varying ϕ for $\theta = 0.02$ and $\theta = -0.08$ we obtain the best-fit results shown in Tab. 4.5. The full PMNS matrix and the deviations of the mixing angles caused by the perturbation θ are given in Eqs. (C.55), and (C.56) - (C.57) of App. C.3.2.
The breaking of Z_3 also affects the Jarlskog invariant as follows

$$\begin{aligned} J \approx \frac{\cos(2\psi)}{6\sqrt{3}} &+ \frac{1}{12}\theta\left(\sqrt{6}\sin(2\psi)\cos(\phi) - \sqrt{2}\sin(2\psi)\sin(\phi)\right) \\ &+ \frac{1}{24}\theta^2\left(-3\sqrt{3}\cos(2\psi) - \sin(2\psi)\sin(\phi) + \sqrt{3}\right) , \end{aligned} \tag{4.51}$$

and therefore induces CP violation in neutrino oscillations. Since the obtained Jarlskog invariant can be of the order 10^{-2} (compare Tab. 4.5), the Z_3 symmetry breaking can generate a sizable CP phase of about $\delta^L_{\text{CP}} \approx 0.3$ in the case of negative θ values.

θ	Hierarchy	$\sin^2\theta_{12}$	$\sin^2\theta_{23}$	$\sin^2\theta_{13}$	J	ϕ
0.02	NH	0.349	0.388	0.0214	4.7×10^{-3}	-0.219π
	IH		0.599	0.0216	3.0×10^{-3}	0.551π
-0.08	NH	0.302	0.447	0.0217	-1.8×10^{-2}	-0.234π
	IH		0.615	0.0216	-1.2×10^{-2}	0.570π

Table 4.5: Approximate values of the PMNS mixing angles and the Jarlskog invariant J after Z_3 breaking for the benchmark points $\theta = 0.02$ and $\theta = -0.08$. The best fit was obtained by varying ϕ.

Flavor-Violating Higgs decays

The CMS measurement of $h \to \mu\tau$ is equivalent to a bound on the off-diagonal Yukawa couplings [198]

$$0.0019(0.0008) < \sqrt{|y_{\mu\tau}|^2 + |y_{\tau\mu}|^2} < 0.0032(0.0036) \text{ @ } 68\%(95\%) \text{ C.L.} , \tag{4.52}$$

assuming for simplicity that $h \to \mu\tau$ is the only additional contribution to the SM Higgs decay width. The result in Eq. (4.52) is compatible with the current bounds $\mathcal{B}(\tau \to \mu\gamma) < 4.4 \times 10^{-8}$ @ 90% C.L. and $\mathcal{B}(\tau \to e\gamma) < 3.3 \times 10^{-8}$ @ 90% [6]. However, while small compared to $y_{\mu\tau}$, $y_{e\mu}$ is tightly constrained by $\mathcal{B}(\mu \to e\gamma) < 5.7 \times 10^{-13}$ [199], which consequently restricts the allowed values of θ and m_a (or m_H). The corresponding diagrams mediating these processes in our model are shown in Fig. 4.1. Analytically, the branching ratio of $l \to l'\gamma$ is given by [51]

$$\mathcal{B}(l \to l'\gamma) = \frac{\tau_l \alpha_{\text{EM}} m_l^5}{64\pi^4} \left(|c_L|^2 + |c_R|^2 \right), \tag{4.53}$$

where c_L and c_R are the Wilson coefficients denoting left-handed and right-handed scalar currents, respectively. To calculate c_L and c_R, one-loop (see Fig. 4.1) and two-loop contributions are taken into account, since the latter can dominate the branching ratio in certain regions of the parameter space. The full set of equations is shown in Eqs. (C.60)-(C.63) of App. C.3.4 and was taken from Refs. [51, 200].

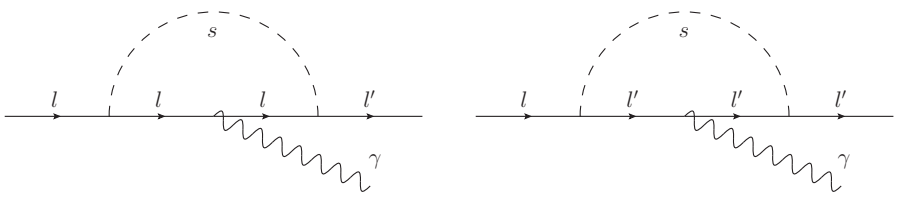

Figure 4.1: Leading order diagrams for $l \to l'\gamma$ with flavor-violating Higgs boson couplings, where $s = h, H, a, \eta$ and $l, l' = e, \mu, \tau$.

Using Eqs. (C.54), (4.45), and (4.48) we determine numerically the allowed values of θ and m_H that can explain the $2.4\,\sigma$ anomaly in $h \to \mu\tau$ and at the same time respect the bound on $\mathcal{B}(\mu \to e\gamma)$. Scanning the parameter space for negative and positive values of θ, we find that a window opens up for rather light masses of the extra scalars H and η in the vicinity of the SM Higgs boson mass, where the regions complying with either $\mathcal{B}(\mu \to e\gamma)$ or $\mathcal{B}(h \to \mu\tau)$ overlap, as shown in Figs. 4.2. In these regions the contributions of the Higgs h to $\mathcal{B}(\mu \to e\gamma)$ are partly canceled by the contributions of the neutral scalars H and η, allowing for larger flavor-violating Yukawa couplings. The viable parameter space at 68% C.L.(95% C.L.) and $m_\eta = 200\,\text{GeV}$

$$\begin{aligned} \theta &\in [0.002\,(0.001), 0.090\,(0.104)] \quad \cap \quad m_H \in [126\,(126), 204\,(214)]\ \text{GeV}\,, \\ -\theta &\in [0.001\,(0.004), 0.082\,(0.082)] \quad \cap \quad m_H \in [127\,(126), 190\,(190)]\ \text{GeV}\,, \end{aligned} \tag{4.54}$$

is practically symmetric around $\theta = 0$, while the analysis of the lepton mixing showed a slight preference for negative θ, as pointed out in the previous subsection.
Like in Sec. 3.1.3, the T and S parameters measuring the oblique corrections to the SM can be used to confine the scalar mass spectrum. By requiring that ΔT and ΔS lie inside the experimentally determined ellipsis, as seen in Fig. 4.3, we can derive the allowed masses of the charged scalars $m_{H^\pm}$ for the given range of 126 GeV $\lesssim m_H \lesssim$ 200GeV and $m_\eta = 200$ GeV. The parabolic shape denotes the values of ΔT and ΔS, which stay inside the ellipsis for 116 GeV $< m_{H^\pm} <$ 240 GeV. The loop expressions used for the computation (replacing the scalar couplings) can be found in App. C.1.3.

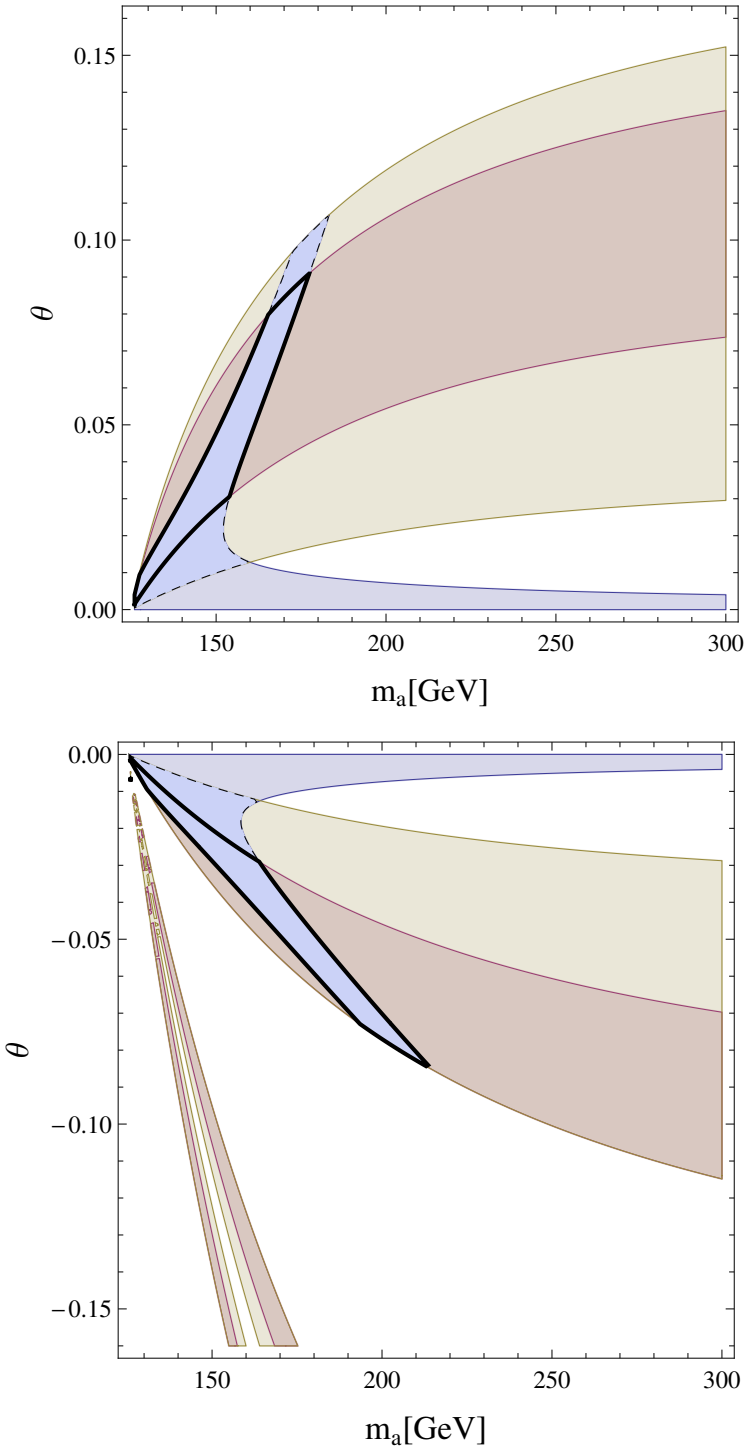

Figure 4.2: Parameter values leading to $|y_{\mu\tau}|$ required by CMS data on $h \to \mu\tau$ in brown (68% C.L.) and yellow (95% C.L.) for positive and negative θ, respectively. The parameter regions shaded in blue are allowed by $\mathcal{B}(\mu \to e\gamma) < 5.7 \times 10^{-13}$. The solid (dashed) lines mark the $1\,\sigma$ ($2\,\sigma$) intervals of $|y_{\mu\tau}|$ where the excess in $h \to \mu\tau$ and $\mathcal{B}(\mu \to e\gamma)$ can be accommodated simultaneously.

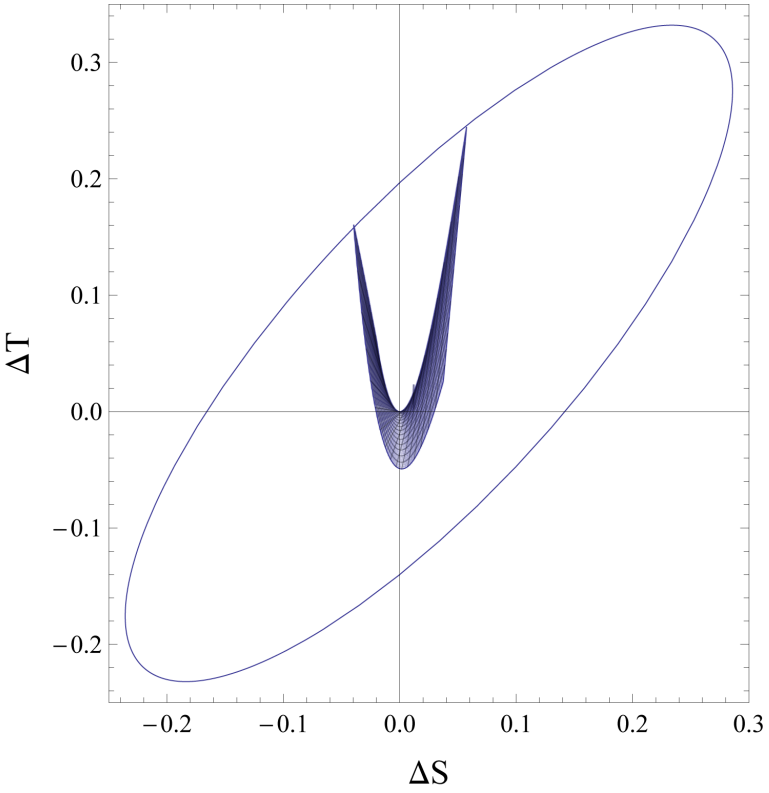

Figure 4.3: The ΔS-ΔT plane, where the ellipsis denotes the experimentally allowed region at 95% C.L. [201]. The origin $\Delta S = \Delta T = 0$ corresponds to the SM value, with $m_h = 125.5$ GeV and $m_t = 176$ GeV. The shape inside the ellipsis denotes the values of ΔT and ΔS as the scalar mass is varied in the range 126 GeV $\lesssim m_H \lesssim$ 200 GeV. Requiring that ΔT and ΔS stay inside the experimental limits yields the allowed mass range 116 GeV $< m_{H^\pm} <$ 240 GeV.

Using the determined $1\,\sigma$ parameter ranges [Eq. (4.54)], we can make predictions for other rare decays, including the decays $l \to l'\gamma$ and $l \to 3l'$. The flavor-violating modes $\mathcal{B}(\tau \to 3\mu) < 2.1 \times 10^{-8}$, $\mathcal{B}(\tau \to 3e) < 2.7 \times 10^{-8}$, and $\mathcal{B}(\mu \to 3e) < 1.0 \times 10^{-12}$ [6] are approximately given by

$$\mathcal{B}(l \to 3l') = -\frac{\tau_l \alpha_{\rm EM}^2 m_l^5}{72(2\pi)^5}\left[12\log\frac{m_l'^2}{m_l^2} + 29 + 6\log 4\right]\left(|c_L|^2 + |c_R|^2\right), \qquad (4.55)$$

assuming that loop diagrams in the spirit of Fig. 4.1 (γ decays into l^+l^-) dominate over the tree-level exchange of a neutral scalar field [51].

Our predictions for $0.01 \lesssim \theta \lesssim 0.09$, $126\,\text{GeV} \lesssim m_H \lesssim 204\,\text{GeV}$ ($m_\eta = 200\,\text{GeV}$),

$$\begin{aligned}
\mathcal{B}(\tau \to \mu\gamma) &\in (0.3 - 1.3) \times 10^{-8}\,, & \mathcal{B}(\tau \to e\gamma) &\in (0.3 - 1.3) \times 10^{-8}\,,\\
\mathcal{B}(\tau \to 3\mu) &\in (1.9 - 8.1) \times 10^{-10}\,, & \mathcal{B}(\tau \to 3e) &\in (0.9 - 4.1) \times 10^{-9}\,,\\
\mathcal{B}(h \to e\tau) &\in (0.4 - 1.2) \times 10^{-2}\,, & \mathcal{B}(h \to e\mu) &\in (1.5 - 4.2) \times 10^{-5}\,,
\end{aligned}$$

and for $-0.08 \lesssim \theta \lesssim -0.01$, $127\,\text{GeV} \lesssim m_H \lesssim 190\,\text{GeV}$,

$$\begin{aligned}
\mathcal{B}(\tau \to \mu\gamma) &\in (0.3-1.2)\times 10^{-8}\,, & \mathcal{B}(\tau \to e\gamma) &\in (0.3-1.2)\times 10^{-8}\,,\\
\mathcal{B}(\tau \to 3\mu) &\in (2.0-7.6)\times 10^{-10}\,, & \mathcal{B}(\tau \to 3e) &\in (1.1-4.1)\times 10^{-9}\,,\\
\mathcal{B}(h \to e\tau) &\in (0.5-1.4)\times 10^{-2}\,, & \mathcal{B}(h \to e\mu) &\in (1.5-4.1)\times 10^{-5}\,,
\end{aligned}$$

are throughout below the current bounds, but not too small to be out of reach for future experiments. A measurement of the $h \to e\tau$ channel using the newest LHC data should be the fastest way to rule out this model in the near future, as our prediction for this channel is unambiguously connected to $h \to \mu\tau$ and expected to be the same order of magnitude. This is shown by the ratio

$$\frac{\mathcal{B}(h \to \mu\tau)}{\mathcal{B}(h \to e\tau)} \approx \frac{|y_{\mu\tau}|^2}{|y_{e\tau}|^2} \approx \frac{(c_{\alpha_L}+s_{\alpha_L})^2}{(c_{\alpha_L}-s_{\alpha_L})^2}\,, \tag{4.56}$$

which is approximately 1 for small values of θ. Using Eqs. (3.75) and (4.51), we also predict a nonvanishing leptonic CP phase $\delta^L_{\text{CP}} \approx 0.3$ at $\theta = -0.08$, the maximal value still in agreement with the lepton mixing angles. MINOS and NOvA are planning to measure δ^L_{CP} in the near future. The latest results from T2K, however, point towards nearly maximal CP violation in the lepton sector with $\delta^L_{\text{CP}} = [-3.13, -0.39]$ (NH), $[-2.09, -0.74]$ (IH) at 90% C.L. [202].

While the neutral scalars H and η may be well hidden thanks to their tiny Yukawa couplings, it becomes increasingly unlikely that light scalar states remain undetected in the accumulating LHC Run 2 data. Together with the updated measurements of $h \to \mu\tau$, the rather fine-tuned parameter space indicates that the initial CMS report may indeed just be a statistical fluctuation. The T and S parameters also point to light charged scalars, while the study of $h \to \gamma\gamma$ in App. C.3.3 could not provide complementary limits on the Higgs parameter space. Furthermore, although not excluded yet, our distinct prediction $\mathcal{B}(h \to e\tau) \sim \mathcal{B}(h \to \mu\tau)$ is already in tension with first searches for LFV in the $h \to e\tau$ channel [73]. To conclude, a multi-Higgs model would be the most logical solution to explain the large flavor violation reported in $h \to \mu\tau$. However, while it is possible to find a viable region in parameter space, the corresponding predictions should manifest themselves at the LHC right now.

4.2 CHARGED SCALARS, DISCRETE SYMMETRIES, AND $R_{D^{(*)}}$

Among the many unresolved anomalies, the deviation in $R_{D^{(*)}}$ is particularly intriguing since it has a high statistical significance of more than $4\,\sigma$ after combining all existent measurements. It is intuitive to explain this charged current anomaly that seems to prefer τ over e and μ final states with charged Higgses, whose couplings typically scale with the fermion masses (see Fig. 1.12).

The widely studied 2HDM type II, however, cannot fulfill the requirements imposed by experimental data, calling for more elaborate extensions [41]. A possibility is to consider a more general flavor structure realized by the 2HDM type III [203] or a third Higgs doublet. In this section we study whether 3HDMs with flavor symmetries can shed light on the excess in $\overline{B} \to D^{(*)}\tau\overline{\nu}$ decays.

After reviewing the challenges in 2HDMs in Sec. 4.2.1, we extend the framework in Sec. 4.2.2 to 3HDMs focusing on the charged scalar interactions to make predictions for

$R_{D^{(*)}}$. We further discuss how the most popular discrete flavor symmetries with triplet representations affect these predictions and apply the framework to the S_4 flavor model presented in Sec. 4.1.

4.2.1 *2HDM type II and III*

The challenges of building a model to explain $R_{D^{(*)}}$ go way beyond modifying the $\overline{B} \to D^{(*)}\tau\overline{\nu}$ channel. In fact, the NP model should not only accommodate R_D, R_{D^*} and $\overline{B} \to \tau\overline{\nu}$ at the same time, but also the $B^0_{s,d} - \overline{B}^0_{s,d}$ oscillations and the radiative decays $b \to q\gamma$, $q = s, d$. Multi-Higgs extensions typically affect all of these observables simultaneously without an additional mechanism to forbid specific couplings. In that respect discrete flavor symmetries are particularly useful. The task becomes even more challenging when taking into account the shape of the measured q^2 distribution provided by BaBar [41].

One of the most studied extensions of the SM, the 2HDM type II requires particularly large values of $\frac{\tan^2\beta}{m^2_{H^\pm}}$ to accommodate the excess in $R_{D^{(*)}}$ [41]. Such large $\tan\beta$ values modify the q^2 spectra of $\overline{B} \to D^{(*)}\tau\overline{\nu}$ in an undesired fashion and thereby disfavor the 2HDM type II. Moreover, the model provides only one scalar operator which cannot fit the three observables R_D, R_{D^*} and $\mathcal{B}(\overline{B}^\pm \to \tau\overline{\nu})$ at the same time.

To accommodate the channels simultaneously, a more general flavor structure with both Higgses coupling to all quarks is necessary.[2] The relevant effective Hamiltonian is

$$\mathcal{H}_{\text{eff}} = C_{\text{SM}} O_{\text{SM}} + C_R O_{SR} + C_L O_{SL}, \tag{4.57}$$

with

$$\begin{aligned} O_{\text{SM}} &= [\overline{c}\gamma_\mu P_L b][\overline{\tau}\gamma_\mu P_L \nu_\tau]\,, \\ O_{SR} &= [\overline{c} P_R b][\overline{\tau} P_L \nu_\tau]\,, \\ O_{SL} &= [\overline{c} P_L b][\overline{\tau} P_L \nu_\tau]\,, \end{aligned} \tag{4.58}$$

in the limit of massless neutrinos. While the 2HDM type II provides only C_R in addition to C_{SM}, the type III also allows for a nonzero C_L, which can be used to explain the data. In type III the ratios are modified in the following way [203]:

$$\begin{aligned} R_D &= R_D^{\text{SM}} \left(1 + 1.5\text{Re}\left[\frac{C_R + C_L}{C_{\text{SM}}}\right] + 1.0\left|\frac{C_R + C_L}{C_{\text{SM}}}\right|^2\right), \\ R_{D^*} &= R_{D^*}^{\text{SM}} \left(1 + 0.12\text{Re}\left[\frac{C_R - C_L^{cb}}{C_{\text{SM}}}\right] + 0.05\left|\frac{C_R - C_L}{C_{\text{SM}}}\right|^2\right), \end{aligned} \tag{4.59}$$

where $R^{\text{SM}}_{D^{(*)}}$ is the SM value of the respective observable. The Wilson coefficients in turn are determined by the charged scalar Yukawa couplings $\Gamma^{L(R)H^\pm}$

$$C_{R(L)} = -\frac{1}{M^2_{H^\pm}} \Gamma^{L(R)H^\pm}_{cb} \Gamma^{LH^{\pm *}}_{\nu\tau}\,, \qquad C_{\text{SM}} = \frac{4G_F}{\sqrt{2}} V_{cb}\,, \tag{4.60}$$

which can be extracted from the respective Yukawa Lagrangian.

[2] Anomalously enhanced charged Higgs couplings in the flipped 2HDM are another possibility [204].

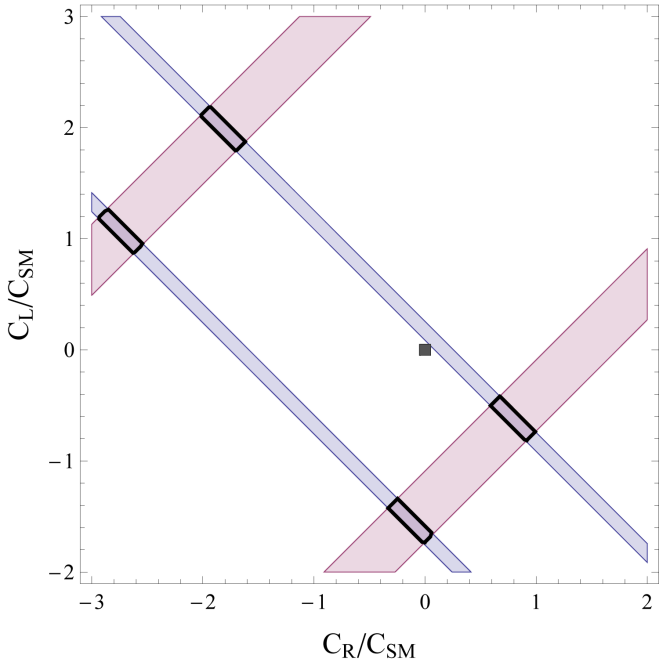

Figure 4.4: Constraints on C_R - C_L from R_D (blue) and R_{D^*} (red) narrow the parameter space down to tiny viable regions. The gray dot marks the SM value.

Depicting the constraints from R_D and R_{D^*} in the C_R - C_L plane (see Fig. 4.4), we find that explaining both ratios simultaneously may require fine-tuning even in 2HDMs with flavor violation. A full flavor analysis based on the 2HDM type III has been done in Ref. [203].

4.2.2 *3HDMs with Flavor Symmetries*

The additional charged scalars and mixing angles of the 3HDM result in a more complicated charged scalar Lagrangian. Specific assumptions about the flavor structure simplify the couplings at the expense of less freedom to fit the observables. Alternatively, discrete flavor symmetries can be exploited to obtain relations among the scalar mixing angles by simplifying the 3HDM scalar potential.
The charged scalar interactions are easiest described in the Higgs basis, where

$$\langle \phi^h_{1,0} \rangle = v, \quad \langle \phi^h_{2,0} \rangle = 0, \quad \text{and} \quad \langle \phi^h_{3,0} \rangle = 0 \tag{4.61}$$

with $v^2 = v^2_{\text{SM}} = v_1^2 + v_2^2 + v_3^2$ and the Higgs basis doublets take the form

$$\phi^h_1 = \begin{pmatrix} G^+ \\ \frac{1}{\sqrt{2}}(v + H_1 + G_0) \end{pmatrix}, \quad \phi^h_{2,3} = \begin{pmatrix} H^+_{2,3} \\ \frac{1}{\sqrt{2}}(H_{2,3} + iA_{2,3}) \end{pmatrix}. \tag{4.62}$$

In this notation the Goldstone bosons G_0 and G^+ that are absorbed by the gauge bosons are located in the doublet ϕ^h_1. As shown in Sec. 2.2.2, the charged Higgs couplings are then described by nondiagonal matrices η and ξ that vanish in the SM limit. The Higgs basis rotation depends only on the VEV alignment preferred by the 3HDM potential and is given by Eq. (2.37).

The charged scalar Lagrangian for the quarks is then written as

$$\begin{aligned}-\mathcal{L}_{ud}^{\pm} =& \overline{u}_i (V_{ik}^{\mathrm{CKM}} \widetilde{\eta}_{kj}^{d} P_R - \widetilde{\eta}_{ik}^{u*} V_{kj}^{\mathrm{CKM}} P_L) d_j H_2^+ \\ &+ \overline{u}_i (V_{ik}^{\mathrm{CKM}} \widetilde{\xi}_{kj}^{d} P_R - \widetilde{\xi}_{ik}^{u*} V_{kj}^{\mathrm{CKM}} P_L) d_j H_3^+ + \mathrm{h.c.}\,,\end{aligned} \tag{4.63}$$

where

$$V_L^{u,d} \eta_{ij}^{u,d} V_R^{u,d\dagger} = \widetilde{\eta}_{ij}^{u,d}\,, \qquad V_L^{u,d} \xi_{ij}^{u,d} V_R^{u,d\dagger} = \widetilde{\xi}_{ij}^{u,d}\,. \tag{4.64}$$

The matrices $V_{L,R}^{u,d}$ entering $\widetilde{\eta}^{u,d}$ and $\widetilde{\xi}^{u,d}$ transform the fermions into their mass bases and can be derived from

$$V_L^{u,d} y_{ij}^{u,d} V_R^{u,d\dagger} = \frac{1}{v} m^{u,d} \quad \text{and} \quad V_{\mathrm{CKM}} = V_L^u V_L^{d,\dagger}\,, \tag{4.65}$$

where $y_{ij}^{u,d}$ are the couplings of the doublet ϕ_1^h. In the same fashion the charged lepton couplings read ($V^{\mathrm{PMNS}} \equiv U$)

$$-\mathcal{L}_l^{\pm} = \overline{\nu}_{iL} \left[U_{ik}^T \widetilde{\eta}_{kj}^{l} H_2^+ + U_{ik}^T \widetilde{\xi}_{kj}^{l} H_3^+ \right] l_{jR} + \mathrm{h.c.} \tag{4.66}$$

Keeping in mind that the $H_{2,3}^{\pm}$ fields still have to be transformed into the mass basis

$$\begin{pmatrix} H_2^{\pm} \\ H_3^{\pm} \end{pmatrix} = \begin{pmatrix} \cos\rho & \sin\rho \\ -\sin\rho & \cos\rho \end{pmatrix} \begin{pmatrix} H_b^{\pm} \\ H_c^{\pm} \end{pmatrix}, \tag{4.67}$$

we can derive the couplings $\Gamma^{L(R)H^{\pm}}$ for quarks from Eq. (4.63)

$$\begin{aligned}\Gamma_{cb}^{LH_b^{\pm}} &= V_{ck}^{\mathrm{CKM}} (\widetilde{\eta}_{kb}^{d} \cos\rho - \widetilde{\xi}_{kb}^{d} \sin\rho)\,, \\ \Gamma_{cb}^{LH_c^{\pm}} &= V_{ck}^{\mathrm{CKM}} (\widetilde{\eta}_{kb}^{d} \sin\rho + \widetilde{\xi}_{kb}^{d} \cos\rho)\,, \\ \Gamma_{cb}^{RH_b^{\pm}} &= -(\widetilde{\eta}_{ck}^{u*} \cos\rho - \widetilde{\xi}_{ck}^{u*} \sin\rho) V_{ki}^{\mathrm{CKM}}\,, \\ \Gamma_{cb}^{RH_c^{\pm}} &= -(\widetilde{\eta}_{ck}^{u*} \sin\rho + \widetilde{\xi}_{ck}^{u*} \cos\rho) V_{kb}^{\mathrm{CKM}}\,,\end{aligned} \tag{4.68}$$

where we implicitly use the Einstein notation for repeated indices. In the charged lepton sector we have (after summing over the neutrino states)

$$\begin{aligned}\Gamma_{\nu\tau}^{LH_b^{\pm}} &= \sum_{f=1}^{3} U_{fk}^T \left[\widetilde{\eta}_{k\tau}^{l} \cos\rho - \widetilde{\xi}_{k\tau}^{l} \sin\rho \right]\,, \\ \Gamma_{\nu\tau}^{LH_c^{\pm}} &= \sum_{f=1}^{3} U_{fk}^T \left[\widetilde{\eta}_{k\tau}^{l} \sin\rho + \widetilde{\xi}_{k\tau}^{l} \cos\rho \right]\,.\end{aligned} \tag{4.69}$$

Finally, in the Higgs mass basis the relevant Wilson coefficients are

$$C_{R(L)} = -\left(\frac{1}{m_{H_b^{\pm}}^2} \Gamma_{cb}^{L(R)H_b^{\pm}} \Gamma_{\nu\tau}^{LH_b^{\pm}\,*} + \frac{1}{m_{H_c^{\pm}}^2} \Gamma_{cb}^{L(R)H_c^{\pm}} \Gamma_{\nu\tau}^{LH_c^{\pm}\,*} \right)\,, \tag{4.70}$$

which we can combine with Eqs. (4.68) and (4.69) to estimate the impact on $R_{D^{(*)}}$. To make more specific predictions we study in the following how discrete symmetries affect the charged Higgs interactions in the 3HDM.

Discrete Symmetries

For this analysis we assume that the three scalar doublets are unified into a triplet representation of a flavor symmetry. The scalar interactions can then be studied for the VEV alignments that minimize the scalar potential. These were derived systematically for the A_4-, S_4- and $\Delta(27)$-symmetric 3HDM potentials using geometric minimization [120]. Their global minima are

$$v(1,0,0)\,, \qquad v(1,1,1)\,, \tag{4.71}$$

plus two complex VEV alignments for each of the groups. Discussing the additional source of CP violation entailed by these complex VEVs is beyond the scope of this work. Focusing therefore on the real alignments we obtain the Higgs basis rotations $R_{v00} = I$ and R_{vvv} given in Eq. (2.38).
The shape of the scalar potential decides over the global minimum and also determines the scalar mass eigenstates fixing the angle ρ in the charged Higgs interactions. Quartic couplings in the scalar potential can lead to deviations from these alignments, which, for the sake of simplicity, are neglected here as they produce only subleading effects.
The general A_4-symmetric 3HDM potential [119]

$$\begin{aligned} V(\phi) = -\mu^2 \sum_{i=1}^{3} \phi_i^\dagger \phi_i + \alpha \left(\sum_{i=1}^{3} \phi_i^\dagger \phi_i \right)^2 + \sum_{i,j=1, i\neq j}^{3} \Big(\beta (\phi_i^\dagger \phi_i)(\phi_j^\dagger \phi_j) + \gamma |\phi_i^\dagger \phi_j|^2 \Big) \\ + \Big(\delta \left[(\phi_1^\dagger \phi_2)^2 + (\phi_2^\dagger \phi_3)^2 + (\phi_3^\dagger \phi_1)^2 \right] + \text{h.c.} \Big) \quad (\mu, \alpha, \beta, \gamma, \delta, \sigma \in \mathbb{R})\,. \end{aligned} \tag{4.72}$$

extends to S_4 in the case that δ is real, which we adopt in the following. Hence, most statements regarding the A_4 potential also apply to S_4 and vice versa. An interesting feature of the S_4 potential is that the VEV alignments $v(1,1,1)$ and $v(1,0,0)$ and their respective Higgs basis rotations already diagonalize the charged Higgs couplings without further ado. As a consequence, the mixing angle ρ is zero and the charged scalar couplings can simply be derived from the Higgs basis Lagrangian with

$$\begin{aligned} v_1 = v_2 = v_3 \ : \quad & m^2_{H^\pm_{1,2}} = m^2_{H^\pm_{b,c}} = -v^2(\gamma + \delta), \\ v_2 = v_3 = 0 \ : \quad & m^2_{H^\pm_{1,2}} = m^2_{H^\pm_{b,c}} = v^2(\gamma - \delta). \end{aligned} \tag{4.73}$$

Therefore, in both alignments the Wilson coefficients $C_{R(L)}$ reduce to

$$C_R = -\frac{1}{m^2_{H^\pm_{b,c}}} \sum_{m=1}^{3} V_{cn}^{\text{CKM}} \left[\widetilde{\eta}^d_{nb} U^\dagger_{mk} \widetilde{\eta}^{l*}_{k\tau} + \widetilde{\xi}^d_{nb} U^\dagger_{mk} \widetilde{\xi}^{l*}_{k\tau} \right], \tag{4.74}$$

$$C_L = \frac{1}{m^2_{H^\pm_{b,c}}} \sum_{m=1}^{3} \left[\widetilde{\eta}^u_{cn} V_{nb}^{\text{CKM}} U^\dagger_{mk} \widetilde{\eta}^{l*}_{k\tau} + \widetilde{\xi}^u_{cn} V_{nb}^{\text{CKM}} U^\dagger_{mk} \widetilde{\xi}^{l*}_{k\tau} \right] \tag{4.75}$$

and since the contributions of $H_b^\pm$ and $H_c^\pm$ are indistinguishable because of their mass degeneracy, we can further replace $\widetilde{\eta} + \widetilde{\xi} \to \widetilde{\eta}'$ yielding

$$C_R = -\frac{1}{m^2_{H^\pm_{b,c}}} \sum_{m=1}^{3} V_{cn}^{\text{CKM}} \widetilde{\eta}^{d\prime}_{nb} U^\dagger_{mk} \widetilde{\eta}^{l\prime *}_{k\tau}\,, \tag{4.76}$$

$$C_L = \frac{1}{m^2_{H^\pm_{b,c}}} \sum_{m=1}^{3} \widetilde{\eta}^{u\prime}_{cn} V_{nb}^{\text{CKM}} U^\dagger_{mk} \widetilde{\eta}^{l\prime *}_{k\tau}\,. \tag{4.77}$$

For the $\Delta(27)$ symmetric potential

$$\begin{aligned} V(\phi) = &-\mu^2 \sum_{i=1}^{3} \phi_i^\dagger \phi_i + \alpha \left(\sum_{i=1}^{3} \phi_i^\dagger \phi_i \right)^2 + \sum_{i,j=1, i\neq j}^{3} \left[\beta (\phi_i^\dagger \phi_i)(\phi_j^\dagger \phi_j) + \gamma |\phi_i^\dagger \phi_j|^2 \right] \\ &+ \left(\delta \left[(\phi_1^\dagger \phi_2)(\phi_1^\dagger \phi_3) + (\phi_2^\dagger \phi_3)(\phi_2^\dagger \phi_1) + (\phi_3^\dagger \phi_1)(\phi_3^\dagger \phi_2) \right] + \text{h.c.} \right) \end{aligned} \tag{4.78}$$

with $\mu, \alpha, \beta, \gamma \in \mathbb{R}, \delta \in \mathbb{C}$, the charged Higgs masses are

$$\begin{aligned} v_1 = v_2 = v_3 \ : \quad & m^2_{H^\pm_{1,2}} = m^2_{H^\pm_{b,c}} = -v^2(\gamma + \text{Re}\,\delta)\,, \\ v_2 = v_3 = 0 \ : \quad & m^2_{H^\pm_{1,2}} = m^2_{H^\pm_{b,c}} = -v^2\beta\,. \end{aligned} \tag{4.79}$$

Thanks to the discrete symmetry, also here the Higgs basis transformations diagonalize the charged Higgs Yukawa couplings with $\rho = 0$. Therefore the Wilson coefficients $C_{R(L)}$ are again given by Eqs. (4.76) and (4.77).
In conclusion, the highly symmetric VEV alignments of symmetries with triplet representations greatly simplify the charged Higgs couplings of 3HDMs. Since the charged Higgs bosons are degenerate in mass, the 3HDM is reduced by the flavor symmetry to an effective 2HDM type III. This generic feature disfavors some of the most popular models based on A_4 or S_4 that are motivated by neutrino mixing data as candidates to explain the $R_{D^{(*)}}$ anomaly. An example using the S_4 flavor model of Sec. 4.1 is discussed in the following subsection.

S_4 Model Example

Using the S_4 model of Sec. 4.1 as an example, the matrices η^l, ξ^l, V_L, and V_R are derived easily from the basic structure of the charged lepton sector. The scalar triplet ϕ acquires VEVs in the alignment $\frac{v}{\sqrt{3}}(1,1,1)$, hence the Lagrangian is transformed into the Higgs basis via the R_{vvv} rotation given in Eq. (2.38). The ϕ_1^h couplings are given by the matrix y^l, which has to be diagonalized yielding the unitary matrices $V^l_{L,R}$. Explicitly,

$$y^l = \frac{1}{v}\sqrt{\frac{2}{3}} \begin{pmatrix} m_e & m_\mu & m_\tau \\ \omega^2 m_e & \omega m_\mu & m_\tau \\ \omega m_e & \omega^2 m_\mu & m_\tau \end{pmatrix}, \qquad \omega = e^{\frac{2i\pi}{3}}\,, \tag{4.80}$$

is diagonalized by a bi-unitary transformation $V_L y^l V_R^\dagger$ with

$$V_L = \frac{1}{\sqrt{3}} \begin{pmatrix} 1 & \omega & \omega^2 \\ 1 & \omega^2 & \omega \\ 1 & 1 & 1 \end{pmatrix} \qquad \text{and} \qquad V_R = \text{diag}(1,1,1)\,. \tag{4.81}$$

The matrices V_L and V_R in turn determine the entries of $\widetilde{\eta}^l$ and $\widetilde{\xi}^l$ that eventually fix the charged Higgs couplings. In agreement with Eq. (4.73) the charged scalar masses are degenerate, therefore their couplings cannot be distinguished in an experiment and we can redefine $\widetilde{\eta}^l + \widetilde{\xi}^l \equiv \widetilde{\eta}^{l\prime}$, which is precisely

$$\widetilde{\eta}^{l\prime} = -\frac{\sqrt{2}}{v} \begin{pmatrix} 0 & m_\mu & m_\tau \\ m_e & 0 & m_\tau \\ m_e & m_\mu & 0 \end{pmatrix}. \tag{4.82}$$

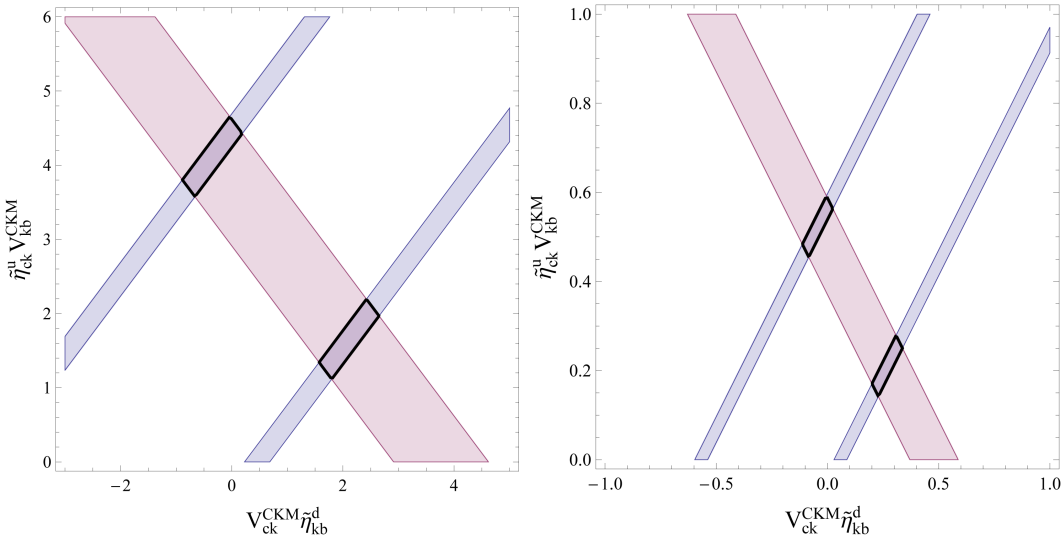

Figure 4.5: Constraints from R_D (blue) and R_{D^*} (red) in the $V^{\mathrm{CKM}}\widetilde{\eta}^{d\prime}$ - $\widetilde{\eta}^{u\prime}V^{\mathrm{CKM}}$ plane with $\Gamma^{LH^\pm}_{\nu\tau} = -\frac{2\sqrt{2}}{v}m_\tau, m_{H^\pm} = 200$ GeV (a) and $\Gamma^{LH^\pm}_{\nu\tau} = -1, m_{H^\pm} = 500$ GeV (b).

In conclusion, the sum of the charged lepton contributions $\Gamma^{LH^\pm}_{\nu\tau}$ entering the Wilson coefficients $C_{R(L)}$ is

$$\Gamma^{LH^\pm}_{\nu\tau} = -\frac{\sqrt{2}m_\tau}{v}\sum_{i=1}^{2}\sum_{j=1}^{3}U_{ij} = -a\frac{\sqrt{2}m_\tau}{v}\,, \tag{4.83}$$

where a is an order one coefficient defined by the sum of the PMNS matrix elements. Using this result (assuming for simplicity $a \approx 1$) and the constraints from R_D and R_{D^*}, Eq. (4.59), we can determine the values of $\widetilde{\eta}^{d,u\prime}$ required to explain the ratios. As Fig. 4.5 (a) shows, the anomaly could be explained by pure up-type flavor violation in some region of the parameter space. However, $\widetilde{\eta}^{u\prime}$ has to be at the minimum order 1, which implies flavor-violating couplings at least of the order of the top Yukawa for $m_{H^\pm} = 200$ GeV. More realistically though, the charged Higgs masses should be much heavier to avoid tension with rare B decays and direct searches via decays into $W^\pm$ gauge bosons. This in turn would require even larger $\widetilde{\eta}^{u\prime}$ couplings to account for $R_{D^{(*)}}$.

Fig. 4.5 (b) depicts an alternative scenario with order one lepton couplings and charged Higgs masses of 500 GeV. In this scenario up-type flavor violation may be much smaller, but the large LFV should be checked against processes such as $\mu \to e\gamma$.

Since Higgs couplings to fermions are typically of the order of $m_f/v_{\mathrm{SM}} \ll 1$, it is difficult to explain the origin of such large flavor-violating couplings in a multi-Higgs framework with discrete symmetries. We therefore conclude that charged scalars may not be the ideal candidates to explain the $R_{D^{(*)}}$ anomaly and take another approach to the B meson puzzle in the following section.

4.3 COMMON ORIGIN OF B DECAYS AND NEUTRINO MASSES

TeV scale leptoquarks modifying $b \to sll$ and $b \to \bar{c}l\nu$ transitions are among the most prominent solutions to the flavor puzzles posed by low-energy precision B physics. Viable candidates to explain the observables R_K and $R_{D^{(*)}}$ include the scalar leptoquarks S_0 and S_1 [186, 205–211], and the vector leptoquarks V_0 and $V_{1/2}$ [212–214]. Attempts have been made using leptoquarks to draw connections beyond B physics to other unexplained phenomena, such as neutrino masses [147, 215–222], $0\nu\beta\beta$ decay [223, 224], $g-2$ [62, 225, 226], $h \to \mu\tau$ [226, 227], and even the diphoton excess near 750 GeV reported in 2015 [228, 229]. Vector leptoquarks in particular have been shown to be excellent candidates to explain the latter without the need of introducing many additional fermions [228, 230]. For a recent review on leptoquark physics, see Ref. [231]. Conveniently, constraints from B-physics force the leptoquarks into a testable range, $1\,\text{TeV} \lesssim M \lesssim 50\,\text{TeV}$, with an upper bound on their mass dictated by the $B_s - \overline{B}_s$ mixing phase [205].

In this section we explore the possibility of such TeV scale leptoquarks being responsible for low-scale neutrino masses, thereby connecting several currently unresolved phenomena of the SM. The idea of leptoquarks as the origin of neutrino masses has been considered before, but previous attempts expected lighter leptoquarks with small couplings or involve two loops, where one of the leptoquarks cannot be linked to the B anomalies as it couples only to up-type quarks. Explaining R_K and R_D, on the other hand, requires sizable couplings to down-type quarks and charged leptons, posing a challenge to combine the seemingly distinct observables.

To this end we propose viable flavor patterns based on an FN framework for the scalar leptoquarks S_1 and $S_{1/2}$, and for the vector leptoquarks V_0 and $V_{1/2}$ to accommodate the B physics anomalies and neutrino masses. Even the diphoton excess can be addressed in this model, which is discussed in chapter 5.2. The FN mechanism reproduces the fermion mass hierarchies and the quark mixing in good agreement with experimental data [85], while the neutrino-leptoquark interactions give rise to the large leptonic mixing angles.

We introduce the necessary tools in the context of the scalar leptoquark model with S_1 and $S_{1/2}$ in Sec. 4.3.1 and discuss under which conditions this model can accommodate the R_K anomaly and neutrino masses. For the sake of clarity, a more thorough analysis using the vector leptoquarks V_0 and $V_{1/2}$ is postponed to Sec. 4.3.2. These leptoquarks additionally account for the observed deviations in $R_{D^{(*)}}$ and consequently require a more intricate model realization.

4.3.1 *A Scalar Leptoquark Model for R_K and Neutrino Masses*

The mixing of two leptoquarks induced by a $\Delta L = 2$ Higgs boson coupling is not only crucial for generating Majorana neutrino masses, it can also affect the B meson observables if these two leptoquarks both contribute to down-type quark transitions. To explore whether the B meson anomalies and neutrino masses can actually be combined in one framework, we start from a minimal model based on the scalar leptoquarks S_1 and $S_{1/2}$. The section is divided into three parts. First we study the leptoquark mixing

and their effects on R_K, then we discuss the generation of neutrino masses, and finally we propose some ideas to combine the two processes.

Leptoquark Mixing and R_K

As shown in Ref. [205], the deviation in R_K is best explained by (axial) vector operators that, unlike scalar operators, affect $B \to Kll$ but leave $B_s \to ll$ unchanged. Due to Fierz rearrangement [150], the desired vector operators are induced by scalar leptoquarks with electric charge $2/3$ or $-4/3$ that couple to down-type quarks and charged leptons. In light of neutrino mass generation we focus only on the $2/3$ leptoquarks, whose mixing can induce a Majorana mass as depicted in Fig. 4.7. Their corresponding quantum numbers are listed in Tab. 4.6.

Leptoquark	$(SU(3)_C, SU(2)_L)_{U(1)_Y}$	Q_{EM}	B	L
$S_{1/2}$	$(3,2)_{1/6}$	$(-1/3, 2/3)$	$1/3$	-1
S_1	$(3,3)_{-1/3}$	$(2/3, -1/3, -4/3)$	$1/3$	1

Table 4.6: Quantum numbers of the scalar leptoquarks with electric charge $2/3$ that can account for the R_K anomaly as well as neutrino masses. B and L here refer to baryon and lepton number, respectively.

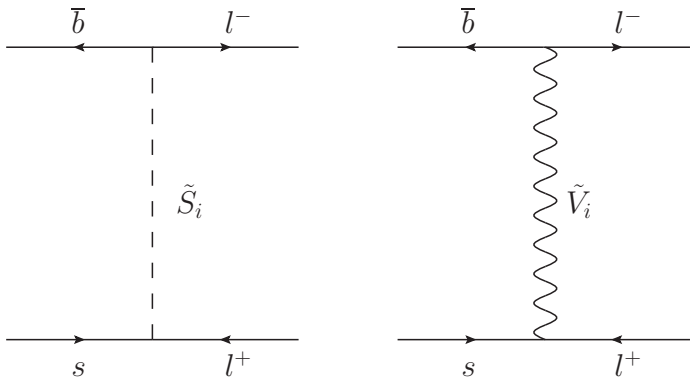

Figure 4.6: $\overline{b} \to \overline{s}ll$ transition mediated by the scalar $\tilde{S}_i$ $(i = 1, 2)$ (left) and vector leptoquark $\tilde{V}_i$ $(i = 1, 2)$ mass eigenstates (right), defined in Eq. (4.90) and Eq. (4.127), respectively.

To study effects on R_K it is convenient to work with a flavor-changing $|\Delta B| = |\Delta S| = 1$ effective Hamiltonian, integrating out the heavy degrees of freedom

$$\mathcal{H}_{\text{eff}} = -4\frac{G_F}{\sqrt{2}} V_{tb} V_{ts}^* \frac{\alpha_e}{4\pi} \sum_i C_i \mathcal{O}_i \,, \tag{4.84}$$

where G_F is the Fermi constant, α_e the electromagnetic coupling, V_{ud} the CKM matrix elements, and C_i are the Wilson coefficients of their operators $\mathcal{O}_i$.

By adding the leptoquarks listed in Tab. 4.6 to the SM field content we can write down interactions of the form

$$-\mathcal{L}^S_{\rm LQ} = \lambda^R_{S_{1/2}} \overline{d} P_L L S_{1/2} + \lambda^L_{S_1} \overline{Q^c} P_L i\tau_2 S_1^\dagger L + \text{h.c.} \tag{4.85}$$

After Fierz rearrangement these leptoquarks generate the effective (axial) vector operators

$$\begin{aligned} \mathcal{O}_9 &= [\bar{s}\gamma^\mu P_L b] \left[\bar{l}\gamma_\mu l\right], \\ \mathcal{O}_{10} &= [\bar{s}\gamma^\mu P_L b] \left[\bar{l}\gamma_\mu\gamma_5 l\right], \end{aligned} \tag{4.86}$$

and their chirality flipped counterparts $\mathcal{O}'_{9,10}$ by interchanging the chiral projectors P_L and P_R. A comparison with Eq. (4.84) yields ($l = e, \mu$),

$$\begin{aligned} S_1: \quad C_9^l &= -C_{10}^l = \frac{\pi}{\alpha_e} \frac{\left(\lambda^L_{sl}\right)^* \lambda^L_{bl}}{V_{tb}V_{ts}^*} \frac{\sqrt{2}}{2m^2_{S_1} G_F}, \\ S_{1/2}: \quad C_{10}^{\prime l} &= -C_9^{\prime l} = \frac{\pi}{\alpha_e} \frac{\lambda^R_{sl} \left(\lambda^R_{bl}\right)^*}{V_{tb}V_{ts}^*} \frac{\sqrt{2}}{4m^2_{S_{1/2}} G_F}, \end{aligned} \tag{4.87}$$

where the ql indices denote one element of the matrix λ^L.
As shown in Refs. [147, 232], two leptoquarks sharing the same electric charge Q will eventually mix through a coupling with the SM Higgs boson via

$$\begin{aligned} V(S_i, H) = \quad & -(m'^2_{S_i} - g_{S_i} H^\dagger H) S_i^\dagger S_i \\ & + h_S H i\tau_2 S_1 S_{1/2}^\dagger + \text{h.c.} \quad (i = 1, 1/2), \end{aligned} \tag{4.88}$$

with $m^2_{S_i} \equiv m'^2_{S_i} - g_{S_i} v^2_{\rm SM}$. The last term, in particular, accounts for the mixing and hence induces neutrino masses if $h_S \neq 0$.
The resulting leptoquark mass eigenstates are a mixture of flavor states with the $Q_{\rm EM}$ charges $2/3$, $-1/3$, and a distinct $-4/3$ state

$$\begin{aligned} M^2_{2/3} &= M^2_{-1/3} = \begin{pmatrix} m'^2_{S_1} - g_{S_1} v^2_{\rm SM} & h_S v_{\rm SM} \\ h_S v_{\rm SM} & m'^2_{S_{1/2}} - g_{S_{1/2}} v^2_{\rm SM} \end{pmatrix}, \\ M^2_{-4/3} &= m'^2_{S_1} - g_{S_1} v^2_{\rm SM}. \end{aligned} \tag{4.89}$$

The rotation angle α diagonalizing the $M^2_{2/3}$ matrix is determined by

$$\begin{pmatrix} \tilde{S}_1 \\ \tilde{S}_2 \end{pmatrix} = R \begin{pmatrix} S_1 \\ S_{1/2} \end{pmatrix}_{2/3}, \quad R = \begin{pmatrix} \cos\alpha & -\sin\alpha \\ \sin\alpha & \cos\alpha \end{pmatrix} \tag{4.90}$$

$$\text{and} \quad \tan 2\alpha = \frac{2h_S v_{\rm SM}}{m^2_{S_{1/2}} - m^2_{S_1}}, \tag{4.91}$$

where $\tilde{S}_i$ denotes the leptoquark mass eigenstates. The mixing shifts the absolute leptoquark masses and induces additional (pseudo-)scalar and tensor operators potentially affecting $\mathcal{B}(B_s \to ll)$ and $\mathcal{B}(B \to Kll)$. Their Wilson coefficients are

$$C_S = C_P = \frac{\pi \lambda^R_{sl} \left(\lambda^L_{bl}\right)^*}{4\alpha_e \sqrt{2} G_F V_{tb} V_{ts}^*} \sin 2\alpha \left(\frac{1}{m^2_{\tilde{S}_2}} - \frac{1}{m^2_{\tilde{S}_1}}\right) \tag{4.92}$$

with similar expressions for C'_P and C'_S directly depending on the mixing angle α. For $m^2_{S_{1/2}} \gg m^2_{S_1}$ the coefficients simplify to

$$C_S = C_P \approx -\frac{\pi}{4\alpha_e\sqrt{2}G_F V_{tb}V_{ts}^*}\frac{h_S v_{\rm SM}\lambda^R_{sl}\left(\lambda^L_{bl}\right)^*}{m^2_{S_{1/2}}m^2_{S_1}}\,, \tag{4.93}$$

$$-C'_P = C'_S \approx -\frac{\pi}{4\alpha_e\sqrt{2}G_F V_{tb}V_{ts}^*}\frac{h_S v_{\rm SM}\lambda^L_{sl}\left(\lambda^R_{bl}\right)^*}{m^2_{S_{1/2}}m^2_{S_1}}\,, \tag{4.94}$$

$$C_T = (C_S + C'_S)/4\,, \qquad C_{T_5} = (C_S - C'_S)/4\,. \tag{4.95}$$

The Wilson coefficients $C_{S,P,T}$ are suppressed by a factor $h_S v_{\rm SM}/|\Delta m^2_S|$, with $\Delta m^2_S \equiv m^2_{S_{1/2}} - m^2_{S_1}$, and are therefore less relevant at low energies, but should be taken into account in the case of degenerate leptoquark masses. In the limit of small mixing, the shift of the leptoquark masses also becomes negligible for determining R_K.
As shown, e.g., in Ref. [218], the dimensional parameter h_S cannot be arbitrarily large, but is in fact limited by the condition of positive leptoquark masses and the perturbativity of the theory to

$$h_S \leq m_{S_1}m_{S_{1/2}}/v_{\rm SM}\,. \tag{4.96}$$

The R_K measurement by LHCb implies at $1\,\sigma$ [205]

$$0.7 \lesssim \ {\rm Re}\,[X^e - X^\mu] \lesssim 1.5\,, \quad \text{with} \quad X^l = C^l_9 - C^l_{10} = 2C^l_9\,. \tag{4.97}$$

Hence, with the combination of S_1 and $S_{1/2}$ we obtain in the case of small leptoquark mixing

$$\begin{aligned} X^e - X^\mu = \frac{\pi}{\sqrt{2}\alpha_e G_F V_{tb}V_{ts}^*}\Bigg\{ &\frac{2}{m^2_{S_1}}\left[\left(\lambda^L_{se}\right)^*\lambda^L_{be} - \left(\lambda^L_{s\mu}\right)^*\lambda^L_{b\mu}\right] \\ &- \frac{1}{m^2_{S_{1/2}}}\left[\lambda^R_{se}\left(\lambda^R_{be}\right)^* - \lambda^R_{s\mu}\left(\lambda^R_{b\mu}\right)^*\right]\Bigg\}\,. \end{aligned} \tag{4.98}$$

By considering all constraints on leptoquark couplings to down-type quarks and charged leptons, the authors of Ref. [186] came up with a "data-driven" pattern that complies with all current bounds and can produce a visible signal in $b \to sll$ processes:

$$\lambda_{ql} \sim \lambda_0 \begin{pmatrix} \rho_d\kappa & \rho_d & \rho_d \\ \rho\kappa & \rho & \rho \\ \kappa & 1 & 1 \end{pmatrix} \tag{4.99}$$

with the allowed parameter ranges (assuming $\lambda_0 \approx 1$)

$$\begin{aligned} &\rho_d \lesssim 0.02\,, \qquad \kappa \lesssim 0.5\,, \qquad 10^{-4} \lesssim \rho \lesssim 1\,, \\ &\frac{\kappa}{\rho} \lesssim 0.5\,, \qquad \frac{\rho_d}{\rho} \lesssim 1.6\,. \end{aligned} \tag{4.100}$$

The constraints leading to this pattern are summarized explicitly in Sec. 4.3.2. The overall scale λ_0 is fixed by Eqs. (4.97), (4.98), and the leptoquark masses m_{S_i}, where $\lambda_0 \simeq \mathcal{O}(10^{-2})$ corresponds to light leptoquarks of a few TeV, while $\lambda_0 \approx 1$ implies heavy

leptoquarks. Assuming for simplicity that both λ^L and λ^R follow this pattern – many other possibilities are plausible, too – Eq. (4.98) simplifies to

$$X^e - X^\mu = \frac{\pi}{\sqrt{2}\alpha_e G_F V_{tb} V_{ts}^*} \lambda_0^2 \rho(\kappa^2 - 1) \left(\frac{2}{m_{S_1}^2} - \frac{1}{m_{S_{1/2}}^2} \right) . \tag{4.101}$$

This can be matched perfectly well to Eq. (4.97) for a suitable choice of couplings and leptoquark masses. If, e.g., the leptoquark masses are strongly hierarchical with $m_{S_{1/2}} \gg m_{S_1}$, the mixing between them is minimized, thereby rendering additional (pseudo-)scalar and tensor operators negligible. R_K is then almost exclusively determined by S_1. It is noteworthy that, if $S_{1/2}$ indeed contributes significantly to R_K, the measurement of R_{K^*} will be a smoking gun of NP since right-handed currents lead to deviations in the double ratio $\frac{R_{K^*}}{R_K} \neq 1$ [206].

Generating Neutrino Masses

If at least two leptoquarks with couplings to the same type of quarks are present, a Majorana neutrino mass as depicted in Fig. 4.7 can be obtained at one-loop level. As pointed out in Refs. [147, 233], this mass term is generated by leptoquark mixing with the Higgs boson and depends on the leptoquark couplings $\lambda^{L,R}$ as well as on the strength of their mixing. This is particularly interesting in models where a combination of two leptoquarks is considered to explain the measured B meson anomalies.

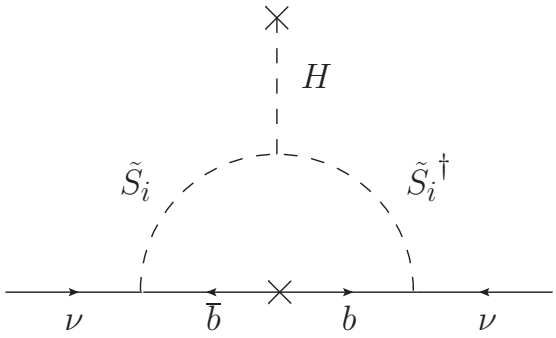

Figure 4.7: Majorana neutrino mass generated at one-loop level through a $\Delta L = 2$ leptoquark-Higgs coupling.

Assuming that the scalar leptoquarks S_1 and $S_{1/2}$ are used simultaneously to reproduce R_K, the contributions to the neutrino mass matrix read

$$\begin{aligned} M_{ii'}^\nu = \frac{3}{16\pi^2} \sum_{j=1,2} \sum_{k=d,s,b} & m_k B_0(0, m_k^2, m_{S_j}^2) R_{j1} R_{j2} \\ & \times \left[\left(\lambda_{S_{1/2}}^R\right)_{ki} \left(\lambda_{S_1}^L\right)_{ki'} + \left(\lambda_{S_{1/2}}^R\right)_{ki'} \left(\lambda_{S_1}^L\right)_{ki} \right] \end{aligned}$$

where R_{jl} are the elements of the rotation matrix diagonalizing the leptoquark mass matrix. Following Ref. [217], we consider only the finite part of the Passarino-Veltman

function B_0 since the divergences cancel out due to $R_{11}R_{12} = -R_{21}R_{22} = \sin 2\alpha$. In the relevant leptoquark mass range $1\,\text{TeV} \lesssim m_{S_j} \lesssim 50\,\text{TeV}$ B_0 is limited to

$$B_0(0, m_k^2, m_{S_j}^2) = \frac{m_k^2 \log(m_k^2) - m_{S_j}^2 \log(m_{S_j}^2)}{m_k^2 - m_{S_j}^2} \lesssim 8\,. \tag{4.102}$$

Starting from the data-driven pattern shown in Eq. (4.99), we can estimate the absolute neutrino mass scale generated by the leptoquark couplings. The pattern is strongly hierarchical in terms of quark families since the light generations are tightly constrained by kaon phenomenology. Therefore, it is clear that the bottom quark will dominate the loop assuming that λ^L and λ^R have a similar structure. The latter does not have to be the case, and other plausible scenarios are discussed in the remainder of this section. Considering only the dominant bottom quark loop we obtain

$$M_{ii'}^{\nu} \approx \underbrace{\frac{3}{16\pi^2} m_b \sin 2\alpha \Delta B_0}_{\equiv a} \left[\left(\lambda_{S_{1/2}}^R\right)_{bi} \left(\lambda_{S_1}^L\right)_{bi'} + \left(\lambda_{S_{1/2}}^R\right)_{bi'} \left(\lambda_{S_1}^L\right)_{bi} \right] \tag{4.103}$$

with

$$\Delta B_0 \equiv \left[B_0(0, m_b^2, m_{S_{1/2}}^2) - B_0(0, m_b^2, m_{S_1}^2) \right]\,, \tag{4.104}$$

and after inserting Eq. (4.105)

$$M_{ii'}^{\nu} \propto a \cdot \lambda_0^2 \begin{pmatrix} \kappa^2 & \kappa & \kappa \\ \kappa & 1 & 1 \\ \kappa & 1 & 1 \end{pmatrix}, \tag{4.105}$$

while the neutrino mass eigenstates in terms of the leptoquark couplings are given by

$$m_1^{\nu} = 0\,, \qquad m_{2(3)}^{\nu} = a \left\{ \sum_i \lambda_{bi}^L \lambda_{bi(+)}^R \sqrt{\sum_i \left(\lambda_{bi}^L\right)^2 \sum_i \left(\lambda_{bi}^R\right)^2} \right\}\,, \tag{4.106}$$

with $\lambda_{S_{1/2}}^R \equiv \lambda^R$, $\lambda_{S_1}^L \equiv \lambda^L$, and $i = e, \mu, \tau$. In agreement with Ref. [217], one mass eigenstate is exactly zero if either only down-type or up-type quarks generate neutrino masses.

Judging from Eqs. (4.105) and (4.106), a small breaking of the $\mu - \tau$ symmetry of the original pattern is required to obtain two nonzero neutrino masses, and – if leptoquarks are the sole origin of lepton mixing – to reproduce the PMNS mixing matrix observed in neutrino oscillations. Since we perform only an order-of-magnitude estimation, this problem is ignored for the moment.

Moreover, the rough estimate using the data-driven pattern yields an eigenvalue of order one times the bottom quark mass, which lies in the GeV range. Taking into account that λ_0 can be as small as $\mathcal{O}(10^{-2})$, we can suppress the neutrino mass scale by another four orders of magnitude. It then comes down to explaining the smallness of the parameter a to reduce the mass scale by another five orders of magnitude. We can either attribute this to a tiny mixing of the leptoquarks with the SM Higgs, or a degeneracy among the leptoquark masses, for which the difference of Passarino-Veltman functions

$$\Delta B_0 \approx \log\left[\frac{m_{S_{1/2}}^2}{m_{S_1}^2}\right] \qquad \left(m_b^2 \ll m_{S_i}^2\right) \tag{4.107}$$

approaches zero. In this limit $\tan 2\alpha$ [cf. Eq. (4.91)] goes to infinity leading to maximal mixing among the leptoquarks. As a result $\sin 2\alpha = 0.5$ will take its maximal but finite value. As stated earlier, however, with $|\Delta m_S^2|$ becoming small, additional scalar, pseudoscalar and tensor $b \to sll$-inducing operators become relevant that have to be taken into account in the computation of R_K.
Interestingly, the mixing is minimized in the opposite scenario with strongly hierarchical leptoquark masses $m_{S_{1/2}} \gg m_{S_1}$. The extent is limited by the upper bound on the leptoquark mass $m_S \lesssim 50\,\text{TeV}$ to comply with the phase measured in $B_s^0 - \overline{B}_s^0$ mixing. $\Delta B_0 \approx 7.8$ then takes its maximal value, while $\tan 2\alpha$ is suppressed by a factor of up to 2500. Last but not least, one can also argue with the smallness of $h_S v_{\text{SM}}$ compared to Δm_S^2 to reduce the mixing by a few orders of magnitude.
In the following section we concentrate on alternative setups to suppress the absolute neutrino mass by adopting different structures for the coupling matrices λ^L and λ^R, including an FN mechanism.

Alternative Setups

As stated above, λ^L and λ^R need not necessarily have the same pattern. Distinct couplings together with a slight breaking of the $\mu - \tau$ symmetry are actually favored by neutrino oscillation experiments requiring two nonzero neutrino mass eigenstates and large mixing angles. The latter dictate certain relations between the leptoquark couplings to explain the hierarchy of the mixing angles $\theta_{13} < \theta_{12} < \theta_{23}$, assuming that leptoquarks alone are responsible for the leptonic mixing [217]:

$$\begin{aligned} \lambda^L_{qe}\lambda^R_{q\tau} + \lambda^L_{q\tau}\lambda^R_{qe} &\ll \lambda^L_{q\mu}\lambda^R_{q\tau} + \lambda^L_{q\tau}\lambda^R_{q\mu}\,, \\ \lambda^L_{q\mu}\lambda^R_{q\tau} + \lambda^L_{q\tau}\lambda^R_{q\mu} &\gtrsim \lambda^L_{q\mu}\lambda^R_{q\mu} - \lambda^L_{q\tau}\lambda^R_{q\tau}\,. \end{aligned} \tag{4.108}$$

Furthermore, the couplings in λ^L and λ^R do not have to be the same order of magnitude. One or the other could have significantly smaller couplings to the SM fermions, effectively rendering the corresponding leptoquark redundant for the explanation of the R_K anomaly, while at the same time reducing the absolute neutrino mass scale considerably.
In the case that only one leptoquark contributes to the B meson sector, a third possibility opens up that forces one of the leptoquarks to couple exclusively to lighter quark generations, e.g.,

$$\lambda \simeq \begin{pmatrix} \eta_{de} & \eta_{d\mu} & \eta_{d\tau} \\ 0 & 0 & 0 \\ 0 & 0 & 0 \end{pmatrix}, \qquad \lambda \simeq \begin{pmatrix} 0 & 0 & 0 \\ \eta_{se} & \eta_{s\mu} & \eta_{s\tau} \\ 0 & 0 & 0 \end{pmatrix}. \tag{4.109}$$

The η_{sl} and η_{dl} entries are constrained to be small by experimental data and will, therefore, lower the neutrino mass scale. Moreover, the mass scale is further suppressed by the light quark masses $m_s, m_d \ll m_b$ now dominating the loop. Consequently, the requirements for the leptoquark-Higgs mixing are much more relaxed compared to the previous scenarios.
Finally, if one leptoquark couples solely to up-type quarks while the other one does not, neutrino masses can be generated only at two-loop level [218]. This mechanism sufficiently suppresses the neutrino mass scale, but is independent of the B meson anomalies.

A quick numerical example will demonstrate that some reasonable choice of parameter values can indeed combine the R_K measurement with the light neutrino mass scale at one-loop level. Starting from the patterns

$$\lambda^L_{S_1} \sim \lambda_0 \begin{pmatrix} \rho_d\kappa & \rho_d & \rho_d \\ \rho\kappa & \rho & \rho \\ \kappa & 1 & 1 \end{pmatrix}, \qquad \lambda^R_{S_{1/2}} \sim \begin{pmatrix} \eta_{de} & \eta_{d\mu} & \eta_{d\tau} \\ \eta_{se} & \eta_{s\mu} & \eta_{s\tau} \\ \eta_{be} & \eta_{b\mu} & \eta_{b\tau} \end{pmatrix}, \tag{4.110}$$

where the η_{ql} are arbitrary constants, the neutrino mass matrix $M^\nu_{ii'}$ is approximately given by

$$\begin{aligned} M^\nu_{ii'} &\approx a \begin{pmatrix} 2\eta_{be}\kappa & \kappa\eta_{b\mu}+\eta_{be} & \kappa\eta_{b\tau}+\eta_{be} \\ \kappa\eta_{b\mu}+\eta_{be} & 2\eta_{b\mu} & \eta_{b\tau}+\eta_{b\mu} \\ \kappa\eta_{b\tau}+\eta_{be} & \eta_{b\tau}+\eta_{b\mu} & 2\eta_{b\tau} \end{pmatrix} \\ \text{with} \quad a &= \frac{3\lambda_0}{16\pi^2} m_b \sin 2\alpha \log\left[\frac{m^2_{S_{1/2}}}{m^2_{S_1}}\right]. \end{aligned} \tag{4.111}$$

In the limit $m_{S_1} \approx 1\,\text{TeV} \ll m_{S_{1/2}} \approx 50\,\text{TeV}$, S_1 will be the dominant contribution to R_K. Choosing λ_0, κ and $\rho \sim \mathcal{O}(\epsilon)$ with $\epsilon \approx 0.2$ will then comply with flavor physics precision measurements and yield $0.7 \lesssim \text{Re}\,[X^e - X^\mu] \lesssim 1.5$ implied by R_K at $1\,\sigma$.
By using a specific ansatz for the leptoquark couplings, e.g., $\eta_{ql} \simeq m_q m_l / v^2_{\text{SM}}$, we are able to pin down the neutrino masses. Such hierarchical patterns are motivated by and easily obtained in FN-type flavor models, where the fermion mass hierarchies are explained through an additional $U(1)_{\text{FN}}$ family symmetry.
As an example, let us consider the fermion and leptoquark charges listed in Tab. 4.7, which can reproduce the SM fermion mass hierarchies ($\epsilon \approx 0.2$)

$$\begin{aligned} m_u &: m_c : m_t \approx \epsilon^8 : \epsilon^4 : 1\,, \\ m_d &: m_s : m_b \approx \epsilon^7 : \epsilon^5 : \epsilon^3\,, \\ m_e &: m_\mu : m_\tau \approx \epsilon^9 : \epsilon^5 : \epsilon^3\,, \end{aligned} \tag{4.112}$$

with some minor deviations in the CKM mixing matrix. We denote the Wolfenstein parameter here ϵ instead of λ to avoid confusion with the leptoquark matrices $\lambda^{L,R}$. The FN charges can be expressed in terms of the free parameter $Q_{\text{FN}}(\tau) \equiv q_\tau$, which always cancels out in the leptoquark interactions of Eq. (4.85). Furthermore, demanding $U(1)_{\text{FN}}$ invariance of the interaction $Hi\tau_2 S_1 S^\dagger_{1/2}$ essential for neutrino masses, dictates the FN charge assignment $Q(S_1) = Q(S_{1/2})$, provided that the Higgs charge $Q(H) = 0$. This implies $q_\tau = 6$ but does not affect the leptoquark-fermion couplings.
The resulting leptoquark textures are the following:

$$\lambda^L_{S_1} \simeq \begin{pmatrix} \epsilon^4 & \epsilon^3 & \epsilon^3 \\ \epsilon^3 & \epsilon^2 & \epsilon^2 \\ \epsilon^2 & \epsilon & \epsilon \end{pmatrix}, \qquad \lambda^R_{S_{1/2}} \simeq \begin{pmatrix} \epsilon^3 & \epsilon^2 & \epsilon^2 \\ \epsilon^6 & \epsilon^5 & \epsilon^5 \\ \epsilon^9 & \epsilon^8 & \epsilon^8 \end{pmatrix}, \tag{4.113}$$

which correspond to $\lambda_0 \approx \epsilon$, $\rho \approx \epsilon, \rho_d \approx \epsilon^2$ and $\kappa \approx \epsilon$ of the data-driven pattern, cf. Eq. (4.105). Note that the charges were chosen such that one of the patterns is inverse hierarchical in terms of quark generations, i.e., coupling strongly to d and weakly to b quarks. This has some interesting phenomenological implications not only for neutrino masses. By accommodating the two leptoquarks simultaneously in the FN

Field	Q_1	Q_2	Q_3	d	s	b	u	c	t
$U(1)_{\text{FN}}$	2	1	0	9	6	3	10	5	0

Field	L_1	L_2	L_3	e	μ	τ	S_1	$S_{1/2}$	H
$U(1)_{\text{FN}}$	$q_\tau+1$	q_τ	q_τ	$q_\tau+10$	$q_\tau+5$	$q_\tau+3$	$q_\tau-1$	$11-q_\tau$	0

Table 4.7: Possible $U(1)_{\text{FN}}$ quantum numbers consistent with the SM fermion mass hierarchies and V_{CKM} to obtain the patterns discussed in Eq. (4.113). The condition $Q(S_1) = Q(S_{1/2})$ implies $q_\tau = 6$.

flavor symmetry, one of the leptoquarks always suppresses the strong couplings of the other, consequently leading to naturally-light neutrino masses. Since

$$m_s \approx m_b \epsilon^2\,, \quad m_d \approx m_b \epsilon^4\,, \tag{4.114}$$

and therefore

$$m_q \lambda^R_{qi} \lambda^L_{qi'} \approx m_b \epsilon^9 \qquad (q = b, s, d)\,, \tag{4.115}$$

all quark loops contribute equally to Eq. (4.102), resulting in an additional factor of 3 in our estimate of the neutrino mass scale. For $h_S = 1\,\text{TeV}$, we find

$$m^\nu_3 \approx 0.30\,\text{eV}, \qquad m^\nu_2 \approx 0.01\,\text{eV}, \qquad m^\nu_1 = 0, \tag{4.116}$$

which approximates the expected neutrino mass scale quite well. The structure shown in Eq. (4.111) also guarantees three nonzero mixing angles implying that leptoquarks could very well be the sole origin of neutrino masses and mixings. Obtaining the observed mass squared differences Δm^2_{atm} and Δm^2_{sol} and the exact mixing angle values, however, would require an explicit model realization, which is reserved for the vector leptoquarks discussed in Sec. 4.3.2.

Note that the leptoquark patterns should be rotated into the mass bases of the respective fields before analyzing their impact on flavor observables. Since we make only order-of-magnitude estimates, the rotation matrices are neglected in this discussion keeping in mind that due to the FN mechanism the mixing matrices are approximately diagonal. With that said, the mass basis transformations are taken into account in the more detailed analysis of the vector leptoquark model in Sec. 4.3.2.

Inverse hierarchical patterns like in Eq. (4.113) can induce $0\nu\beta\beta$ decay and the resulting limits can be even more stringent than those from LHC searches [215, 223]. This is particularly interesting since one of the leptoquarks interacts strongly with the first quark generation. The $0\nu\beta\beta$ decay requires leptoquark couplings to up-type quarks that in our framework are only provided by S_1. Consequent mixing with $S_{1/2}$ then generates the operator [223]

$$\underbrace{\lambda^L_{u\nu} \lambda^R_{de} \frac{h_S v_{\text{SM}}}{m^2_{S_{1/2}} m^2_{S_1}}}_{\equiv C} \left[\overline{\nu} P_R e^c\right] \left[\overline{u} P_R d\right]\,. \tag{4.117}$$

which is because of our limited leptoquark content the only contribution to the $0\nu\beta\beta$ decay. Hence, the expression for the half-life simplifies to

$$T_{1/2}^{0\nu\beta\beta} = \left(|\mathcal{M}_{GT}|^2 \tilde{a} \frac{2}{G_F^2} C^2 \right)^{-1} , \tag{4.118}$$

where $\mathcal{M}_{GT}$ is the nuclear matrix element and $\tilde{a}$ is a function of the electron mass and the nuclear radius. For ^{76}Ge, $|\mathcal{M}_{GT}|^2\tilde{a} = 6.52 \times 10^{-10}$ was obtained numerically in Ref. [223] and afterwards corrected by a factor of 4 in Ref. [234].
The best bound on the half-life of ^{76}Ge is currently provided by GERDA [27] with

$$T_{1/2}^{0\nu\beta\beta}(^{76}\text{Ge}) > 2.1 \times 10^{25}\,\text{yr}. \tag{4.119}$$

Using the leptoquark patterns shown in Eq. (4.113), we obtain $\lambda_{11}^L \lambda_{11}^R = \epsilon^7$ and consequently

$$T_{1/2}^{0\nu\beta\beta}(^{76}\text{Ge}) \approx \frac{2.5 \times 10^{21}\,\text{yr}}{(\sin 2\alpha)^2} \frac{m_{S_{1/2}}^4 m_{S_1}^4}{\Delta m_S^4 (\text{TeV})^4} . \tag{4.120}$$

For our numerical example with $m_{S_{1/2}} \simeq 50\,\text{TeV}$, $m_{S_1} \simeq 1\,\text{TeV}$ and $h_S = 1\,\text{TeV}$, the $0\nu\beta\beta$ half-life results in

$$T_{1/2}^{0\nu\beta\beta}(^{76}\text{Ge}) \approx 9.7 \times 10^{29}\,\text{yr} . \tag{4.121}$$

If the hierarchy of $\lambda_{S_{1/2}}^R$ is even stronger, i.e., $m_d \approx m_b \epsilon^5$, it is possible to suppress the neutrino mass scale while getting dangerously close to the current $0\nu\beta\beta$ bound. In the scenario of almost degenerate leptoquark masses, $m_{S_1} \simeq 1\,\text{TeV}$ and $m_{S_{1/2}} \simeq 2\,\text{TeV}$, $S_{1/2}$ still does not contribute to R_K due to its tiny s and b quark couplings. Yet, as opposed to the previous example, the mixing is now significantly enhanced with $\alpha \approx 0.01$ for $h_S = 0.1\,\text{TeV}$. The extra suppression of $\lambda_{S_{1/2}}^R$ then compensates for the strong leptoquark mixing to keep the neutrino masses in the eV range. These values thus yield

$$T_{1/2}^{0\nu\beta\beta}(^{76}\text{Ge}) \approx 2.7 \times 10^{26}\,\text{yr} , \tag{4.122}$$

which lies within the expected sensitivity of GERDA phase II. We conclude that the $0\nu\beta\beta$ limit is respected thanks to the small leptoquark mixing, but could in principle allow for an observation of the $0\nu\beta\beta$ decay in the near future. Another interesting and important task would be to study the washout effect on the baryon asymmetry of the Universe but this is beyond the scope of the present analysis [235].

4.3.2 $R_K, R_{D^{(*)}}$ *and Neutrino Masses with Vector Leptoquarks*

While scalar leptoquarks can be used to combine R_K with neutrino masses, their vector counterparts can additionally accommodate $R_{D^{(*)}}$ and the 750 GeV diphoton excess recently observed by CMS and ATLAS [74, 75]. In fact, also scalar leptoquarks can easily provide the large $\mathcal{O}(1)$ couplings necessary to account for the deviation in $R_{D^{(*)}}$. However, such couplings are in tension with $B \to X_s \nu\nu$ measurements, implying that possible solutions are strongly fine-tuned [211]. The vector leptoquark V_0 plays a special part in the anomaly puzzle by providing all the vital interactions for $R_{D^{(*)}}$ and R_K

while not coupling down-type quarks to neutrinos, which is crucial for $B \to X_s \nu\nu$. A model exploiting this unique property of V_0 is presented in the following section.
First we review how R_K and $R_{D^{(*)}}$ can be explained with the vector leptoquarks V_0 and $V_{1/2}$, highlighting the differences and caveats compared to the scalar leptoquark framework. After summarizing the flavor constraints briefly, we embed the vector particles in an FN symmetry to obtain appropriate hierarchical patterns. The neutrino masses and the favored model parameter space are discussed in the final part of the section.

R_K and $R_{D^{(*)}}$

Recently, an analysis based on a $U(2)^5$ flavor symmetry also concluded that among the many possible leptoquark mediators, the $(3,1)_{2/3}$ vector leptoquark V_0 is the most suitable to explain the anomalies in the B meson sector [214]. Here we take a different approach to shaping the leptoquark couplings by embedding them into a $U(1)$ FN framework. While Ref. [214] focused on constraints from the flavor sector, we study in addition how these patterns affect neutrino masses and even the diphoton excess (see Sec. 5.2). To extend the framework to neutrino masses, we introduce a second leptoquark $V_{1/2}$ that mixes with V_0 through a $\Delta L = 2$ Higgs boson coupling. The quantum numbers of these leptoquarks are summarized in Tab. 4.8.

Leptoquark	$(SU(3)_C, SU(2)_L)_{U(1)_Y}$	Q_{EM}	B	L
$V_{1/2}$	$(3,2)_{1/6}$	$(2/3, -1/3)$	$1/3$	1
V_0	$(3,1)_{2/3}$	$2/3$	$1/3$	-1

Table 4.8: Quantum numbers of the considered leptoquarks with electric charge $2/3$ that can account for the R_K and R_D anomalies as well as neutrino masses. B and L here refer to baryon and lepton number, respectively.

Adding $V_{1/2}$ and V_0 to the SM field content leads to the following interactions

$$-\mathcal{L}^V_{\text{LQ}} = \lambda^L_{V_0} \overline{Q} \gamma^\mu L V_{0,\mu} + \lambda^R_{V_{1/2}} \overline{u^c} \gamma^\mu L V^\dagger_{1/2,\mu} + \text{h.c.} \tag{4.123}$$

Note that the $V_{1/2}$ leptoquark shares its quantum numbers with the gauge bosons arising in $SU(5) \to SU(3)_C \otimes SU(2) \otimes U(1)_Y$ breaking. To avoid rapid proton decay, which is a typical feature of minimal $SU(5)$ models, we assume an underlying symmetry that forbids dangerous diquark operators emerging with $V_{1/2}$.
Like the scalar leptoquarks, the vector particles sharing the same electric charge eventually mix via

$$\begin{aligned} V(V_i, H) = &- (m'^2_{V_i} - g_{V_i} H^\dagger H) V^\dagger_{i,\mu} V^\mu_i \\ &+ h_V H i\tau_2 V^\mu_{1/2} V^\dagger_{0\mu} + \text{h.c.} \quad (i = 0, 1/2)\,, \end{aligned} \tag{4.124}$$

where $h_V \neq 0$ is crucial for nonzero neutrino masses and $m^2_{V_i} \equiv m'^2_{V_i} - g_{V_i} H^\dagger H$. Again, the h_V parameter is limited by the condition of positive leptoquark masses and the perturbativity of the theory to

$$h_V \leq m_{V_0} m_{V_{1/2}} / v_{\text{SM}}\,. \tag{4.125}$$

The leptoquark mass eigenstates are a mixture of flavor states with $Q_{\rm EM}$ charge $2/3$ and a distinct $-1/3$ state stemming from $V_{1/2}$,

$$\begin{aligned} M^2_{2/3} &= \begin{pmatrix} m'^2_{V_0} - g_{V_0} v^2_{\rm SM} & h_V v_{\rm SM} \\ h_V v_{\rm SM} & m'^2_{V_{1/2}} - g_{V_{1/2}} v^2_{\rm SM} \end{pmatrix}, \\ M^2_{-1/3} &= m'^2_{V_{1/2}} - g_{V_{1/2}} v^2_{\rm SM}\,. \end{aligned} \tag{4.126}$$

The rotation angle α mixing the $2/3$ states is here given by

$$\begin{pmatrix} \tilde{V}_1 \\ \tilde{V}_2 \end{pmatrix} = R \begin{pmatrix} V_0 \\ V_{1/2} \end{pmatrix}, \qquad \tan 2\alpha = \frac{2 h_V v_{\rm SM}}{m^2_{V_{1/2}} - m^2_{V_0}} \equiv \frac{2 h_V v_{\rm SM}}{\Delta m^2_V}\,, \tag{4.127}$$

where $\tilde{V}_i$ denotes the mass eigenstates.
The left-handed currents induced by V_0^L are sufficient to explain the SM deviations so that $V_{1/2}$ only acts as an auxiliary particle to induce neutrino masses. The leptoquark $V_{1/2}$ itself does not couple directly to down-type quarks, but will do so through its mixing with V_0. However, as the leptoquark mixing is required to be small in order to generate naturally-light neutrino masses, any effects on R_K or $R_{D^{(*)}}$ from $V_{1/2}$ are negligible, which implies also that $R_{K^*} = R_K$.
With these considerations, the computation of R_K is simplified compared to the scalar leptoquark case since $V_{1/2}$ does not contribute to the B meson sector. The comparison with Eq. (4.84) yields ($l = e, \mu$),

$$C_9^l = -C_{10}^l = \frac{\pi}{\alpha_e} \frac{\lambda^{L\,*}_{sl} \lambda^L_{bl}}{V_{tb} V^*_{ts}} \frac{\sqrt{2}}{2 m^2_{V_0} G_F}\,, \tag{4.128}$$

Hence, we obtain

$$X^e - X^\mu = \frac{\pi}{\sqrt{2} \alpha_e G_F V_{tb} V^*_{ts} m^2_{V_0}} \left(\lambda^{L*}_{se} \lambda^L_{be} - \lambda^{L*}_{s\mu} \lambda^L_{b\mu} \right), \tag{4.129}$$

which is equivalent to

$$\lambda^{L*}_{se} \lambda^L_{be} - \lambda^{L*}_{s\mu} \lambda^L_{b\mu} \simeq (1.8 \pm 0.7) \cdot 10^{-3} \frac{m^2_{V_0}}{\rm TeV^2}\,. \tag{4.130}$$

In conclusion, if the leptoquark mass is around 1 TeV, the corresponding product of couplings has to be of the order ϵ^4 to accommodate the R_K data.
While a variety of operators contribute to the tree-level process $b \to \bar{c} l \nu$ depicted in Fig. 4.8, several authors pointed out that the vector operator $\mathcal{O}_V$ gives an excellent fit to the $R_{D^{(*)}}$ data [212, 213, 236],

$$\mathcal{O}_V = [\bar{c} \gamma^\mu P_L b] \, [l \gamma_\mu \nu_l]\,. \tag{4.131}$$

In leptoquark UV completions this operator can be provided by both the $(3,3)_{2/3}$ and $(3,1)_{2/3}$ vector leptoquarks V_1 and V_0. The scalar operators $\mathcal{O}_{SL}$ and $\mathcal{O}_{SR}$ can also explain the data but are fine-tuned and in tension with the measured q^2 spectra. This disfavors, e.g, generic 2HDM solutions with a charged scalar contribution as argued in Sec. 4.2. In our framework the purely left-handed couplings of the leptoquark V_0 generate $\mathcal{O}_V$ with the Wilson coefficient

$$C^{cb}_{L,l\nu} = \frac{1}{2\sqrt{2} G_F V_{cb} m^2_{V_0}} \lambda^L_{bl} \lambda^{L*}_{c\nu}\,, \tag{4.132}$$

which translates to the constraint [212, 213]

$$\lambda^L_{b\tau}\lambda^{L*}_{c\nu_\tau} - \lambda^L_{b\mu}\lambda^{L*}_{c\nu_\mu} \simeq (0.18 \pm 0.04)\frac{m^2_{V_0}}{\text{TeV}^2}\,. \tag{4.133}$$

Explaining the measurement hence requires a mild hierarchy between the second and the third column of λ^L with $\mathcal{O}(1)$ third generation couplings. Furthermore, any explanation of $R_{D^{(*)}}$ must also accommodate the SM-like branching ratio of $B \to \tau\overline{\nu}$ [237], requiring further suppression of leptoquark couplings to up quarks.

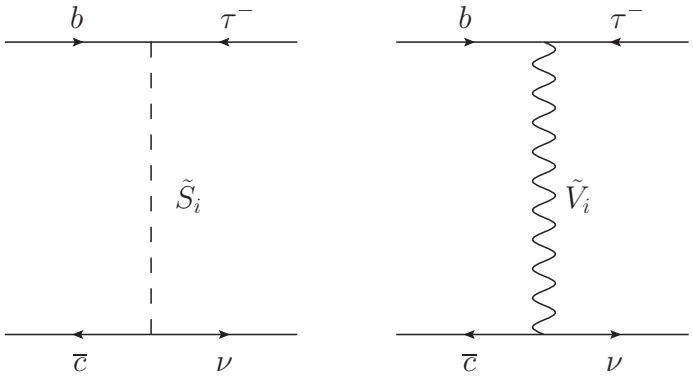

Figure 4.8: The $b \to \bar{c}\tau\nu$ decay induced by the scalar $\tilde{S}_i$ $(i = 1, 2)$ (left) and vector leptoquark $\tilde{V}_i$ $(i = 1, 2)$ mass eigenstates (right).

Constraints

Besides the $B \to X_s\nu\nu$ measurement, which is evaded strategically by utilizing the V_0 leptoquark, lepton flavor- and universality-violating processes involving down-type quarks have to be considered in leptoquark model building. Rare kaon decay data places stringent constraints on the first two quark generations [150],

$$|\lambda^L_{d\mu}\lambda^{L*}_{s\mu}| \lesssim \frac{m^2_{\text{LQ}}}{(183\,\text{TeV})^2}\,. \tag{4.134}$$

Assuming $m_{\text{LQ}} \approx 1$ TeV, this implies $|\lambda^L_{d\mu}\lambda^{L*}_{s\mu}| \lesssim \epsilon^6$ with $\epsilon \simeq 0.2$. The couplings required to explain R_K and R_D can also be combined to induce flavor violation. These final states are limited for instance by $B^- \to K^-\mu\tau$ [213, 238],

$$|\lambda^L_{b\tau}\lambda^L_{s\mu}| + |\lambda^L_{b\mu}\lambda^L_{s\tau}| \lesssim \epsilon\frac{m^2_{\text{LQ}}}{\text{TeV}^2}\,. \tag{4.135}$$

On the other hand, constraints from flavor-violating top decays such as $t \to b\tau\nu_\tau$ are rather weak,

$$|\lambda^L_{b\tau}\lambda^L_{t\nu_\tau}| \lesssim 4.8\frac{m^2_{\text{LQ}}}{\text{TeV}^2}\,, \tag{4.136}$$

as opposed to the flavor-violating lepton decay $\mu \to e\gamma$, measured by MEG, which constrains [186, 199]

$$|\lambda^L_{qe}\lambda^L_{q\mu}| \lesssim \frac{m^2_{\rm LQ}}{(34\,{\rm TeV})^2}\,. \tag{4.137}$$

Thus $|\lambda^L_{qe}\lambda^L_{q\mu}| \lesssim \epsilon^4$, assuming again $m_{\rm LQ} \approx 1$ TeV.
Summarizing the above constraints, an ideal pattern (excluding possible texture-zero solutions) to account for R_K and $R_{D^{(*)}}$ and to comply with experimental searches would read

$$\lambda^L \simeq \begin{pmatrix} \epsilon^6 & \epsilon^4 & \epsilon^3 \\ \epsilon^4 & \epsilon^3 & \epsilon \\ \epsilon^3 & \epsilon & 1 \end{pmatrix}. \tag{4.138}$$

The matrix λ^L is *a priori* a general matrix. The symmetric pattern in Eq. (4.138) is chosen for simplicity while satisfying the experimental constraints. In the following section we study possible $U(1)$ charge assignments to generate such a pattern in an FN framework based on the two leptoquarks V_0 and $V_{1/2}$.

Vector Leptoquark Model

Like in the scalar leptoquark model, the left-handed quark charges are fixed by the CKM matrix, whereas the fermion mass hierarchies, cf. Eq. (4.112), dictate the corresponding right-handed field charges. As long as the origin of neutrino masses is unclear, some freedom remains in the choice of the leptonic FN charges. Furthermore, the interaction $Hi\tau_2 V^\mu_{1/2} V^\dagger_{0\mu}$ essential for neutrino masses and mixing, implies $Q(V_0) = Q(V_{1/2})$ if the Higgs charge $Q(H) = 0$.
Evidently, obtaining the ideal pattern given in Eq. (4.138) requires the $\overline{Q}_i$ charges $(3, 1, 0)$. Such choice of charges, however, leads to a small Cabibbo angle and large mixing among the second and third quark generations contrary to experimental observations. Bearing a little fine-tuning to explain $R_{D^{(*)}}$ we will therefore focus on the $\overline{Q}_i$ charges $(3, 2, 0)$, which are a better fit to the CKM matrix.
The resulting charge assignments can again be expressed in terms of $Q(L_3) \equiv q_\tau$, allowing one to suppress the right-handed couplings λ^R by choosing different integer values for q_τ,

$$\lambda^L_{V_0} \simeq \begin{pmatrix} \epsilon^6 & \epsilon^4 & \epsilon^3 \\ \epsilon^5 & \epsilon^3 & \epsilon^2 \\ \epsilon^3 & \epsilon & 1 \end{pmatrix}, \qquad \lambda^R_{V_{1/2}} \simeq \begin{pmatrix} \epsilon^{8+2q_\tau} & \epsilon^{6+2q_\tau} & \epsilon^{5+2q_\tau} \\ \epsilon^{5+2q_\tau} & \epsilon^{3+2q_\tau} & \epsilon^{2+2q_\tau} \\ \epsilon^{3+2q_\tau} & \epsilon^{1+2q_\tau} & \epsilon^{2q_\tau} \end{pmatrix}, \tag{4.139}$$

e.g., for $q_\tau = 5$ we obtain

$$\lambda^R_{V_{1/2}} \simeq \begin{pmatrix} \epsilon^{18} & \epsilon^{16} & \epsilon^{15} \\ \epsilon^{15} & \epsilon^{13} & \epsilon^{12} \\ \epsilon^{13} & \epsilon^{11} & \epsilon^{10} \end{pmatrix}. \tag{4.140}$$

Note that in the present scenario both patterns are hierarchical resulting in interesting phenomenological consequences. As opposed to the scalar leptoquark case, the free

parameter q_τ does not cancel in the leptoquark interactions involving $V_{1/2}$, leading to a severe suppression of the corresponding couplings. Large integer values of q_τ not only explain the small neutrino masses, but also render $V_{1/2}$ negligible in all flavor processes. The $0\nu\beta\beta$ half-life is also way beyond the reach of current or next-generation experiments due to the suppressed first generation couplings.

Field	$\overline{Q}_1$	$\overline{Q}_2$	$\overline{Q}_3$	d	s	b	u	c	t
$U(1)_{\rm FN}$	3	2	0	4	3	3	5	2	0

Field	L_1	L_2	L_3	e	μ	τ	V_0	$V_{1/2}^\dagger$	H
$U(1)_{\rm FN}$	$q_\tau+3$	$q_\tau+1$	q_τ	$q_\tau-6$	$q_\tau-4$	$q_\tau-3$	$-q_\tau$	q_τ	0

Table 4.9: Possible $U(1)_{\rm FN}$ quantum numbers to obtain a flavor model with natural fermion mass hierarchies and approximate CKM mixing in good agreement with experimental data. Choosing $q_\tau = 5$ results in the vector leptoquark patterns shown in Eq. (4.140), while larger values of $q_\tau > 5$ will gradually suppress λ^R couplings even further.

The FN charges yield the following fermion mass matrices up to $\mathcal{O}(1)$ coefficients

$$M_u \simeq \begin{pmatrix} \epsilon^8 & \epsilon^5 & \epsilon^3 \\ \epsilon^7 & \epsilon^4 & \epsilon^2 \\ \epsilon^5 & \epsilon^2 & 1 \end{pmatrix}, \quad M_d \simeq \begin{pmatrix} \epsilon^7 & \epsilon^6 & \epsilon^6 \\ \epsilon^6 & \epsilon^5 & \epsilon^5 \\ \epsilon^4 & \epsilon^3 & \epsilon^3 \end{pmatrix}, \quad M_l \simeq \begin{pmatrix} \epsilon^9 & \epsilon^7 & \epsilon^6 \\ \epsilon^7 & \epsilon^5 & \epsilon^4 \\ \epsilon^6 & \epsilon^4 & \epsilon^3 \end{pmatrix}. \tag{4.141}$$

The fermion mixing matrices that are required to rotate $\lambda^{L,R}$ into the mass basis follow directly from Tab. 4.9 and are approximately given by

$$\begin{aligned} V_{u,d}^L &\simeq \begin{pmatrix} 1 & \epsilon & \epsilon^3 \\ \epsilon & 1 & \epsilon^2 \\ \epsilon^3 & \epsilon^2 & 1 \end{pmatrix}, \quad V_l^{L,R} \simeq \begin{pmatrix} 1 & \epsilon^2 & \epsilon^3 \\ \epsilon^2 & 1 & \epsilon \\ \epsilon^3 & \epsilon & 1 \end{pmatrix}, \\ V_u^R &\simeq \begin{pmatrix} 1 & \epsilon^3 & \epsilon^5 \\ \epsilon^3 & 1 & \epsilon^2 \\ \epsilon^5 & \epsilon^2 & 1 \end{pmatrix}, \quad V_d^R \simeq \begin{pmatrix} 1 & \epsilon & \epsilon \\ \epsilon & 1 & 1 \\ \epsilon & 1 & 1 \end{pmatrix}. \end{aligned} \tag{4.142}$$

Although the mixing between the second and third lepton generation is enhanced, the FN mechanism is not feasible to explain the large PMNS mixing angles. Instead, the fundamental difference between the hierarchical CKM and the anarchic PMNS matrix is attributed to neutrino-leptoquark interactions.
The patterns $\lambda^{L,R}$ have to be rotated into their respective mass bases to account for the CKM and PMNS mixing. These new matrices are defined as follows:

$$\begin{aligned} \tilde{\lambda}_{dl}^L &= V_d^L \lambda_{V_0}^L V_l^{L\dagger}, & \tilde{\lambda}_{u\nu}^L &= V_u^L \lambda_{V_0}^L V_\nu^{L\dagger}, \\ \tilde{\lambda}_{ul}^R &= V_u^R \lambda_{V_{1/2}}^R V_l^{L\dagger}, & \tilde{\lambda}_{u\nu}^R &= V_u^R \lambda_{V_{1/2}}^R V_\nu^{L\dagger}. \end{aligned} \tag{4.143}$$

Since all relevant mixing matrices of Eq. (4.142) are approximately diagonal, the general structure of the leptoquark patterns $\lambda^{L,R}$ remains unchanged when rotating from the

symmetry into the fermion mass basis. We can henceforth assume $\tilde{\lambda}^{L,R} \simeq \lambda^{L,R}$, with one exception being $\tilde{\lambda}^L_{u\nu}$ that receives large mixing from V^L_ν. The magnitudes of the mixing parameters in V^L_ν can be derived from the experimentally observed PMNS mixing matrix combined with our predictions for V^L_l. From

$$U_{\rm PMNS} = V_l^{L\dagger} V_\nu^L \quad \Leftrightarrow \quad V_\nu^{L\dagger} = U^\dagger_{\rm PMNS} V_l^{L\dagger} \tag{4.144}$$

we infer

$$V_\nu^{L\dagger} \sim \begin{pmatrix} 1 & 1 & \epsilon \\ 1 & 1 & 1 \\ \epsilon & 1 & 1 \end{pmatrix}, \quad \tilde{\lambda}^L_{u\nu} \simeq \begin{pmatrix} \epsilon^4 & \epsilon^3 & \epsilon^3 \\ \epsilon^3 & \epsilon^2 & \epsilon^2 \\ \epsilon & 1 & 1 \end{pmatrix}. \tag{4.145}$$

All of the obtained patterns are valid only up to $\mathcal{O}(1)$ coefficients, allowing us to estimate the extent of tuning required to accommodate the observables R_K and $R_{D^{(*)}}$. Including the $\mathcal{O}(1)$ coefficients a_{ql}, the relevant coupling matrices read

$$\tilde{\lambda}^L_{dl} = \begin{pmatrix} a_{de}\epsilon^6 & a_{d\mu}\epsilon^4 & a_{d\tau}\epsilon^3 \\ a_{se}\epsilon^5 & a_{s\mu}\epsilon^3 & a_{s\tau}\epsilon^2 \\ a_{be}\epsilon^3 & a_{b\mu}\epsilon & a_{b\tau} \end{pmatrix}, \quad \tilde{\lambda}^L_{u\nu} = \begin{pmatrix} a_{ue}\epsilon^4 & a_{u\mu}\epsilon^3 & a_{u\tau}\epsilon^3 \\ a_{ce}\epsilon^3 & a_{c\mu}\epsilon^2 & a_{c\tau}\epsilon^2 \\ a_{te}\epsilon & a_{t\mu} & a_{t\tau} \end{pmatrix}. \tag{4.146}$$

By comparing with Eq. (4.130) we deduce

$$a^*_{b\mu} a_{s\mu} \simeq -(1.1 \pm 0.4) \frac{m^2_{V_0}}{\text{TeV}^2}, \tag{4.147}$$

which is a perfect match with R_K data for $m_{V_0} \approx 1$ TeV. On the other hand, the measurement of $R_{D^{(*)}}$ demands [Eq. (4.133)]

$$a_{b\tau} a^*_{c\tau} - 0.2 \cdot a_{b\mu} a^*_{c\mu} \simeq (4.5 \pm 1.0) \frac{m^2_{V_0}}{\text{TeV}^2}, \tag{4.148}$$

which requires a little more fine-tuning that can be accommodated easily with couplings mildly larger than 1.

Since the $\tilde{\lambda}^L_{u\nu}$ couplings are slightly enhanced due to the large neutrino mixing, it is suggestive to study up-type flavor transitions to make predictions for D meson decay channels with dineutrino final states. Charm constraints are relatively weak compared to those from the kaon sector, cf. Ref. [239].

In our framework, the most promising channel to search for BSM physics is $D^+ \to \pi^+ \nu\nu$, governed by the couplings $|\tilde{\lambda}^L_{c\nu} \tilde{\lambda}^L_{u\nu}| \approx \epsilon^5$, while predictions for other channels involving charged lepton final states suffer more severe suppression to comply with K physics.

Generating Neutrino Masses

Like in the scalar leptoquark case, the $\Delta L = 2$ coupling of the vector leptoquarks to the SM Higgs boson generates Majorana neutrino masses at one-loop level as shown in Fig. 4.9.

The magnitude of the neutrino mass depends on the leptoquark mixing, governed by the dimensionful parameter h_V, and on the leptoquark couplings $\lambda^{L,R}$. Explicitly, the contribution to the Majorana neutrino mass from V_0 and $V_{1/2}$ is given by [217]

$$M^\nu_{ii'} = \frac{3}{16\pi^2} \sum_{j=1,2} \sum_{k=u,c,t} m_k B_0(0, m_k^2, m^2_{V_j}) R_{j1} R_{j2} \left[\lambda^R_{ki} \lambda^L_{ki'} + \lambda^R_{ki'} \lambda^L_{ki} \right], \tag{4.149}$$

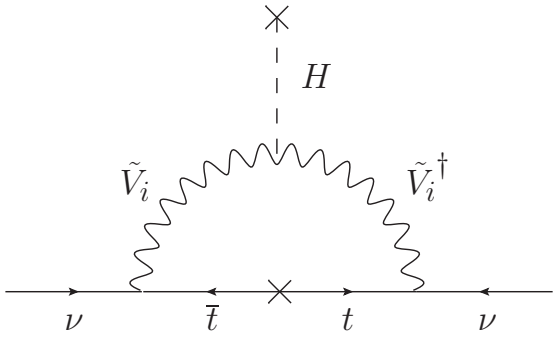

Figure 4.9: One-loop Majorana neutrino mass generated by Higgs-leptoquark mixing.

where m_{V_j} is the mass of the leptoquark V_j and m_k is the quark mass, while B_0 denotes the finite part of the Passarino-Veltman function. A few comments regarding the loop regularization are in order. As seen, for instance, in the unitary gauge

$$\frac{-i}{k^2 - m_V^2}\left[g_{\mu\nu} + \frac{k_\mu k_\nu}{m_V^2}\right], \tag{4.150}$$

the vector leptoquark propagator causes divergences that result in a bad UV behavior. Analogous to the Higgs and the $W^\pm$ bosons in the SM, a heavy Higgs giving masses to the leptoquarks can cancel these divergences. The details, however, depend on the specific UV completion. An example where neutrino masses are mediated by a massive gauge boson is given in Ref. [240]. Here, massive bosons emerge through the breaking of a $SU(3)_C \otimes SU(3)_L \otimes U(1)_X$ gauge group and the UV behavior is well defined. Another example is shown in Ref. [241] for an $SU(2)_N$ extension of the SM, where the $SU(2)_N$ gauge bosons generate a nonzero neutrino mass.
The remaining infinities contained in the Passarino-Veltman function drop out when summing over both leptoquarks like in the scalar leptoquark case. The function B_0, therefore, takes into account only the finite part of the Passarino-Veltman integral.
Stringent constraints can arise if the UV completion does not entail additional particles to cancel the divergences of the vector boson propagator. Such limits, e.g., from radiative charged lepton decays $l \to l'\gamma$, are studied in Ref. [214] based on the vector leptoquark $(3,1)_{2/3}$ in a $U(2)^5$ flavor model.
Using the leptoquark patterns discussed in Eqs. (4.139) and (4.140), we can estimate the absolute neutrino mass scale generated by the leptoquark couplings. Since the patterns are strongly hierarchical in terms of quark families, we consider only the dominating top quark contribution to $M^\nu_{ii'}$. Hence, we obtain

$$M^\nu_{ii'} \approx \underbrace{\frac{3}{32\pi^2} m_t \sin 2\alpha \Delta B_0}_{\equiv a}\left[\lambda^R_{ti}\lambda^L_{ti'} + \lambda^R_{ti'}\lambda^L_{ti}\right], \tag{4.151}$$

with

$$\Delta B_0 \equiv B_0(0, m_t^2, m^2_{V_{1/2}}) - B_0(0, m_t^2, m^2_{V_0}), \tag{4.152}$$

and the neutrino mass eigenstates

$$m_1^\nu = 0, \qquad m_{2(3)}^\nu = a\left\{\sum_i \lambda_{ti}^L \lambda_{ti}^R \,{}^{-}_{(+)} \sqrt{\sum_i \left(\lambda_{ti}^L\right)^2 \sum_i \left(\lambda_{ti}^R\right)^2}\right\} \tag{4.153}$$

with $i = e, \mu, \tau$. Since again one neutrino mass eigenstate is zero, the model predicts a normal neutrino mass hierarchy with a small effective Majorana mass beyond the reach of current $0\nu\beta\beta$ experiments.
Inserting Eqs. (4.139) and (4.140) into Eq. (4.151) yields

$$M_{ii'}^\nu \propto a \cdot \begin{pmatrix} \epsilon^{16} & \epsilon^{14} & \epsilon^{13} \\ \epsilon^{14} & \epsilon^{12} & \epsilon^{11} \\ \epsilon^{13} & \epsilon^{11} & \epsilon^{10} \end{pmatrix}, \quad \text{and} \quad m_3^\nu \sim a \cdot \epsilon^{10}\,. \tag{4.154}$$

Therefore, the factor a must be sufficiently small to push the neutrino mass scale below eV, which is achieved by virtue of small leptoquark mixing. In the limit of small α the parameter a can be approximated as

$$a \approx \frac{3}{16\pi^2} m_t \frac{h_V v_{\rm SM}}{\Delta m_V^2} \log\left[\frac{m_{V_{1/2}}^2}{m_{V_0}^2}\right], \tag{4.155}$$

implying

$$\frac{h_V v_{\rm SM}}{\Delta m_V^2} \log\left[\frac{m_{V_{1/2}}^2}{m_{V_0}^2}\right] \lesssim 0.9 \times 10^{-3} \tag{4.156}$$

to make neutrino masses sufficiently light. The smallness of a can be attributed to the smallness of the dimensionful coupling h_V or a large mass splitting Δm_V^2 of the contributing leptoquarks. Possible solutions of Eq. (4.156) are depicted in Fig. 4.10 for different powers of $\lambda^R \sim \epsilon^8, \epsilon^{10}$, and ϵ^{12}. In Fig. 4.11 we plot m_3^ν in terms of $m_{V_{1/2}}$ for $\lambda^R \sim \epsilon^{10}$ and $h_V = 0.1, 0.5$, and 1 TeV, showing that light neutrino masses favor a large leptoquark mass splitting with natural values of h_V.
Since one neutrino mass eigenstate is exactly zero, one can solve the eigenvalue equation $M^\nu v_0 = 0$ with

$$v_0^T = \frac{(1, -w, w')}{\sqrt{1 + w^2 + w'^2}} \tag{4.157}$$

to obtain analytical expressions for the neutrino mixing angles as a function of the leptoquark couplings $\lambda_{t\nu}^{L,R}$, assuming that the charged leptons are approximately diagonal [217]. It is

$$w = \frac{\lambda_{t\tau}^R \lambda_{te}^L - \lambda_{te}^R \lambda_{t\tau}^L}{\lambda_{t\tau}^R \lambda_{t\mu}^L - \lambda_{t\mu}^R \lambda_{t\tau}^L} \approx t_{12} \frac{c_{23}}{c_{13}} + t_{13} s_{23}\,, \tag{4.158}$$

$$w' = \frac{\lambda_{t\mu}^R \lambda_{te}^L - \lambda_{te}^R \lambda_{t\mu}^L}{\lambda_{t\tau}^R \lambda_{t\mu}^L - \lambda_{t\mu}^R \lambda_{t\tau}^L} \approx t_{12} \frac{s_{23}}{c_{13}} - t_{13} c_{23}\,, \tag{4.159}$$

where $s_{ij} = \sin\theta_{ij}$, $c_{ij} = \cos\theta_{ij}$, and $t_{ij} = \tan\theta_{ij}$, with the PMNS angles θ_{12}, θ_{23}, θ_{13}. Hence, to explain the large PMNS mixing w and w' both should be nonzero and sizable.

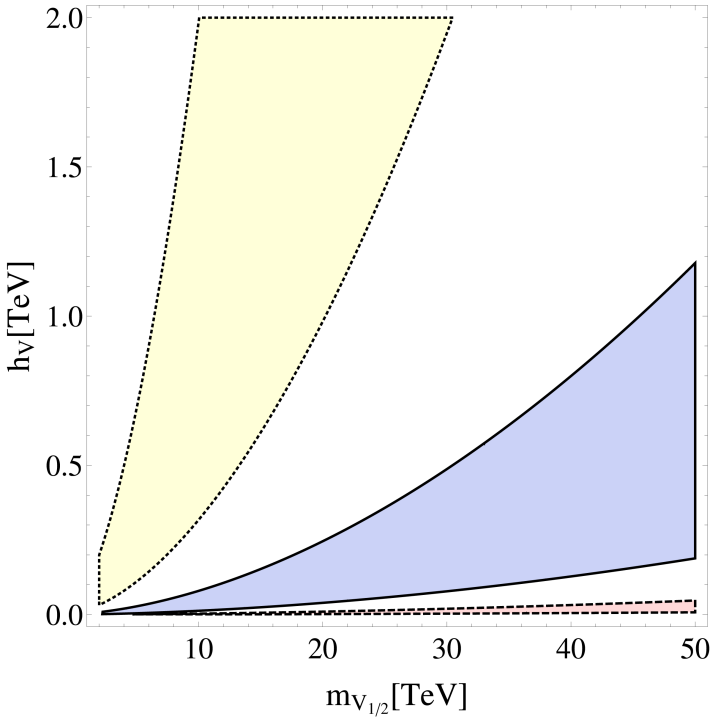

Figure 4.10: Allowed regions of the trilinear leptoquark-Higgs coupling h_V and $m_{V_{1/2}}$ requiring that the largest neutrino mass eigenstate $m_\nu \lesssim 0.3$ eV and $m_{V_0} \simeq 1$ TeV. The three distinct regions correspond to different powers of the dominating coupling $\lambda^R_{t\nu} \simeq \epsilon^8$ (red, dashed), ϵ^{10} (blue, solid) and ϵ^{12} (yellow, dotted).

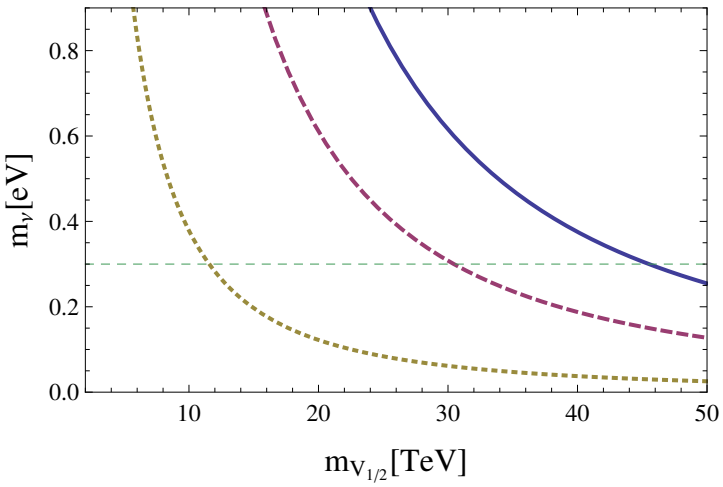

Figure 4.11: The largest neutrino mass as a function of $m_{V_{1/2}}$ for $m_{V_0} = 1$ TeV, $\lambda^R_{t\nu} \simeq \epsilon^{10}$ and $h_V = 1$ TeV (blue, solid), 0.5 TeV (red, dashed), and 0.1 TeV (yellow, dotted). The horizontal, dashed line defines a conservative upper limit on the absolute neutrino mass scale.

By evaluating w and w' for Eqs. (4.139) and (4.140) we find that their values depend heavily on the undetermined $\mathcal{O}(1)$ FN parameters

$$w = \frac{y_{31} - y_{13}}{y_{32} - y_{23}}\epsilon^2\,, \qquad w' = \frac{y_{21} - y_{12}}{y_{32} - y_{23}}\epsilon^3\,, \tag{4.160}$$

where the y_{ij} denote products of $\mathcal{O}(1)$ coefficients from $\lambda^{L,R}$. Because of the possible cancellation in the denominator, w and w' can oscillate quickly with small changes of the $\mathcal{O}(1)$ parameters, explaining also large neutrino mixing easily by permitting some extent of tuning.
With many free $\mathcal{O}(1)$ FN parameters to match to only five physical observables (Δm^2_{atm}, $\Delta m^2_{\text{sol}}, \theta_{12}$, θ_{13}, θ_{23}), the system is underconstrained and has many viable solutions. On condition that all coefficients in Eq. (4.141) are approximately $\mathcal{O}(1)$, the benchmark point

$$\begin{aligned} \lambda^L_{te} &\approx 5.1\,\epsilon^3\,, & \lambda^R_{te} &\approx 3.0\,\epsilon^{13}\,, \\ \lambda^L_{t\mu} &\approx 1.4\,\epsilon\,, & \lambda^R_{t\mu} &\approx 2.1\,\epsilon^{11}\,, \\ \lambda^L_{t\tau} &\approx 0.2\,, & \lambda^R_{t\tau} &\approx -0.8\,\epsilon^{10}\,, \end{aligned} \tag{4.161}$$

provides a good fit to neutrino oscillation data, yielding

$$\begin{aligned} &\Delta m^2_{\text{atm}} = 2.5 \times 10^{-3}\,\text{eV}^2, \quad \Delta m^2_{\text{sol}} = 7.6 \times 10^{-5}\,\text{eV}^2, \\ &\theta_{12} = 33.3^\circ, \qquad \theta_{13} = 8.5^\circ, \qquad \theta_{23} = 42.0^\circ\,. \end{aligned} \tag{4.162}$$

The model parameter space can be confined further by extending the framework to account for other BSM phenomena. This includes resonances in the diphoton channel, such as the 750 GeV excess reported recently by CMS and ATLAS, which could forebode novel leptoquark interactions. A model connecting the vector leptoquarks V_0 and $V_{1/2}$ with the 750 GeV diphoton resonance is discussed in Sec. 5.2.
It should be noted that the vector leptoquark setup cannot be considered complete as we do not discuss the mechanism of mass generation for the vector leptoquarks. This could for example be accomplished through the breaking of a larger gauge group under which the vector leptoquarks are charged or by interpreting them as composite states [242]. Possible gauge groups that give rise to leptoquarks were discussed in Sec. 2.3.2.

4.4 CONCLUSIONS

To address the recently reported anomalies in $h \to \mu\tau$, R_K, and $R_{D^{(*)}}$ we have constructed models based on extended Higgs sectors as well as leptoquark mediators.
We explain the $h \to \mu\tau$ data using a 3HDM with LFT, where strongly constrained FCNCs are suppressed by virtue of a residual Z_3 symmetry. A small breaking of this symmetry can give rise to LFV Higgs decays, occurring naturally in the model due to $SU(2)$ singlet scalars in the scalar potential. The sizable signal in $h \to \mu\tau$ channel is a consequence of the mixing between an SM-like Higgs and an exotic neutral scalar accounting for the $2.4\,\sigma$ deviation from the SM. The model predicts large branching fractions for $h \to e\mu$ and $h \to e\tau$ as well, where the latter will be a decisive measurement for its exclusion.
Although the multi-Higgs framework is an intuitive choice to explain the $h \to \mu\tau$ anomaly, the solution is restricted by $\mu \to e\gamma$ to a rather fine-tuned region in the

parameter space. Only if the additional neutral scalars are light they can partly cancel Higgs-loop contributions to $l \to l'\gamma$, allowing for large flavor-violating Yukawa couplings. The first searches in the $h \to e\tau$ channel are consistent with the SM prediction and support the updated results of $h \to \mu\tau$ [73]. Furthermore, the absence of light exotic scalars in the new LHC Run 2 data indicates that the initial excess is likely to be a statistical fluctuation.

Charged scalars arising in multi-Higgs models are also potential candidates to explain the observed deviation manifest in the ratio $R_{D^{(*)}}$. We studied charged Higgs interactions in 3HDMs with respect to the excess in $B \to D^{(*)}\tau\nu$ decays for constraints on the flavor-violating couplings and the charged Higgs masses. We find that the required values are fine-tuned and in tension with experimental searches involving charged scalars. Applying the popular discrete symmetries A_4, S_4, and $\Delta(27)$ to the 3HDM scalar potential does not provide further insight on the origin of such parameter values, and instead disfavors them as an explanation for $R_{D^{(*)}}$.

A more promising approach to solving the B meson flavor puzzle are leptoquark models. Two scalar leptoquarks can generate neutrino masses at one-loop level and simultaneously explain the anomalies in R_K and $R_{D^{(*)}}$. This is possible if these leptoquarks mix weakly with the SM Higgs boson to induce a $\Delta L = 2$ effective Majorana mass term. We have demonstrated this by constructing two models based on the scalar leptoquarks S_1 and $S_{1/2}$, and the vector leptoquarks V_0 and $V_{1/2}$, respectively.

By exploiting an FN mechanism to modify the leptoquark couplings we have shown that addressing several issues at the same time is entirely feasible and need not be overly fine-tuned. Weak Higgs-leptoquark mixing will lead to naturally small neutrino masses and protect the tightly constrained B decays from additional flavor-changing $|\Delta B| = |\Delta S| = 1$ scalar and tensor operators. At the same time, the leptoquark couplings to b and s quarks may still be strong enough to produce visible signals in $B \to Kll$ decays, with leptoquark masses confined to the testable region $1\,\text{TeV} \lesssim M \lesssim 50\,\text{TeV}$. The vector leptoquark model can even provide the large $\mathcal{O}(1)$ couplings needed to explain $R_{D^{(*)}}$ without interfering with other rare decays. The total additional field content includes no more than two leptoquarks and one SM singlet scalar. Only one additional symmetry is required to shape the fermion mass matrices and leptoquark couplings to comply with experimental data.

Our analysis shows that a mild mass hierarchy of the leptoquarks is favored to explain the lightness of neutrino masses. In Sec. 5.2 we explore how this prediction can be combined with a potential excess in the diphoton channel, taking the 750 GeV resonance as an example to confine the parameter space of leptoquark masses.

5

PROBING MODELS WITH DIPHOTON RESONANCES

Recently, the ATLAS and CMS collaborations reported an excess of events above the expected background in the diphoton final state [74, 75]. This was very promising as both collaborations observed the excess at an invariant mass of about 750 GeV, and with a local statistical significance of $3.9\,\sigma$ (ATLAS) and $3.4\,\sigma$ (CMS).
This diphoton resonance has generated much activity in the community, amounting to more than 500 publications on the topic, including both model-independent studies of the excess as well as interpretations of the resonance itself. The most popular explanations are summarized in Ref. [78], reviewing the progress of the field since the announcement of the excess.
Despite the resonance being just a statistical fluctuation, the diphoton final state can be a powerful tool for NP searches thanks to its clear signature over the low background. The Higgs discovery in 2012 in the same channel further emphasizes the importance of this particular decay mode.
In this chapter we use the 750 GeV diphoton excess to explore different model interpretations of diphoton resonances. To this end we tie the resonance to the model field content and symmetries, exploiting it for unique predictions. Both frameworks presented here fall into the everybody's model category outlined in Sec. 1.2.4, although some exceptional properties separate them from the standard scenario. In Sec. 5.1, we extend the S_3 flavor model of Sec. 3.1 to interpret the excess as the FN flavon, thereby linking the origin of the fermion masses and mixings to the resonance scale. In Sec. 5.2 we demonstrate how vector leptoquarks can naturally enhance the diphoton cross section without a plethora of new particles or excessive fine-tuning. In both frameworks, the diphoton resonance pinpoints where the NP is manifest in the model, setting the stage for targeted experimental searches.

5.1 THE EXCESS IN LIGHT OF THE S_3 FLAVOR SYMMETRY

The first analysis of the diphoton resonance is based on the S_3 flavor model proposed in Sec. 3.1, which is modified to account for the reported excess at 750 GeV. To this end, the fermion sector is extended with four exotic quarks with electric charge $\frac{5}{3}$, grouped into two S_3 doublets, i.e., $T_L = (T_{1L}, T_{2L})$, $T_R = (T_{1R}, T_{2R})$. The exotic fields are color charged and thereby enhance the production rate of the resonance through gluon fusion. The decay rate into the diphoton final state is then further increased by their large electric charge.
The present framework differs from the generic everybody's model outlined in Sec. 1.2.4 by the pattern of flavor symmetries shaping the Yukawa interactions. Charging the

exotic quark fields under the Z_{14} symmetry ties them to the FN scale with the flavon χ acting as the scalar resonance at 750 GeV. This unique link between the flavor puzzle and the diphoton channel allows for immediate testing of the flavor symmetry and the involved exotic particles.
Since charged stable particles would interfere with early structure formation [243], the model is supplemented with a charged scalar ρ^+ that permits the exotic quarks to decay into SM fermions. The assignments of the new fields to the symmetry groups are summarized in Tab. 5.1. The original particle content and the purpose of the symmetries were specified in Tabs. 3.2 and 3.1.

Field	$SU(3)_C$	$SU(2)_L$	$Q_{\rm EM}$	S_3	Z_3	Z_3'	Z_{14}
$T_L = (T_{1L}, T_{2L})$	**3**	**1**	5/3	**2**	0	0	0
$T_R = (T_{1R}, T_{2R})$	**3**	**1**	5/3	**2**	0	0	1
ρ^+	**1**	**1**	1	**1**	0	0	0

Table 5.1: New particle content and assignments under the flavor symmetries to account for the diphoton excess at 750 GeV.

The new particle content gives rise to the following Yukawa Lagrangian

$$\begin{aligned}
-\mathcal{L}_Y^q &= y_T \overline{T}_L T_R \chi + \varepsilon_\rho \overline{q}_{3L} \phi_2 T_R \frac{\xi \chi \rho^-}{\Lambda^3} + y_{1\rho} \overline{T}_L U_R \rho^+ \frac{\chi}{\Lambda} + y_{2\rho} \overline{T}_L U_R \rho^+ \frac{\zeta^3 \chi}{\Lambda^4} \\
&\quad + \varepsilon_{33}^{(\rho)} \overline{q}_{3L} \phi_1 u_{3R} \frac{\rho^-}{\Lambda} + \varepsilon_{33}^{(\rho)} \overline{q}_{3L} \widetilde{\phi}_1 d_{3R} \frac{\rho^+ \chi^3}{\Lambda^4} + \varepsilon_{23}^{(\rho)} \overline{q}_{3L} \widetilde{\phi}_2 d_{2R} \frac{\rho^+ \chi^3}{\Lambda^4} \\
&\quad + \varepsilon_{32}^{(\rho)} \overline{q}_{3L} \phi_2 U_R \frac{\xi \rho^- \chi}{\Lambda^3} + \text{h.c.}\,, \qquad (5.1) \\
-\mathcal{L}_Y^l &= \varepsilon_{21}^{(\rho)} \bar{l}_{2L} \phi_1 \nu_{1R} \frac{\rho^+}{\Lambda} + \varepsilon_{33}^{(l)} \bar{l}_{3L} \widetilde{\phi}_1 l_{3R} \frac{\chi^3 \rho^+}{\Lambda^4} + \varepsilon_{23}^{(l)} \bar{l}_{2L} \widetilde{\phi}_1 l_{3R} \frac{\chi^3 \rho^+}{\Lambda^4} \\
&\quad + \varepsilon_{22}^{(\rho)} \bar{l}_{2L} \phi_1 \nu_{2R} \frac{\rho^+}{\Lambda} + \varepsilon_{31}^{(\rho)} \bar{l}_{3L} \phi_1 \nu_{1R} \frac{\rho^+}{\Lambda} + \varepsilon_{32}^{(\rho)} \bar{l}_{3L} \phi_1 \nu_{2R} \frac{\rho^+}{\Lambda} + \text{h.c.}\,,
\end{aligned}$$

where $\mathcal{L}_Y^q$ and $\mathcal{L}_Y^l$ denote the quark and lepton interactions, respectively, omitting for simplicity Yukawa interactions with ρ^+ of dimension nine and higher.

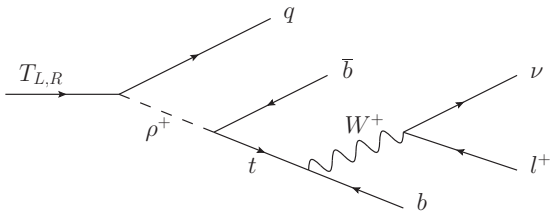

Figure 5.1: Preferred decay chain for the detection of the exotic quarks $T_{L,R}$ at the LHC ($q = u, c, t$). Being pair-produced, the heavy particles should result in an excess of events in the dilepton opposite-sign final state, accompanied by six jets and missing energy.

Following Eq. (5.1), T_L and T_R decay dominantly into up-type quarks and ρ^+, which in turn preferably decays into top and bottom quarks since the lepton decay channels are either suppressed by $\lambda^6 \frac{v^2}{\Lambda^2}$, or kinematically forbidden as $M_{\nu_R} > m_{\rho^+}$. Consequently, the top partners can be searched at the LHC through their decay channel $T_{1(2)} \to \rho^+ u(c) \to t\bar{b}u(c) \to W\bar{b}bu(c) \to l^+ 3j \not{E}_T$, as depicted in Fig. 5.1. Being pair produced via gluon fusion (cf. Fig. 5.2), the exotic quarks should hence appear as an excess of events in the dilepton opposite-sign final state.

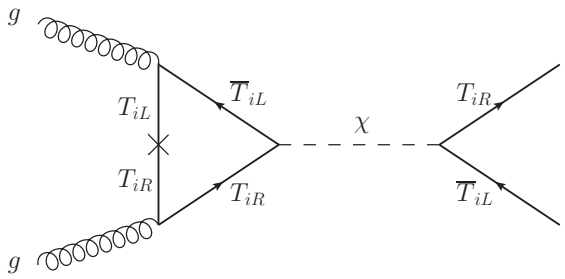

Figure 5.2: Dominant production mechanism of the top partners $T_{L,R}$ at the LHC.

The Z_{14} breaking scalar χ attributed to the resonance is predominantly produced via gluon fusion through triangular loop diagrams with T_1 and T_2. The scalar can subsequently decay through the same loops into the diphoton final state, as depicted in Fig. 5.3. The corresponding total cross section $\sigma_{\gamma\gamma} \equiv \sigma(pp \to \chi \to \gamma\gamma)$ is a function of the gluon production rate $\Gamma(gg \to \chi)$ and the consequent decay rate into photons $\Gamma(\gamma\gamma \to \chi)$

$$\Gamma(gg \to \chi) = K^{gg} \frac{\alpha_s^2 m_\chi^3}{32\pi^3 v_\chi^2} \left| F_{1/2}(x_T) \right|^2 , \tag{5.2}$$

$$\Gamma(\gamma\gamma \to \chi) = \frac{\alpha^2 m_\chi^3}{64\pi^3 v_\chi^2} \left| N_c Q_T^2 F_{1/2}(x_T) \right|^2 , \tag{5.3}$$

where $m_\chi \simeq 750\,\text{GeV}$ denotes the resonance mass, $x_T = 4m_T^2/m_\chi^2$, $m_T = y_T v_\chi$, and $K^{gg} \sim 1.5$ accounts for higher order QCD corrections. $F_{1/2}(x)$ is the fermion loop function contributing to $h \to \gamma\gamma$, which is used here to compute $\sigma_{\gamma\gamma}$. This loop function is given by

$$F_{1/2}(x) = 2\,x\Big[1 + (1-x) f(x)\Big] , \quad f(x) = \Big(\arcsin\sqrt{1/x}\Big)^2 \tag{5.4}$$

with $x_T > 1 \Leftrightarrow 4m_T > m_\chi$. Finally, we obtain

$$\sigma_{\gamma\gamma} \equiv \sigma(pp \to \chi \to \gamma\gamma) = \frac{\pi^2}{8s} \frac{\Gamma(\gamma\gamma \to \chi)\Gamma(gg \to \chi) f_{gg}}{m_\chi \Gamma_{\text{tot}}} \tag{5.5}$$

with Γ_{tot} as the total decay width of χ, and the gluon luminosity function f_{gg}, evaluated at $\sqrt{s} = 13$ TeV using MSTW2008 [244]

$$f_{gg} = \int_{m_\chi^2/s}^1 f_g(x) f_g(m_\chi^2/(xs)) \frac{\mathrm{d}x}{x} = 2141.7 , \tag{5.6}$$

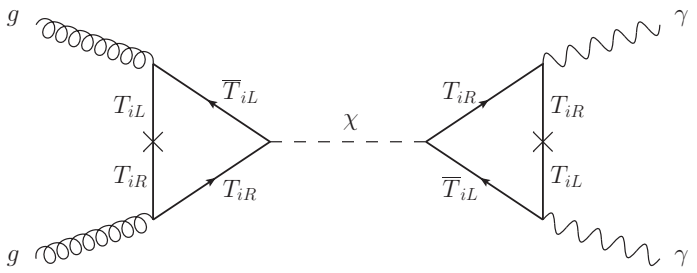

Figure 5.3: Complete process of production and decay of the scalar resonance χ to explain the observed signal in the diphoton final state.

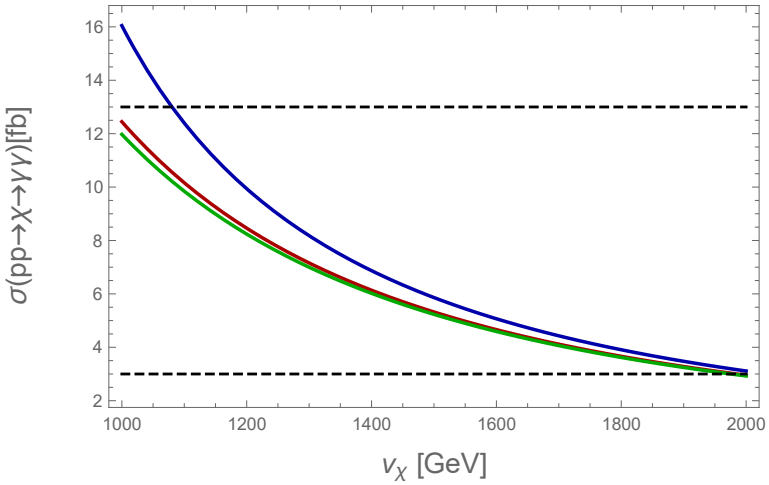

Figure 5.4: Total cross section $\sigma(pp \to \chi \to \gamma\gamma)$ as a function of v_χ for different values of the exotic quark Yukawa couplings $y_{T_i} \sim 0.5$ (blue), 1 (red) and 1.5 (green), assuming $\sqrt{s} = 13$ TeV and $\alpha_s(m_\chi/2) \simeq 0.1$. The horizontal lines denote the experimentally allowed limits of the original diphoton signal given by ATLAS and CMS, which amount to 10 ± 3 fb and 6 ± 3 fb, respectively.

where f_g is the gluon distribution function.
We assume for simplicity unified and natural Yukawa couplings of the exotic quarks $y_{T_i} \sim 1$, amounting to $\sigma_{\gamma\gamma} \approx 8$ fb with $v_\chi \approx 1.2$ TeV. This is well within the limits given by the ATLAS and CMS experiments [245]

$$\sigma_{\text{ATLAS}} = 10 \pm 3 \text{ fb}\,, \qquad \sigma_{\text{CMS}} = 6 \pm 3 \text{ fb}\,. \tag{5.7}$$

The total cross section is shown in Fig. 5.4 as a function of v_χ for different values of the exotic quark Yukawa couplings. The cross section depends crucially on the VEV v_χ as well as on the Yukawa couplings, which if sizable can also enhance σ significantly in particular for lower v_χ values.
If we further require that σ be within the experimental limits given by ATLAS and CMS, we predict v_χ to be smaller than 2 TeV, which on the one hand sets the Z_{14} breaking scale $\Lambda \lesssim 10$ TeV, and on the other hand forces the expected particle masses of χ and the exotic quarks T_i into a testable region.

5.2 DIPHOTON RESONANCE WITH VECTOR LEPTOQUARKS

A plethora of explanations has been considered by various authors since the announcement of the excess until its dismissal, among them also leptoquark mediators. While pure scalar leptoquark solutions face difficulties regarding unitarity, vector leptoquarks can explain the signal rather elegantly thanks to a sizable loop factor. The beauty of the vector leptoquark solution is that it does not come with numerous exotic fermions to artificially enhance the diphoton decay mode. We demonstrate this using the vector leptoquark model presented in Sec. 4.3.2 and not only explain but also utilize the excess to pin down the leptoquark masses.
The vector leptoquarks in our model can interact with the scalar resonance χ through the hypothetical interaction

$$-\mathcal{L}_{V\chi} = \kappa_{V_i} \chi V^{\dagger}_{\mu,i} V^{\mu}_{i} + \text{h.c.}\,, \tag{5.8}$$

where $i = 0, \frac{1}{2}$. The scale of the dimensionful parameter κ_{V_i} is thus far undetermined, however bounded from above by unitarity constraints. The scale where the theory breaks down can be roughly inferred from elastic $V_{i,\mu}V^{i,\mu} \to V_{i,\mu}V^{i,\mu}$ scattering, given by $\sqrt{s} \sim 4\sqrt{\pi} m^2_{V_i}/|\kappa_{V_i}|$ [228]. In the following we will assume natural TeV-scale values for κ_{V_i} to comply with perturbative unitarity.

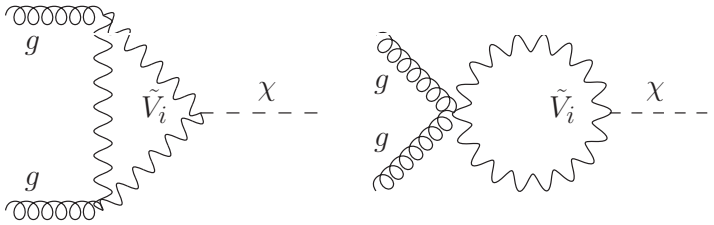

Figure 5.5: Dominating diagrams contributing to $\sigma(pp \to \chi)$.

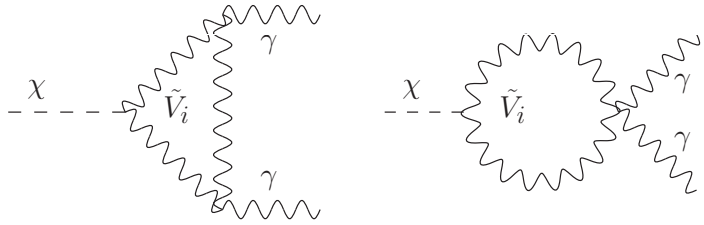

Figure 5.6: Diagrams contributing to $\Gamma(\chi \to \gamma\gamma)$.

In the narrow width approximation, the total cross section $\sigma_{\gamma\gamma}$ is a product of the χ production and its subsequent decay rate into two photons. χ production from $q\overline{q}$ initial states is possible, however, strongly suppressed either by small leptoquark couplings [cf. Eqs. (4.139) and (4.140)] or small values of the parton distribution functions at $\sqrt{s} = 13$ TeV [245] (Tab. 1.3). The only partly competitive channel in terms of luminosity, $d\overline{d} \to \chi$, is additionally suppressed compared to gluon fusion by a factor of

$|\lambda^L_{d\tau}|^2 = \epsilon^6$ due to the FN symmetry. Hence, since χ is predominantly produced via gluon fusion we can compute $\sigma_{\gamma\gamma}$ via Eq. (5.5) with

$$\Gamma_{gg} \equiv \Gamma(\chi \to gg) = \frac{\alpha_s^2 m_\chi^3 K^{gg}}{128\pi^3} \left| \sum_i \frac{\kappa_{V_i} F_1(\tau_{V_i})}{m_{V_i}^2} \right|^2 , \tag{5.9}$$

$$\Gamma_{\gamma\gamma} \equiv \Gamma(\chi \to \gamma\gamma) = \frac{\alpha_e^2 m_\chi^3}{256\pi^3} \left| \sum_i \frac{\kappa_{V_i} N_c Q_{V_i}^2 F_1(\tau_{V_i})}{m_{V_i}^2} \right|^2 , \tag{5.10}$$

where $i = 0, \frac{1}{2}$. We furthermore approximate $\Gamma_{tot} \approx \Gamma_{gg}$. Like in the previous analysis, $f_{gg} = 2141.7$, $N_c = 3$ for the vector leptoquarks running in the loop and α_s is the strong coupling constant. $F_1(\tau)$ denotes the loop factor for a spin-1 particle given by [168]

$$F_1(\tau) = \frac{1}{\tau^2} \left[2\tau^2 + 3\tau + 3(2\tau - 1) \arcsin^2 \sqrt{\tau} \right] , \tag{5.11}$$

and $\tau_{V_i} = m_\chi^2/(4m_{V_i}^2) < 1$. The loop factor $F_1(\tau)$ was originally computed in Ref. [167] to account for the $W^\pm$ gauge boson contribution to the radiative decay $h \to \gamma\gamma$ in the SM. The unphysical degrees of freedom of the vector bosons can cause loop divergences that have to be dealt with. These divergences were regularized using the nonlinear R_ξ gauge [246], in which the vector-boson propagator reads

$$\frac{-i}{k^2 - M_V^2} \left[g_{\mu\nu} + \frac{(\xi - 1) k_\mu k_\nu}{k^2 - \xi M_V^2} \right] . \tag{5.12}$$

It is shown in Ref. [246] that all divergences cancel out separately in the vector-boson and the Faddeev-Popov ghost sector, resulting in a finite and gauge-independent theory. $F_1(\tau)$ acquires large values for vector leptoquarks compared to scalar particles. Assuming leptoquark masses ranging from ~ 0.8 to 50 TeV as dictated by $R_K, R_{D^{(*)}}$ and the $B_s - \overline{B}_s$ mixing phase, the loop factors remain near constant with

$$\frac{|F_1(\tau)|}{|F_0(\tau)|} \approx 20 , \qquad \frac{|F_1(\tau)|}{|F_{1/2}(\tau)|} \approx 5, \tag{5.13}$$

in the relevant mass region.

Depending on the dimensionful couplings κ_{V_i}, typical values of Γ_{gg}/m_χ and $\Gamma_{\gamma\gamma}/m_\chi$ are $\mathcal{O}(10^{-4})$ and $\mathcal{O}(10^{-6})$, respectively. In our setup, at the benchmark point $\kappa_{V_i} = \frac{4}{3} m_{V_i}$, $m_{V_0} = 1$ TeV and $m_{V_{1/2}} = 20$ TeV we have

$$\frac{\Gamma_{gg}}{m_\chi} \simeq 2 \cdot 10^{-4} , \quad \frac{\Gamma_{\gamma\gamma}}{m_\chi} \simeq 8 \cdot 10^{-7} , \quad \sigma_{\gamma\gamma} \simeq 4 \text{ fb} . \tag{5.14}$$

Therefore, the estimated dijet cross section at 13 TeV is 4 pb, leading to a cross section $\simeq 0.8$ pb at 8 TeV. Currently the ATLAS and CMS collaborations do not provide dijet limits at $\sqrt{s} = 13$ TeV for resonance masses below 1 TeV. The $\sqrt{s} = 8$ TeV ATLAS and CMS analyses presented in Refs. [247,248] set a limit of $\sigma_{jj} < 1$ pb for a 1 TeV resonance coupling dominantly to gg. For a mass of 750 GeV the limit shown by ATLAS is of the order of 10 pb. Hence within the interesting region of parameter space considered here, the dijet limits are satisfied.

As V_0 and $V_{1/2}$ carry hypercharge, they necessarily decay via $\chi \to Z\gamma$ and $\chi \to ZZ$. Limits on these final states from experimental collaborations already exist. Here we

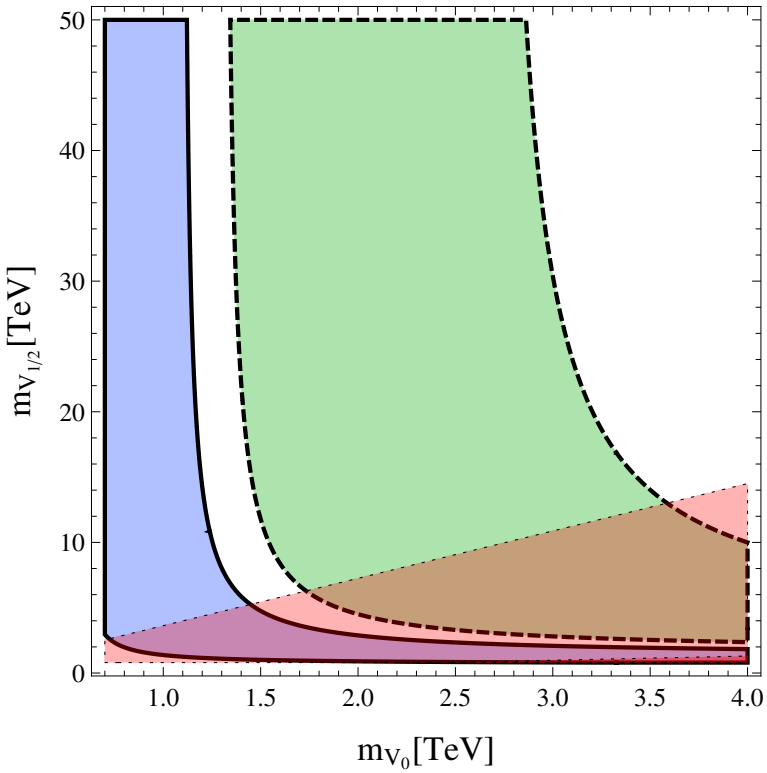

Figure 5.7: Parameter regions yielding $\sigma_{\gamma\gamma} \in (3, 13)$ fb as measured by ATLAS and CMS, where $\sigma_{\gamma\gamma}$ is shown as a function of the leptoquark masses m_{V_0} and $m_{V_{1/2}}$ for different values of the dimensionful couplings $\kappa_{V_i} = \frac{10}{3} m_{V_i}$ (green, dashed) and $\frac{4}{3} m_{V_i}$ (blue, solid). The constraint (5.15) with $r = 0.28$ from WW, ZZ and $Z\gamma$ limits is superimposed in red.

take a rather simplistic viewpoint and assess the viability of our scenario without explicitly calculating the cross sections for $Z\gamma$, and ZZ final states. This can be done by estimating the ratios of χ partial widths. The partial widths $\chi \to Z\gamma$ and $\chi \to ZZ$ are suppressed compared to $\Gamma_{\gamma\gamma}$ by $2\tan^2\theta_W$ and $\tan^4\theta_W$, respectively, and existing bounds on these channels can be easily evaded. More importantly, $V_{1/2}$ is an $SU(2)$ doublet with enhanced rates $\Gamma_{Z\gamma}/\Gamma_{\gamma\gamma} \approx 2/\tan^2\theta_W$, $\Gamma_{ZZ}/\Gamma_{\gamma\gamma} \approx 1/\tan^4\theta_W$. In addition, the decay to two W bosons is possible as well with a strongly enhanced rate $\Gamma_{WW}/\Gamma_{\gamma\gamma} \approx 2/\sin^2\theta_W$ [245]. The experimental limits are satisfied for

$$\frac{|\kappa_{V_{1/2}}|}{m^2_{V_{1/2}}} < r \times \frac{|\kappa_{V_0}|}{m^2_{V_0}}, \tag{5.15}$$

with $r \approx 3.1$ if the κ couplings have the same sign and $r \approx 0.28$ if they have opposite signs. The difference arises due to constructive or destructive interference from the contribution of $SU(2)$ and $U(1)$ coupling components to the decay widths. By using this constraint we quantify the impact of diboson final-state limits in our analysis.
The width of χ is dominated by the decay to gluons and is typically small, $\Gamma_{\text{tot}} \approx \Gamma_{gg} \approx 0.3$ GeV. We make no attempt to explain a potentially large width as suggested by ATLAS within this setup.

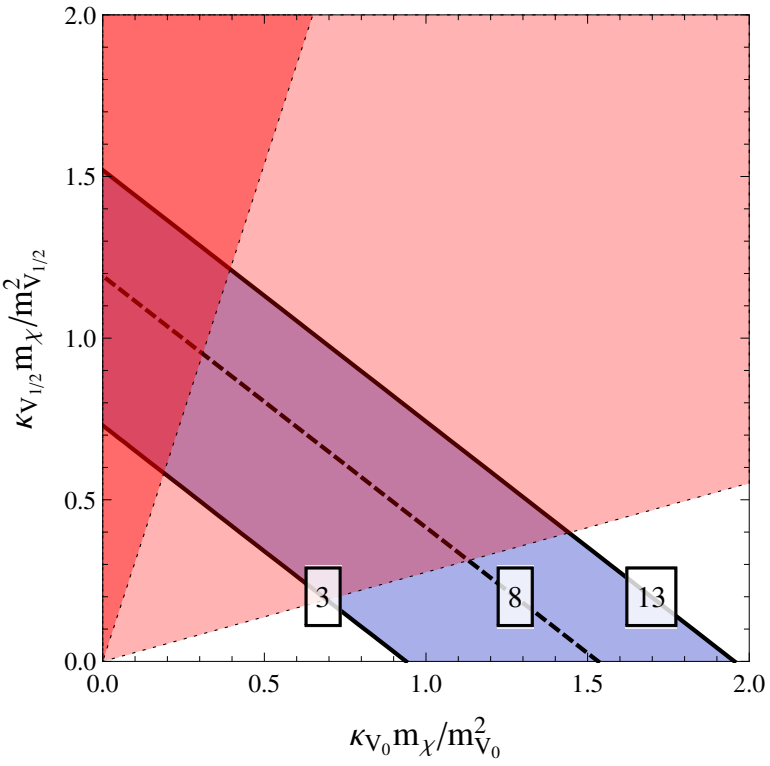

Figure 5.8: Parameter regions yielding $\sigma_{\gamma\gamma} \in (3, 13)$ fb as measured by ATLAS and CMS. $\sigma_{\gamma\gamma}$ as a function of the effective parameters $\kappa_{V_i} m_\chi / m^2_{V_i}$. The lines denote values of constant $\sigma_{\gamma\gamma}$ in fb. The constraint Eq. (5.15) with $r = 0.28$ (light shade) and $r = 3.1$ (dark shade) from WW, ZZ and $Z\gamma$ limits is superimposed in red.

In the following we determine the allowed parameter ranges of κ_{V_i} and m_{V_i} to reproduce the total cross sections measured by ATLAS and CMS in the diphoton channel near 750 GeV, cf. Eq. (5.7).
Taking into account that $m_{V_0} \sim 1$ TeV is needed to reproduce the R_K and R_D data, we obtain the allowed parameter regions displayed in Figs. 5.7 and 5.8 as a function of the dimensionful couplings κ_{V_i} and the leptoquark masses m_{V_i}, respectively. The parameter space favoring the diphoton cross section opens up notably if the second leptoquark is much heavier, yielding a large Δm^2_V that is also favored by neutrino mass generation. Fig. 5.7 shows $\sigma_{\gamma\gamma}$ in the range of $3 - 13$ fb, for two different values of dimensionful couplings κ_{V_i}. The parameter space excluded by WW, ZZ, and $Z\gamma$ searches is depicted in red. This constraint is derived using Eq. (5.15). In Fig. 5.7 only the more stringent constraint, applicable if the κ couplings have opposite signs, is shown; the case of same sign exhibits no appreciable constraint.
In Fig. 5.8 we depict $\sigma_{\gamma\gamma}$ as a function of $\kappa_{V_i} m_\chi / m^2_{V_i}$. We fix the loop factor $F_1(\tau) \sim 7$, after explicitly verifying that $F_1(\tau)$ varies only by 3% in the relevant region of the parameter space. The residual dependence on the masses from the loop function is hence small and is ignored. As $\kappa_{V_0} m_\chi / m^2_{V_0}$ and $\kappa_{V_{1/2}} m_\chi / m^2_{V_{1/2}}$ increase, the corresponding diphoton cross section increases and the observed excess can be explained with, e.g., $\kappa_{V_0} m_\chi / m^2_{V_0} \approx 1$ and $\kappa_{V_{1/2}} m_\chi / m^2_{V_{1/2}} < 0.8$. The shaded red areas denote the parameter space excluded by WW, ZZ, and $Z\gamma$ searches derived from Eq. (5.15). The darker shade

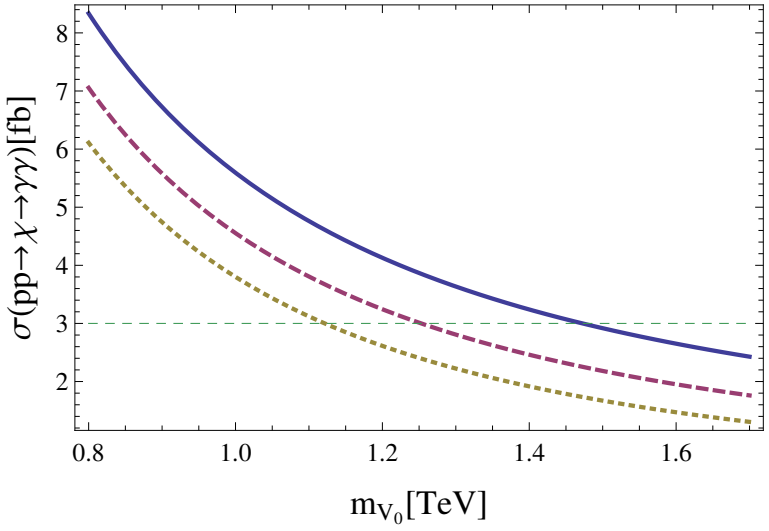

Figure 5.9: $\sigma_{\gamma\gamma}$ as a function of m_{V_0} for $m_{V_{1/2}} = 5$ TeV (blue, solid), 10 TeV (red, dashed), 50 TeV (yellow, dotted) with $\kappa_{V_i} = \frac{4}{3} m_{V_i}$. The horizontal, dashed lines correspond to the lower limit given by the ATLAS and CMS diphoton measurements.

applies in the case of same-sign κ couplings resulting in the limits $\kappa_{V_0} m_\chi / m_{V_0}^2 \gtrsim 0.2$ and $\kappa_{V_{1/2}} m_\chi / m_{V_{1/2}}^2 \lesssim 1.2$. The more constraining case of opposite-sign κ couplings is depicted in light red giving the limits $\kappa_{V_0} m_\chi / m_{V_0}^2 \gtrsim 0.7$ and $\kappa_{V_{1/2}} m_\chi / m_{V_{1/2}}^2 \lesssim 0.4$

In Fig. 5.9 we show the behavior of $\sigma_{\gamma\gamma}$ in terms of m_{V_0} for different choices of $m_{V_{1/2}}$ with $\kappa_{V_i} = \frac{4}{3} m_{V_i}$. The diphoton cross section decreases with large leptoquark masses and a mass $m_{V_0} \approx 1$ TeV is preferred in good agreement with the input from rare B decays. For a given value of $m_{V_{1/2}}$, the diphoton cross section requirement yields an upper bound on m_{V_0}. In the case $m_{V_{1/2}} = 50$ TeV, $m_{V_0} > 1.1$ TeV results in a too low diphoton cross section, while $m_{V_{1/2}} = 5$ TeV requires $m_{V_0} < 1.5$ TeV.

The benchmark point $m_{V_0} = 1$ TeV, $m_{V_{1/2}} = 30$ TeV, $\kappa_{V_i} = \frac{4}{3} m_{V_i}$ yields $\sigma \approx 4.0$ fb conforming to Eq. (5.7). Intriguingly, the combined results of neutrino mass generation and the 750 GeV diphoton excess point to a similar region in the parameter space of leptoquark masses. As shown in Fig. 5.10 the overlay of all constraints points at a light leptoquark $m_{V_0} \approx 1$ TeV together with a heavy $m_{V_{1/2}} \gtrsim 20$ TeV, depending on the size of the trilinear couplings κ_{V_i} and h_V.

By embedding the diphoton resonance in the leptoquark framework, we are able to place upper bounds on the leptoquark masses that are more stringent than the limits from the flavor sector or neutrino masses. This result shows that a full understanding of the diphoton final state is vital for model predictions, i.e., future resonances in this channel may prove crucial for distinguishing between the viable frameworks.

5.3 CONCLUSIONS

Future resonances in the diphoton channel can probe a variety of models. Inspired by the 750 GeV excess, we have illustrated this using the model based on the discrete S_3 flavor symmetry and the vector leptoquark model supplemented with the $U(1)_{\text{FN}}$.

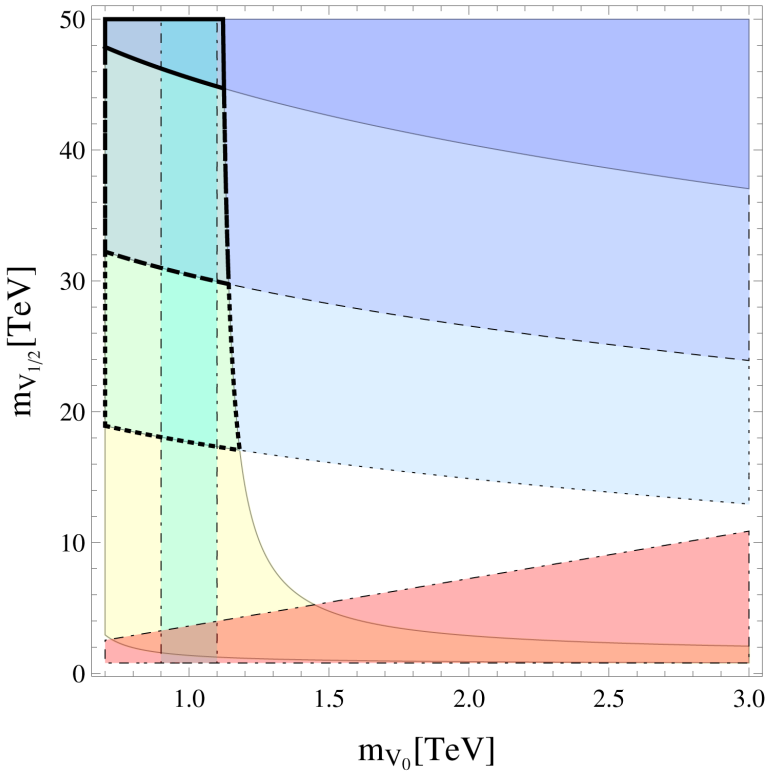

Figure 5.10: Fit results of the 750 GeV diphoton excess (yellow) superimposed with constraints from neutrino mass generation (blue) in the leptoquark parameter space for $\kappa_{V_i} = \frac{4}{3} m_{V_i}$ and $h_V = 0.2$ TeV (dotted), 0.5 TeV (dashed), 1 TeV (solid). The cyan overlay (dotted/dashed) denotes regions favored by low-energy B physics. The constraints favor a combination of a light V_0 and a heavy $V_{1/2}$ with $m_{V_0} \approx 1$ TeV and $m_{V_{1/2}} \gtrsim 20$ TeV, depending on the scale of the trilinear couplings κ_{V_i} and h_V. The constraint (5.15) with $r = 0.28$ from WW, ZZ and $Z\gamma$ limits is superimposed in red excluding all $m_{V_0} > 1.5$ TeV.

By introducing heavy exotic fermions charged under Z_{14} we connected the flavon of the S_3 model with the 750 GeV scalar resonance. The diphoton cross section then dictates the size of the flavon VEV and consequently the exotic fermion masses as well as the Z_{14} breaking scale. The NP scale should be no higher than 10 TeV implying that the framework could be probed in the near future.
In the second model the vector leptoquarks couple to the resonance scalar, thereby naturally enhancing the diphoton cross section. Here the resonance provides complementary constraints to neutrino mass generation and confines the parameter space of leptoquark masses. It is shown that $m_{V_0} \approx 1$ TeV and $m_{V_{1/2}} \approx 30$ TeV fit the data well, whereas $m_{V_0} > 1.5$ TeV is excluded by diboson searches.
These results indicate that if the 750 GeV excess were not a statistical fluctuation it could provide valuable input on the model parameters. Future signals in this channel can therefore help to sift through the large number of flavor models.

6

SUMMARY AND CONCLUSIONS

Since the LHC started taking data in 2008, all measurements have been consistent with the SM predictions, rapidly closing in on models with new physics at the electroweak or even TeV scale. Despite this incredible success, some questions remain unclear. In this thesis we attempted to tackle issues regarding the origin of flavor: the disparate quark and lepton mixings, the hierarchies of the Yukawa couplings, and the source of the neutrino masses. Besides these concerns, recent experiments uncovered several anomalies hinting at a possible violation of lepton flavor and universality. These include a signal in $h \to \mu\tau$ decays and deviations in the ratios R_K and $R_{D^{(*)}}$, which indicate NP in the lepton sector. Motivated by the diverse measurements in the flavor sector, we used model building as a means to find a possible common origin of the anomalies and the flavor puzzle.

In Chapter 3 we constructed two models to unify the masses and mixings of the SM fermions. Special features and predictions distinguish the frameworks from the many flavor models existing in the literature. The first model utilizes the nonabelian S_3 symmetry with two Higgs doublets to separate the interactions in the different fermion sectors. The fermion mass hierarchies are explained with natural order one Yukawa couplings thanks to a Z_{14} FN symmetry. Due to a special case of Yukawa alignment the framework is free of FCNCs in the down-type and the charged lepton sector and thus evades rare decay constraints effortlessly. However, the model can be probed with searches for $t \to cg$ and $t \to hc$ in the future, where sizable flavor violation is still possible.

The second model is an extended $SU(5)$ GUT supplemented with an $A_4 \times U(1)$ flavor symmetry, which attempts to address problems of grand unification as well as the flavor puzzle simultaneously. The link between the flavor and the unification scale is achieved by promoting the $SU(5)$ adjoint representation **24** to the FN flavon. The model contains several light scalars that should be observable in experiments, but due to the many free parameters it is difficult to provide testable predictions.

Both models can accommodate the experimental data very well. However, the large parameter space shows that it is challenging to find an elegant model accounting for the discrepancy between the quark and lepton mixings.

In Chapter 4 we focused on the flavor anomalies and proposed three models based on extended Higgs sectors and leptoquark mediators to explain the observables $\mathcal{B}(h \to \mu\tau)$, R_K, and $R_{D^{(*)}}$. NP at the EW scale is necessary to generate the large signal in $h \to \mu\tau$, which can be provided by additional Higgs doublets. We explore a 3HDM and utilize the S_4 symmetry to relate the large leptonic mixing to the flavor-violating Higgs decays. The allowed region where $h \to \mu\tau$ and the constraints from $\mu \to e\gamma$ can be accommodated

at the same time is small and forces the additional scalar states to be in the region of $200 - 300$ GeV. This prediction is already in tension with experimental searches, which will increase if evidence of NP remains absent in the accumulating LHC Run 2 data. Furthermore, large flavor violation is also expected in $h \to e\tau$ in this framework, which has not been reported yet by experiments. Although multi-Higgs models are an intuitive approach to the anomaly, our solution is fine-tuned and supports the hint that the excess might disappear in the near future.

Besides $h \to \mu\tau$, also the anomaly in $R_{D^{(*)}}$ could be attributed to charged Higgs bosons arising in 3HDMs. We studied how the flavor symmetries A_4, S_4, and $\Delta(27)$ shape the charged scalar interactions with respect to $b - c$ and $\tau - \nu$ couplings and concluded that the large deviation reported in $R_{D^{(*)}}$ cannot originate from flavor symmetries.

Two models based on the scalar leptoquarks S_1 and $S_{1/2}$ and the vector leptoquarks V_0 and $V_{1/2}$, respectively, are viable alternatives to explain the B meson anomalies. Of all the models formulated in this thesis, the vector leptoquark model is the most successful in combining several phenomena with a small amount of field content and symmetries. For the first time we were able to connect the anomalies R_K and $R_{D^{(*)}}$ with the small neutrino mass scale and the large PMNS mixing. An FN mechanism dictates sizable leptoquark couplings to $b - \mu$ and $b - \tau$, while the weak leptoquark-Higgs mixing induces naturally-small neutrino masses. This is possible if the leptoquark masses reside at ~ 1 TeV and $\gtrsim 30$ TeV, respectively, which implies that one leptoquark should manifest in the LHC data soon.

The fact that the flavor problem can be tackled with such fundamentally different frameworks makes testable predictions crucial. It is therefore imperative to study the scalar phenomenology of each model extensively. An attractive channel to probe NP scenarios is the diphoton final state because of its low background at the LHC. We find that the $h \to \gamma\gamma$ channel places the most stringent bounds on the parameter space of the S_3 flavor model (Sec. 3.1).

Other resonances in the diphoton channel can further constrain the parameter space if they are linked to the model phenomenology. In chapter 5 we utilized the 750 GeV diphoton excess reported in December 2015 to show how incorporating possible future signals in this final state can increase the models' predictivity. By extending the S_3 and the vector leptoquark flavor models to account for the resonance we were able to confine the parameter space of the exotic field content. In the S_3 model the FN flavon acted as the scalar resonance and thereby connected the excess with the flavor symmetry breaking scale and the exotic particle masses. The Z_{14} symmetry responsible for the fermion masses and mixing patterns should be broken below 10 TeV to accommodate the resonance at 750 GeV. In the second example, the vector leptoquarks enhanced the diphoton signal through their dimensional coupling to the scalar resonance and their large loop factor. By requiring that the vector leptoquarks reproduce the total cross sections reported by ATLAS and CMS, we were able to pinpoint their masses.

In summary, it is possible to accommodate the different measurements in the flavor sector with model building. However, finding a simple yet elegant framework is challenging and leads to many solutions which vary in complexity and predictivity. The models introducing NP at the TeV or even the EW scale will soon be put to the test by LHC Run 2 data.

A

MEASUREMENTS AND SM PREDICTIONS

A.1 MASSES AND MIXING ANGLES

In this section we collect the experimental values of SM parameters referred to in the models of this thesis. The quark, lepton, and neutrino masses are listed in Tabs. A.1 and A.2. Information on the CKM and PMNS mixing angles can be found in Tabs. A.3 – A.6.

Mass	Value	Mass	Value	Mass	Value
m_d	$0.0029^{+0.0005}_{-0.0004}$	m_u	$0.00145^{+0.00056}_{-0.00045}$	m_e	0.00051
m_s	$0.0577^{+0.0168}_{-0.0157}$	m_c	0.635 ± 0.086	m_μ	0.10565
m_b	$2.820^{+0.090}_{-0.040}$	m_t	$172.1 \pm 0.6 \pm 0.9$	m_τ	1.77686 ± 0.00012

Table A.1: Experimental values of the fermion masses at the M_Z scale in GeV [155].

Observable	$\Delta m^2_{21}(10^{-5}\text{eV}^2)$	$\Delta m^2_{31}(10^{-3}\text{eV}^2)$	
Best fit ($\pm 1\,\sigma$)	$7.49^{+0.19}_{-0.17}$	NH:	$+2.526^{+0.039}_{-0.037}$
		IH:	$-2.518^{+0.038}_{-0.037}$
3σ	$7.02 \to 8.08$	NH:	$+2.413 \to +2.645$
		IH:	$-2.634 \to -2.406$

Table A.2: Neutrino mass squared splittings for normal and inverted hierarchy, respectively. The values were taken from the newest NU-Fit 2.2 data [13].

Observable	$\sin\theta_{12}$	$\sin\theta_{23}$	$\sin\theta_{13}$	δ
Best fit	0.2254	0.0413	0.00350	68°

Table A.3: Experimental values of the CKM mixing angles and the CP phase δ obtained from the NU-Fit 2.2 data [13].

Element	Central $\pm 3\sigma$	Element	Central $\pm 3\sigma$	Element	Central $\pm 3\sigma$
$\lvert V_{ud}\rvert$	$0.97425^{+0.00022}_{-0.00032}$	$\lvert V_{cd}\rvert$	$0.22529^{+0.00100}_{-0.00098}$	$\lvert V_{td}\rvert$	$0.00868^{+0.00027}_{-0.00058}$
$\lvert V_{us}\rvert$	$0.22542^{+0.00101}_{-0.00097}$	$\lvert V_{cs}\rvert$	$0.97339^{+0.00024}_{-0.00024}$	$\lvert V_{ts}\rvert$	$0.04107^{+0.00094}_{-0.00161}$
$\lvert V_{ub}\rvert$	$0.00371^{+0.00027}_{-0.00020}$	$\lvert V_{cb}\rvert$	$0.04180^{+0.00097}_{-0.00164}$	$\lvert V_{tb}\rvert$	$0.99912^{+0.00007}_{-0.00004}$

Table A.4: Experimental values of the CKM matrix elements. Each matrix element is constrained by various channels independently, which are taken into account in the global fit performed by CKMfitter [185].

Observable	$\sin^2\theta_{12}$	$\sin^2\theta_{23}$	$\sin^2\theta_{13}$
Best fit ($\pm 1\,\sigma$)	$0.308^{+0.013}_{-0.012}$	NH: $0.440^{+0.023}_{-0.019}$	NH: $0.02163^{+0.00074}_{-0.00074}$
		IH: $0.584^{+0.018}_{-0.022}$	IH: $0.02175^{+0.00075}_{-0.00074}$
3σ	$0.273 \to 0.349$	NH: $0.388 \to 0.630$	NH: $0.01938 \to 0.02388$
		IH: $0.398 \to 0.634$	IH: $0.01950 \to 0.02403$

Table A.5: Leptonic mixing angles for normal and inverted hierarchy, respectively. The values were taken from the newest NU-Fit 2.2 data [13].

Type	Experiments	Dominant	Important
Solar	SNO	θ_{12}	Δm^2_{sol}, θ_{13}
Reactor long baseline	KamLAND	Δm^2_{sol}	θ_{12}, θ_{13}
Reactor medium baseline	Daya-Bay, Reno Double-Chooz	θ_{13}	$\lvert\Delta m^2_{\text{atm}}\rvert$
Atmospheric	SuperKamiokande	θ_{23}	$\lvert\Delta m^2_{\text{atm}}\rvert$, θ_{13}
Accelerator ν_μ disappearance	Minos, NOνA, T2K	$\lvert\Delta m^2_{\text{atm}}\rvert$	θ_{23}
Accelerator ν_e appearance	Minos, NOνA, T2K	δ_{CP}	θ_{13}, θ_{23}, $\pm\Delta m^2_{\text{atm}}$

Table A.6: Overview of experiments that currently measure neutrino oscillation parameters and the observables they are sensitive to [13].

A.2 RARE AND FORBIDDEN DECAY RATES

This appendix contains summary tables of the rare decay branching ratios relevant for this thesis. These are separated into B meson (A.7), K meson (A.8), and lepton decays (A.9).

Channel	$\mathcal{B}_{\text{exp}}$	$\mathcal{B}_{\text{SM}}$
$b \to s\gamma$	$(3.49 \pm 0.19) \times 10^{-4}$	$(3.36 \pm 0.23) \times 10^{-4}$
$b \to see$	$(4.7 \pm 1.3) \times 10^{-6}$	$(4.15 \pm 0.70) \times 10^{-6}$
$b \to s\mu\mu$	$(4.3 \pm 1.3) \times 10^{-6}$	$(4.15 \pm 0.70) \times 10^{-6}$
$B^0 \to \mu\mu$	$(3.9^{+1.6}_{-1.4}) \times 10^{-10}$	$(1.06 \pm 0.09) \times 10^{-10}$
$B_s^0 \to \mu\mu$	$(2.8^{+0.7}_{-0.6}) \times 10^{-9}$	$(3.66 \pm 0.23) \times 10^{-9}$
$B^+ \to \tau^+\nu$	$(1.14 \pm 0.27) \times 10^{-4}$	$(0.76^{+0.08}_{-0.06}) \times 10^{-4}$
Observable	Experiment	SM expectation
R_K	$0.745^{+0.090}_{-0.074} \pm 0.036$	1.0003 ± 0.0001
R_D	0.388 ± 0.047	0.300 ± 0.010
R_{D^*}	0.321 ± 0.021	0.252 ± 0.005

Table A.7: Summary of current measurements in the B meson sector [6, 6, 32, 33, 35–37, 40–43].

Channel	$\mathcal{B}_{\text{exp}}$	$\mathcal{B}_{\text{SM}}$
$K_L \to \mu\mu$	$(6.84 \pm 0.11) \times 10^{-9}$	$\sim (6.64 \pm 0.07) \times 10^{-9}$
$K_L \to ee$	$(8.7^{+5.7}_{-4.1}) \times 10^{-12}$	$\sim 9 \times 10^{-12}$
$K_L \to \mu e$	$< 4.7 \times 10^{-12}$	
$K_L \to \pi^0 \mu e$	$< 7.6 \times 10^{-11}$	
$K_L \to \pi^0 \mu e$	$< 1.7 \times 10^{-10}$	
$K^+ \to \pi^+ \mu^+ e^-$	$< 1.2 \times 10^{-11}$	
$K^+ \to \pi^+ \mu^- e^+$	$< 5.2 \times 10^{-10}$	

Table A.8: Overview of constraints on rare K decays at 90% C.L. The decays with lepton flavor-violating final states are forbidden in the SM without massive neutrinos. The measurements were taken from Ref. [6]

Channel	$\mathcal{B}_{\text{exp}}$
$\mu \to e\gamma$	$< 5.7 \times 10^{-13}$
$\mu N \to eN$	$< 7.0 \times 10^{-13}$
$\mu \to eee$	$< 1.0 \times 10^{-12}$
$\tau \to e\gamma$	$< 3.3 \times 10^{-8}$
$\tau \to \mu\gamma$	$< 4.4 \times 10^{-8}$
$\tau \to eee$	$< 2.7 \times 10^{-8}$
$\tau \to e\mu\mu$	$< 1.7 \times 10^{-8}$
$\tau \to ee\mu$	$< 1.8 \times 10^{-8}$
$\tau \to \mu\mu\mu$	$< 2.1 \times 10^{-8}$

Table A.9: Summary of current limits on processes with CLFV [50, 54, 55, 57, 249].

B

TENSOR PRODUCT RULES

Here we append the group multiplication rules for A_4 and S_4 used in the models of Secs. 3.2 and 4.1.

B.1 MULTIPLICATION RULES OF S_4

The S_4 product rules can be written as [83]

$$\begin{array}{lllllllll}
\mathbf{3}\otimes\mathbf{3} &=& \mathbf{1}\oplus\mathbf{2}\oplus\mathbf{3}\oplus\mathbf{3'}\,, & \mathbf{2}\otimes\mathbf{2} &=& \mathbf{1}\oplus\mathbf{1'}\oplus\mathbf{2}\,, & \mathbf{3}\otimes\mathbf{1'} &=& \mathbf{3'}\,, \\
\mathbf{3'}\otimes\mathbf{3'} &=& \mathbf{1}\oplus\mathbf{2}\oplus\mathbf{3}\oplus\mathbf{3'}\,, & \mathbf{2}\otimes\mathbf{3} &=& \mathbf{3}\oplus\mathbf{3'}\,, & \mathbf{3'}\otimes\mathbf{1'} &=& \mathbf{3}\,, \\
\mathbf{3}\otimes\mathbf{3'} &=& \mathbf{1'}\oplus\mathbf{2}\oplus\mathbf{3}\oplus\mathbf{3'}\,, & \mathbf{2}\otimes\mathbf{3'} &=& \mathbf{3'}\oplus\mathbf{3}\,, & \mathbf{2}\otimes\mathbf{1'} &=& \mathbf{2}\,.
\end{array} \tag{B.1}$$

Explicitly, in the basis adopted in this thesis, which corresponds to Ref. [83], the tensor products read

$$\begin{aligned}
&(\mathbf{A})_{\mathbf{3}}\otimes(\mathbf{B})_{\mathbf{3}} \\
&\qquad = (\mathbf{A}\cdot\mathbf{B})_{\mathbf{1}}\oplus\begin{pmatrix}\mathbf{A}\cdot\Sigma\cdot\mathbf{B}\\ \mathbf{A}\cdot\Sigma^{*}\cdot\mathbf{B}\end{pmatrix}_{\mathbf{2}}\oplus\begin{pmatrix}\{A_yB_z\}\\ \{A_zB_x\}\\ \{A_xB_y\}\end{pmatrix}_{\mathbf{3}}\oplus\begin{pmatrix}[A_yB_z]\\ [A_zB_x]\\ [A_xB_y]\end{pmatrix}_{\mathbf{3'}}\,, \\
&(\mathbf{A})_{\mathbf{3'}}\otimes(\mathbf{B})_{\mathbf{3'}} \\
&\qquad = (\mathbf{A}\cdot\mathbf{B})_{\mathbf{1}}\oplus\begin{pmatrix}\mathbf{A}\cdot\Sigma\cdot\mathbf{B}\\ \mathbf{A}\cdot\Sigma^{*}\cdot\mathbf{B}\end{pmatrix}_{\mathbf{2}}\oplus\begin{pmatrix}\{A_yB_z\}\\ \{A_zB_x\}\\ \{A_xB_y\}\end{pmatrix}_{\mathbf{3}}\oplus\begin{pmatrix}[A_yB_z]\\ [A_zB_x]\\ [A_xB_y]\end{pmatrix}_{\mathbf{3'}}\,, \\
&(\mathbf{A})_{\mathbf{3}}\otimes(\mathbf{B})_{\mathbf{3'}} \\
&\qquad = (\mathbf{A}\cdot\mathbf{B})_{\mathbf{1'}}\oplus\begin{pmatrix}\mathbf{A}\cdot\Sigma\cdot\mathbf{B}\\ -\mathbf{A}\cdot\Sigma^{*}\cdot\mathbf{B}\end{pmatrix}_{\mathbf{2}}\oplus\begin{pmatrix}\{A_yB_z\}\\ \{A_zB_x\}\\ \{A_xB_y\}\end{pmatrix}_{\mathbf{3'}}\oplus\begin{pmatrix}[A_yB_z]\\ [A_zB_x]\\ [A_xB_y]\end{pmatrix}_{\mathbf{3}}\,,
\end{aligned} \tag{B.2}$$

$$(\mathbf{A})_{\mathbf{2}}\otimes(\mathbf{B})_{\mathbf{2}} = \{A_xB_y\}_{\mathbf{1}}\oplus[A_xB_y]_{\mathbf{1'}}\oplus\begin{pmatrix}A_yB_y\\ A_xB_x\end{pmatrix}_{\mathbf{2}}\,, \tag{B.3}$$

$$
\begin{aligned}
&\begin{pmatrix} A_x \\ A_y \end{pmatrix}_{\mathbf{2}} \otimes \begin{pmatrix} B_x \\ B_y \\ B_z \end{pmatrix}_{\mathbf{3}} \\
&\qquad = \begin{pmatrix} (A_x + A_y)B_x \\ (\omega^2 A_x + \omega A_y)B_y \\ (\omega A_x + \omega^2 A_y)B_z \end{pmatrix}_{\mathbf{3}} \oplus \begin{pmatrix} (A_x - A_y)B_x \\ (\omega^2 A_x - \omega A_y)B_y \\ (\omega A_x - \omega^2 A_y)B_z \end{pmatrix}_{\mathbf{3'}}, \\
&\begin{pmatrix} A_x \\ A_y \end{pmatrix}_{\mathbf{2}} \otimes \begin{pmatrix} B_x \\ B_y \\ B_z \end{pmatrix}_{\mathbf{3'}} \\
&\qquad = \begin{pmatrix} (A_x + A_y)B_x \\ (\omega^2 A_x + \omega A_y)B_y \\ (\omega A_x + \omega^2 A_y)B_z \end{pmatrix}_{\mathbf{3'}} \oplus \begin{pmatrix} (A_x - A_y)B_x \\ (\omega^2 A_x - \omega A_y)B_y \\ (\omega A_x - \omega^2 A_y)B_z \end{pmatrix}_{\mathbf{3}},
\end{aligned}
\tag{B.4}
$$

with

$$
\begin{aligned}
\mathbf{A}\cdot\mathbf{B} &= A_x B_x + A_y B_y + A_z B_z, \\
\{A_x B_y\} &= A_x B_y + A_y B_x, \\
[A_x B_y] &= A_x B_y - A_y B_x, \\
\mathbf{A}\cdot\boldsymbol{\Sigma}\cdot\mathbf{B} &= A_x B_x + \omega A_y B_y + \omega^2 A_z B_z, \\
\mathbf{A}\cdot\boldsymbol{\Sigma}^*\cdot\mathbf{B} &= A_x B_x + \omega^2 A_y B_y + \omega A_z B_z,
\end{aligned}
\tag{B.5}
$$

where $\omega = e^{2\pi i/3}$ is a complex square root of unity.

B.2 MULTIPLICATION RULES OF A_4

The A_4 multiplication rules are

$$
\begin{gathered}
\mathbf{3}\otimes\mathbf{3} = \mathbf{3}_s \oplus \mathbf{3}_a \oplus \mathbf{1} \oplus \mathbf{1'} \oplus \mathbf{1''}, \\
\mathbf{1}\otimes\mathbf{1} = \mathbf{1}, \quad \mathbf{1'}\otimes\mathbf{1''} = \mathbf{1}, \quad \mathbf{1'}\otimes\mathbf{1'} = \mathbf{1''}, \quad \mathbf{1''}\otimes\mathbf{1''} = \mathbf{1'},
\end{gathered}
\tag{B.6}
$$

where $\mathbf{3}_s$ and $\mathbf{3}_a$ define the symmetric and antisymmetric triplet combinations, respectively. In terms of the two basis vectors (x_1, y_1, z_1) and (x_2, y_2, z_2), the A_4 triplet products read:

$$
\begin{aligned}
(\mathbf{3}\otimes\mathbf{3})_{\mathbf{1}} &= x_1 y_1 + x_2 y_2 + x_3 y_3, \\
(\mathbf{3}\otimes\mathbf{3})_{\mathbf{1'}} &= x_1 y_1 + \omega x_2 y_2 + \omega^2 x_3 y_3, \\
(\mathbf{3}\otimes\mathbf{3})_{\mathbf{1''}} &= x_1 y_1 + \omega^2 x_2 y_2 + \omega x_3 y_3, \\
(\mathbf{3}\otimes\mathbf{3})_{\mathbf{3}_s} &= (x_2 y_3 + x_3 y_2, x_3 y_1 + x_1 y_3, x_1 y_2 + x_2 y_1), \\
(\mathbf{3}\otimes\mathbf{3})_{\mathbf{3}_a} &= (x_2 y_3 - x_3 y_2, x_3 y_1 - x_1 y_3, x_1 y_2 - x_2 y_1),
\end{aligned}
\tag{B.7}
$$

with $\omega = e^{i\frac{2\pi}{3}}$.

C

MODEL DETAILS

C.1 PHENOMENOLOGY OF THE S_3 FLAVOR MODEL

This appendix contains the detailed computations of the neutrino masses and the PMNS mixing matrix (C.1.1). We also give the loop expressions used in the analysis of the scalar sector, including the rare top decays induced by the exotic scalars (C.1.2) and the T and S parameters (C.1.3). App. C.1.4 deals with the minimization of the scalar potential and the VEV alignment.

C.1.1 *Neutrino Sector*

In this model, the light neutrino mass eigenstates are obtained from a 5×5 dimensional neutrino mass matrix that follows from Eq. (3.10). In the seesaw mechanism type I the light neutrino mass scale is a consequence of the suppression by the heavy Majorana masses, so that

$$\begin{aligned} M_{\nu_L} &= M_\nu^D M_R^{-1} \left(M_\nu^D\right)^T \\ &= \begin{pmatrix} A & F \\ B & E \\ C & D \end{pmatrix} \begin{pmatrix} -\frac{4M_2}{M_{12}^2-4M_1M_2} & \frac{2M_{12}}{M_{12}^2-4M_1M_2} \\ \frac{2M_{12}}{M_{12}^2-4M_1M_2} & -\frac{4M_1}{M_{12}^2-4M_1M_2} \end{pmatrix} \begin{pmatrix} A & B & C \\ F & E & D \end{pmatrix} \\ &\equiv \begin{pmatrix} W^2 & WX\cos\varphi & WY\cos(\varphi-\varrho) \\ WX\cos\varphi & X^2 & XY\cos\varrho \\ WY\cos(\varphi-\varrho) & XY\cos\varrho & Y^2 \end{pmatrix}, \end{aligned} \tag{C.1}$$

with

$$\begin{aligned} W^2 &= -\frac{4\left(M_2A^2-M_{12}AF+M_1F^2\right)}{M_{12}^2-4M_1M_2}, & WX &= \frac{2(BFM_{12}-2ABM_2-2FEM_1+AEM_{12})}{(M_{12}^2-4M_1M_2)\cos\varphi}, \\ X^2 &= -\frac{4\left(M_2B^2-M_{12}BE+M_1E^2\right)}{M_{12}^2-4M_1M_2}, & XY &= \frac{2(BDM_{12}-2BCM_2+CEM_{12}-2DEM_1)}{(M_{12}^2-4M_1M_2)\cos\varphi}, \\ Y^2 &= \frac{4\left(M_2C^2-M_{12}CD+M_1D^2\right)}{M_{12}^2-4M_1M_2}, & WY &= \frac{2(CFM_{12}-2ACM_2-2FDM_1+ADM_{12})}{(M_{12}^2-4M_1M_2)\cos(\varphi-\varrho)}, \end{aligned}$$

and

$$\begin{pmatrix} A & F \\ B & E \\ C & D \end{pmatrix} \equiv \begin{pmatrix} \lambda^3\varepsilon_{11}^{(\nu)}\frac{v_2}{\sqrt{2}} & \lambda^3\varepsilon_{12}^{(\nu)}\frac{v_2}{\sqrt{2}} \\ \varepsilon_{21}^{(\nu)}\frac{v_1}{\sqrt{2}} & \varepsilon_{22}^{(\nu)}\frac{v_3}{\sqrt{2}} \\ \varepsilon_{31}^{(\nu)}\frac{v_1}{\sqrt{2}} & \varepsilon_{33}^{(\nu)}\frac{v_3}{\sqrt{2}} \end{pmatrix}. \tag{C.2}$$

For simplicity we set $\varphi = \varrho$ and $\kappa \equiv \cos\phi$, resulting in

$$M_{\nu_L} = \begin{pmatrix} W^2 & \kappa WX & WY \\ \kappa WX & X^2 & \kappa XY \\ WY & \kappa XY & Y^2 \end{pmatrix} . \tag{C.3}$$

A matrix with this structure can be diagonalized with a rotation matrix V_ν, which for NH is given by

$$V_\nu^{\text{NH}} = \begin{pmatrix} -\frac{Y}{\sqrt{W^2+Y^2}} & \frac{W}{\sqrt{W^2+Y^2}}\sin\theta_\nu & \frac{W}{\sqrt{W^2+Y^2}}\cos\theta_\nu \\ 0 & \cos\theta_\nu & -\sin\theta_\nu \\ \frac{W}{\sqrt{W^2+Y^2}} & \frac{Y}{\sqrt{W^2+Y^2}}\sin\theta_\nu & \frac{Y}{\sqrt{W^2+Y^2}}\cos\theta_\nu \end{pmatrix} , \quad \text{with} \quad \tan\theta_\nu = -\sqrt{\frac{m_3 - X^2}{X^2 - m_2}} , \tag{C.4}$$

while for IH it is

$$V_\nu^{\text{IH}} = \begin{pmatrix} \frac{W}{\sqrt{W^2+Y^2}} & -\frac{Y}{\sqrt{W^2+Y^2}}\sin\theta_\nu & -\frac{Y}{\sqrt{W^2+Y^2}}\cos\theta_\nu \\ 0 & \cos\theta_\nu & -\sin\theta_\nu \\ \frac{Y}{\sqrt{W^2+Y^2}} & \frac{W}{\sqrt{W^2+Y^2}}\sin\theta_\nu & \frac{W}{\sqrt{W^2+Y^2}}\cos\theta_\nu \end{pmatrix} , \quad \text{with} \quad \tan\theta_\nu = -\sqrt{\frac{m_2 - X^2}{X^2 - m_1}} . \tag{C.5}$$

Finally, the corresponding two nonvanishing neutrino masses in these cases are

$$m_{\nu_\mp} = \frac{1}{2}\left(W^2 + X^2 + Y^2 \mp \sqrt{\left(W^2 - X^2 + Y^2\right)^2 - 4\kappa^2 X^2 \left(W^2 + Y^2\right)} \right) . \tag{C.6}$$

The smallness of the active neutrinos masses is a consequence of their scaling with the inverse of the large Majorana neutrino masses, as expected from the type I seesaw mechanism.

The PMNS matrix now follows directly from $V_{\text{PMNS}} = V_l^\dagger V_\nu$ using Eq. (3.20), and Eqs. (C.4) and (C.5) for NH and IH, respectively,

$$V_{\text{PMNS}} = \begin{cases} \begin{pmatrix} -\frac{Y}{\sqrt{W^2+Y^2}} & \frac{Ws_{\theta_\nu}}{\sqrt{W^2+Y^2}} & \frac{Wc_{\theta_\nu}}{\sqrt{W^2+Y^2}} \\ \frac{Ws_{\theta_l}}{\sqrt{W^2+Y^2}} & c_{\theta_l}c_{\theta_\nu} + \frac{Ys_{\theta_l}s_{\theta_\nu}}{\sqrt{W^2+Y^2}} & \frac{Yc_{\theta_\nu}s_{\theta_l}}{\sqrt{W^2+Y^2}} - c_{\theta_l}s_{\theta_\nu} \\ \frac{Wc_{\theta_l}}{\sqrt{W^2+Y^2}} & \frac{Yc_{\theta_l}s_{\theta_\nu}}{\sqrt{W^2+Y^2}} - c_{\theta_\nu}s_{\theta_l} & s_{\theta_l}s_{\theta_\nu} + \frac{Yc_{\theta_l}c_{\theta_\nu}}{\sqrt{W^2+Y^2}} \end{pmatrix} & \text{(NH)} \\ \begin{pmatrix} \frac{W}{\sqrt{W^2+Y^2}} & -\frac{Ys_{\theta_\nu}}{\sqrt{W^2+Y^2}} & -\frac{Yc_{\theta_\nu}}{\sqrt{W^2+Y^2}} \\ \frac{Ys_{\theta_l}}{\sqrt{W^2+Y^2}} & c_{\theta_l}c_{\theta_\nu} + \frac{Ws_{\theta_\nu}s_{\theta_l}}{\sqrt{W^2+Y^2}} & \frac{Ws_{\theta_l}c_{\theta_\nu}}{\sqrt{X^2+Y^2}} - c_{\theta_l}s_{\theta_\nu} \\ \frac{Yc_{\theta_l}}{\sqrt{W^2+Y^2}} & \frac{Ws_{\theta_\nu}c_{\theta_l}}{\sqrt{W^2+Y^2}} - c_{\theta_\nu}s_{\theta_l} & s_{\theta_l}s_{\theta_\nu} + \frac{Wc_{\theta_l}c_{\theta_\nu}}{\sqrt{W^2+Y^2}} \end{pmatrix} & \text{(IH)} \end{cases} . \tag{C.7}$$

By comparing with the standard parametrization we can derive the mixing angles for NH and IH, shown in Eqs. (3.26) and (3.27).

C.1.2 *Loop-Induced Top Quark Decays*

The loop-induced top quark decays studied in Sec. 3.1.3 were calculated using the loop factors provided in Ref. [163]. For completeness, the analytic expressions for the decay rates are summarized in this appendix.

The radiative decays $t \to cV(V = \gamma, Z, g)$ can be expressed in terms of the form factors $A^{(V)}, B^{(V)}, C^{(V)}, D^{(V)}$. Each form factor $F = A, B, C, D$ in turn contains a sum of five different contributions

$$F^{(V)} = F_h^{(V)} + F_H^{(V)} + F_A^{(V)} + F_C^{(V)} + F_M^{(V)}\,, \tag{C.8}$$

where the lower index denotes the contributing scalar (C for "charged" and M for "mixed" h-A contributions), and the upper index corresponds to the outgoing gauge boson.

In this notation the decay rates are given by

$$\Gamma(t \to c\gamma) = \frac{1}{(16\pi^2)^2}\frac{1}{8\pi}\left(|C^\gamma|^2 + |D^\gamma|^2\right)\,, \tag{C.9}$$

$$\begin{aligned}\Gamma(t \to cZ) = \frac{1}{(16\pi^2)^2}\frac{1}{16\pi m_t}&\left(1 - \frac{M_Z^2}{m_t^2}\right)\left(\frac{m_t^2}{M_Z^2} - 1\right)\\ &\times\Big[(m_t^2 + 2M_Z^2)\left(|A^Z|^2 + |B^Z|^2\right) - 6M_Z^2(A^{Z*}C^Z - B^{Z*}D^Z)\\ &\quad + M_Z^2\left(\frac{M_Z^2}{m_t^2} + 2\right)\left(|C^Z|^2 + |D^Z|^2\right)\Big]\,,\end{aligned} \tag{C.10}$$

$$\Gamma(t \to cg) = \frac{1}{(16\pi^2)^2}\frac{1}{8\pi}\frac{N^2-1}{2N}\left(|C^g|^2 + |D^g|^2\right)\,. \tag{C.11}$$

The reader is referred to Ref. [163] for the complete expressions of each form factor $F^{(V)}$.

C.1.3 *Loop Expressions for the T and S Parameters*

This section deals with the technical details of the T and S parameter analysis. To emphasize the contributions arising from new physics, the T and S are split into $T \equiv T_{\rm SM} + \Delta T$ and $S \equiv S_{\rm SM} + \Delta S$, where $T_{\rm SM}$ and $S_{\rm SM}$ are the SM contributions given by

$$T_{SM} = -\frac{3}{16\pi\cos^2\theta_W}\ln\left(\frac{m_h^2}{m_W^2}\right)\,, \tag{C.12}$$

$$S_{SM} = \frac{1}{12\pi}\ln\left(\frac{m_h^2}{m_W^2}\right)\,, \tag{C.13}$$

while ΔT and ΔS contain all the contributions involving the exotic heavy scalars

$$\begin{aligned}\Delta T \simeq & -\frac{3\cos^2(\alpha-\beta)}{16\pi\cos^2\theta_W}\ln\left(\frac{m_{H^0}^2}{m_h^2}\right) \\ & + \frac{1}{16\pi^2 v^2 \alpha_{\rm EM}(M_Z)}\left[m_{H^\pm}^2 - F\left(m_{A^0}^2, m_{H^\pm}^2\right)\right] \\ & + \frac{\sin^2(\alpha-\beta)}{16\pi^2 v^2 \alpha_{\rm EM}(M_Z)}\left[F\left(m_h^2, m_{A^0}^2\right) - F\left(m_h^2, m_{H^\pm}^2\right)\right] \\ & + \frac{\cos^2(\alpha-\beta)}{16\pi^2 v^2 \alpha_{\rm EM}(M_Z)}\left[F\left(m_{H^0}^2, m_{A^0}^2\right) - F\left(m_{H^0}^2, m_{H^\pm}^2\right)\right],\end{aligned} \tag{C.14}$$

$$\begin{aligned}\Delta S \simeq \frac{1}{12\pi}\Bigg[&\cos^2(\alpha-\beta)\ln\left(\frac{m_{H^0}^2}{m_h^2}\right) + \sin^2(\alpha-\beta)\,K\left(m_h^2, m_{A^0}^2, m_{H^\pm}^2\right) \\ &+ \cos^2(\alpha-\beta)\,K\left(m_{H^0}^2, m_{A^0}^2, m_{H^\pm}^2\right)\Bigg],\end{aligned} \tag{C.15}$$

with the functions [250]

$$F\left(m_1^2, m_2^2\right) = \frac{m_1^2 m_2^2}{m_1^2 - m_2^2}\ln\left(\frac{m_1^2}{m_2^2}\right), \qquad \lim_{m_2\to m_1} F\left(m_1^2, m_2^2\right) = m_1^2, \tag{C.16}$$

$$\begin{aligned}K\left(m_1^2, m_2^2, m_3^2\right) = \frac{1}{\left(m_2^2 - m_1^2\right)^3}\Bigg\{& m_1^4\left(3m_2^2 - m_1^2\right)\ln\left(\frac{m_1^2}{m_3^2}\right) \\ & - m_2^4\left(3m_1^2 - m_2^2\right)\ln\left(\frac{m_2^2}{m_3^2}\right) \\ & - \frac{1}{6}\left[27m_1^2 m_2^2\left(m_1^2 - m_2^2\right) + 5\left(m_2^6 - m_1^6\right)\right]\Bigg\},\end{aligned} \tag{C.17}$$

and the properties

$$\begin{aligned}\lim_{m_1\to m_2} K(m_1^2, m_2^2, m_3^2) &= K_1(m_2^2, m_3^2), \\ \lim_{m_2\to m_3} K(m_1^2, m_2^2, m_3^2) &= K_2(m_1^2, m_3^2), \\ \lim_{m_1\to m_3} K(m_1^2, m_2^2, m_3^2) &= K_2(m_2^2, m_3^2),\end{aligned} \tag{C.18}$$

where

$$\begin{aligned}K_1(m_2^2, m_3^2) &= \ln\left(\frac{m_2^2}{m_3^2}\right), \\ K_2(m_1^2, m_3^2) &= \frac{1}{6\left(m_1^2 - m_3^2\right)^3}\Big(-5m_1^6 + 27m_1^4 m_3^2 - 27m_1^2 m_3^4 \\ &\qquad + 6\left(m_1^6 - 3m_1^4 m_3^2\right)\ln\left(\frac{m_1^2}{m_3^2}\right) + 5m_3^6\Big).\end{aligned} \tag{C.19}$$

The corresponding Feynman diagrams contributing to ΔT and ΔS are shown in Figs. C.1 and C.2, respectively.

C.1.4 *Decoupling and S_3 VEVs*

The full symmetry is broken in two subsequent steps taking place at different energy scales. The respective $SU(2)$ singlet scalars inducing the breaking of the flavor symmetry

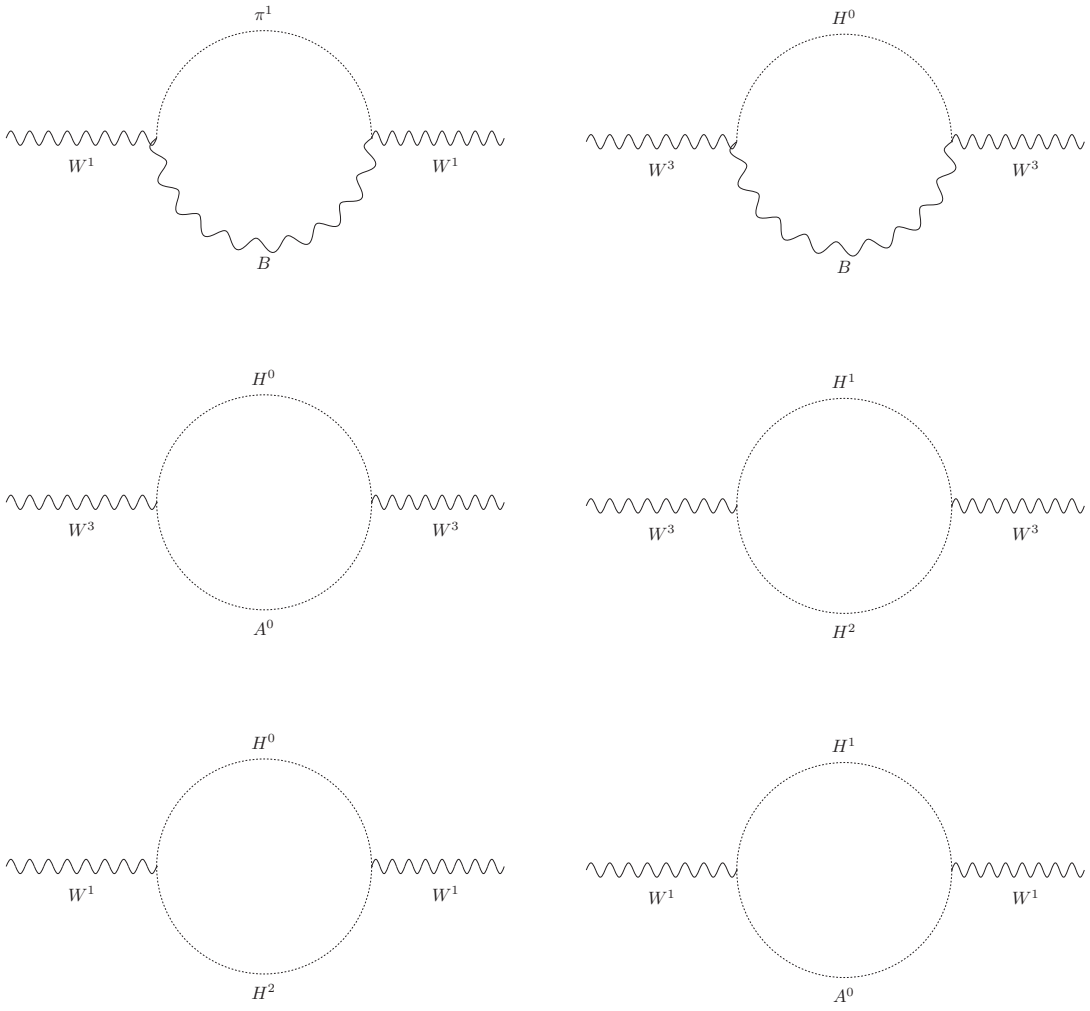

Figure C.1: One-loop Feynman diagrams contributing to the T parameter. The fields H^1 and H^2 are linear combinations of the charged Higgses $H^\pm$, similarly to how the $W^\pm$ gauge bosons are defined in terms of W^1 and W^2. Likewise, the fields π^1 and π^2 are linear combinations of the charged Goldstone bosons $\pi^\pm$.

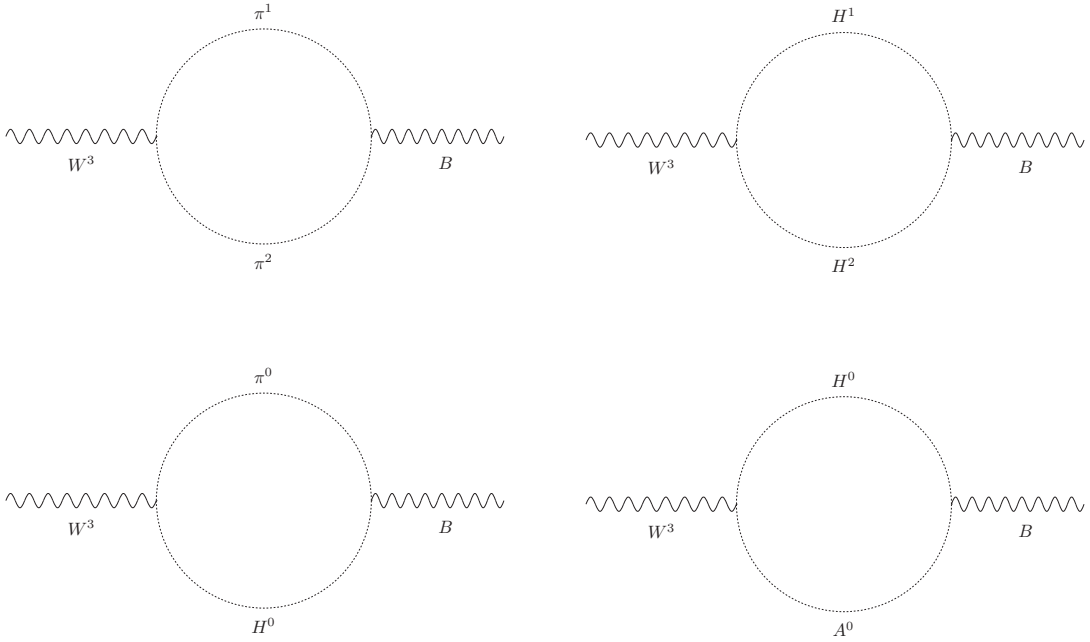

Figure C.2: One-loop Feynman diagrams contributing to the S parameter. The fields H^1 and H^2 are linear combinations of the charged Higgses $H^\pm$.

are assumed to acquire VEVs much larger than the EW breaking scale. According to the method of recursive expansion [251], the mixing between the scalar $SU(2)$ singlets and doublets is of the order of $\frac{v_{1,2}}{\lambda\Lambda}$ with $v_{1,2} \sim \mathcal{O}(100\text{ GeV})$ and $\Lambda \gg \Lambda_{\text{EW}}$. Since the mixing is strongly suppressed by the new breaking scale Λ, the singlet scalars effectively decouple from the Higgs doublets and are therefore negligible in the analysis of the low-energy scalar potential. We also checked numerically that the masses of the $SU(2)$ doublet scalars are nearly unaffected by SM singlet VEVs of $\mathcal{O}(500\,\text{GeV})$ and higher. For simplicity we assume a CP invariant scalar potential with only real couplings. In the regime where the VEVs decouple, the relevant terms for determining the direction of the ξ VEV in the S_3-space are

$$V(\xi) = -\mu_\xi^2(\xi\xi)_1 + \gamma_{\xi,3}(\xi\xi)_2\xi + \kappa_{\xi,1}(\xi\xi)_1(\xi\xi)_1 + \kappa_{\xi,2}(\xi\xi)_2(\xi\xi)_2 + \kappa_{\xi,3}\left[(\xi\xi)_{\mathbf{2}}\,\xi\right]_{\mathbf{2}}\xi, \tag{C.20}$$

From the minimization conditions of the high-energy scalar potential, we find the following relations:

$$\begin{aligned}
\frac{\partial\langle V\rangle}{\partial v_{\xi_1}} &= 2v_{\xi_1}\left[\mu_\xi^2 + 2\left(\kappa_{\xi,1}+\kappa_{\xi,2}+\kappa_{\xi,3}\right)\left(v_{\xi_1}^2+v_{\xi_2}^2\right)\right] + 3\gamma_{\xi,3}\left(v_{\xi_2}^2 - v_{\xi_1}^2\right) = 0\,,\\
\frac{\partial\langle V\rangle}{\partial v_{\xi_2}} &= 2v_{\xi_2}\left\{\left[\mu_\xi^2 + 2\left(\kappa_{\xi,1}+\kappa_{\xi,2}+\kappa_{\xi,3}\right)\left(v_{\xi_1}^2+v_{\xi_2}^2\right)\right] + 3\gamma_{\xi,3}v_{\xi_1}\right\} = 0\,.
\end{aligned} \tag{C.21}$$

The analysis of the minimization equations yields for a large range of the parameter space the following VEV direction for ξ:

$$\langle \xi \rangle = v_\xi \, (1, 0) \ . \tag{C.22}$$

Inserting the vacuum configuration (C.22) into Eq. (C.21), we find the relation between the parameters and the magnitude of the VEV

$$\mu_\xi^2 = -\frac{v_\xi}{2} \left[2 \left(\kappa_{\xi,1} + \kappa_{\xi,2} + \kappa_{\xi,3} \right) v_\xi - 3\gamma_{\xi,3} \right] \ , \tag{C.23}$$

which can be fulfilled in a large region of the parameter space. These results shows that the VEV direction for the S_3 doublet ξ in Eq. (3.3) is consistent with a global minimum of the scalar potential of our model.

C.2 FERMION MASSES AND MIXINGS IN $SU(5)$

This appendix deals with the details of the $SU(5)$ GUT model presented in Sec. 3.2, starting with the complete expressions for the fermion Yukawa interactions (App. C.2.1), followed by discussions of the scalar sector (App. C.2.2), and the CKM mixing (App. C.2.3).

C.2.1 *Yukawa Lagrangian*

The particle content and symmetry assignments listed in Tab. 3.7 lead to the following Yukawa interactions:

$$
\begin{aligned}
\mathcal{L}^{\nu}_{\text{Yuk}} &= \lambda_\nu \left(\psi^i S_i\right)_{\mathbf{1}} N_R + M_N \overline{N}_R N_R^c + \text{h.c.}\,, \\
\mathcal{L}^{d,l}_{\text{Yuk}} &= \frac{\alpha_1}{\Lambda}\left(\frac{\Sigma_l^k \Sigma_k^l}{\Lambda^2}\right)^{a_{\mathbf{1}}} \left(\psi^i \xi\right)_{\mathbf{1}} H^{j(1)} \Psi^{(1)}_{ij} + \frac{\alpha_2}{\Lambda}\left(\frac{\Sigma_l^k \Sigma_k^l}{\Lambda^2}\right)^{a_{\mathbf{2}}} \left(\psi^i \xi\right)_{\mathbf{1''}} H^{j(1)} \Psi^{(2)}_{ij} \\
&\quad + \frac{\alpha_3}{\Lambda}\left(\frac{\Sigma_l^k \Sigma_k^l}{\Lambda^2}\right)^{a_{\mathbf{3}}} \left(\psi^i \xi\right)_{\mathbf{1'}} H^{j(1)} \Psi^{(3)}_{ij} + \frac{\beta_1}{\Lambda}\left(\frac{\Sigma_l^k \Sigma_k^l}{\Lambda^2}\right)^{b_{\mathbf{1}}} \left(\psi^i \xi\right)_{\mathbf{1}} \Phi_i^{jk} \Psi^{(1)}_{jk} \\
&\quad + \frac{\beta_2}{\Lambda}\left(\frac{\Sigma_l^k \Sigma_k^l}{\Lambda^2}\right)^{b_2} \left(\psi^i \xi\right)_{\mathbf{1''}} \Phi_i^{jk} \Psi^{(2)}_{jk} + \frac{\beta_3}{\Lambda}\left(\frac{\Sigma_l^k \Sigma_k^l}{\Lambda^2}\right)^{b_3} \left(\psi^i \xi\right)_{\mathbf{1'}} \Phi_i^{jk} \Psi^{(3)}_{jk}\,, \\
\mathcal{L}^{u}_{\text{Yuk}} &= \varepsilon^{ijklp} \left\{ \gamma_{12}\left(\frac{\Sigma_n^m \Sigma_m^n}{\Lambda^2}\right)^{x_{12}} \Psi^{(1)}_{ij} H^{(3)}_p \Psi^{(2)}_{kl} \right. \\
&\quad + \gamma_{22}\left(\frac{\Sigma_n^m \Sigma_m^n}{\Lambda^2}\right)^{x_{22}} \Psi^{(2)}_{ij} H^{(2)}_p \Psi^{(2)}_{kl} + \gamma_{11}\left(\frac{\Sigma_n^m \Sigma_m^n}{\Lambda^2}\right)^{x_{11}} \Psi^{(1)}_{ij} H^{(4)}_p \Psi^{(1)}_{kl} \\
&\quad + \gamma_{23}\left(\frac{\Sigma_n^m \Sigma_m^n}{\Lambda^2}\right)^{x_{23}} \Psi^{(2)}_{ij} H^{(4)}_p \Psi^{(3)}_{kl} + \gamma_{32}\left(\frac{\Sigma_n^m \Sigma_m^n}{\Lambda^2}\right)^{x_{32}} \Psi^{(3)}_{ij} H^{(4)}_p \Psi^{(2)}_{kl} \\
&\quad + \gamma_{13}\left(\frac{\Sigma_n^m \Sigma_m^n}{\Lambda^2}\right)^{x_{13}} \Psi^{(1)}_{ij} H^{(2)}_p \Psi^{(3)}_{kl} + \gamma_{31}\left(\frac{\Sigma_n^m \Sigma_m^n}{\Lambda^2}\right)^{x_{31}} \Psi^{(3)}_{ij} H^{(2)}_p \Psi^{(1)}_{kl} \\
&\quad \left. + \gamma_{33}\left(\frac{\Sigma_n^m \Sigma_m^n}{\Lambda^2}\right)^{x_{33}} \Psi^{(3)}_{ij} H^{(3)}_p \Psi^{(3)}_{kl} + \gamma_{21}\left(\frac{\Sigma_n^m \Sigma_m^n}{\Lambda^2}\right)^{x_{21}} \Psi^{(2)}_{ij} H^{(3)}_p \Psi^{(1)}_{kl} \right\}\,,
\end{aligned}
\tag{C.24}
$$

where $\mathcal{L}^{\nu}_{\text{Yuk}}$, $\mathcal{L}^{d,l}_{\text{Yuk}}$, and $\mathcal{L}^{u}_{\text{Yuk}}$ correspond to the neutrino, down-type, and up-type quark Yukawa terms, respectively. Since the down-type quarks and charged leptons are in the same $SU(5)$ multiplets, the $\mathcal{L}^{d,l}_{\text{Yuk}}$ Lagrangian also generates the charged lepton masses. The projection of the triplets on the corresponding singlet is denoted by the subscripts $\mathbf{1}, \mathbf{1'}, \mathbf{1''}$. The dimensionless couplings α_i, β_i and γ_{ij} $(i,j = 1,2,3)$ are $\mathcal{O}(1)$ parameters. And finally, the Froggatt-Nielsen charges fulfill the following relations:

$$
\begin{aligned}
a_i &= Q_i^{\Psi} + Q^{\psi} + Q_1^H + Q^{\xi}\,, & b_i &= Q_i^{\Psi} + Q^{\psi} + Q^{\Phi} + Q^{\xi}\,, \\
x_{12} &= x_{21} = Q_1^{\Psi} + Q_2^{\Psi} + Q_{\mathbf{5}}^{(3)}\,, & x_{33} &= Q_3^{\Psi} + Q_3^{\Psi} + Q_{\mathbf{5}}^{(3)}\,, \\
x_{13} &= x_{31} = Q_1^{\Psi} + Q_3^{\Psi} + Q_{\mathbf{5}}^{(2)}\,, & x_{22} &= Q_2^{\Psi} + Q_2^{\Psi} + Q_{\mathbf{5}}^{(2)}\,, \\
x_{23} &= x_{32} = Q_2^{\Psi} + Q_3^{\Psi} + Q_{\mathbf{5}}^{(4)}\,, & x_{11} &= Q_1^{\Psi} + Q_1^{\Psi} + Q_{\mathbf{5}}^{(4)}\,.
\end{aligned}
\tag{C.25}
$$

Since the scalar S participates only in neutrino interactions, we choose for its FN charge

$$
Q^S = -Q^{\psi} \tag{C.26}
$$

to cancel the lepton charge separating the neutrino masses from the FN mechanism. To relate the quark masses with the quark mixing parameters, we set:

$$
\kappa = \frac{\Sigma_l^k \Sigma_k^l}{\Lambda^2} = \frac{15 v_\Sigma^2}{2\Lambda^2} = \frac{\Lambda_{GUT}}{\Lambda} = \lambda\,. \tag{C.27}
$$

where $\lambda = 0.225$ corresponds to Wolfenstein parameter of the CKM matrix.

C.2.2 *Scalar Sector*

We consider the following VEV patterns of the scalars fields in the model. The VEV alignment known to break $SU(5)$ down to the SM group is [252]

$$\left\langle \Sigma^i_j \right\rangle = v_\Sigma \,\mathrm{diag}\left(1,1,1,-\frac{3}{2},-\frac{3}{2}\right), \qquad i,j=1,2,3,4,5. \tag{C.28}$$

The fields $H^{(h)}$ $(h=1,2,3,4)$ and Φ then induce the EW symmetry breaking by acquiring the VEVs [127, 253]

$$\begin{array}{rclrcl} \left\langle H^{(h)}_i \right\rangle &=& v^{(h)}_H \delta_{i5}\,, & & & \\ \left\langle \Phi^p_{p5} \right\rangle &=& v_\Phi = -\frac{1}{3}\left\langle \Phi^4_{45} \right\rangle\,, & p &=& 1,2,3,5, \\ \left\langle \Phi^i_{j5} \right\rangle &=& v_\Phi \left(\delta^i_j - 4\delta^i_4\delta^4_j\right)\,, & i,j &=& 1,2,3,4,5\,. \end{array} \tag{C.29}$$

Since the Z_2 symmetry is unbroken, the VEV of the A_4 triplet S must vanish

$$v^i_S = 0, \qquad i=1,2,3. \tag{C.30}$$

The A_4 potential is minimized by the following alignments of χ and ξ:

$$\langle \chi \rangle = \frac{v_\chi}{\sqrt{2}}(-1,0,1)\,, \qquad \langle \xi \rangle = \frac{v_\xi}{\sqrt{3}}(1,1,1)\,. \tag{C.31}$$

Note that the flavons are aligned in different directions of the group space to generate the mismatch between the neutrino and the charged lepton mixings, required by the large PMNS mixing angles. The vacuum $\langle \xi \rangle$ preserves a Z_3 subgroup of A_4, which has been extensively studied by many authors (see, e.g., Refs. [90, 254, 255] or Sec. 4.1 for a detailed study of the Z_3 subgroup).
Finally, to induce the breaking shown in Eq. (3.61), the VEVs of the scalars fulfill the hierarchy

$$\Lambda_{\mathrm{EW}} \sim v_H, v_\Phi \ll v_\chi \ll v_\xi, v_\sigma \sim \Lambda_{\mathrm{GUT}}\,. \tag{C.32}$$

Because of the many uncorrelated parameters, the scalar potential can be adjusted to yield the required pattern of scalar masses evading experimental searches. Therefore, also the loop effects of the heavy scalars to certain observables can be suppressed by an appropriate choice of parameters. Fortunately, all these adjustments do not affect the charged fermion and neutrino sector, which is completely controlled by the fermion-Higgs Yukawa couplings and the combinations of $U(1)_f$ FN charges. Since the model is not predictive in the scalar sector, the full expression for the scalar potential is omitted from this section. A complete study of the scalar sector, also with respect to possible dark matter candidates, is reserved for a future publication.

C.2.3 *CKM matrix*

As demonstrated in Sec. 3.2.2, the CKM matrix is solely determined by the up-quark sector. It can be shown that

$$M_U = m_t \begin{pmatrix} y\lambda^{10} & f\lambda^9 e^{i\tau\sigma} & b\lambda^3 \\ f\lambda^9 e^{i\tau\sigma} & a\lambda^4 e^{i\sigma(1+\tau)} & c\lambda^2 e^{i\sigma} \\ b\lambda^3 & c\lambda^2 e^{i\sigma} & d e^{i\sigma} \end{pmatrix} \tag{C.33}$$

is an appropriate structure to reproduce the CKM elements as well as J and the CP phase δ, where y, a, b, c, d and f are $\mathcal{O}(1)$ parameters. This structure can be obtained by setting the FN charges to

$$\begin{array}{lllllllll} x_{11} & = & 10\,, & x_{12} & = & 9\,, & x_{13} & = & 3\,, \\ x_{23} & = & 2\,, & x_{22} & = & 4\,, & x_{33} & = & 0\,, \end{array} \tag{C.34}$$

and assuming

$$v_H^{(2)} \sim v_H^{(3)} \sim v_H^{(4)} \sim \frac{v}{\sqrt{2}}\,, \quad |\gamma_{ij}| \sim \frac{1}{4}\,, \quad i,j = 1,2,3. \tag{C.35}$$

Consequently, we obtain

$$\begin{aligned} \frac{1}{m_t^2} M_U M_U^\dagger = & \begin{pmatrix} b^2\lambda^6 & bc\lambda^5 e^{-i\sigma} & bd\lambda^3 e^{-i\sigma} \\ bc\lambda^5 e^{i\sigma} & c^2\lambda^4 & cd\lambda^2 \\ bd\lambda^3 e^{i\sigma} & cd\lambda^2 & d^2 \end{pmatrix} \\ & + \begin{pmatrix} \lambda^{18}\left(f^2 + y^2\lambda^2\right) & f\lambda^{13}\left(e^{-i\sigma\tau} y\lambda^6 + a e^{-i\sigma}\right) & \lambda^{11}\left(by\lambda^2 + ce^{i\sigma(\tau-1)} f\right) \\ f\lambda^{13}\left(e^{i\sigma\tau} y\lambda^6 + a e^{i\sigma}\right) & \lambda^8\left(f^2\lambda^{10} + a^2\right) & e^{i\sigma\tau}\lambda^6\left(bf\lambda^6 + ac\right) \\ by\lambda^{13} + ce^{-i\sigma(\tau-1)} f\lambda^{11} & e^{-i\sigma\tau}\lambda^6\left(bf\lambda^6 + ac\right) & \lambda^4\left(c^2 + b^2\lambda^2\right) \end{pmatrix}, \end{aligned} \tag{C.36}$$

where the first term is the leading order contribution to $M_U M_U^\dagger$, while the second one is crucial to generate the up and charm quark masses.
Since $V_{\rm CKM}$ is determined only by V_U, another expression can be used to relate Eq. (C.36) directly to the CKM matrix

$$\begin{aligned} M_U M_U^\dagger &= V_{\rm CKM}^\dagger {\rm diag}\left(m_u^2, m_c^2, m_t^2\right) V_{\rm CKM} \\ &\simeq m_t^2 \begin{pmatrix} |V_{td}|^2 & V_{td}^\dagger V_{ts} & V_{td}^\dagger V_{tb} \\ V_{ts}^\dagger V_{td} & |V_{ts}|^2 & V_{ts}^\dagger V_{tb} \\ V_{tb}^\dagger V_{td} & V_{tb}^\dagger V_{ts} & |V_{tb}|^2 \end{pmatrix}, \end{aligned} \tag{C.37}$$

where $V_{tq} (q = d, s, b)$ denote the respective elements of the CKM matrix.
By using the Wolfenstein parameterization of the CKM matrix [86]

$$V_{\rm CKM} \simeq \begin{pmatrix} 1 - \frac{\lambda^2}{2} & \lambda & W\lambda^3(\rho - i\eta) \\ -\lambda & 1 - \frac{\lambda^2}{2} & W\lambda^2 \\ W\lambda^3(1 - \rho - i\eta) & -W\lambda^2 & 1 \end{pmatrix}, \tag{C.38}$$

with

$$\begin{array}{lllllllll} \lambda & = & 0.22535 \pm 0.00065\,, & & W & = & 0.811^{+0.022}_{-0.012}\,, \\ \overline{\rho} & = & 0.131^{+0.026}_{-0.013}\,, & & \overline{\eta} & = & 0.345^{+0.013}_{-0.014}\,, \end{array} \tag{C.39}$$

and

$$\overline{\rho} \simeq \rho\left(1 - \frac{\lambda^2}{2}\right), \qquad \overline{\eta} \simeq \eta\left(1 - \frac{\lambda^2}{2}\right), \tag{C.40}$$

we can connect the model parameters with the experimental observables.

As a result, we obtain for

$$M_U M_U^\dagger \simeq \\ m_t^2 \begin{pmatrix} W^2\lambda^6\left[\eta^2+(\rho-1)^2\right] & W^2\lambda^5(-i\eta+\rho-1) & W\lambda^3(i\eta-\rho+1) \\ W^2\lambda^5(i\eta+\rho-1) & W^2\lambda^4 & -W\lambda^2 \\ W\lambda^3(-i\eta-\rho+1) & -W\lambda^2 & 1 \end{pmatrix}, \tag{C.41}$$

Comparing Eqs. (C.36) and (C.41), we find the following relations:

$$b \simeq W\sqrt{\eta^2+(\rho-1)^2}\,, \quad c \simeq -W\,, \quad d \simeq 1\,, \quad \sigma \simeq \arctan\left(-\frac{\eta}{1-\rho}\right). \tag{C.42}$$

Since $d \simeq 1$, the quark mixing in our model is described by the effective dimensionless parameters b, c, σ, τ and λ, where the latter is fixed by the ratio of the grand unification scale Λ_{GUT} and the cutoff Λ of our model.

We fit the remaining $\mathcal{O}(1)$ parameters in Eq. (C.33) to reproduce the up-type quark mass spectrum and quark mixing parameters. The results are shown in Tab. 3.11 for the best-fit values

$$y = 0.2 \quad f = 0.39\,, \quad a = 0.26\,, \quad \tau = 2.9\,. \tag{C.43}$$

C.3 DETAILS OF THE S_4 TRIALITY MODEL

In this appendix we discuss the technical details of the S_4 flavor model with LFT, including a comprehensive study of the quark masses and mixings (App. C.3.1), the consequences of the Z_3 breaking (App. C.3.2), and the computation of the radiative decays (App. C.3.4). A complete overview of the model content can be found in Tab. C.1.

C.3.1 *Quark Masses and Mixings*

Following from Tab. 4.4, the relevant $S_4 \otimes Z_2'' \otimes Z_6 \otimes Z_{12}$ -invariant Yukawa terms for the up-type quark sector are

$$\begin{aligned} -\mathcal{L}^{(U)} = {} & y_1^{(t)}\,[Q\phi]_{3'}\,t_R\frac{\rho}{\Lambda} + \frac{y_2^{(t)}}{\Lambda}Q\,[\phi\rho]_{3'}\,t_R + x_1^{(t)}\,[Q\phi]_3\,t_R\frac{\varphi}{\Lambda} + \frac{x_2^{(t)}}{\Lambda}Q\,[\phi\varphi]_{3'}\,t_R \\ & + y_1^{(c)}\,[Q\phi]_{3'}\,c_R\frac{\rho}{\Lambda} + \frac{y_2^{(c)}}{\Lambda}Q\,[\phi\rho]_{3'}\,c_R + x_1^{(c)}\,[Q\phi]_3\,c_R\frac{\varphi}{\Lambda} + \frac{x_2^{(c)}}{\Lambda}Q\,[\phi\varphi]_{3'}\,c_R \\ & + x_0^{(u)}\,[Q\phi]_1\,u_R\frac{\Omega_2^3}{\Lambda^3} + y_1^{(u)}\,[Q\phi]_{3'}\,u_R\frac{\rho\Omega_1^2}{\Lambda^3} + y_2^{(u)}Q\,[\phi\rho]_{3'}\,u_R\frac{\Omega_1^2}{\Lambda^3} \\ & + x_1^{(u)}\,[Q\phi]_{3'}\,u_R\frac{\varphi\Omega_1^2}{\Lambda^3} + x_2^{(u)}Q\,[\phi\varphi]_{3'}\,u_R\frac{\Omega_1^2}{\Lambda^3}\,, \end{aligned} \tag{C.44}$$

Field	$SU(2)_L$	S_4	Z_2	Z_2'	Z_2''	Z_6	Z_{12}
$L = (L_e, L_\mu, L_\tau)$	**2**	**3′**					
τ_R	**1**	**1**					3
$l_R = (e_R, \mu_R)$	**1**	**2**					5
N_{1R}	**1**	**1**	1				
N_{2R}	**1**	**1**	1	1			
$Q = (Q_1, Q_2, Q_3)$	**2**	**3′**			1		
u_R	**1**	**1**					6
c_R	**1**	**1**					
t_R	**1**	**1**					
d_R	**1**	**1**				3	6
s_R	**1**	**1**				3	
b_R	**1**	**1**				3	
$\phi = (\phi_1, \phi_2, \phi_3)$	**2**	**3′**					
η_1	**1**	**1**					-1
η_2	**1**	**1′**					-1
χ	**1**	**3′**	1				
ξ	**1**	**3**	1				
σ	**1**	**3′**	1	1			
ζ	**1**	**3**	1	1			
ρ	**1**	**3′**			1		
φ	**1**	**3**			1		
Ω_1	**1**	**1**					3
Ω_2	**1**	**1**			1		2
Ω_3	**1**	**1**				1	

Table C.1: The complete particle content and symmetries used in the model. The empty entries denote uncharged fields.

and for the down-type quarks

$$\begin{aligned}
-\mathcal{L}^{(D)} = {} & y_1^{(b)} \left[Q\phi\right]_{3'} b_R \frac{\rho\Omega_3^3}{\Lambda^4} + \frac{y_2^{(b)}}{\Lambda} Q \left[\phi\rho\right]_{3'} b_R \frac{\Omega_3^3}{\Lambda^3} + x_1^{(b)} \left[Q\phi\right]_3 b_R \frac{\varphi\Omega_3^3}{\Lambda^4} \\
& + \frac{x_2^{(b)}}{\Lambda} Q \left[\phi\varphi\right]_{3'} b_R \frac{\Omega_3^3}{\Lambda^3} + y_1^{(s)} \left[Q\phi\right]_{3'} s_R \frac{\rho\Omega_3^3}{\Lambda^4} + \frac{y_2^{(b)}}{\Lambda} Q \left[\phi\rho\right]_{3'} s_R \frac{\Omega_3^3}{\Lambda^3} \\
& + x_1^{(s)} \left[Q\phi\right]_3 s_R \frac{\varphi\Omega_3^3}{\Lambda^4} + \frac{x_2^{(s)}}{\Lambda} Q \left[\phi\varphi\right]_{3'} s_R \frac{\Omega_3^3}{\Lambda^3} + x_0^{(d)} \left[Q\phi\right]_1 d_R \frac{\Omega_2^2\Omega_3^3}{\Lambda^5} \\
& + y_1^{(d)} \left[Q\phi\right]_{3'} d_R \frac{\rho\Omega_1^2\Omega_3^3}{\Lambda^6} + y_2^{(d)} Q \left[\phi\rho\right]_{3'} d_R \frac{\Omega_1^2\Omega_3^3}{\Lambda^6} \\
& + x_1^{(d)} \left[Q\phi\right]_3 d_R \frac{\varphi\Omega_1^2\Omega_3^3}{\Lambda^6} + x_2^{(d)} Q \left[\phi\varphi\right]_{3'} d_R \frac{\Omega_1^2\Omega_3^3}{\Lambda^6} \,.
\end{aligned} \tag{C.45}$$

Then the quark mass matrices shown in Eq. (4.29) satisfy the following relation:

$$M_q M_q^\dagger \equiv \begin{pmatrix} X_q & Y_q e^{i\theta_{aq}} & Y_q e^{i\theta_{bq}} \\ Y_q e^{-i\theta_{aq}} & U_q & V_q e^{i\theta_{cq}} \\ Y_q e^{-i\theta_{bq}} & V_q e^{-i\theta_{cq}} & U_q \end{pmatrix} \tag{C.46}$$

where X_q, Y_q, V_q and U_q are real parameters and

$$\theta_{aq} = \theta_{1q} + \theta_{2q} \,, \qquad \theta_{bq} = \theta_{1q} - \theta_{2q} \,. \tag{C.47}$$

For the sake of simplicity we assume $\theta_{cq} = \theta_{bq} - \theta_{aq}$, so that the relevant physical part of the quark mass matrices can be rewritten as follows:

$$M_q M_q^\dagger = P_q J_q P_q^\dagger \,, \quad P_q = \mathrm{diag}(1, e^{-i\theta_{aq}}, e^{-i\theta_{cq}}) \,, \quad J_q = \begin{pmatrix} X_q & Y_q & Y_q \\ Y_q & U_q & V_q \\ Y_q & V_q & U_q \end{pmatrix} . \tag{C.48}$$

The matrix J_q corresponds to a modification of the Fukuyama-Nishiura texture proposed in [154] and is diagonalized by an orthogonal matrix R_q as follows:

$$R_q J_q R_q^T = diag\left(-m_{q1}^2, m_{q2}^2, m_{q3}^2\right) , \qquad R_q = \begin{pmatrix} c_q & s_q & 0 \\ -\frac{s_q}{\sqrt{2}} & \frac{c_q}{\sqrt{2}} & -\frac{1}{\sqrt{2}} \\ -\frac{s_q}{\sqrt{2}} & \frac{c_q}{\sqrt{2}} & \frac{1}{\sqrt{2}} \end{pmatrix} , \tag{C.49}$$

where

$$c_q = \sqrt{\frac{m_{q2}^2 - X_q}{m_{q2}^2 + m_{q1}^2}} \,, \qquad s_q = \sqrt{\frac{m_{q1}^2 + X_q}{m_{q2}^2 + m_{q1}^2}} \,, \tag{C.50}$$

with the quark masses

$$\begin{aligned}
-m_{q1}^2 &= \frac{1}{2}\left(U_q + V_q + X_q - \sqrt{\left(X_q - U_q - V_q\right)^2 + 8Y_q^2}\right) , \\
m_{q2}^2 &= \frac{1}{2}\left(U_q + V_q + X_q + \sqrt{\left(X_q - U_q - V_q\right)^2 + 8Y_q^2}\right) , \\
m_{q3}^2 &= U_q - V_q \,.
\end{aligned} \tag{C.51}$$

Furthermore, for the CKM matrix we obtain

$$V_{\text{CKM}} = O_U^T P_{UD} O_D \tag{C.52}$$
$$= \begin{pmatrix} c_U c_D + \frac{1}{2} s_U s_D \left(e^{i\vartheta} + e^{i\varrho}\right) & c_U s_D - \frac{1}{2} s_U c_D \left(e^{i\vartheta} + e^{i\varrho}\right) & \frac{1}{2} s_U \left(e^{i\vartheta} - e^{i\varrho}\right) \\ s_U c_D - \frac{1}{2} c_U s_D \left(e^{i\vartheta} + e^{i\varrho}\right) & s_U s_D + \frac{1}{2} c_U c_D \left(e^{i\vartheta} + e^{i\varrho}\right) & \frac{1}{2} c_U \left(e^{i\varrho} - e^{i\vartheta}\right) \\ \frac{1}{2} s_D \left(e^{i\vartheta} - e^{i\varrho}\right) & \frac{1}{2} c_D \left(e^{i\varrho} - e^{i\vartheta}\right) & \frac{1}{2} \left(e^{i\vartheta} + e^{i\varrho}\right) \end{pmatrix},$$

where $P_{UD} = P_U^\dagger P_D = \text{diag}\left(1, e^{i\vartheta}, e^{i\varrho}\right)$, with $\vartheta = \theta_{aU} - \theta_{aD}$ and $\varrho = \theta_{bU} - \theta_{bD}$. Using the values of the quark masses at the M_Z scale shown in Table A.1 and varying the parameters $X_{U,D}$, ϑ and ϱ we fit the magnitudes of the CKM matrix elements, the CP-violating phase and the Jarlskog invariant J to the experimental values shown in Table C.2.

Observable	Model value	Experiment ($\pm 1\,\sigma$)
$\lvert V_{ud}\rvert$	0.974	$0.97425^{+0.00022}_{-0.00032}$
$\lvert V_{us}\rvert$	0.225	$0.22542^{+0.00101}_{-0.00097}$
$\lvert V_{ub}\rvert$	0.00351	$0.00371^{+0.00027}_{-0.00020}$
$\lvert V_{cd}\rvert$	0.225	$0.22529^{+0.00100}_{-0.00090}$
$\lvert V_{cs}\rvert$	0.973	$0.97339^{+0.00024}_{-0.00024}$
$\lvert V_{cb}\rvert$	0.0412	$0.04180^{+0.00097}_{-0.00164}$
$\lvert V_{td}\rvert$	0.00867	$0.00868^{+0.00027}_{-0.00058}$
$\lvert V_{ts}\rvert$	0.0404	$0.04107^{+0.00094}_{-0.00161}$
$\lvert V_{tb}\rvert$	0.999	$0.99912^{+0.00007}_{-0.00004}$
J	2.95×10^{-5}	$(2.96^{+0.20}_{-0.16}) \times 10^{-5}$
δ	69.2°	68°

Table C.2: Model values and the corresponding measurements of the up-type quark masses and CKM parameters at the M_Z scale. The experimental values were taken from Refs. [6, 155].

For the values

$$\begin{aligned} X_U &= 2.90 \times 10^{-3}\,\text{GeV}^2\,, & \vartheta &= 87.9^\circ\,, \\ X_D &= 1.38 \times 10^{-4}\,\text{GeV}^2\,, & \varrho &= 92.6^\circ\,, \end{aligned} \tag{C.53}$$

the obtained magnitudes of the CKM matrix elements, the CP-violating phase and the Jarlskog invariant are in excellent agreement with the experimental data.

C.3.2 *Z_3 Breaking*

In this section we append the full expressions used to determine the consequences of the perturbed VEV alignment. After Z_3 breaking the new mixing angle ϑ between the

CP-even neutral scalars can be expressed in terms of the scalar masses $m_h \approx 125\,\text{GeV}$ and $m_{\phi^0_{a,R}} \equiv m_a$

$$\begin{aligned}
\tan 2\vartheta &= \frac{A}{B} \qquad \text{with} \\
A &= s_\theta\{c_\theta[4m_a^2m_h^2s_\theta^2(2-7s_\theta^2)+4m_h^4(4+4s_\theta^2-7s_\theta^4) \\
&\quad -8m_a^4(2-5s_\theta^2+3s_\theta^4)]-4\sqrt{2}s_\theta[4m_h^4(2-3s_\theta^2+s_\theta^4) \\
&\quad +m_a^2m_h^2(2-7s_\theta^2+4s_\theta^4)+m_a^4(6-19s_\theta^2+15s_\theta^4)]\}\,, \\
B &= 2m_a^2m_h^2(4-16s_\theta^2+17s_\theta^4+4\sqrt{2}c_\theta s_\theta^5-7s_\theta^6) \\
&\quad +m_h^4(-1+2s_\theta^2)(4+4s_\theta^2-7s_\theta^4+4\sqrt{2}c_\theta s_\theta(-2+s_\theta^2)) \\
&\quad +m_a^4(-4+12s_\theta^2-11s_\theta^4+5s_\theta^6-2\sqrt{2}c_\theta s_\theta(4-14s_\theta^2+13s_\theta^4))\,.
\end{aligned} \tag{C.54}$$

The PMNS matrix receives corrections caused by the perturbation of the VEV alignment. These are approximately given by

$$\begin{aligned}
U \;\simeq\; & \begin{pmatrix}
\frac{c_\psi}{\sqrt{3}}-\frac{e^{i\phi-\frac{2i\pi}{3}}s_\psi}{\sqrt{3}} & \frac{e^{\frac{2i\pi}{3}}}{\sqrt{3}} & \frac{e^{-\frac{2i\pi}{3}}c_\psi}{\sqrt{3}}+\frac{e^{-i\phi}s_\psi}{\sqrt{3}} \\
\frac{c_\psi}{\sqrt{3}}-\frac{e^{i\phi+\frac{2i\pi}{3}}s_\psi}{\sqrt{3}} & \frac{e^{-\frac{2i\pi}{3}}}{\sqrt{3}} & \frac{e^{\frac{2i\pi}{3}}c_\psi}{\sqrt{3}}+\frac{e^{-i\phi}s_\psi}{\sqrt{3}} \\
\frac{c_\psi}{\sqrt{3}}-\frac{e^{i\phi}s_\psi}{\sqrt{3}} & \frac{1}{\sqrt{3}} & \frac{c_\psi}{\sqrt{3}}+\frac{e^{-i\phi}s_\psi}{\sqrt{3}}
\end{pmatrix} \\
& +\theta\begin{pmatrix}
-\sqrt{\frac{2}{3}}c_\psi+\frac{e^{i\phi+\frac{2i\pi}{3}}s_\psi}{\sqrt{6}}+\frac{e^{i\phi}s_\psi}{\sqrt{6}} & -\frac{1}{\sqrt{6}}-\frac{e^{-\frac{2i\pi}{3}}}{\sqrt{6}} & -\frac{(e^{\frac{2i\pi}{3}}+1)c_\psi}{\sqrt{6}}-\sqrt{\frac{2}{3}}e^{-i\phi}s_\psi \\
\frac{e^{i\phi}s_\psi}{\sqrt{6}}-\frac{e^{i\phi-\frac{2i\pi}{3}}s_\psi}{\sqrt{6}} & -\frac{1}{\sqrt{6}}+\frac{e^{\frac{2i\pi}{3}}}{\sqrt{6}} & \frac{e^{-\frac{2i\pi}{3}}c_\psi}{\sqrt{6}}-\frac{c_\psi}{\sqrt{6}} \\
\sqrt{\frac{2}{3}}c_\psi-\frac{e^{i\phi-\frac{2i\pi}{3}}s_\psi}{\sqrt{6}}-\frac{e^{i\phi+\frac{2i\pi}{3}}s_\psi}{\sqrt{6}} & \frac{e^{-\frac{2i\pi}{3}}}{\sqrt{6}}+\frac{e^{\frac{2i\pi}{3}}}{\sqrt{6}} & -\frac{c_\psi}{\sqrt{6}}+\sqrt{\frac{2}{3}}e^{-i\phi}s_\psi
\end{pmatrix} \\
& +\theta^2\begin{pmatrix}
\frac{1}{4}\sqrt{3}c_\psi-\frac{1}{4}\sqrt{3}e^{i\phi+\frac{2i\pi}{3}}s_\psi & \frac{1}{4}\sqrt{3}e^{-\frac{2i\pi}{3}} & \frac{1}{4}\sqrt{3}e^{\frac{2i\pi}{3}}c_\psi+\frac{1}{4}\sqrt{3}e^{-i\phi}s_\psi \\
\frac{1}{4}\sqrt{3}e^{i\phi-\frac{2i\pi}{3}}s_\psi-\frac{1}{4}\sqrt{3}c_\psi & -\frac{1}{4}\sqrt{3}e^{\frac{2i\pi}{3}} & -\frac{1}{4}\sqrt{3}e^{-\frac{2i\pi}{3}}c_\psi-\frac{1}{4}\sqrt{3}e^{-i\phi}s_\psi \\
0 & 0 & 0
\end{pmatrix},
\end{aligned} \tag{C.55}$$

whereas the deviations in the mixing angles caused by the perturbation θ are accounted for by

$$\begin{aligned}
\sin^2\theta_{12} &= \frac{\left(-\frac{3\theta^2}{8}+\frac{\theta}{2\sqrt{2}}+\frac{1}{2}\right)^2+\left(-\frac{1}{8}\sqrt{3}\theta^2-\frac{\theta}{2\sqrt{6}}-\frac{1}{2\sqrt{3}}\right)^2}{f\left(\theta,\psi,\phi\right)}\,, \\
\sin^2\theta_{13} &= \left(\left(-\frac{\sqrt{3}\theta^2}{8}-\frac{\theta}{2\sqrt{6}}-\frac{1}{2\sqrt{3}}\right)c_\psi+\left(\frac{\sqrt{3}\theta^2}{4}-\sqrt{\frac{2}{3}}\theta+\frac{1}{\sqrt{3}}\right)s_\psi c_\phi\right)^2 \\
&\quad +\left(\left(\frac{3\theta^2}{8}-\frac{\theta}{2\sqrt{2}}-\frac{1}{2}\right)c_\psi-\left(\frac{\sqrt{3}\theta^2}{4}-\sqrt{\frac{2}{3}}\theta+\frac{1}{\sqrt{3}}\right)s_\psi s_\phi\right)^2\,, \\
\sin^2\theta_{23} &= \frac{\left(\left(\frac{\sqrt{3}\theta^2}{8}-\frac{1}{2}\sqrt{\frac{3}{2}}\theta-\frac{1}{2\sqrt{3}}\right)c_\psi+\left(\frac{1}{\sqrt{3}}-\frac{\sqrt{3}\theta^2}{4}\right)s_\psi c_\phi\right)^2}{f\left(\theta,\psi,\phi\right)} \\
&\quad +\frac{\left(\left(\frac{3\theta^2}{8}-\frac{\theta}{2\sqrt{2}}+\frac{1}{2}\right)c_\psi-\left(\frac{1}{\sqrt{3}}-\frac{\sqrt{3}\theta^2}{4}\right)s_\psi s_\phi\right)^2}{f\left(\theta,\psi,\phi\right)}\,,
\end{aligned} \tag{C.56}$$

with

$$f(\theta,\psi,\phi) = -\left\{\left(\frac{3\theta^2}{8} - \frac{\theta}{2\sqrt{2}} - \frac{1}{2}\right)c_\psi - \left(\frac{\sqrt{3}\theta^2}{4} - \sqrt{\frac{2}{3}}\theta + \frac{1}{\sqrt{3}}\right)s_\psi s_\phi\right\}^2 \\ -\left\{\left(-\frac{\sqrt{3}\theta^2}{8} - \frac{\theta}{2\sqrt{6}} - \frac{1}{2\sqrt{3}}\right)c_\psi + \left(\frac{\sqrt{3}\theta^2}{4} - \sqrt{\frac{2}{3}}\theta + \frac{1}{\sqrt{3}}\right)s_\psi c_\phi\right\}^2 + 1\,. \tag{C.57}$$

C.3.3 *Limits from $h \to \gamma\gamma$*

In the spirit of Sec. 3.1.3, where a thorough analysis of the scalar sector was crucial to exclude large parts of the parameter space, we perform a study of the $h \to \gamma\gamma$ channel in the present framework.
As shown in the previous section, small Z_3 breaking perturbations allow to successfully accommodate the experimental CMS data on the $h \to \mu\tau$ excess. Consequently and in order to make definite predictions, it is reasonable to neglect these perturbations in the computation of the Higgs diphoton decay rate. Here, the $h \to \gamma\gamma$ decay receives additional contributions from loops with charged scalars $\phi^\pm_{(a,b)}$ resulting in a potential diphoton excess, cf. Fig. 3.5 in Sec. 3.1.3. The $\Gamma(h \to \gamma\gamma)$ decay rate as well as the loop expressions coincide with those given in Eqs. (3.53) and (3.56). The relevant trilinear coupling entering $\Gamma(h \to \gamma\gamma)$ is

$$\lambda_{h\phi_s^\pm\phi_s^\mp} = \frac{2}{3}(3\alpha + 2\beta - \gamma - \delta)\,v = \frac{2\left(m_h^2 - m^2_{\phi_s^\pm}\right)}{v}, \qquad s = a, b. \tag{C.58}$$

The ratio $R_{\gamma\gamma}$, defined in Eq. (3.58) is compared with the respective measurements from CMS and ATLAS, Eq. (3.59), to limit the charged scalar masses.
Fig. C.3 shows the sensitivity of the ratio $R_{\gamma\gamma}$ under variations of the charged Higgs masses $m_{\phi_s^\pm}$ $(s = a, b)$, between 200 GeV and 1 TeV. Requiring that the $h \to \gamma\gamma$ signal stays within the range $1.14 \lesssim R_{\gamma\gamma} \lesssim 1.17$ (the central values of the recent CMS and ATLAS results, respectively), yields the bound 200 GeV$\lesssim m_{\phi^\pm_{a,b}} \lesssim$ 205 GeV for the charged Higgs boson masses. However, considering the large experimental errors of the measurements, the masses are barely constrained at all by the $h \to \gamma\gamma$ rate. This is due to the fact that the diphoton cross section is dominated by the SM particles, which behave SM-like in the unbroken Z_3 limit. A back-reaction of the Z_3 breaking on the quark sector could possibly modify the top quark coupling and thereby cause deviations from the measured $h \to \gamma\gamma$ rate. A thorough study of the quark sector is, however, beyond the scope of this work.

C.3.4 *Computation of the Radiative Decays $l \to l'\gamma$*

The radiative decays $l \to l'\gamma$ provide the strongest bounds on flavor-violating Yukawa couplings in our model, therefore it is imperative to compute these decays with reasonable precision. The branching ratio of $l \to l'\gamma$ can be written as

$$\mathcal{B}(l \to l'\gamma) = \frac{\tau_l \alpha_{\mathrm{EM}} m_l^5}{64\pi^4}\left(|c_L|^2 + |c_R|^2\right), \tag{C.59}$$

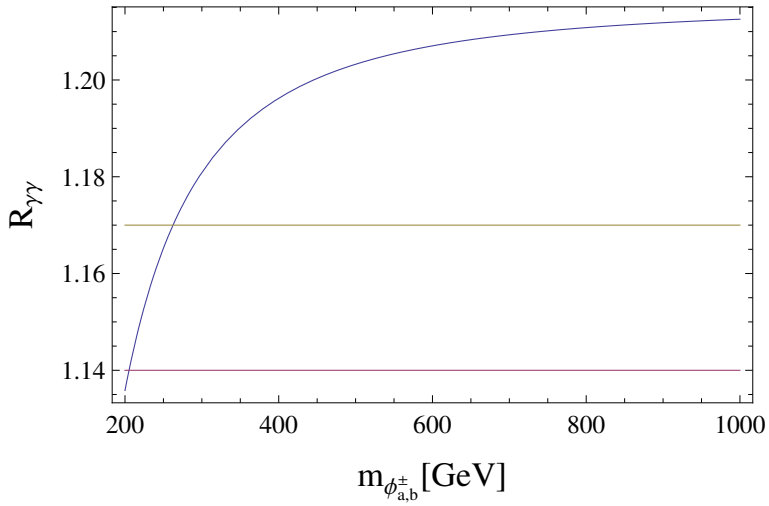

Figure C.3: The ratio $R_{\gamma\gamma}$ is shown as a function of $m_{\phi_s^\pm}$ $(s = a, b)$ for $a_{htt} = 1$. The horizontal lines correspond to the central values of the $R_{\gamma\gamma}$ measurements by CMS and ATLAS, equal to $1.14^{+0.26}_{-0.23}$ and 1.17 ± 0.27, respectively [169, 170].

where in the following the Wilson coefficients $c_{L,R}$ are calculated up to order two. Because of the strong hierarchy of the Yukawa couplings in our model $|y_{l'l}| \gg |y_{ll'}|$ the contributions from c_L to $\mathcal{B}(l \to l'\gamma)$ can be neglected. The one-loop expressions corresponding to the diagrams in Fig. 4.1 are given by [51]

$$c_R^{1\text{Loop}} \simeq \frac{1}{4m_l} \int_0^1 \delta(1-u-v-w) \frac{v\, w\, m_l\, y_{l'l}\, y_{ll}^* + (u+v)\, m_l\, y_{l'l}\, y_{ll}}{w\, m_s^2 - v\, w\, m_l^2 + (u+v)\, m_l^2 - u\, v\, q^2} du\, dv\, dw \tag{C.60}$$

with $s = h, H, \eta_I, \phi_{a,R}, \phi_{a,I}$. Specifically in the case of $\mu \to e\gamma$ the two-loop contributions with a top quark and a W boson running in the loop have to be taken into account as they can dominate the cross section in certain regions of the parameter space [51, 200]. The analytical expressions for the top-loops are

$$\begin{aligned} c_R^{t\gamma} &= -\frac{8}{3}\kappa \frac{v}{m_t} y_{\mu\tau} \left[\text{Re}(y_{tt}) f(z_{ts}) - i\text{Im}(y_{tt}) g(z_{ts}) \right], \\ c_R^{tZ} &= -4\kappa \frac{(1 - 4s^2_{\theta_\text{W}})(1 - \frac{8}{3}s^2_{\theta_\text{W}})v}{16 s^2_{\theta_\text{W}} c^2_{\theta_\text{W}}} y_{\mu\tau} \left[\text{Re}(y_{tt}) \tilde{f}(z_{ts}) - i\text{Im}(y_{tt}) \tilde{g}(z_{ts}) \right] \end{aligned} \tag{C.61}$$

with $\theta_W \simeq 28.74°$ and

$$\begin{aligned} f(z) =& \frac{z}{2} \int_0^1 \frac{1 - 2x(1-x)}{x(1-x) - z} \log \frac{x(1-x)}{z} dx\,, \\ g(z) =& \frac{z}{2} \int_0^1 \frac{1}{x(1-x) - z} \log \frac{x(1-x)}{z} dx\,, \\ h(z) =& \frac{z}{2} \int_0^1 \frac{1}{z - x(1-x)} \left[1 + \frac{z}{z - x(1-x)} \log \frac{x(1-x)}{z} \right] dx\,, \\ \tilde{f}(x,y) =& \frac{y f(x)}{y-x} + \frac{x f(y)}{x-y}\,, \qquad \tilde{g}(x,y) = \frac{y g(x)}{y-x} + \frac{x g(y)}{x-y}\,, \\ z_{ij} =& \frac{m_i^2}{m_j^2}\,, \quad \text{and} \quad \kappa = \frac{\alpha}{2\sqrt{2}\pi} G_F \frac{v}{m_l}\,. \end{aligned} \tag{C.62}$$

The W-loop expressions on the other hand are

$$
\begin{aligned}
c_R^{W\gamma} &= \kappa\, y_{\mu\tau}\left[3f(z_{Ws}) + (5+\frac{3}{4})g(z_{Ws}) + \frac{3}{4})h(z_{Ws}) + \frac{f(z_{Ws})-g(z_{Ws})}{2z_{Ws}}\right], \\
c_R^{WZ} &= \kappa\frac{1-4s^2_{\theta_{\rm W}}}{4s^2_{\theta_{\rm W}}} y_{\mu\tau}\left[\frac{1}{2}(5-t^2_{\theta_{\rm W}})\tilde{f}(z_{ts},z_{WZ}) + \frac{1}{2}(7-3t^2_{\theta_{\rm W}})\tilde{g}(z_{ts},z_{WZ})\right. \\
&\quad \left. + \frac{3}{4}g(z_{ts}) + \frac{3}{4}h(z_{ts}) + \frac{1}{4z_{ts}}(1-t^2_{\theta_{\rm W}})(\tilde{f}(z_{ts},z_{WZ}) - \tilde{g}(z_{ts},z_{WZ}))\right].
\end{aligned}
\tag{C.63}
$$

The corresponding diagrams of these loop contributions can be found in, e.g., Fig. 12 of Ref. [51].

BIBLIOGRAPHY

[1] S. L. Glashow. *Partial Symmetries of Weak Interactions.* Nucl. Phys., 22:pp. 579–588 [1961]. doi:10.1016/0029-5582(61)90469-2.

[2] S. Weinberg. *A Model of Leptons.* Phys. Rev. Lett., 19:pp. 1264–1266 [1967]. doi:10.1103/PhysRevLett.19.1264.

[3] F. Abe et al. *Observation of top quark production in $\bar{p}p$ collisions.* Phys. Rev. Lett., 74:pp. 2626–2631 [1995]. doi:10.1103/PhysRevLett.74.2626.

[4] G. Aad et al. *Observation of a new particle in the search for the Standard Model Higgs boson with the ATLAS detector at the LHC.* Phys. Lett., B716:pp. 1–29 [2012]. doi:10.1016/j.physletb.2012.08.020.

[5] S. Chatrchyan et al. *Observation of a new boson at a mass of 125 GeV with the CMS experiment at the LHC.* Phys. Lett., B716:pp. 30–61 [2012]. doi:10.1016/j.physletb.2012.08.021.

[6] K. A. Olive et al. *Review of Particle Physics.* Chin. Phys., C38:p. 090001 [2014]. doi:10.1088/1674-1137/38/9/090001.

[7] P. Langacker. *Grand Unified Theories and Proton Decay.* Phys. Rept., 72:p. 185 [1981]. doi:10.1016/0370-1573(81)90059-4.

[8] S. L. Glashow, J. Iliopoulos, and L. Maiani. *Weak Interactions with Lepton-Hadron Symmetry.* Phys. Rev., D2:pp. 1285–1292 [1970]. doi:10.1103/PhysRevD.2.1285.

[9] J. K. Ahn et al. *Observation of Reactor Electron Antineutrino Disappearance in the RENO Experiment.* Phys. Rev. Lett., 108:p. 191802 [2012]. doi:10.1103/PhysRevLett.108.191802.

[10] F. P. An et al. *Observation of electron-antineutrino disappearance at Daya Bay.* Phys. Rev. Lett., 108:p. 171803 [2012]. doi:10.1103/PhysRevLett.108.171803.

[11] Y. Abe et al. *First Measurement of θ_{13} from Delayed Neutron Capture on Hydrogen in the Double Chooz Experiment.* Phys. Lett., B723:pp. 66–70 [2013]. doi:10.1016/j.physletb.2013.04.050.

[12] P. F. Harrison, D. H. Perkins, and W. G. Scott. *A Redetermination of the neutrino mass squared difference in tri - maximal mixing with terrestrial matter effects.* Phys. Lett., B458:pp. 79–92 [1999]. doi:10.1016/S0370-2693(99)00438-4.

[13] M. C. Gonzalez-Garcia, M. Maltoni, and T. Schwetz. *Updated fit to three neutrino mixing: status of leptonic CP violation.* JHEP, 11:p. 052 [2014]. doi:10.1007/JHEP11(2014)052.

[14] J. Garayoa and T. Schwetz. *Neutrino mass hierarchy and Majorana CP phases within the Higgs triplet model at the LHC.* JHEP, 03:p. 009 [2008]. doi:10.1088/1126-6708/2008/03/009.

[15] B. Pontecorvo. *Mesonium and anti-mesonium.* Sov. Phys. JETP, 6:p. 429 [1957]. [Zh. Eksp. Teor. Fiz.33,549(1957)].

[16] Q. R. Ahmad et al. *Measurement of the rate of $\nu_e + d \rightarrow p + p + e^-$ interactions produced by ^8B solar neutrinos at the Sudbury Neutrino Observatory.* Phys. Rev. Lett., 87:p. 071301 [2001]. doi:10.1103/PhysRevLett.87.071301.

[17] Y. Fukuda et al. *Evidence for oscillation of atmospheric neutrinos.* Phys. Rev. Lett., 81:pp. 1562–1567 [1998]. doi:10.1103/PhysRevLett.81.1562.

[18] P. A. R. Ade et al. *Planck 2015 results. XIII. Cosmological parameters.* Astron. Astrophys., 594:p. A13 [2016]. doi:10.1051/0004-6361/201525830.

[19] S. Mertens. *Status of the KATRIN Experiment and Prospects to Search for keV-mass Sterile Neutrinos in Tritium β-decay.* Phys. Procedia, 61:pp. 267–273 [2015]. doi:10.1016/j.phpro.2014.12.043.

[20] E. Giusarma, M. Gerbino, O. Mena, S. Vagnozzi, S. Ho, and K. Freese. *On the improvement of cosmological neutrino mass bounds.* Unpublished manuscript. arXiv:1605.04320 [2016].

[21] S. Weinberg. *Baryon and Lepton Nonconserving Processes.* Phys. Rev. Lett., 43:pp. 1566–1570 [1979]. doi:10.1103/PhysRevLett.43.1566.

[22] P. Minkowski. *$\mu \rightarrow e\gamma$ at a Rate of One Out of 10^9 Muon Decays?* Phys. Lett., B67:pp. 421–428 [1977]. doi:10.1016/0370-2693(77)90435-X.

[23] K. S. Babu and V. S. Mathur. *Radiatively Induced Seesaw Mechanism for Neutrino Masses.* Phys. Rev., D38:p. 3550 [1988]. doi:10.1103/PhysRevD.38.3550.

[24] J. Schechter and J. W. F. Valle. *Neutrinoless Double beta Decay in $SU(2) \times U(1)$ Theories.* Phys. Rev., D25:p. 2951 [1982]. doi:10.1103/PhysRevD.25.2951.

[25] K. S. Krane. *Introductory nuclear physics.* Wiley, New York, NY [1988].

[26] S. M. Bilenky and C. Giunti. *Neutrinoless double-beta decay: A brief review.* Mod. Phys. Lett., A27:p. 1230015 [2012]. doi:10.1142/S0217732312300157.

[27] M. Agostini et al. *Results on Neutrinoless Double-β Decay of ^{76}Ge from Phase I of the GERDA Experiment.* Phys. Rev. Lett., 111(12):p. 122503 [2013]. doi:10.1103/PhysRevLett.111.122503.

[28] A. Gando et al. *Search for Majorana Neutrinos near the Inverted Mass Hierarchy Region with KamLAND-Zen.* Phys. Rev. Lett., 117(8):p. 082503 [2016]. doi:10.1103/PhysRevLett.117.109903, 10.1103/PhysRevLett.117.082503. [Addendum: Phys. Rev. Lett.117,no.10,109903(2016)].

[29] M. Bongrand. *Latest NEMO-3 Results and Status of SuperNEMO.* Phys. Procedia, 61:pp. 211–220 [2015]. doi:10.1016/j.phpro.2014.12.034.

[30] J. J. Gomez-Cadenas et al. *Present status and future perspectives of the NEXT experiment.* Adv. High Energy Phys., 2014:p. 907067 [2014]. doi:10.1155/2014/907067.

[31] T. Konno. *Status and prospects of the Belle II experiment.* J. Phys. Conf. Ser., 627(1):p. 012009 [2015]. doi:10.1088/1742-6596/627/1/012009.

[32] M. Misiak et al. *Updated NNLO QCD predictions for the weak radiative B-meson decays.* Phys. Rev. Lett., 114(22):p. 221801 [2015]. doi:10.1103/PhysRevLett.114.221801.

[33] Y. Amhis et al. *Averages of B-Hadron, C-Hadron, and τ-lepton properties as of early 2012.* Unpublished manuscript. arXiv:1207.1158 [2012].

[34] A. Ali, P. Ball, L. T. Handoko, and G. Hiller. *A Comparative study of the decays $B \to (K, K^*)\ell^+\ell^-$ in standard model and supersymmetric theories.* Phys. Rev., D61:p. 074024 [2000]. doi:10.1103/PhysRevD.61.074024.

[35] C. Bobeth, M. Gorbahn, T. Hermann, M. Misiak, E. Stamou, and M. Steinhauser. *$B_{s,d} \to l^+l^-$ in the Standard Model with Reduced Theoretical Uncertainty.* Phys. Rev. Lett., 112:p. 101801 [2014]. doi:10.1103/PhysRevLett.112.101801.

[36] V. Khachatryan et al. *Observation of the rare $B_s^0 \to \mu^+\mu^-$ decay from the combined analysis of CMS and LHCb data.* Nature, 522:pp. 68–72 [2015]. doi:10.1038/nature14474.

[37] J. Charles et al. *Current status of the Standard Model CKM fit and constraints on $\Delta F = 2$ New Physics.* Phys. Rev., D91(7):p. 073007 [2015]. doi:10.1103/PhysRevD.91.073007.

[38] R. Aaij et al. *Measurement of Form-Factor-Independent Observables in the Decay $B^0 \to K^{*0}\mu^+\mu^-$.* Phys. Rev. Lett., 111:p. 191801 [2013]. doi:10.1103/PhysRevLett.111.191801.

[39] G. Hiller and F. Kruger. *More model independent analysis of $b \to s$ processes.* Phys. Rev., D69:p. 074020 [2004]. doi:10.1103/PhysRevD.69.074020.

[40] R. Aaij et al. *Test of lepton universality using $B^+ \to K^+\ell^+\ell^-$ decays.* Phys. Rev. Lett., 113:p. 151601 [2014]. doi:10.1103/PhysRevLett.113.151601.

[41] J. P. Lees et al. *Measurement of an Excess of $\bar{B} \to D^{(*)}\tau^-\bar{\nu}_\tau$ Decays and Implications for Charged Higgs Bosons.* Phys. Rev., D88(7):p. 072012 [2013]. doi:10.1103/PhysRevD.88.072012.

[42] R. Aaij et al. *Measurement of the ratio of branching fractions $\mathcal{B}(\bar{B}^0 \to D^{*+}\tau^-\bar{\nu}_\tau)/\mathcal{B}(\bar{B}^0 \to D^{*+}\mu^-\bar{\nu}_\mu)$.* Phys. Rev. Lett., 115(11):p. 111803 [2015]. doi:10.1103/PhysRevLett.115.159901, 10.1103/PhysRevLett.115.111803. [Addendum: Phys. Rev. Lett.115,no.15,159901(2015)].

[43] M. Huschle et al. *Measurement of the branching ratio of $\bar{B} \to D^{(*)}\tau^-\bar{\nu}_\tau$ relative to $\bar{B} \to D^{(*)}\ell^-\bar{\nu}_\ell$ decays with hadronic tagging at Belle.* Phys. Rev., D92(7):p. 072014 [2015]. doi:10.1103/PhysRevD.92.072014.

[44] S. Fajfer, J. F. Kamenik, and I. Nisandzic. *On the $B \to D^*\tau\bar{\nu}_\tau$ Sensitivity to New Physics.* Phys. Rev., D85:p. 094025 [2012]. doi:10.1103/PhysRevD.85.094025.

[45] HFAG. *Average of $R(D)$ and $R(D^*)$ for EPS-HEP 2015.* `http://www.slac.stanford.edu/xorg/hfag/semi/eps15/eps15_dtaunu.html` [2015]. [Online; accessed 27-September-2016].

[46] S. Descotes-Genon, L. Hofer, J. Matias, and J. Virto. *Global analysis of $b \to s\ell\ell$ anomalies.* JHEP, 06:p. 092 [2016]. doi:10.1007/JHEP06(2016)092.

[47] J. H. Christenson, J. W. Cronin, V. L. Fitch, and R. Turlay. *Evidence for the 2π Decay of the K_2^0 Meson.* Phys. Rev. Lett., 13:pp. 138–140 [1964]. doi:10.1103/PhysRevLett.13.138.

[48] S. M. Bilenky and B. Pontecorvo. *Lepton Mixing and Neutrino Oscillations.* Phys. Rept., 41:pp. 225–261 [1978]. doi:10.1016/0370-1573(78)90095-9.

[49] S. Mihara, J. P. Miller, P. Paradisi, and G. Piredda. *Charged Lepton Flavor-Violation Experiments.* Ann. Rev. Nucl. Part. Sci., 63:pp. 531–552 [2013]. doi:10.1146/annurev-nucl-102912-144530.

[50] A. M. Baldini et al. *Search for the Lepton Flavour Violating Decay $\mu^+ \to e^+\gamma$ with the Full Dataset of the MEG Experiment.* Eur. Phys. J., C76(8):p. 434 [2016]. doi:10.1140/epjc/s10052-016-4271-x.

[51] R. Harnik, J. Kopp, and J. Zupan. *Flavor Violating Higgs Decays.* JHEP, 03:p. 026 [2013]. doi:10.1007/JHEP03(2013)026.

[52] C. Schwanda. *Charged Lepton Flavour Violation at Belle and Belle II.* Nucl. Phys. Proc. Suppl., 248-250:pp. 67–72 [2014]. doi:10.1016/j.nuclphysbps.2014.02.013.

[53] A. M. Baldini et al. *MEG Upgrade Proposal.* Unpublished manuscript. arXiv:1301.7225 [2013].

[54] K. Hayasaka et al. *Search for Lepton Flavor Violating Tau Decays into Three Leptons with 719 Million Produced $\tau^+\tau^-$ Pairs.* Phys. Lett., B687:pp. 139–143 [2010]. doi:10.1016/j.physletb.2010.03.037.

[55] U. Bellgardt et al. *Search for the Decay $\mu^+ \to e^+e^+e^-$.* Nucl. Phys., B299:pp. 1–6 [1988]. doi:10.1016/0550-3213(88)90462-2.

[56] A. Blondel et al. *Research Proposal for an Experiment to Search for the Decay $\mu \to eee$.* Unpublished manuscript. arXiv:1301.6113 [2013].

[57] W. H. Bertl et al. *A Search for muon to electron conversion in muonic gold.* Eur. Phys. J., C47:pp. 337–346 [2006]. doi:10.1140/epjc/s2006-02582-x.

[58] R. M. Carey et al. *Proposal to search for $\mu^- N \to e^- N$ with a single event sensitivity below 10^{-16}.* Unpublished manuscript. `http://inspirehep.net/record/809087` [2008].

[59] N. H. Tran. *Status of the COMET Experiment at J-PARC.* JPS Conf. Proc., 1:p. 013006 [2014]. doi:10.7566/JPSCP.1.013006.

[60] T. Aoyama, M. Hayakawa, T. Kinoshita, and M. Nio. *Tenth-Order QED Contribution to the Electron $g-2$ and an Improved Value of the Fine Structure Constant.* Phys. Rev. Lett., 109:p. 111807 [2012]. doi:10.1103/PhysRevLett.109.111807.

[61] D. Hanneke, S. F. Hoogerheide, and G. Gabrielse. *Cavity Control of a Single-Electron Quantum Cyclotron: Measuring the Electron Magnetic Moment.* Phys. Rev., A83:p. 052122 [2011]. doi:10.1103/PhysRevA.83.052122.

[62] M. Bauer and M. Neubert. *Minimal Leptoquark Explanation for the $R_{D^{(*)}}$, R_K, and $(g-2)_\mu$ Anomalies.* Phys. Rev. Lett., 116(14):p. 141802 [2016]. doi:10.1103/PhysRevLett.116.141802.

[63] G. Aad et al. *Evidence for the Higgs-boson Yukawa coupling to tau leptons with the ATLAS detector.* JHEP, 04:p. 117 [2015]. doi:10.1007/JHEP04(2015)117.

[64] S. Chatrchyan et al. *Evidence for the 125 GeV Higgs boson decaying to a pair of τ leptons.* JHEP, 05:p. 104 [2014]. doi:10.1007/JHEP05(2014)104.

[65] G. Aad et al. *Search for the $b\bar{b}$ decay of the Standard Model Higgs boson in associated $(W/Z)H$ production with the ATLAS detector.* JHEP, 01:p. 069 [2015]. doi:10.1007/JHEP01(2015)069.

[66] C. Vernieri. *Search for the Higgs boson in the $\mathrm{b\bar{b}}$ decay channel using the CMS detector.* Nucl. Part. Phys. Proc., 273-275:pp. 733–739 [2016]. doi:10.1016/j.nuclphysbps.2015.09.112.

[67] G. Aad et al. *Search for the Standard Model Higgs boson decay to $\mu^+\mu^-$ with the ATLAS detector.* Phys. Lett., B738:pp. 68–86 [2014]. doi:10.1016/j.physletb.2014.09.008.

[68] G. Aad et al. *Measurements of the Higgs boson production and decay rates and constraints on its couplings from a combined ATLAS and CMS analysis of the LHC pp collision data at $\sqrt{s} = 7$ and 8 TeV.* JHEP, 08:p. 045 [2016]. doi:10.1007/JHEP08(2016)045.

[69] M. Bona et al. *Model-independent constraints on $\Delta F = 2$ operators and the scale of new physics.* JHEP, 03:p. 049 [2008]. doi:10.1088/1126-6708/2008/03/049.

[70] V. Khachatryan et al. *Search for Lepton-Flavour-Violating Decays of the Higgs Boson.* Phys. Lett., B749:pp. 337–362 [2015]. doi:10.1016/j.physletb.2015.07.053.

[71] G. Aad et al. *Search for lepton-flavour-violating $H \to \mu\tau$ decays of the Higgs boson with the ATLAS detector.* JHEP, 11:p. 211 [2015]. doi:10.1007/JHEP11(2015)211.

[72] G. Aad et al. *Search for lepton-flavour-violating decays of the Higgs and Z bosons with the ATLAS detector.* Unpublished manuscript. arXiv:1604.07730 [2016].

[73] V. Khachatryan et al. *Search for lepton flavour violating decays of the Higgs boson to $e\tau$ and $e\mu$ in proton-proton collisions at $\sqrt{s} = 8$ TeV.* Submitted to: Phys. Lett. B [2016].

[74] V. Khachatryan et al. *Search for Resonant Production of High-Mass Photon Pairs in Proton-Proton Collisions at $\sqrt{s}$ =8 and 13 TeV.* Phys. Rev. Lett., 117(5):p. 051802 [2016]. doi:10.1103/PhysRevLett.117.051802.

[75] M. Aaboud et al. *Search for resonances in diphoton events at $\sqrt{s}$=13 TeV with the ATLAS detector.* JHEP, 09:p. 001 [2016]. doi:10.1007/JHEP09(2016)001.

[76] CMS Collaboration. *Search for resonant production of high mass photon pairs using* $12.9\,\mathrm{fb}^{-1}$ *of proton-proton collisions at* $\sqrt{s} = 13$ TeV *and combined interpretation of searches at 8 and 13 TeV.* Unpublished manuscript. `http://cds.cern.ch/record/2205245` [2016].

[77] The ATLAS collaboration. *Search for scalar diphoton resonances with 15.4 fb^{-1} of data collected at $\sqrt{s}$=13 TeV in 2015 and 2016 with the ATLAS detector.* Unpublished manuscript. `http://cds.cern.ch/record/2206154` [2016].

[78] A. Strumia. *Interpreting the 750 GeV digamma excess: a review.* Unpublished manuscript. arXiv:1605.09401 [2016].

[79] S. Pakvasa and H. Sugawara. *Discrete Symmetry and Cabibbo Angle.* Phys. Lett., B73:pp. 61–64 [1978]. doi:10.1016/0370-2693(78)90172-7.

[80] W. Grimus. *Discrete symmetries, roots of unity, and lepton mixing.* J. Phys., G40:p. 075008 [2013]. doi:10.1088/0954-3899/40/7/075008.

[81] R. M. Fonseca and W. Grimus. *Classification of lepton mixing matrices from finite residual symmetries.* JHEP, 09:p. 033 [2014]. doi:10.1007/JHEP09(2014)033.

[82] M. Holthausen, M. Lindner, and M. A. Schmidt. *CP and Discrete Flavour Symmetries.* JHEP, 04:p. 122 [2013]. doi:10.1007/JHEP04(2013)122.

[83] H. Ishimori, T. Kobayashi, H. Ohki, Y. Shimizu, H. Okada, and M. Tanimoto. *Non-Abelian Discrete Symmetries in Particle Physics.* Prog. Theor. Phys. Suppl., 183:pp. 1–163 [2010]. doi:10.1143/PTPS.183.1.

[84] H. Georgi. *Lie algebras in particle physics.* Front. Phys., 54:pp. 1–320 [1999].

[85] C. D. Froggatt and H. B. Nielsen. *Hierarchy of Quark Masses, Cabibbo Angles and CP Violation.* Nucl. Phys., B147:pp. 277–298 [1979]. doi:10.1016/0550-3213(79)90316-X.

[86] L. Wolfenstein. *Parametrization of the Kobayashi-Maskawa Matrix.* Phys. Rev. Lett., 51:p. 1945 [1983]. doi:10.1103/PhysRevLett.51.1945.

[87] A. Bilal. *Lectures on Anomalies*. Unpublished manuscript. arXiv:0802.0634 [2008].

[88] Ya. B. Zeldovich, I. Yu. Kobzarev, and L. B. Okun. *Cosmological Consequences of the Spontaneous Breakdown of Discrete Symmetry*. Zh. Eksp. Teor. Fiz., 67:pp. 3–11 [1974]. [Sov. Phys. JETP40,1(1974)].

[89] E. Ma and G. Rajasekaran. *Softly broken A_4 symmetry for nearly degenerate neutrino masses*. Phys. Rev., D64:p. 113012 [2001]. doi:10.1103/PhysRevD.64.113012.

[90] G. Altarelli and F. Feruglio. *Tri-bimaximal neutrino mixing, A_4 and the modular symmetry*. Nucl. Phys., B741:pp. 215–235 [2006]. doi:10.1016/j.nuclphysb.2006.02.015.

[91] J. Heeck, M. Holthausen, W. Rodejohann, and Y. Shimizu. *Higgs $\to \mu\tau$ in Abelian and non-Abelian flavor symmetry models*. Nucl. Phys., B896:pp. 281–310 [2015]. doi:10.1016/j.nuclphysb.2015.04.025.

[92] G. Hiller, D. Loose, and K. Schönwald. *Leptoquark Flavor Patterns & B Decay Anomalies*. Submitted to: JHEP. arXiv:1609.08895 [2016].

[93] Y. Kajiyama, M. Raidal, and A. Strumia. *The Golden ratio prediction for the solar neutrino mixing*. Phys. Rev., D76:p. 117301 [2007]. doi:10.1103/PhysRevD.76.117301.

[94] V. D. Barger, S. Pakvasa, T. J. Weiler, and K. Whisnant. *Bimaximal mixing of three neutrinos*. Phys. Lett., B437:pp. 107–116 [1998]. doi:10.1016/S0370-2693(98)00880-6.

[95] A. de Gouvea and H. Murayama. *Neutrino Mixing Anarchy: Alive and Kicking*. Phys. Lett., B747:pp. 479–483 [2015]. doi:10.1016/j.physletb.2015.06.028.

[96] R. Bousso, D. M. Katz, and C. Zukowski. *Anthropic Origin of the Neutrino Mass from Cooling Failure*. Phys. Rev., D92(2):p. 025037 [2015]. doi:10.1103/PhysRevD.92.025037.

[97] H. Cardenas, A. C. B. Machado, V. Pleitez, and J. A. Rodriguez. *Higgs decay rate to two photons in a model with two fermiophobic-Higgs doublets*. Phys. Rev., D87(3):p. 035028 [2013]. doi:10.1103/PhysRevD.87.035028.

[98] A. G. Dias, A. C. B. Machado, and C. C. Nishi. *An S_3 Model for Lepton Mass Matrices with Nearly Minimal Texture*. Phys. Rev., D86:p. 093005 [2012]. doi:10.1103/PhysRevD.86.093005.

[99] S. Dev, R. R. Gautam, and L. Singh. *Broken S_3 Symmetry in the Neutrino Mass Matrix and Non-Zero θ_{13}*. Phys. Lett., B708:pp. 284–289 [2012]. doi:10.1016/j.physletb.2012.01.051.

[100] D. Meloni. *S_3 as a flavour symmetry for quarks and leptons after the Daya Bay result on θ_{13}*. JHEP, 05:p. 124 [2012]. doi:10.1007/JHEP05(2012)124.

[101] F. González Canales, A. Mondragón, M. Mondragón, U. J. Saldaña Salazar, and L. Velasco-Sevilla. *Quark sector of S_3 models: classification and comparison with experimental data.* Phys. Rev., D88:p. 096004 [2013]. doi:10.1103/PhysRevD.88.096004.

[102] E. Ma and B. Melic. *Updated S_3 model of quarks.* Phys. Lett., B725:pp. 402–406 [2013]. doi:10.1016/j.physletb.2013.07.015.

[103] Y. Kajiyama, H. Okada, and K. Yagyu. *Electron/Muon Specific Two Higgs Doublet Model.* Nucl. Phys., B887:pp. 358–370 [2014]. doi:10.1016/j.nuclphysb.2014.08.009.

[104] V. V. Vien and H. N. Long. *Neutrino mass and mixing in the 3-3-1 model and S_3 flavor symmetry with minimal Higgs content.* Zh. Eksp. Teor. Fiz., 145:pp. 991–1009 [2014]. doi:10.7868/S0044451014060044, 10.1134/S1063776114050173. [J. Exp. Theor. Phys.118,no.6,869(2014)].

[105] D. Das, U. K. Dey, and P. B. Pal. *S_3 symmetry and the quark mixing matrix.* Phys. Lett., B753:pp. 315–318 [2016]. doi:10.1016/j.physletb.2015.12.038.

[106] L. J. Hall and G. G. Ross. *Discrete Symmetries and Neutrino Mass Perturbations for θ_{13}.* JHEP, 11:p. 091 [2013]. doi:10.1007/JHEP11(2013)091.

[107] F. Bazzocchi and L. Merlo. *Neutrino Mixings and the S_4 Discrete Flavour Symmetry.* Fortsch. Phys., 61:pp. 571–596 [2013]. doi:10.1002/prop.201200123.

[108] C. S. Lam. *The Unique Horizontal Symmetry of Leptons.* Phys. Rev., D78:p. 073015 [2008]. doi:10.1103/PhysRevD.78.073015.

[109] F. Bazzocchi and S. Morisi. *S_4 as a natural flavor symmetry for lepton mixing.* Phys. Rev., D80:p. 096005 [2009]. doi:10.1103/PhysRevD.80.096005.

[110] H. Ishimori and T. Kobayashi. *Towards Minimal S_4 Lepton Flavor Model.* JHEP, 10:p. 082 [2011]. doi:10.1007/JHEP10(2011)082.

[111] S. Morisi and E. Peinado. *An S_4 model for quarks and leptons with maximal atmospheric angle.* Phys. Rev., D81:p. 085015 [2010]. doi:10.1103/PhysRevD.81.085015.

[112] A. E. Carcamo Hernandez, I. de Medeiros Varzielas, S. G. Kovalenko, H. Päs, and I. Schmidt. *Lepton masses and mixings in an A_4 multi-Higgs model with a radiative seesaw mechanism.* Phys. Rev., D88(7):p. 076014 [2013]. doi:10.1103/PhysRevD.88.076014.

[113] I. de Medeiros Varzielas and D. Pidt. *UV completions of flavour models and large θ_{13}.* JHEP, 03:p. 065 [2013]. doi:10.1007/JHEP03(2013)065.

[114] H. Ishimori and E. Ma. *New Simple A_4 Neutrino Model for Nonzero θ_{13} and Large δ_{CP}.* Phys. Rev., D86:p. 045030 [2012]. doi:10.1103/PhysRevD.86.045030.

[115] S. F. King, S. Morisi, E. Peinado, and J. W. F. Valle. *Quark-Lepton Mass Relation in a Realistic A_4 Extension of the Standard Model.* Phys. Lett., B724:pp. 68–72 [2013]. doi:10.1016/j.physletb.2013.05.067.

[116] G. C. Branco, P. M. Ferreira, L. Lavoura, M. N. Rebelo, M. Sher, and J. P. Silva. *Theory and phenomenology of two-Higgs-doublet models.* Phys. Rept., 516:pp. 1–102 [2012]. doi:10.1016/j.physrep.2012.02.002.

[117] A. Pich and P. Tuzon. *Yukawa Alignment in the Two-Higgs-Doublet Model.* Phys. Rev., D80:p. 091702 [2009]. doi:10.1103/PhysRevD.80.091702.

[118] E. A. Paschos. *Diagonal Neutral Currents.* Phys. Rev., D15:p. 1966 [1977]. doi:10.1103/PhysRevD.15.1966.

[119] V. Keus, S. F. King, and S. Moretti. *Three-Higgs-doublet models: symmetries, potentials and Higgs boson masses.* JHEP, 01:p. 052 [2014]. doi:10.1007/JHEP01(2014)052.

[120] A. Degee, I. P. Ivanov, and V. Keus. *Geometric minimization of highly symmetric potentials.* JHEP, 02:p. 125 [2013]. doi:10.1007/JHEP02(2013)125.

[121] S. F. King and C. Luhn. *Neutrino Mass and Mixing with Discrete Symmetry.* Rept. Prog. Phys., 76:p. 056201 [2013]. doi:10.1088/0034-4885/76/5/056201.

[122] E. Ma. *Quark and Lepton Flavor Triality.* Phys. Rev., D82:p. 037301 [2010]. doi:10.1103/PhysRevD.82.037301.

[123] G. G. Ross. *GRAND UNIFIED THEORIES.* Westview Press [1985].

[124] H. Georgi and S. L. Glashow. *Unity of All Elementary Particle Forces.* Phys. Rev. Lett., 32:pp. 438–441 [1974]. doi:10.1103/PhysRevLett.32.438.

[125] A. J. Buras, J. R. Ellis, M. K. Gaillard, and D. V. Nanopoulos. *Aspects of the Grand Unification of Strong, Weak and Electromagnetic Interactions.* Nucl. Phys., B135:pp. 66–92 [1978]. doi:10.1016/0550-3213(78)90214-6.

[126] R. N. Mohapatra. *Supersymmetric grand unification.* In *Supersymmetry, supergravity and supercolliders. Proceedings, Theoretical Advanced Study Institute in elementary particle physics, TASI'97, Boulder, USA, June 2-27, 1997*, pp. 601–657 [1997].

[127] H. Georgi and C. Jarlskog. *A New Lepton - Quark Mass Relation in a Unified Theory.* Phys. Lett., B86:pp. 297–300 [1979]. doi:10.1016/0370-2693(79)90842-6.

[128] P. Nath and P. Fileviez Perez. *Proton stability in grand unified theories, in strings and in branes.* Phys. Rept., 441:pp. 191–317 [2007]. doi:10.1016/j.physrep.2007.02.010.

[129] H. Nishino et al. *Search for Proton Decay via p —¿ e+ pi0 and p —¿ mu+ pi0 in a Large Water Cherenkov Detector.* Phys. Rev. Lett., 102:p. 141801 [2009]. doi:10.1103/PhysRevLett.102.141801.

[130] J. R. Ellis and M. K. Gaillard. *Fermion Masses and Higgs Representations in $SU(5)$*. Phys. Lett., B88:pp. 315–319 [1979]. doi:10.1016/0370-2693(79)90476-3.

[131] S. F. King, C. Luhn, and A. J. Stuart. *A Grand $\Delta(96) \times SU(5)$ Flavour Model*. Nucl. Phys., B867:pp. 203–235 [2013]. doi:10.1016/j.nuclphysb.2012.09.021.

[132] P. S. Bhupal Dev, B. Dutta, R. N. Mohapatra, and M. Severson. *θ_{13} and Proton Decay in a Minimal $SO(10) \times S_4$ model of Flavor*. Phys. Rev., D86:p. 035002 [2012]. doi:10.1103/PhysRevD.86.035002.

[133] S. Antusch, S. F. King, and M. Spinrath. *Measurable Neutrino Mass Scale in $A_4 \times SU(5)$*. Phys. Rev., D83:p. 013005 [2011]. doi:10.1103/PhysRevD.83.013005.

[134] C. Hagedorn, S. F. King, and C. Luhn. *A SUSY GUT of Flavour with $S4 \times SU(5)$ to NLO*. JHEP, 06:p. 048 [2010]. doi:10.1007/JHEP06(2010)048.

[135] H. Ishimori, Y. Shimizu, and M. Tanimoto. *S_4 Flavor Symmetry of Quarks and Leptons in $SU(5)$ GUT*. Prog. Theor. Phys., 121:pp. 769–787 [2009]. doi:10.1143/PTP.121.769.

[136] S. M. Barr. *A New Symmetry Breaking Pattern for $SO(10)$ and Proton Decay*. Phys. Lett., B112:pp. 219–222 [1982]. doi:10.1016/0370-2693(82)90966-2.

[137] G. K. Leontaris and J. D. Vergados. *Neutrino masses in flipped $SU(5)$*. Phys. Lett., B305:pp. 242–251 [1993]. doi:10.1016/0370-2693(93)90114-W.

[138] H. Fritzsch and P. Minkowski. *Unified Interactions of Leptons and Hadrons*. Annals Phys., 93:pp. 193–266 [1975]. doi:10.1016/0003-4916(75)90211-0.

[139] H. Georgi. *The State of the Art – Gauge Theories*. AIP Conf. Proc., 23:pp. 575–582 [1975]. doi:10.1063/1.2947450.

[140] F. Buccella and C. A. Savoy. *Intermediate symmetries in the spontaneous breaking of supersymmetric SO(10)*. Mod. Phys. Lett., A17:pp. 1239–1248 [2002]. doi:10.1142/S0217732302007429.

[141] A. V. Kuznetsov and N. V. Mikheev. *Vector leptoquarks could be rather light?* Phys. Lett., B329:pp. 295–299 [1994]. doi:10.1016/0370-2693(94)90775-7.

[142] R. R. Volkas. *Prospects for mass unification at low-energy scales*. Phys. Rev., D53:pp. 2681–2698 [1996]. doi:10.1103/PhysRevD.53.2681.

[143] A. Blumhofer and B. Lampe. *A Low-energy compatible $SU(4)$ type model for vector leptoquarks of mass ≤ 1 TeV*. Eur. Phys. J., C7:pp. 141–148 [1999]. doi:10.1007/s100529900965.

[144] N. V. Mikheev, M. L. Zilberman, and L. A. Vasilevskaya. *Neutrino radiative decay in an external electromagnetic field via vector leptoquark*. Phys. Lett., B390:pp. 227–233 [1997]. doi:10.1016/S0370-2693(96)01369-X.

[145] T. Fukuyama. *$SO(10)$ GUT in Four and Five Dimensions: A Review*. Int. J. Mod. Phys., A28:p. 1330008 [2013]. doi:10.1142/S0217751X13300081.

[146] K. S. Babu and R. N. Mohapatra. *Predictive neutrino spectrum in minimal SO(10) grand unification.* Phys. Rev. Lett., 70:pp. 2845–2848 [1993]. doi:10.1103/PhysRevLett.70.2845.

[147] M. Hirsch, H. V. Klapdor-Kleingrothaus, and S. G. Kovalenko. *New low-energy leptoquark interactions.* Phys. Lett., B378:pp. 17–22 [1996]. doi:10.1016/0370-2693(96)00419-4.

[148] O. U. Shanker. *$\pi\ell$ 2, $K\ell$ 3 and $K^0 - \bar{K}0$ Constraints on Leptoquarks and Supersymmetric Particles.* Nucl. Phys., B204:pp. 375–386 [1982]. doi:10.1016/0550-3213(82)90196-1.

[149] G. Aad et al. *Searches for scalar leptoquarks in pp collisions at $\sqrt{s}$ = 8 TeV with the ATLAS detector.* Eur. Phys. J., C76(1):p. 5 [2016]. doi:10.1140/epjc/s10052-015-3823-9.

[150] S. Davidson, D. C. Bailey, and B. A. Campbell. *Model independent constraints on leptoquarks from rare processes.* Z. Phys., C61:pp. 613–644 [1994]. doi:10.1007/BF01552629.

[151] J. C. Pati and A. Salam. *Lepton Number as the Fourth Color.* Phys. Rev., D10:pp. 275–289 [1974]. doi:10.1103/PhysRevD.10.275, 10.1103/PhysRevD.11.703.2. [Erratum: Phys. Rev.D11,703(1975)].

[152] T. Hübsch. *Advanced Concepts in Particle and Field Theory.* Cambridge University Press [2015]. ISBN 9781107097483, 9781316371763.

[153] I. Dorsner, S. Fajfer, and N. Kosnik. *Heavy and light scalar leptoquarks in proton decay.* Phys. Rev., D86:p. 015013 [2012]. doi:10.1103/PhysRevD.86.015013.

[154] A. E. Cárcamo Hernández and I. de Medeiros Varzielas. *Viable textures for the fermion sector.* J. Phys., G42(6):p. 065002 [2015]. doi:10.1088/0954-3899/42/6/065002.

[155] K. Bora. *Updated values of running quark and lepton masses at GUT scale in SM, 2HDM and MSSM.* Horizon, 2 [2013].

[156] G. Bhattacharyya and D. Das. *Scalar sector of two-Higgs-doublet models: A minireview.* Pramana, 87(3):p. 40 [2016]. doi:10.1007/s12043-016-1252-4.

[157] H. Serodio. *Yukawa Alignment in a Multi Higgs Doublet Model: An effective approach.* Phys. Lett., B700:pp. 133–138 [2011]. doi:10.1016/j.physletb.2011.04.069.

[158] I. de Medeiros Varzielas. *Family symmetries and alignment in multi-Higgs doublet models.* Phys. Lett., B701:pp. 597–600 [2011]. doi:10.1016/j.physletb.2011.06.042.

[159] G. Aad et al. *Search for top quark decays $t \to qH$ with $H \to \gamma\gamma$ using the ATLAS detector.* JHEP, 06:p. 008 [2014]. doi:10.1007/JHEP06(2014)008.

[160] CMS Collaboration. *Combined multilepton and diphoton limit on $t \to cH$.* Unpublished manuscript. `http://cds.cern.ch/record/1666526` [2014].

[161] C. S. Kim, Y. W. Yoon, and X.-B. Yuan. *Exploring top quark FCNC within 2HDM type III in association with flavor physics.* JHEP, 12:p. 038 [2015]. doi:10.1007/JHEP12(2015)038.

[162] T. P. Cheng and M. Sher. *Mass Matrix Ansatz and Flavor Nonconservation in Models with Multiple Higgs Doublets.* Phys. Rev., D35:p. 3484 [1987]. doi:10.1103/PhysRevD.35.3484.

[163] D. Atwood, L. Reina, and A. Soni. *Phenomenology of two Higgs doublet models with flavor changing neutral currents.* Phys. Rev., D55:pp. 3156–3176 [1997]. doi:10.1103/PhysRevD.55.3156.

[164] S. Chatrchyan et al. *Search for Flavor-Changing Neutral Currents in Top-Quark Decays $t \to Zq$ in pp Collisions at $\sqrt{s} = 8$ TeV.* Phys. Rev. Lett., 112(17):p. 171802 [2014]. doi:10.1103/PhysRevLett.112.171802.

[165] G. Aad et al. *Search for flavour-changing neutral current top-quark decays to qZ in pp collision data collected with the ATLAS detector at $\sqrt{s} = 8$ TeV.* Eur. Phys. J., C76(1):p. 12 [2016]. doi:10.1140/epjc/s10052-015-3851-5.

[166] M. A. Shifman, A. I. Vainshtein, M. B. Voloshin, and V. I. Zakharov. *Low-Energy Theorems for Higgs Boson Couplings to Photons.* Sov. J. Nucl. Phys., 30:pp. 711–716 [1979]. [Yad. Fiz.30,1368(1979)].

[167] J. F. Gunion, H. E. Haber, G. L. Kane, and S. Dawson. *The Higgs Hunter's Guide.* Front. Phys., 80:pp. 1–404 [2000].

[168] A. Djouadi. *The Anatomy of electro-weak symmetry breaking. II. The Higgs bosons in the minimal supersymmetric model.* Phys. Rept., 459:pp. 1–241 [2008]. doi:10.1016/j.physrep.2007.10.005.

[169] V. Khachatryan et al. *Observation of the diphoton decay of the Higgs boson and measurement of its properties.* Eur. Phys. J., C74(10):p. 3076 [2014]. doi:10.1140/epjc/s10052-014-3076-z.

[170] G. Aad et al. *Measurement of Higgs boson production in the diphoton decay channel in pp collisions at center-of-mass energies of 7 and 8 TeV with the ATLAS detector.* Phys. Rev., D90(11):p. 112015 [2014]. doi:10.1103/PhysRevD.90.112015.

[171] M. E. Peskin and T. Takeuchi. *Estimation of oblique electroweak corrections.* Phys. Rev., D46:pp. 381–409 [1992]. doi:10.1103/PhysRevD.46.381.

[172] D. Marzocca, S. T. Petcov, A. Romanino, and M. Spinrath. *Sizeable θ_{13} from the Charged Lepton Sector in $SU(5)$, (Tri-)Bimaximal Neutrino Mixing and Dirac CP Violation.* JHEP, 11:p. 009 [2011]. doi:10.1007/JHEP11(2011)009.

[173] S. Antusch, C. Gross, V. Maurer, and C. Sluka. *A flavour GUT model with $\theta_{13}^{PMNS} \simeq \theta_C/\sqrt{2}$.* Nucl. Phys., B877:pp. 772–791 [2013]. doi:10.1016/j.nuclphysb.2013.11.003.

[174] M.-C. Chen and K. T. Mahanthappa. *Fermion masses and mixing and CP violation in $SO(10)$ models with family symmetries.* Int. J. Mod. Phys., A18:pp. 5819–5888 [2003]. doi:10.1142/S0217751X03017026.

[175] S. Nandi and K. Tanaka. *Masses and Mixing Angles in $SU(5)$ Gauge Model.* Phys. Lett., B92:pp. 107–110 [1980]. doi:10.1016/0370-2693(80)90315-9.

[176] P. Kalyniak and J. N. Ng. *Symmetry Breaking Patterns in $SU(5)$ With Nonminimal Higgs Fields.* Phys. Rev., D26:p. 890 [1982]. doi:10.1103/PhysRevD.26.890.

[177] I. Dorsner and P. Fileviez Perez. *Unification versus proton decay in $SU(5)$.* Phys. Lett., B642:pp. 248–252 [2006]. doi:10.1016/j.physletb.2006.09.034.

[178] F. Wang and Y.-X. Li. *Generalized Froggatt-Nielsen Mechanism.* Eur. Phys. J., C71:p. 1803 [2011]. doi:10.1140/epjc/s10052-011-1803-2.

[179] Y. H. Ahn, S. K. Kang, and C. S. Kim. *Spontaneous CP Violation in A_4 Flavor Symmetry and Leptogenesis.* Phys. Rev., D87(11):p. 113012 [2013]. doi:10.1103/PhysRevD.87.113012.

[180] S. Khalil, S. Salem, and M. Allam. *$SU(5)$ Octet Scalar at the LHC.* Phys. Rev., D89:p. 095011 [2014]. doi:10.1103/PhysRevD.91.119908, 10.1103/PhysRevD.89.095011. [Erratum: Phys. Rev.D91,119908(2015)].

[181] A. E. Carcamo Hernandez, R. Martinez, and F. Ochoa. *Radiative seesaw-type mechanism of quark masses in $SU(3)_C \otimes SU(3)_L \otimes U(1)_X$.* Phys. Rev., D87(7):p. 075009 [2013]. doi:10.1103/PhysRevD.87.075009.

[182] A. Gando et al. *Measurement of the double-β decay half-life of ^{136}Xe with the KamLAND-Zen experiment.* Phys. Rev., C85:p. 045504 [2012]. doi:10.1103/PhysRevC.85.045504.

[183] I. Abt et al. *A New Ge^{76} Double Beta Decay Experiment at LNGS: Letter of Intent.* Unpublished manuscript. arXiv:hep-ex/0404039 [2004].

[184] C. E. Aalseth et al. *The Majorana Experiment.* Nucl. Phys. Proc. Suppl., 217:pp. 44–46 [2011]. doi:10.1016/j.nuclphysbps.2011.04.063.

[185] J. Charles, A. Hocker, H. Lacker, S. Laplace, F. R. Le Diberder, J. Malcles, J. Ocariz, M. Pivk, and L. Roos. *CP violation and the CKM matrix: Assessing the impact of the asymmetric B factories.* Eur. Phys. J., C41(1):pp. 1–131 [2005]. doi:10.1140/epjc/s2005-02169-1.

[186] I. de Medeiros Varzielas and G. Hiller. *Clues for flavor from rare lepton and quark decays.* JHEP, 06:p. 072 [2015]. doi:10.1007/JHEP06(2015)072.

[187] A. Dery, A. Efrati, Y. Nir, Y. Soreq, and V. Susič. *Model building for flavor changing Higgs couplings.* Phys. Rev., D90:p. 115022 [2014]. doi:10.1103/PhysRevD.90.115022.

[188] C.-J. Lee and J. Tandean. *Lepton-Flavored Scalar Dark Matter with Minimal Flavor Violation.* JHEP, 04:p. 174 [2015]. doi:10.1007/JHEP04(2015)174.

[189] A. Celis, V. Cirigliano, and E. Passemar. *Disentangling new physics contributions in lepton flavour violating τ decays.* Nucl. Part. Phys. Proc., 273-275:pp. 1664–1670 [2016]. doi:10.1016/j.nuclphysbps.2015.09.269.

[190] D. Aristizabal Sierra and A. Vicente. *Explaining the CMS Higgs flavor violating decay excess.* Phys. Rev., D90(11):p. 115004 [2014]. doi:10.1103/PhysRevD.90.115004.

[191] A. Crivellin, G. D'Ambrosio, and J. Heeck. *Addressing the LHC flavor anomalies with horizontal gauge symmetries.* Phys. Rev., D91(7):p. 075006 [2015]. doi:10.1103/PhysRevD.91.075006.

[192] G. Bhattacharyya, P. Leser, and H. Pas. *Exotic Higgs boson decay modes as a harbinger of S_3 flavor symmetry.* Phys. Rev., D83:p. 011701 [2011]. doi:10.1103/PhysRevD.83.011701.

[193] Q.-H. Cao, A. Damanik, E. Ma, and D. Wegman. *Probing Lepton Flavor Triality with Higgs Boson Decay.* Phys. Rev., D83:p. 093012 [2011]. doi:10.1103/PhysRevD.83.093012.

[194] G. Bhattacharyya, P. Leser, and H. Pas. *Novel signatures of the Higgs sector from S_3 flavor symmetry.* Phys. Rev., D86:p. 036009 [2012]. doi:10.1103/PhysRevD.86.036009.

[195] G. Bhattacharyya, I. de Medeiros Varzielas, and P. Leser. *A common origin of fermion mixing and geometrical CP violation, and its test through Higgs physics at the LHC.* Phys. Rev. Lett., 109:p. 241603 [2012]. doi:10.1103/PhysRevLett.109.241603.

[196] ATLAS Collaboration. *An update to the combined search for the Standard Model Higgs boson with the ATLAS detector at the LHC using up to 4.9 fb^{-1} of pp collision data at $\sqrt{s}$ = 7 TeV.* Unpublished manuscript. `http://cds.cern.ch/record/1430033` [2012].

[197] CMS Collaboration. *Combination of SM, SM4, FP Higgs boson searches.* Unpublished manuscript. `http://cds.cern.ch/record/1429928` [2012].

[198] I. Doršner, S. Fajfer, A. Greljo, J. F. Kamenik, N. Košnik, and I. Nišandžic. *New Physics Models Facing Lepton Flavor Violating Higgs Decays at the Percent Level.* JHEP, 06:p. 108 [2015]. doi:10.1007/JHEP06(2015)108.

[199] J. Adam et al. *New constraint on the existence of the $\mu^+ \to e^+\gamma$ decay.* Phys. Rev. Lett., 110:p. 201801 [2013]. doi:10.1103/PhysRevLett.110.201801.

[200] D. Chang, W. S. Hou, and W.-Y. Keung. *Two-loop contributions of flavor changing neutral Higgs bosons to $\mu \to e\gamma$.* Phys. Rev., D48:pp. 217–224 [1993]. doi:10.1103/PhysRevD.48.217.

[201] M. Baak, M. Goebel, J. Haller, A. Hoecker, D. Ludwig, K. Moenig, M. Schott, and J. Stelzer. *Updated Status of the Global Electroweak Fit and Constraints on New Physics.* Eur. Phys. J., C72:p. 2003 [2012]. doi:10.1140/epjc/s10052-012-2003-4.

[202] M. Scott. *Recent results from T2K*. In *30th Rencontres de Physique de La Vallée d'Aoste La Thuile, Aosta valley, Italy, March 6-12, 2016* [2016].

[203] A. Crivellin, A. Kokulu, and C. Greub. *Flavor-phenomenology of two-Higgs-doublet models with generic Yukawa structure*. Phys. Rev., D87(9):p. 094031 [2013]. doi:10.1103/PhysRevD.87.094031.

[204] L. Dhargyal. *$R(D^{(*)})$ and $\mathcal{B}(B \to \tau\nu_\tau)$ in a Flipped/Lepton-Specific 2HDM with anomalously enhanced charged Higgs coupling to τ/b*. Phys. Rev., D93(11):p. 115009 [2016]. doi:10.1103/PhysRevD.93.115009.

[205] G. Hiller and M. Schmaltz. *R_K and future $b \to s\ell\ell$ physics beyond the standard model opportunities*. Phys. Rev., D90:p. 054014 [2014]. doi:10.1103/PhysRevD.90.054014.

[206] G. Hiller and M. Schmaltz. *Diagnosing lepton-nonuniversality in $b \to s\ell\ell$*. JHEP, 02:p. 055 [2015]. doi:10.1007/JHEP02(2015)055.

[207] S. Sahoo and R. Mohanta. *Study of the rare semileptonic decays $B_d^0 \to K^* l^+ l^-$ in scalar leptoquark model*. Phys. Rev., D93(3):p. 034018 [2016]. doi:10.1103/PhysRevD.93.034018.

[208] S. Sahoo and R. Mohanta. *Leptoquark effects on $b \to s\nu\bar{\nu}$ and $B \to K l^+ l^-$ decay processes*. New J. Phys., 18(1):p. 013032 [2016]. doi:10.1088/1367-2630/18/1/013032.

[209] R. Alonso, B. Grinstein, and J. Martin Camalich. *Lepton universality violation and lepton flavor conservation in B-meson decays*. JHEP, 10:p. 184 [2015]. doi:10.1007/JHEP10(2015)184.

[210] D. Bečirević, S. Fajfer, and N. Košnik. *Lepton flavor nonuniversality in $b \to s l^+ l^-$ processes*. Phys. Rev., D92(1):p. 014016 [2015]. doi:10.1103/PhysRevD.92.014016.

[211] Y. Sakaki, M. Tanaka, A. Tayduganov, and R. Watanabe. *Testing leptoquark models in $\bar{B} \to D^{(*)}\tau\bar{\nu}$*. Phys. Rev., D88(9):p. 094012 [2013]. doi:10.1103/PhysRevD.88.094012.

[212] M. Freytsis, Z. Ligeti, and J. T. Ruderman. *Flavor models for $\bar{B} \to D^{(*)}\tau\bar{\nu}$*. Phys. Rev., D92(5):p. 054018 [2015]. doi:10.1103/PhysRevD.92.054018.

[213] S. Fajfer and N. Košnik. *Vector leptoquark resolution of R_K and $R_{D^{(*)}}$ puzzles*. Phys. Lett., B755:pp. 270–274 [2016]. doi:10.1016/j.physletb.2016.02.018.

[214] R. Barbieri, G. Isidori, A. Pattori, and F. Senia. *Anomalies in B-decays and $U(2)$ flavour symmetry*. Eur. Phys. J., C76(2):p. 67 [2016]. doi:10.1140/epjc/s10052-016-3905-3.

[215] J. C. Helo, M. Hirsch, H. Päs, and S. G. Kovalenko. *Short-range mechanisms of neutrinoless double beta decay at the LHC*. Phys. Rev., D88:p. 073011 [2013]. doi:10.1103/PhysRevD.88.073011.

[216] U. Mahanta. *Neutrino masses and mixing angles from leptoquark interactions.* Phys. Rev., D62:p. 073009 [2000]. doi:10.1103/PhysRevD.62.073009.

[217] D. Aristizabal Sierra, M. Hirsch, and S. G. Kovalenko. *Leptoquarks: Neutrino masses and accelerator phenomenology.* Phys. Rev., D77:p. 055011 [2008]. doi:10.1103/PhysRevD.77.055011.

[218] K. S. Babu and J. Julio. *Two-Loop Neutrino Mass Generation through Leptoquarks.* Nucl. Phys., B841:pp. 130–156 [2010]. doi:10.1016/j.nuclphysb.2010.07.022.

[219] M. Kohda, H. Sugiyama, and K. Tsumura. *Lepton number violation at the LHC with leptoquark and diquark.* Phys. Lett., B718:pp. 1436–1440 [2013]. doi:10.1016/j.physletb.2012.12.048.

[220] Y. Cai, J. D. Clarke, M. A. Schmidt, and R. R. Volkas. *Testing Radiative Neutrino Mass Models at the LHC.* JHEP, 02:p. 161 [2015]. doi:10.1007/JHEP02(2015)161.

[221] D. Aristizabal Sierra, A. Degee, L. Dorame, and M. Hirsch. *Systematic classification of two-loop realizations of the Weinberg operator.* JHEP, 03:p. 040 [2015]. doi:10.1007/JHEP03(2015)040.

[222] J. C. Helo, M. Hirsch, T. Ota, and F. A. Pereira dos Santos. *Double beta decay and neutrino mass models.* JHEP, 05:p. 092 [2015]. doi:10.1007/JHEP05(2015)092.

[223] M. Hirsch, H. V. Klapdor-Kleingrothaus, and S. G. Kovalenko. *New leptoquark mechanism of neutrinoless double beta decay.* Phys. Rev., D54:pp. R4207–R4210 [1996]. doi:10.1103/PhysRevD.54.R4207.

[224] H. Päs and W. Rodejohann. *Neutrinoless Double Beta Decay.* New J. Phys., 17(11):p. 115010 [2015]. doi:10.1088/1367-2630/17/11/115010.

[225] K.-m. Cheung. *Muon anomalous magnetic moment and leptoquark solutions.* Phys. Rev., D64:p. 033001 [2001]. doi:10.1103/PhysRevD.64.033001.

[226] S. Baek and K. Nishiwaki. *Leptoquark explanation of $h \to \mu\tau$ and muon $(g-2)$.* Phys. Rev., D93(1):p. 015002 [2016]. doi:10.1103/PhysRevD.93.015002.

[227] K. Cheung, W.-Y. Keung, and P.-Y. Tseng. *Leptoquark induced rare decay amplitudes $h \to \tau^{\mp}\mu^{\pm}$ and $\tau \to \mu\gamma$.* Phys. Rev., D93(1):p. 015010 [2016]. doi:10.1103/PhysRevD.93.015010.

[228] C. W. Murphy. *Vector Leptoquarks and the 750 GeV Diphoton Resonance at the LHC.* Phys. Lett., B757:pp. 192–198 [2016]. doi:10.1016/j.physletb.2016.03.076.

[229] M. Bauer and M. Neubert. *Flavor anomalies, the 750 GeV diphoton excess, and a dark matter candidate.* Phys. Rev., D93(11):p. 115030 [2016]. doi:10.1103/PhysRevD.93.115030.

[230] J. de Blas, J. Santiago, and R. Vega-Morales. *New vector bosons and the diphoton excess.* Phys. Lett., B759:pp. 247–252 [2016]. doi:10.1016/j.physletb.2016.05.078.

[231] I. Doršner, S. Fajfer, A. Greljo, J. F. Kamenik, and N. Košnik. *Physics of leptoquarks in precision experiments and at particle colliders.* Phys. Rept., 641:pp. 1–68 [2016]. doi:10.1016/j.physrep.2016.06.001.

[232] N. Kosnik. *Model independent constraints on leptoquarks from $b \to s\ell^+\ell^-$ processes.* Phys. Rev., D86:p. 055004 [2012]. doi:10.1103/PhysRevD.86.055004.

[233] W. Buchmuller, R. Ruckl, and D. Wyler. *Leptoquarks in Lepton - Quark Collisions.* Phys. Lett., B191:pp. 442–448 [1987]. doi:10.1016/S0370-2693(99)00014-3, 10.1016/0370-2693(87)90637-X. [Erratum: Phys. Lett.B448,320(1999)].

[234] H. Päs, M. Hirsch, and H. V. Klapdor-Kleingrothaus. *Improved bounds on SUSY accompanied neutrinoless double beta decay.* Phys. Lett., B459:pp. 450–454 [1999]. doi:10.1016/S0370-2693(99)00711-X.

[235] F. F. Deppisch, J. Harz, M. Hirsch, W.-C. Huang, and H. Päs. *Falsifying High-Scale Baryogenesis with Neutrinoless Double Beta Decay and Lepton Flavor Violation.* Phys. Rev., D92(3):p. 036005 [2015]. doi:10.1103/PhysRevD.92.036005.

[236] L. Calibbi, A. Crivellin, and T. Ota. *Effective Field Theory Approach to $b \to s\ell\ell'$, $B \to K^{(*)}\nu\overline{\nu}$ and $B \to D^{(*)}\tau\nu$ with Third Generation Couplings.* Phys. Rev. Lett., 115:p. 181801 [2015]. doi:10.1103/PhysRevLett.115.181801.

[237] J. P. Lees et al. *Evidence of $B^+ \to \tau^+\nu$ decays with hadronic B tags.* Phys. Rev., D88(3):p. 031102 [2013]. doi:10.1103/PhysRevD.88.031102.

[238] J. P. Lees et al. *A search for the decay modes $B^\pm \to h^\pm\tau^\pm l$.* Phys. Rev., D86:p. 012004 [2012]. doi:10.1103/PhysRevD.86.012004.

[239] S. de Boer and G. Hiller. *Flavor and new physics opportunities with rare charm decays into leptons.* Phys. Rev., D93(7):p. 074001 [2016]. doi:10.1103/PhysRevD.93.074001.

[240] S. M. Boucenna, R. M. Fonseca, F. Gonzalez-Canales, and J. W. F. Valle. *Small neutrino masses and gauge coupling unification.* Phys. Rev., D91(3):p. 031702 [2015]. doi:10.1103/PhysRevD.91.031702.

[241] E. Ma and J. Wudka. *Vector-Boson-Induced Neutrino Mass.* Phys. Lett., B712:pp. 391–395 [2012]. doi:10.1016/j.physletb.2012.05.008.

[242] A. E. Carcamo Hernandez. *Composite Vectors and Scalars in Theories of Electroweak Symmetry Breaking.* Ph.D. thesis, Pisa, Scuola Normale Superiore [2011].

[243] A. Kudo and M. Yamaguchi. *Inflation with low reheat temperature and cosmological constraint on stable charged massive particles.* Phys. Lett., B516:pp. 151–155 [2001]. doi:10.1016/S0370-2693(01)00938-8.

[244] A. D. Martin, W. J. Stirling, R. S. Thorne, and G. Watt. *Parton distributions for the LHC.* Eur. Phys. J., C63:pp. 189–285 [2009]. doi:10.1140/epjc/s10052-009-1072-5.

[245] R. Franceschini, G. F. Giudice, J. F. Kamenik, M. McCullough, A. Pomarol, R. Rattazzi, M. Redi, F. Riva, A. Strumia, and R. Torre. *What is the $\gamma\gamma$ resonance at 750 GeV?* JHEP, 03:p. 144 [2016]. doi:10.1007/JHEP03(2016)144.

[246] M. B. Gavela, G. Girardi, C. Malleville, and P. Sorba. *A Nonlinear R_ξ Gauge Condition for the Electroweak $SU(2) \times U(1)$ Model.* Nucl. Phys., B193:pp. 257–268 [1981]. doi:10.1016/0550-3213(81)90529-0.

[247] V. Khachatryan et al. *Search for resonances and quantum black holes using dijet mass spectra in proton-proton collisions at $\sqrt{s} = 8$ TeV.* Phys. Rev., D91(5):p. 052009 [2015]. doi:10.1103/PhysRevD.91.052009.

[248] G. Aad et al. *Search for new phenomena in the dijet mass distribution using $p-p$ collision data at $\sqrt{s} = 8$ TeV with the ATLAS detector.* Phys. Rev., D91(5):p. 052007 [2015]. doi:10.1103/PhysRevD.91.052007.

[249] B. Aubert et al. *Searches for Lepton Flavor Violation in the Decays $\tau^\pm \to e^\pm\gamma$ and $\tau^\pm \to \mu^\pm\gamma$.* Phys. Rev. Lett., 104:p. 021802 [2010]. doi:10.1103/PhysRevLett.104.021802.

[250] S. Bertolini. *Quantum Effects in a Two Higgs Doublet Model of the Electroweak Interactions.* Nucl. Phys., B272:pp. 77–98 [1986]. doi:10.1016/0550-3213(86)90341-X.

[251] W. Grimus and L. Lavoura. *The Seesaw mechanism at arbitrary order: Disentangling the small scale from the large scale.* JHEP, 11:p. 042 [2000]. doi:10.1088/1126-6708/2000/11/042.

[252] L.-F. Li. *Group Theory of the Spontaneously Broken Gauge Symmetries.* Phys. Rev., D9:pp. 1723–1739 [1974]. doi:10.1103/PhysRevD.9.1723.

[253] P. H. Frampton. *Unification of Flavor.* Phys. Lett., B89:pp. 352–354 [1980]. doi:10.1016/0370-2693(80)90140-9.

[254] E. Ma, H. Sawanaka, and M. Tanimoto. *Quark Masses and Mixing with A_4 Family Symmetry.* Phys. Lett., B641:pp. 301–304 [2006]. doi:10.1016/j.physletb.2006.08.062.

[255] G. Altarelli and F. Feruglio. *Tri-bimaximal neutrino mixing from discrete symmetry in extra dimensions.* Nucl. Phys., B720:pp. 64–88 [2005]. doi:10.1016/j.nuclphysb.2005.05.005.